GEOTECHNICAL INVESTIGATIONS AND MONITORING OF ZUANGTUI AREA, AIZAWL, MIZORAM

A THESIS SUBMITTED IN PARTIAL FULFILLMENT OF THE REQUIREMENTS FOR THE DEGREE OF DOCTOR OF PHILOSOPHY

LALHMINGSANGI

MZU REGISTRATION NO.: 2100410

Ph.D. REGISTRATION NO.: MZU/Ph.D./1738 of 16.04.2021

DEPARTMENT OF GEOLOGY

SCHOOL OF EARTH SCIENCES AND NATURAL RESOURCES MANAGEMENT

APRIL, 2024

GEOTECHNICAL INVESTIGATIONS AND MONITORING OF ZUANGTUI AREA, AIZAWL, MIZORAM

BY

LALHMINGSANGI
DEPARTMENT OF GEOLOGY

SUPERVISOR
Dr. V. VANTHANGLIANA

JOINT SUPERVISOR
Dr. LALDINPUIA

Submitted
In partial fulfillment of the requirement of the Degree of Doctor of Philosophy in Geology of Mizoram University, Aizawl

DEPARTMENT OF GEOLOGY

PACHHUNGA UNIVERSITY COLLEGE

(A CONSTITUENT COLLEGE OF MIZORAM UNIVERSITY

Dr.V.Vanthangliana AIZAWL-796001: MIZORAM

SUPERVISOR'S CERTIFICATE

This is to certify that **Lalhmingsangi**, a Ph.D. scholar having MZU Registration No. **2100410** and Ph.D. Registration No. **MZU/Ph.D./1738 of 16.04.2021** has completed a thesis work on "**Geotechnical Investigations and Monitoring of Zuangtui Area, Aizawl, Mizoram**" under my supervision and guidance. This thesis work is a part of fulfilment of the requirements for the Degree of Doctor of Philosophy in Geology of Mizoram University, Aizawl. No part of the study has been published nor presented earlier elsewhere.

(Dr.V.VANGTHANGLIANA) (Dr. LALDINPUIA)

Supervisor Joint Supervisor

DECLARATION

Mizoram University

April, 2024

I, **Lalhmingsangi** , hereby declare that the subject matter of this thesis is the record of work done by me, that the contents of this thesis did not form basis of the award of any previous degree to me or to do the best of my knowledge to anybody else, and that the thesis has not been submitted by me for any research degree in any other University/Institute.

This is being submitted to the Mizoram University for the Degree of Doctor of Philosophy in Geology.

(LALHMINGSANGI)

(Dr. JIMMY LALNUNMAWIA)
Head of Department

(Dr. V.VANTHANGLIANA)
Supervisor

ACKNOWLEDGEMENT

I am deeply grateful to God for blessing me with good health, vitality, supportive teachers, a dedicated research partner, and a loving family throughout the process of working on this thesis

I express my sincere thank to the Departmental Research Committee of Geology, Mizoram University for accepting my research work.

This thesis has been completed under the consistent guidance and supervision of Dr. V.Vanthangliana, my supervisor, Department of Geology, Pachhunga University College and Dr. Laldinpuia, my joint supervisor, Centre for Disaster Management, Mizoram University. I am grateful to Zosangliana Ralte, my research partner, department of Geophysics, Pachhunga University College, who provided invaluable assistance in all aspects of my research including fieldwork and laboratory work. I remain genuinely grateful for their unwavering guidance and support in completing my research work.

I am sincerely grateful to the Department of Geology, Pachhunga University College for generously allowing me to use their Geotechnical Laboratory facilities without any charge. Additionally, I extend my gratitude to the Department of Geology, Mizoram University for providing me with the opportunity to conduct my research under their esteemed institution.

I extend my heartfelt gratitude to Lallawmsanga, Zoramkhuma, Laldinsanga Hnamte, H.Z. Vanlalrochana, Jessy Laltlanzaua and Dr.Lalhlimpuia for their assistance in various aspects of my research.

Last but certainly not least, I am deeply thankful to my family and relatives for their support throughout my research journey.

(LALHMINGSANGI)

TABLE OF CONTENTS

LIST OF TABLES

LIST OF FIGURES

LIST OF EQUATIONS

Eqn. No.	The Equations
4.1	$W=\{(W_2-W_3)/(W_3-W_1)\} \times 100$
4.2	Plasticity Index (I_p)= Liquid Limit (w_L) – Plastic Limit (w_p)
4.3	$I_p = 0.74\ (w_L - 8)$
4.4	(NMC-PL)/ PI
4.5	CI= (LL-W)/(LL-PL)
4.6	$Y_m = \frac{m_2 - m_1}{V_m}$
4.7	$Y_d = \frac{100 Y_m}{100+w}$
4.8	$PDSD = \frac{ASD \times 100}{DSD}$
4.9	$A=A_O/(1-e)$
4.10	Deviatoric stress = L/A_c
4.11	$FoS = \frac{\sum \text{Resisting forces}}{\sum \text{Driving forces}}$
4.12	$I_{d1} = \frac{B-D}{A-D}\ 100$
4.13	$I_{d2} = \frac{C-D}{A-D} 100$
4.14	$W = \frac{W1+W2+W3}{3}$
4.15	$I_L\ (50) = P/\ (DW)^{0.75} \sqrt{D}^*$
4.16	$RQD = 115 - 3.3\ J_v($
4.17	$RQD = 110 - 2.5 J_v$
4.18	$J_v = \sum_{i=1}^{J} \left(\frac{1}{S_i}\right)$
4.19	$J_v = \sum_{i=1}^{J} \left(\frac{1}{S_i}\right) \frac{N_r}{5\sqrt{A}}$
4.20	$\rho_{as} = \frac{\pi(L^2 - l^2)}{2l} \Delta V/I$

LIST OF ABBREVIATIONS

LL	Liquid limit
PL	Plastic limit
NMC	Natural moisture content
CI	Consistency index
PI	Plasticity index
CD	Consolidated drained
RMR	Rock mass rating
UCS	Uniaxial compressive strength
PLI	Point load index
et al.	et alia (and others)
RQD	Rock quality designation
SD	Spacing Discontinuity
SDI	Slake Durability Index
VES	Vertical electrical sounding
EDM	Electronic Distance Measuring Device
LEM	Limit Equilibrium Method
IS	Indian Standard
SL	Shrinkage limit
ZS	Zuangtui soil
ZR	Zuangtui rock

CHAPTER 1

INTRODUCTION

1.1 GENERAL INTRODUCTION

A landslide is the downward movement of a mass of debris, earth or rock down a slope under the influence of gravity (Nemcok et al., 1972; Vernes, 1958, 1978; Hutchinson, 1988; WP/WLI, 1990; Cruden and Vernes, 1996). This broad definition includes a variety of slope failure modes and is not limited to slow-moving, slide-type failure. Mass wasting(Thornbury,1969), mass movement (Sharp,1958), and slope movement(Varnes,1978) are alternate terms used as broadly defined. Landslides can occur due to rainfall-induced, earthquakes, toe erosion due to flooding or river erosion, and other natural causes, as well as anthropogenic causes such as modification of slope, overgrazing, excessive development, etc (Mc Coll, 2021). Rockfall is a block or fragments of rock detached from the slope by toppling, direct falling, or sliding that proceeds by rolling on talus or bouncing down the slope (Varnes, 1987). Based on the types, materials involved, and nature of the movement, a landslide can be of different types like falls, topples, rotational slides, and translational slides (Evans *et al*.,2001). Direct falls of rock from a cliff or steep slope are defined as falls and the forward rotation of rocks is called topple (Singh *et al*.,2016). A movement that is rotational about an axis that is transverse across the slide and is parallel to the surface of the ground is termed a rotational slide. A translational slide is the rotational or backward tilting of the movement along the planar surface (ISRO, 2023). The rate of ground movement is highly controlled by the moisture content, topography, and materials involved (Ahmed,2021).

Landslides are ubiquitous hazards, especially in hilly terrain throughout the world. In India, a landslide is mostly suffered by a state or region with varied climatic and physiographic conditions(Mc Coll, 2022). Excluding snow-covered, 12.6% or 0.42 million sq. km of land cover in India is prone to landslide

hazards. Out of this, 0.09 million sq. km falls under Konkan hills and the region around Western Ghats, 0.01 million sq. km in Eastern Ghats, and the region of North East Himalayas has landslide prone area of about 0.18 million sq. km. Due to hilly and steep topography, the Himalayas and Western Ghats suffered more landslides compared to other states during monsoon (ISRO, 2023). In a hilly area like Mizoram, other than anthropogenic causes, rainfall is one of the most triggering factors as the action of water on soil, rock, and vegetation reduces the strength of the slope stability resulting in environmental damages, loss of human life and destruction on inhabitations (ISRO, 2023). More than 1,000 people die because of landslides every year (Karsli *et al*.2009). Continental-wise, maximum damages due to landslides are suffered by Asia, especially in South Asian countries like India (Froude and Perley, 2018). 15% of the land in India is prone to landslide high-risk zone (GSI, 2001). Countries with the highest landslide risk include Nepal, India, Columbia, and Tajikistan, which are estimated to have several people die because of a landslide of more than one per 1000 sqm (Nadim *et al*.2020). Among the many landslide incidents in India, one of the common fatal landslides is; the Darjeeling landslide where 667 people lost their lives occurred on 4th October 1968 (Biswas & Pal, 2016). On 16th June 2013, a landslide occurred in Uttarakhand due to a flood, and over 5700 people dead were reported (Barik, 2016). 40 people lost their lives because of a fatal landslide that occurred in Amboori in November 2021. A great Guwahati landslide killed around 500 people in September 1948 (KSDMA, 2019). 151 people lost their lives due to the Malin Maharashtra landslide on 30th July 2014(Saha & Prakash, 2019).

Landslide is the most serious hazard in the hilly terrain of North Eastern part of India. More than 50% of natural hazards in Mizoram are due to landslides (Tiwari & Kumar,1996). The large remarkable landslide occurred in the years 1893, 1929, and 1965 in Mizoram(Laldinpuia *et al*.,2013). An increase in urbanization in hilly terrain results in modification of the slope that induced landslide in different parts of Mizoram. Some of the most tragic landslide incidents in Mizoram are; the Hlimen quarry landslide (Tiwari & Kumar, 1996),

the Hunthar landslide (Laldinpuia et al.2013), the Keifang quarry landslide, and the Rangvamual landslide, Zemabawk landslide that occurred on 7th October 2020, Thuampui landslide where 4 people died on 11th June 2021, Zuangtui landslide which is actively moving since 1987, Pullen landslide where the national highway was displaced on 4th October 2020. 17 people lost their lives because of the Laipuitlang rockslide on 11th May 2013 (Laldinpuia *et al*.,2014), Durtlang rockslides that occurred on 2nd July 2019 killed 3 people and injured 8 persons. Four blocks in the BSUP complex were swiped off by these rockslides. The subsidence that occurred in 1994 in areas within Aizawl Venglai and Ramthar resulted in significant destruction and damages resulting in the evacuation of many houses. In 2017 landslide occurred along the highways passing through various districts in Mizoram, particularly affecting Lunglei, Serchip, Lawngtlai, Siaha, and Champhai districts near the Myanmar border, tragically resulting in the deaths of 12 commuters and 877 structures were destroyed due to the impact of the landslide(Lalramdina, 2022).On 16th June 2023, a destructive landslide occurred at Zohnuai Aizawl. Two residential RCC buildings and one ongoing construction of a house at the lower section of the sliding area were destroyed by this incident. Four houses near the incident area were evacuated.

Landslides in North East India are mainly due to topography, undercutting of slopes by streams or rivers, slope modification for development, differential erosion, earthquakes, and the reduction in the strength of engineering properties of rock and soil due to moisture(Bhusan *et al*.,2022).

To decipher the causes, mechanism of failure, and suggestion of mitigation measures, landslides need to be investigated and monitored scientifically. Some of the Geotechnical parameters such as tensile strength, cohesive strength, angle of internal friction, change in pore pressure, permeability, etc. are highly important in the investigation of the affected area(Ahmed *et al*.,2021). Since rock and soil strength decreases depending upon their contact with water, groundwater investigation also plays an important role(Shrestha et al.,2008). Geotechnical methods involve direct investigation of soil and rock properties through techniques

such as drilling, sampling, and laboratory testing. These methods provide valuable data on parameters like soil strength, permeability, and deformation characteristics, which are essential for assessing landslide susceptibility and designing appropriate mitigation measures(Cotecchia *et al*., 2017; Sloan,2013; Jongmans *et al*.,2007). Geophysical methods offer non-invasive techniques for assessing subsurface conditions and detecting geological structures associated with landslide hazards(Jongmans *et al*.,2007; Vyzhya *et al*.,2019). By combining geotechnical and geophysical methods, we can develop a comprehensive understanding of the factors contributing to landslide hazards and implement targeted mitigation strategies (Pasierb *et al*.,2019). This integrated approach enhances the effectiveness of landslide control measures, reduces risks to infrastructure and communities, and promotes sustainable land use planning in landslide-prone areas(Kabeta *et al*.,2023; Pasierb *et al*.,2019).

Monitoring ground movement in landslide-prone areas is critical for understanding the activity level and potential risks associated with such areas(Zieher et al.,2021). Sophisticated equipment like total stations plays a key role in this monitoring process. The monitoring data is crucial for assessing the stability of the area and determining whether it remains active or is stabilizing, and is essential for implementing effective mitigation strategies, issuing timely warnings to residents, and ultimately improving the safety and resilience of communities living in landslide-prone regions (Shible et al.,2023)

According to Laldinpuia (2019), a geological investigation of the Ramhlun Sports Complex area was performed due to the ground movement that occurred in August 2012. 38 houses were vacated affecting 195 persons of 41 families. Monitoring was done using a crack meter and extensometer for two years. Soil samples of the investigated area were analyzed as Atterberg's limit, CBR (California bearing ratio), MDD (maximum dry density), and OMC (optimum moisture content). From the investigation, the interpretation is made that the moisture content of the soil is too high and the CBR and MDD values are low compared to safety standards.

A geological investigation was carried out by Laldinpuia (2014) on Zuangtui road which was affected due to subsidence since 1987. The subsidence rate was measured every month around the retaining wall of Zuangtui Road at 6 points for 7 years. Huge debris flow that occurred every 10 years intervals caused translational slide at the top of the road. Two houses were affected by this slope failure and the socio-economic link road is badly disturbed. Geotechnical studies were carried out at Liapuitlang rockslide and the main triggering factors were interpreted as unsafe cuttings and heavy rainfall(Laldinpuia *et al*.,2014).

For the investigation of groundwater condition in Mizoram Highway-I, an Electrical resistivity survey was done using the vertical electrical sounding technique (H. Laldintluanga, 2022). The electrical resistivity method is used for delineating subsurface conditions(Cho *et al*., 2020; Jianjun *et al*.,2020; Mahmud *et al*.,2022). Validation of geotechnical data and the resistivity data enable the characterization of subsurface lithology which provides important information for the proper and safe construction of any type of structure (Siddiqui *et al*., 2012; Mehmood *et al*.,2020; Mahmud *et al*.,2022). Vertical electrical sounding (VES) techniques are instrumental in understanding groundwater conditions and assessing landslide triggers related to moisture in vulnerable areas(Bahammou *et al*.,2021)

In 2021, the Aizawl Municipal Corporation (AMC) initiated the implementation of the Slope Development and Slope Modification (SDSM) application across all earthwork construction activities within the AMC area. As part of this initiative, geotechnical investigations are conducted for proposed construction areas by qualified geologists. These investigations aim to assess the geological and geotechnical conditions of the site, including factors such as soil composition, stability, and potential risks of slope instability or landslides.

Following the geotechnical investigation, a detailed geotechnical report is generated and reviewed by both geologists and engineers designated by the AMC. This collaborative review process ensures that the geotechnical findings are thoroughly evaluated and understood by all relevant stakeholders. Additionally, it

allows for the identification of any potential hazards or challenges associated with the proposed construction activities.

By implementing the SDSM application and conducting geotechnical investigations, the AMC aims to promote safe and sustainable construction practices within its jurisdiction. This proactive approach to site assessment and risk management helps mitigate potential geotechnical hazards, safeguard infrastructure investments, and enhance overall public safety within the AMC area.

Indeed, the detailed analysis and utilization of both geotechnical and geophysical methods are crucial for understanding subsurface conditions and mechanical properties of rock and soil. This comprehensive approach provides essential information necessary for effective landslide control and mitigation measures.

1.2 LOCATION OF THE STUDY AREA

The selected area Zuangtui is one of the localities in Aizawl under ward no. 1 of the Aizawl Municipal Corporation (AMC) area. It is located between $N23^{0}44'54.54"$ & $E92^{0}44'14.82"$ and $N23^{0}44'53.16"$ & $E092^{0}44'18.6"$ and at 965m above sea level. The area falls under top sheet 84A/9 (Fig. 1).

The study area is around 30km from Lengpui Airport, which is in the western part of Aizawl. Aizawl is connected by air routes from Kolkata, Guwahati, and Imphal. It is connected with Assam and other states of India by NH-54. The Train route reached Bairabi, Kolasib district of Mizoram which is around a 3-hour journey from the study area.

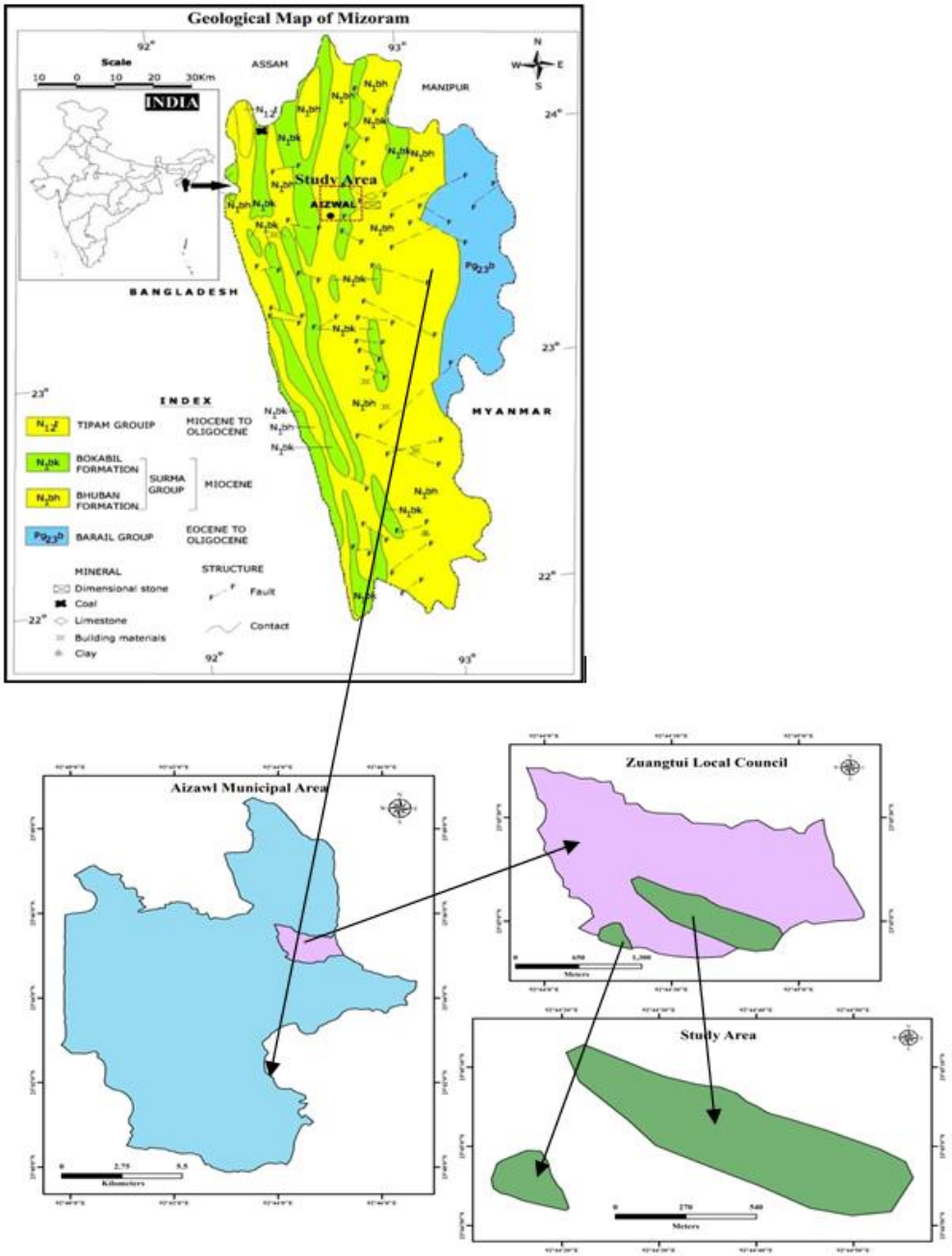

Figure. 1.1. Location map of the study area

1.3. HISTORY OF THE STUDY AREA

The selected area Zuangtui has been suffering ground movement since 1987 where huge debris movement in the N-E direction is observed every 10 years interval at Zuangtui- Thuampui local council border. Rotational type of movement affected in and around 132kV Station, Zuangtui from the 1990s. More than 20 houses were demolished due to active ground movement in the Zuangtui-Thuampui local council border (Figure 1.2.a). Besides residential buildings, Government buildings and churches were also affected. More than 5 Government quarters (P&E quarters) collapsed and the 132KV substation was relocated due to the subsidence. Cracks, fractures, and displacement of the road were observed particularly during the rainy season(Figure 1.2.b)

Gabion walls constructed along road sections to prevent slope failure have experienced bulging, necessitating subsequent reconstruction efforts. Check dams have been constructed at the lower portion of the slope to aid in controlling slope failure. These check dams serve as temporary barriers that impound soil during rainfall or runoff events, reducing erosion and preventing excessive water accumulation that could destabilize the slope.

The construction of permanent reinforced cement concrete buildings is prohibited by Aizawl Municipal Corporation (AMC). Due to active movement especially during monsoon season, some part of the road has been displaced and reconstruction of the road is carried out frequently

(a)

(b)

Figure. 1.2(a) & (b) Landslide in the study area

1.4. SCOPE OF THE STUDY

The description of Mizoram as a young folded mountain with immature sedimentary strata highlights the geological complexity of the region. The presence of soft rocks and high hill slopes, compounded by random faulting and folding, creates inherently unstable slope conditions. In particular, the susceptibility to landslides is exacerbated by the presence of groundwater in loose, weathered soil, and unconsolidated rock formations, particularly pronounced in areas like Aizawl. These factors contribute to frequent landslides during the rainy season, posing significant risks to habitat areas and infrastructure. Given these challenges, understanding the geological and geomechanical properties of the soil and rock is crucial, especially in the context of moisture influence. Conducting geophysical surveys can provide valuable insights into subsurface lithology and groundwater presence, aiding in the assessment of landslide risks. By integrating geotechnical investigations to evaluate material properties and groundwater conditions, it becomes possible to develop effective mitigation strategies to address landslide hazards.

Therefore, the proposed study, aimed at assessing the geological, geomechanical, and hydrogeological characteristics of the region, holds great promise in mitigating ground movement and addressing the challenges faced by communities in Mizoram. By gaining a comprehensive understanding of the underlying geological processes and associated hazards, it becomes possible to implement targeted measures to enhance resilience and safeguard lives and infrastructure in landslide-prone areas.

1.4 OBJECTIVES

The objectives of this study are as follows

a) To assess the geo-mechanical properties of soil and rock.

b) To monitor the rate of ground movement and to determine sub-surface structure

c) To suggest appropriate mitigation measures.

CHAPTER 2

GEOLOGICAL SETTING OF MIZORAM

2.1. REGIONAL GEOLOGY

Understanding the sedimentation and paleogeographic patterns of a region is intricately linked to the tectonic setting and stratigraphic chronology of the area. The tectonic history of the region under study, spanning approximately 2500 kilometers in length and 300 kilometers in width from east to west along the Himalayas, and 1500 kilometers in length and 300 kilometers in width from north to south along the Indo-Burman ranges, is primarily characterized by the collision of the Indian plate with the Eurasian and Burmese plates. This collision has resulted in the formation of the regional tectonic framework. The Himalayan belt is composed of four longitudinal lithotectonic units, each displaying a general northward dipping thrust. These litho-tectonic units are interconnected, forming a continuous belt across the region. Notably, the litho-tectonic and tectonic characteristics of these four units remain relatively consistent along their strike over considerable distances (Gansser 1964). The four units are:

i. The Tethys Himalaya and Trans Himalaya
ii. The Higher Himalaya
iii. The Lower or Lesser Himalaya
iv. The Sub Himalaya

2.2. SURMA BASIN

The Surma basin, dating back to the Neogene period, is defined by several significant post-Barail unconformities and fault systems. These include the Kaladan fault to the east (Nandy et al., 1983), the east-west trending Dauki fault to the north (Nandy et al., 1983), the northeast-southwest trending Disang thrust to the northeast (Sengupta, 1966), the northeast-southwest trending Sylhet fault to the west (Nandy et al., 1983), and the Barisal Chandpur High fault situated beneath the sediments of Bangladesh to the northwest (Sengupta, 1966). The southern boundary of the Surma basin extends to the Arakan coastal area of Myanmar (Malsawma, 2019). This basin

is characterized by a collection of sedimentary formations, including the Surma groups and younger deposits, forming a westward-facing convex fold belt. Stretching approximately 550 kilometers in length and reaching a maximum width of 200 kilometers, the Surma basin encompasses the lower regions of Mizoram, Tripura, and Assam, as well as parts of western Manipur. Additionally, it extends into the Sylhet and Chittagong districts of Bangladesh, along with the Arakan coastal area of Myanmar (Nandy et al.,1983). The Gas province situated in the northeast of Bangladesh within the Surma basin has been significantly influenced by the convergence of two major tectonic movements. These tectonic activities have played a crucial role in shaping the structural configuration and geological characteristics of the Surma basin and its associated petroleum resources (Hillar and Elahi, 1989).

In 1932, Evan established the first lithostratigraphic classification specifically for the tertiary strata that were exposed in the Assam Basin. This classification quickly became a crucial framework for stratigraphic correlation not only within the Assam Basin but also across the broader Bengal Basin. Numerous published and unpublished reports referenced Evan's classification, highlighting its significance in regional geological studies. As scientific disciplines like micro-paleontology, palynology, and seismic stratigraphy advanced over the years, Evan's initial lithostratigraphic scheme underwent refinements and enhancements. Banerji (1984) contributed to these refinements by incorporating micro-paleontological data into the classification process. Similarly, Baksi (1972) and Reimann (1993) used palynology techniques to further develop and refine the classification system. Studies focusing on various aspects such as lithology, fossil assemblages, plant life, and additional geological evidence have provided strong indications that the sediments forming the lower Disang group were deposited in a deep-water environment. The interpretation suggests that these sediments were likely situated on the slopes of turbidites, indicating specific depositional processes and environmental conditions during the formation of these geological units (Roy, 1983).

The contributions of Banerji, Baksi, Reimann, and others exemplify the interdisciplinary nature of geological research and the importance of integrating multiple scientific methods to enhance our understanding of stratigraphy,

sedimentary environments, and geological history. By combining traditional lithostratigraphy with modern techniques such as micro-paleontology and palynology, researchers have been able to refine stratigraphic classifications and gain insights into the depositional settings and geological evolution of the Assam Basin and its surrounding regions. The detailed analysis of sedimentary sequences and associated fossil records provides valuable information about past environments and processes that shaped the landscapes we see today.

Additionally, Salt et al. (1989) and Lindsay et al. (1991), utilizing seismic stratigraphy, further refined the scheme. The sedimentary sequence of the Disang Group, ranging from the Late Cretaceous to the Eocene, represents the oldest exposed strata along the Indo-Burman collision zone (Rao,1983).In contrast, the upper Disang sediments, correlated with the Sylhet limestone, were primarily deposited in a shallow-water environment within a dynamically subsiding basin. The Sylhet limestone is succeeded by a thin argillaceous unit known as the Kopili shale formation, which belongs to the Upper Eocene epoch and has a paralic environment((Uddin and Ahmed,1989 and Reimann, 1993)

Table 2.1: Stratigraphic succession of the Surma basin part of the Bengal basin (revised from Hiller and Elahi, 1988)

Age (approx.)	Group	Foramation	Seismic marker	Thickness(max)(m)
Holocene	Dihing	Alluvium	Yellow	3350
Pleistocene		Dihing Upper Dupi Tila		
Late Pliocene	Dupi Tila	Lower Dupi Tila		
Mid-Pliocene	Tipam	Gurujan Clay Tipam Sandstone		3550
Early Pliocene Miocene	Surma	Lower		3990
		Upper		
Oligocene	Barail	Undifferentiated	Brown	
Paleocene-Eocene	Jaintia	Kopili shale		
		Sylhet Limestone	Red	7200
Pre-Paleocene	Undifferentiated sedimentary rocks(with volcanics) on the continental basement complex		violet blue	

2.2.1. BARAILGROUP

The Barail group, a significant geological formation in the Assam Basin, is characterized by its composition of very-fine to fine-grained sandstone interspersed with siltstone, silty shale, and distinct coal seams(Alam, 1991). This group's deposition is believed to have occurred during a notable regression event, which exposed a substantial portion of the Bengal Basin to sedimentary processes. Evidence of a similar lithological sequence dating to the Oligocene age has been identified along the northern fringe of the Sylhet Trough, adjacent to the southern part of the Dauki Fault (Johnson and Alam, 1991). The depositional environment of the Barail group is predominantly interpreted as a tide-dominated shelf setting (Alam, 1991), indicating significant influences from tidal processes during sedimentation. This suggests that the area experienced regular tidal activity that influenced sediment transport and deposition during the formation of the Barail strata.

In terms of stratigraphy, the Barail formation is characterized by the deposition of a relatively smaller delta system compared to other neighboring formations like the Surma and Tipam groups. The main concentration of this delta system was situated further north in Assam. Over time, stratigraphic records indicate the progradation of this delta system, suggesting gradual extension into the basin (Alam et al., 2003; Biswas and Mukhopadhyay, 2011; Bezbaruah and Muzamil, 2013; Sincavage et al., 2020).

In Southeast Assam, the Barail group is further subdivided into distinct formations known as the Laisong Formation, Jenam Formation, and Renji Formation, each representing specific depositional environments and sedimentary characteristics within the Barail sequence. Similarly, in Northeast Assam, the Barail series is divided into the Tikak Parbat Formation, Borgolai Formation, and Naogaon Formation, reflecting regional variations and stratigraphic complexity (Borooah, 1962).

2.2.2. SURMA GROUP

The primary lithostratigraphic units of the Surma Group are comprised of the Bhuban and Bokabil Formations. Mizoram, situated within the Surma basin, is geologically influenced by faulting to the east, and the folded sediments extend southward into Myanmar (Nandy et al., 1983). Within the Surma Group, the Bhuban Formation is subdivided into distinct units based on the order of superposition, lithological characteristics, and physical properties. These subdivisions include the Lower, Middle, and Upper Bhuban Formations, each representing specific sedimentary sequences and depositional environments within the broader framework of the Surma Group. This detailed stratigraphic division aids in understanding the geological history and evolution of the Surma basin, highlighting the complex interplay of tectonic forces and sedimentary processes that have shaped the landscape of this region over time (Nandy et al., 1983).

2.2.3. TIPAM GROUP

The Tipam Group, dating to the upper Mio-Pliocene period, is positioned above the Surma Group of rocks with unconformity contact. Within the Tipam Group, there are two distinct formations: the Tipam Sandstone Formation and the Girujan Clay Formation (Johnson and Alam, 1991). The Tipam Sandstone Formation is typified by yellowish-brown to reddish-brown coarse-grained sandstone, showcasing features like cross-bedding and ripple-laminated sandstone, alongside minor occurrences of siltstone and mudstone. These sedimentary characteristics strongly indicate a depositional environment dominated by a braided-fluvial system (Johnson and Alam, 1991). In a braided-fluvial system, sediment deposition is influenced by multiple shifting channels that interconnect, creating a complex network of sediment transport and deposition patterns. The presence of cross-bedding and ripple marks further suggests the dynamic nature of this environment, characterized by fluctuating water flow and sediment transport processes(Johnson and Alam, 1991).On the other hand, the Girujan Clay Formation consists of brown, blue, and grey mottled clay. This formation indicates a different depositional environment characterized by lacustrine (lake) and fluvial (river) processes with the

presence of mottled clay suggesting variations in sediment composition and potential fluctuations in water levels within the depositional setting (Reimann, 1993).

2.3. GENERAL GEOLOGY OF MIZORAM

Geological studies were a crucial task in Mizoram due to its remoteness and inaccessibility problems. Among few pioneer geologists Ganju (1975), Ganguly (1975), Jokhan Ram et al.(1984), Shrivastava et al.(1979), Nandy (1972,1983), and Nandy et al.(1983) have contributed a lot in shaping the geology of Mizoram.

Mizoram is a hilly terrain bounded in the West by Tripura and Chittagong Hill Tract, in the East by Chin Hills, in the South by Arakan Hills, and shares its northern boundary with Assam and Tripura states. It covers about 250000 km^2 and is the easternmost extension of the Surma Basin (Borgohain *et al*.,2020).

Geologically Mizoram is a part of the Tripura-Mizoram mio-geosynclinal basin which was formed after the upliftment of the Barail Group of sediment during the Miocene age (Evans, 1964). It is composed of immature sedimentary strata with a succession of arenaceous and argillaceous sediments having a series of N-S trending, longitudinally plunging, anticlines, and synclines (G.S.I, 1974). It is a folded mountain with an alternating succession of shales, mudstones, and sandstones, having a westerly convex with sinuous structural ridges and valleys and characterized by poorly fossiliferous strata (Srivastava et al.,1979)

Dissension among the geologists arose on the occurrence of the Barail Group in Mizoram. The absence of Barail sediments and consideration of Mizoram as only a part of the Surma Group was given by Ganju (1975), Shrivastava *et al*. (1979), and Jokhan Ram *et al*.(1984). Meanwhile, there is a presence of Barail sediments in the Eastern part of Mizoram (Munshi, 1964; Nandy, 1972, 1982), and (Nandy *et al*. 1983).

In the western and north-western parts, Bokabil rocks are encountered in the cores of synclines. At the anticline cores at high altitudes, the Lower Bhuban Formation is observed, while the limbs of the folds and the core of low amplitude reveal the deposition of the Middle Bhuban Formation. Upper Bhuban rocks are

observed in the synclinal cores of the central and eastern parts and also restricted to the anticlinal region of the western part of Mizoram (Jokhan Ram *et al*.1984). Generally, the rock formation has a dip direction either towards the east or west, with a strike of N-S trending. An outcrop of older rock formation is observed towards the eastern side of Mizoram.

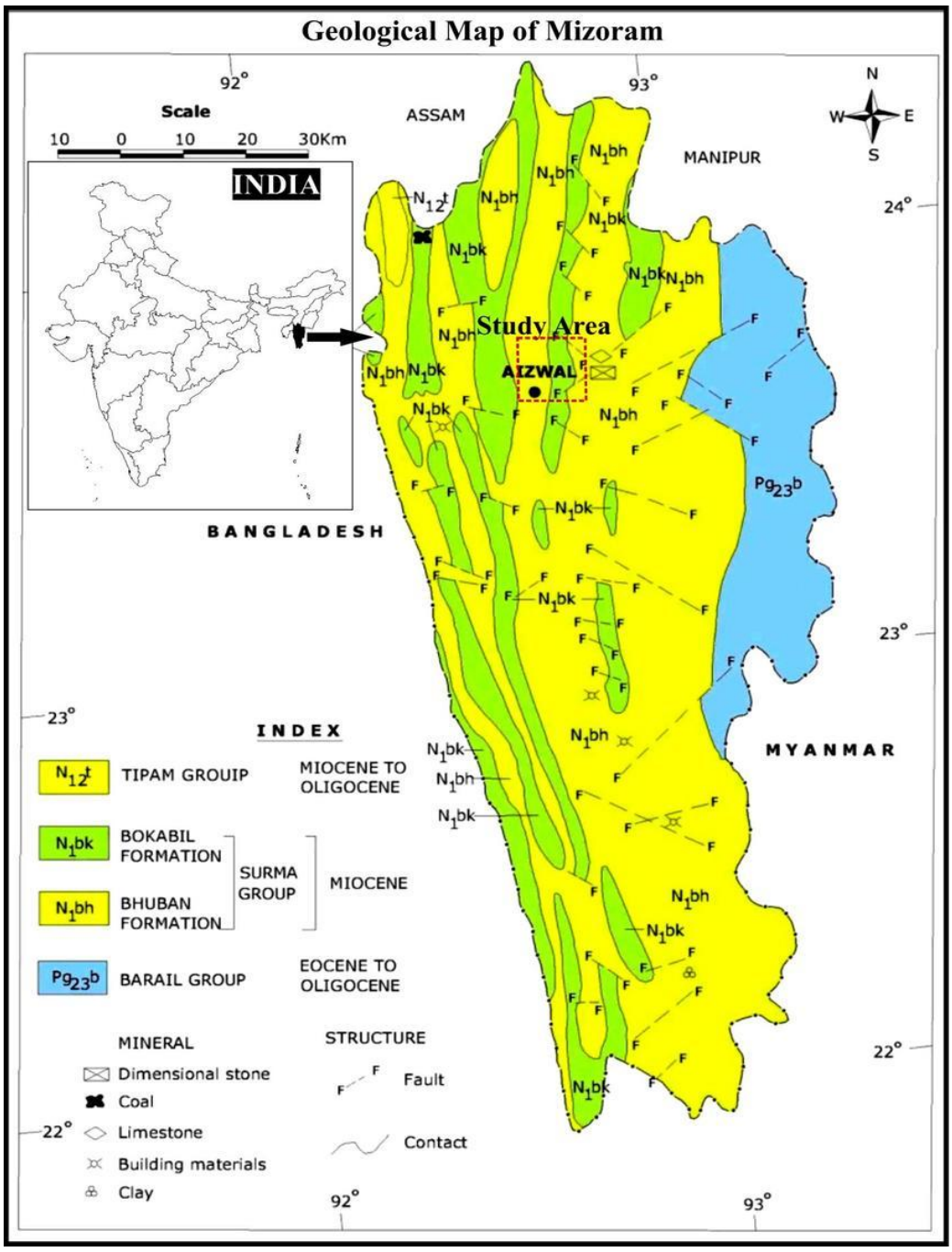

Figure:2.1.General Geological Map of Mizoram State after (Kesari, 2011)

2.3.1. Stratigraphic Succession of Mizoram

Mizoram is a part of the Surma basin and is subsequently faulted to the east. The folded sediments further continue up to Myanmar to the south (Nandy et al. 1983). Generalized stratigraphic succession worked out by Munshi (1964), Nandy *et al.* (1972,1983), Ganju (1975), and Shrivastava *et al*.(1979) is shown in table 2.2

2.3.1.1.Surma group

The major litho unit of the Surma Group is represented by Bhuban and Bokabil Formations. Based on the order of superposition, lithological characters, and physical characteristics, the Bhuban Formation Under the Surma Group is further subdivided into Lower, Middle, and Upper Bhuban Formation(Nandy et al. 1983).

i. Lower Bhuban Formation

The lower and middle Bhuban Formation is marked by the appearance of fine-grained, compact sandstone with thick siltstone/mudstone underlain by dark grey shale. The fined-grained sandstone is moderate to poorly sorted, massive with interlaminations of siltstone and shale. Turbidite features are observed in the shale. The dark shales are thinly laminated, locally splintery, micaceous, compact, and iron-stained (Ganju, 1975)

ii. Middle Bhuban Formation

This Formation comfortably overlies the Lower Bhuban Formation with gradational contact having a thickness of about 3000m. It mainly consists of argillaceous and is characterized by thinly bedded shale, siltstone, and mudstone. The shales are dark grey to greenish grey, usually splinter, and moderately hard. There is an alteration of siltstone, shales, and sandstone. Fine-grained sandstones are laminated and thinly bedded demarcating Middle Bhuban Formation. Sedimentary structures like ripple marks, lenticular and wavy bedding, cross-stratification, and worm burrows with different shapes and sizes are observed in this unit.

iii. Upper Bhuban Formation

The Upper Middle Bhuban Formation is found conformably overlain by the Upper Bhuban Formation with transitional contact. It is mainly arenaceous and is represented by sandstone beds. Thinly bedded sandstone with siltstone and shale is observed in this unit. This unit is exposed in and around the road section of Aizawl and Lunglei. Along the Rangvamual-Sairang section, the formation is found to attain its maximum thickness and is about 1200m. This unit is characterized by several sedimentary structures and traces of fossils like mega fossils, flasers, and lenticular bedding. Sandstone interbedded with shale and the presence of diagenetic nodules are observed (Bharali *et al*. 2017)

Table 2.2 Stratigraphic Succession of Mizoram(After Munshi, 1964; Nandy *et al*.1972,1983;Ganju, 1975; Shrivastava *et al*. 1979)

<table>
<tr><th>Age</th><th>Group</th><th colspan="3">Subgroup</th><th>Formation</th><th>Generalized Lithology</th></tr>
<tr><td>Recent</td><td>Alluvium</td><td colspan="3"></td><td></td><td>Silt,clay and gravel</td></tr>
<tr><td colspan="7">Unconformity</td></tr>
<tr><td>Early Pliocene to Late Miocene</td><td>Tipam (+900m)</td><td colspan="3"></td><td></td><td>Friable sandstone with occasional clay bands</td></tr>
<tr><td colspan="7">Conformable and transitional contact</td></tr>
<tr><td rowspan="8">Miocene

To

Upper Oligocene</td><td rowspan="8">S
U
R
M
A</td><td colspan="3">Bokabil (+950m)</td><td></td><td>Shale, siltstone and sandstone</td></tr>
<tr><td colspan="6">Conformable and transitional contact</td></tr>
<tr><td rowspan="6">B
H
U
B
A
N</td><td></td><td>Upper Bhuban (+1100)</td><td>Arenaceous predominating with sandstone,
Shale and siltstone</td></tr>
<tr><td colspan="3">Conformable and transitional contact</td></tr>
<tr><td></td><td>Middle Bhuban (+3000m)</td><td>Argillaceous predominating with shale, siltstone, shale alteration with sandstone</td></tr>
<tr><td colspan="3">Conformable and transitional contact</td></tr>
<tr><td></td><td>Lower Bhuban (+900)</td><td>Arenaceous predominating with sandstone and silty-shale</td></tr>
<tr><td colspan="6"></td></tr>
<tr><td colspan="7">Unconformity obliterated by faults</td></tr>
<tr><td>Oligocene</td><td>Barail (+3000m)</td><td colspan="3"></td><td></td><td>Shale, siltstone and sandstone</td></tr>
<tr><td colspan="7">Lower contact not seen</td></tr>
</table>

2.3.2. Structure and Tectonics of Mizoram

Structurally, the major structural trends of Mizoram coincide with regional tectonic trends. It falls in the mobile belt of Assam Arakan geosynclines and a series of plunging en-echelon synclines and anticline features are observed (Ganju, 1975). Mizoram has a slightly arcuate shape and is convex on the western side.

Structural complexity gradually increases from west to east where the fold becomes compressed on the eastern side. Tripura- Mizoram border is characterized by overturned, box, and recumbent fold. Aizawl faults are sinistral whereas NW-SE oblique faults like mat fault, Tupui, Saitual, and Sateek faults are dextral (Nandy *et al* 1983)

Tectonically Tripura-Mizoram Surma basin developed due to eastward movement during the period of Eocene where the Indian plate subducted along the Arakan Yoma suture resulting in the formation of the Indo-Burman folded Orogenic Belt (Nandy 1982). The fold belt extends into the Naga Hills and Patkai Range having NE-SW trending and also continues towards the north in Surma Valley and Manipur in the western hills. It extends with NNW-SSE trending into the Arakan Hill of Myanmar (Ganguly, 1975). There is a development of a narrow molasses basin of Tipam marking the west side of the orogen. In the southern part of the Shillong plateau, a bell-shaped Surma basin is exposed sloping towards the Southwest(Sarkar *et al*.1977).

2.4. LOCATION AND GEOLOGY OF THE STUDY AREA

Mizoram, located in northeastern India, is a state known for its scenic landscapes and rich cultural heritage. Its capital city, Aizawl, is situated in the central northern part of the state. Aizawl falls within the geographical coordinates of toposheets 84A/09, 84A/10, and 84A/13, spanning latitudes from 23°39'N to 23°50'N and longitudes from 92°03'39"E to 92°04'47"E.

Within Aizawl, the locality of Zuangtui is situated in ward no. 1 of the Aizawl Municipal Corporation (AMC) area. Zuangtui's coordinates range between approximately 23°44'54.54"N to 23°44'53.16"N latitude and 92°04'14.82"E to

92°04'18.6"E longitude, with an elevation of approximately 965 meters above sea level. This area falls under the top sheet 84A/9 in terms of geographical mapping.

The study area is approximately 30 kilometers away from Lengpui Airport, located in the western part of Aizawl. Lengpui Airport serves as a vital air hub connecting Aizawl to major cities like Kolkata, Guwahati, and Imphal. Additionally, Aizawl is accessible by National Highway 54 (NH-54), which connects it to Assam and other states of India.

For railway connectivity, the nearest train route is to Bairabi in the Kolasib district of Mizoram, which is approximately a 3-hour journey from the study area. This railway link provides important connectivity to Mizoram's neighboring states and facilitates the transportation of goods and passengers to and from Aizawl and surrounding regions.

The study area is situated within the geological context of the Upper Bhuban Formation, which is part of the Surma Group and belongs to the Miocene-Oligocene age. This formation is characterized by the intercalation of sandstone and shale layers, with a notable dip of approximately 40°E observed in the southern part of the area (as reported by the Geological Survey of India in 1974 and 2011).

In terms of surface features, the Upper Bhuban Formation is overlain by thick loose soil, which is a common characteristic observed in this geological setting. Rock exposures within the study area, particularly along the nullah (stream) of the Zuangtui-Thuampui border and along road sections, predominantly exhibit shale formations with a high clay content. The shale formations observed in the study area are indicative of sedimentary deposits that were likely formed in relatively calm aquatic environments.

The lithology observed in the study area exhibits a notable variation in the proportion of sand and clay. This variation in lithological composition reflects different sedimentary conditions and depositional environments that have influenced the geological characteristics of the region. Sand and clay proportions within the observed lithology indicate varying levels of grain size distribution, with sand

representing coarser particles and clay representing finer particles. The presence of shale formations with high clay content is significant, especially in sliding areas, where the cohesive and plastic nature of clay-rich shale plays a critical role in slope stability and landslide susceptibility. Rosette diagram and stereonet projection for the study area are given in Figure 2.1 to Figure 2.6 .

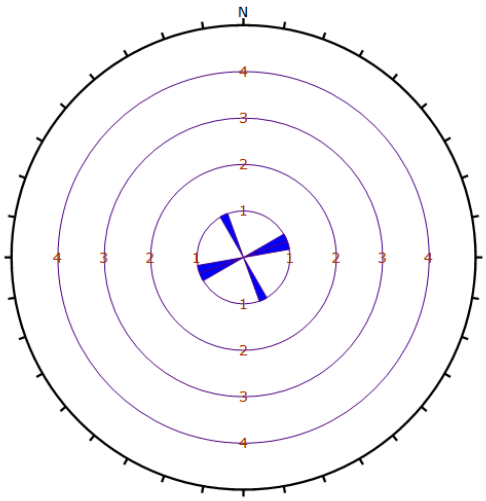

Plot Mode	Rosette
Plot Data	Apparent Strike
Face Normal Trend	0.0
Face Normal Plunge	90.0
Bin Size	10°
Outer Circle	5 planes per arc
Planes Plotted	3
Minimum Angle To Plot	45.0°
Maximum Angle To Plot	90.0°

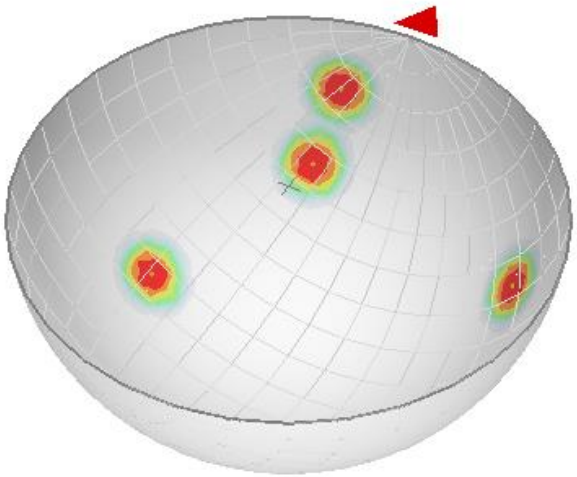

Figure.2.2. Rosette diagram and stereonet for spot 1

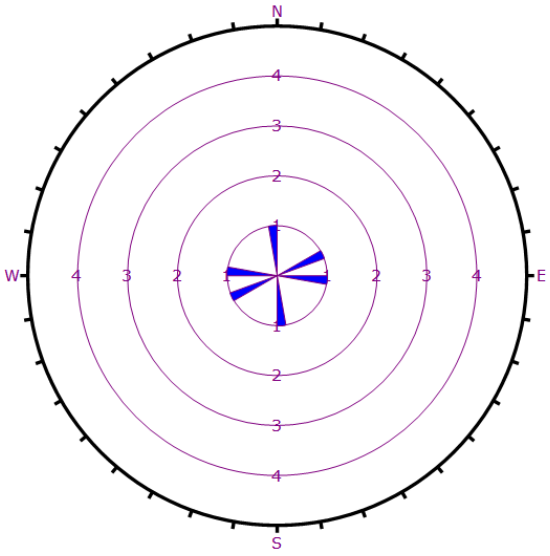

Plot Mode	Rosette
Plot Data	Apparent Strike
Face Normal Trend	0.0
Face Normal Plunge	90.0
Bin Size	10°
Outer Circle	5 planes per arc
Planes Plotted	3
Minimum Angle To Plot	45.0°
Maximum Angle To Plot	90.0°

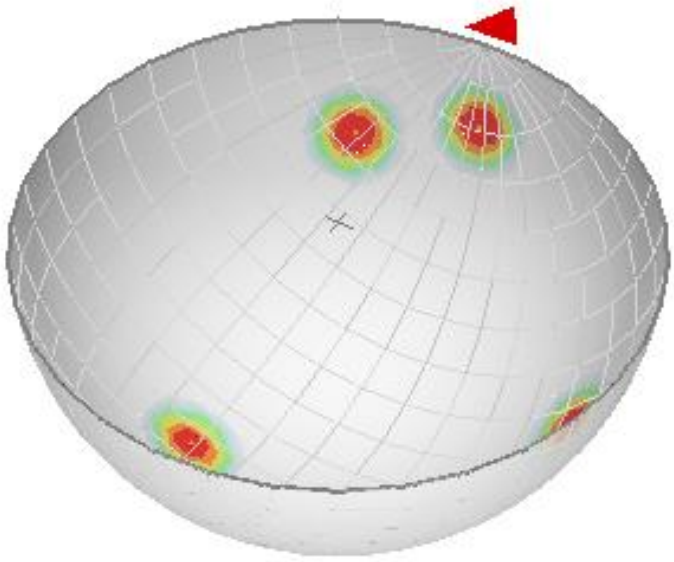

Figure.2.3. Rosette diagram and stereonet for spot 2

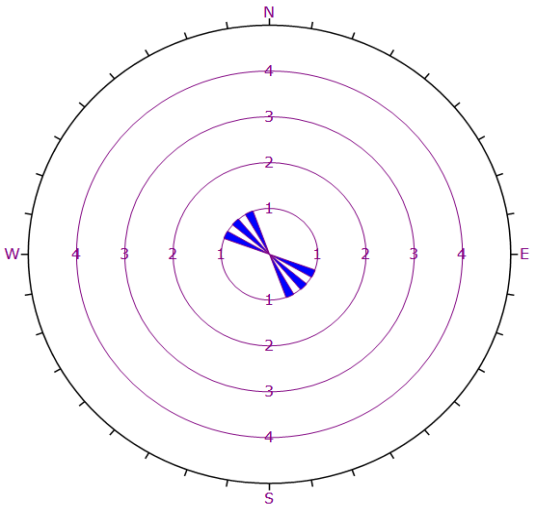

Plot Mode	Rosette
Plot Data	Apparent Strike
Face Normal Trend	0.0
Face Normal Plunge	90.0
Bin Size	10°
Outer Circle	5 planes per arc
Planes Plotted	3
Minimum Angle To Plot	45.0°
Maximum Angle To Plot	90.0°

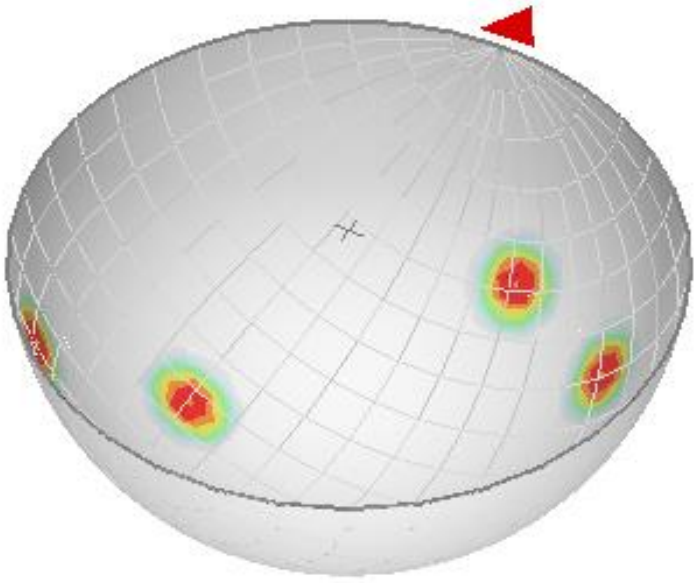

Figure.2.4. Rosette diagram and stereonet for spot 3

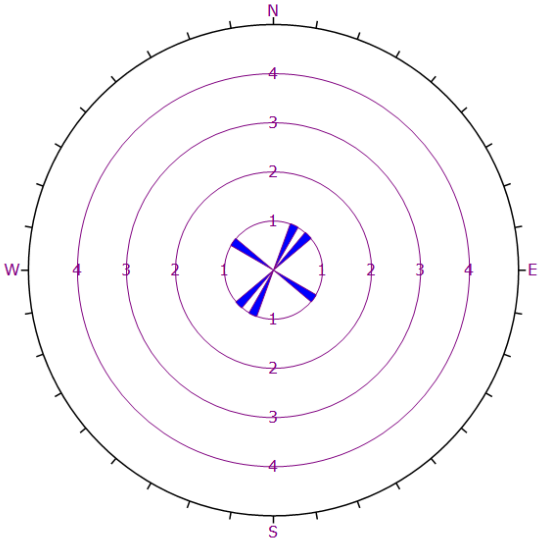

Plot Mode	Rosette
Plot Data	Apparent Strike
Face Normal Trend	0.0
Face Normal Plunge	90.0
Bin Size	10°
Outer Circle	5 planes per arc
Planes Plotted	3
Minimum Angle To Plot	45.0°
Maximum Angle To Plot	90.0°

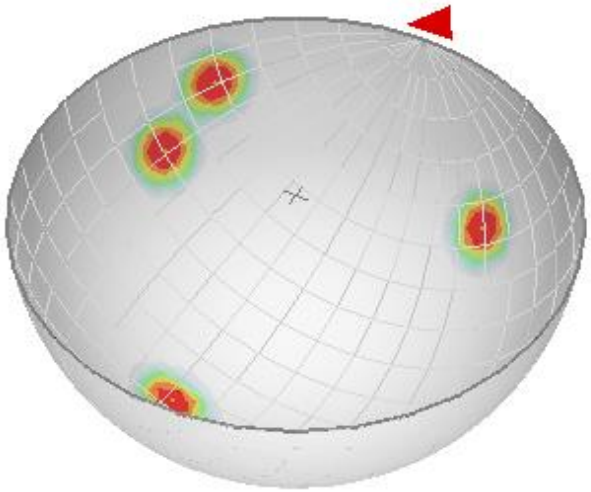

Figure.2.5. Rosette diagram and stereonet for spot 4

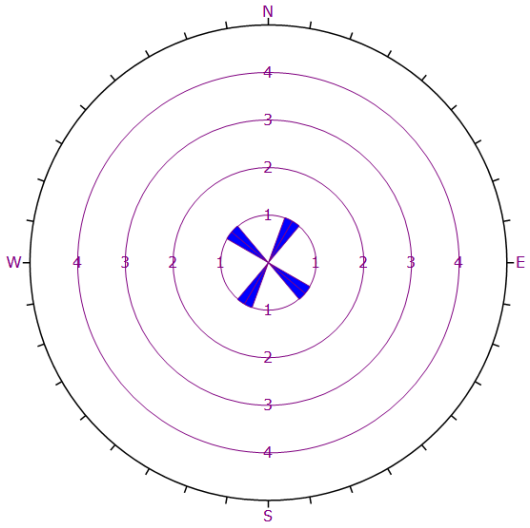

Plot Mode	Rosette
Plot Data	Apparent Strike
Face Normal Trend	0.0
Face Normal Plunge	90.0
Bin Size	10°
Outer Circle	5 planes per arc
Planes Plotted	4
Minimum Angle To Plot	45.0°
Maximum Angle To Plot	90.0°

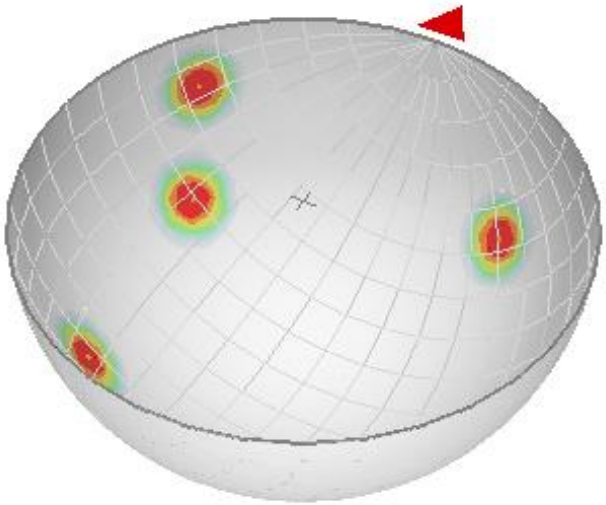

Figure.2.6. Rosette diagram and stereonet for spot 5

CHAPTER 3

LITERATURE REVIEW

In the current study, a comprehensive literature review was undertaken as an integral component of the project. Aligned with the specific goals and objectives of the research, this literature survey focused on relevant topics, drawing from a wide array of journals at both national and international levels.

Geotechnical investigation, geophysical survey, and monitoring are widely done all over the world by many geologists and engineers using different techniques and tools. In the proposed research work, different literature, both international and national which are relevant to the aim and objectives are referred. Among the many obtained kinds of literature, only some review of literature is given below.

Kabeta et al. (2023) used both geotechnical and geophysical methods in investigating the landslide area at Chira town in Ethiopia. The result obtained from the study provided important information in planning, reduction of disaster, and infrastructure design

Christopher W.A.P.P.*et al.* (2023) studied the subsurface conditions of landslide in Badulusirigama, Badulla, Sri Lanka using the resistivity method. A resistivity survey was done using the Schlumberger configuration. The data they obtained reveal that there is a decrease in resistivity three layers with clay layers sandwiched between two layers were obtained and bedrock is not encountered.

Al-Taie, A. J. (2023) The study evaluates the deterioration properties and durability of the rock samples collected from the Rutba-Jezira Zone in the Western part of Iraq. Slake durability test, absorption test, and specific gravity test were performed and the results show a variation in durability and deterioration of the rock in the study area. The study concludes that the variation is due to the presence of secondary constituents which result in rapid deterioration upon alternate drying and wetting.

Kamal, A. M., *et al*.(2022) used the geological and engineering properties of soil to determine the factor responsible for causing shallow landslides in the Kutupalong Rohingya Camp in Cox's Bazar. Bangladesh. The possible extend of landslide is also determined. The study was performed aiming to investigate the effects of engineering properties of soil along with the mineral and chemical composition of the slope in triggering the slope failure. Their results show the weak engineering properties of the soil are highly responsible for the failure of the slope.

Lalhlimpuia *et al*. (2022) conducted a study along five selected sites at Ngaizel road cutting in Mizoram to assess the geo-mechanical conditions of the slope mass using Rock Mass Rating (RMR) and identify hazard-prone areas using the Rockfall Hazard Rating System (RHRS). The findings revealed that the study sites exhibit bad-quality rock mass with an 80% to 90% probability of rockfall occurrence. Calculated scores indicate that all locations fall under the category of High Urgency and are highly prone to rockfall failures, emphasizing the urgent need for risk mitigation measures and slope stabilization interventions in the area. Chen Q.*et al*..

Prodan, M. V.*et al*. (2022) Conducted a laboratory test for siltstone collected from Istria Peninsula, Croatia. For the determination of physical properties, uniaxial compressive strength, mineralogical properties, residual shear strength, and durability of siltstone, they performed different weathering grade tests. They used the fragments of rocks that remained after 5 cycles of the slake durability test to determine the durability. The result revealed that landslides can be triggered by the increase in the weathering process which reduces residual shear strength, durability, and uniaxial compressive strength.

Araujo, J.R.*et al*.(2022) conducted a study on landslides in Portugal taking rainfall as one of the most important parameters. They correlate extreme rainfall and landslide events over Portugal's mainland to predict the future extreme rainfall area. The study greatly helps in conducting preventive measures to reduce the disaster due to rainfall.

Tamrakar, N. K. *et al* (2021), a slake durability test performed for mudrocks in the Siwaliks of Nepal to identify the factors responsible for the erosion and

instability of the slope. Samples were collected and four cycles of slake durability test were conducted. The study reveals that mudrocks with calcareous binding materials are more durable than mudrocks with non-calcareous binding materials and also mudrocks are usually prone to sliding.

Salamov A. M. *et al.* (2021) studied the coastal zone of Takhtakorpu reservoir which is a landslide-prone area and is located in the Southern part of the Great Caucasus Mountain in Azerbaijan. A resistivity survey was done using the vertical electrical sounding (VES) method. The survey revealed that the study area is subjected to dislocations because of the active geodynamic process and also the steepness of the slope and waterlogged problems are the main triggering factors.

Lalitha, M., *et al*. (2021*)* studied landslides in the Western Ghats. He selected 5 major landslide areas for geotechnical investigations. They conclude that the mechanical properties of the soil and pedogenesis of the weathered soil profile are the main triggering factors for various landslides.

Wang, J.Q.,(2021) performed the triaxial automated test to investigate how prior cyclic loading effects consolidated undrained triaxial compression. They found out that the strength of the soil in the sliding zone is greatly affected by prior loading. Under different confining pressures, cycle periods, and a number of cycles, the samples exhibit the characteristics of strain-hardening. They revealed that the failure stress ratio decreases with an increase in the period of cycle and confining pressure

Zieher, T., et al.(2021) studied a deep-seated slow-moving landslide using a total station in the mountainous region of Australia. The study provided the rate of motion and direction of landslides in the study area.

Bahammou, Y, A., et al.(2021) carried out a resistivity survey using the Vertical Electrical Sounding method in the Zaouia Jdida area to delineate the probability of exploring aquifers. The results show the presence of groundwater with fault and fracture zones.

Jianjun, G., et al.(2020) studied a landslide in the eastern part of China using geophysical methods like electrical methods. The subsurface lithology of the landslide was determined in this study

Hernando, P., (2020) compared stable areas and landslides in Bhat Thailand using geotechnical and geological conditions and prepared a landslide susceptibility map. He verified that stable area has low susceptibility to landslides with higher strength of soil and rock.

Misbahudin, M,. (2020) analyzed the landslide susceptibility area in Kabandungan taking five parameters that are slope, aspect, rainfall, lithology, and distance from the road. A Geographical Information System (GIS) was used for mapping landslide susceptibility areas. He concluded that rainfall, deforestation, human activities, and an increase in urbanization as the main triggering factors of landslides in the study area.

Alam, K., *et* al. (2020) evaluated the quality of the reservoir of Barail sandstone. The evaluation is done based on the petrographic and petrophysical characteristics of Barail sandstone. They classified the rock as sub-arkose to sub-litharenite and are moderately mature rock types. The presence of an iron oxide border around quartz indicates the deposition of Barail sandstone under dry conditions.

Amaral, P., *et a*l. (2019) carried out monitoring of ground movement in Fajãzinha Parish, on Flores Island using a total station instrument. Movement of about 57mm,16mm, and 27mm in E, N, and Z components was observed.

Laldinpuia(2019) carried out geotechnical studies and monitoring of landslides at Ramhlun Sports Complex. He monitored the rate of ground movement using the total station. He studied the mechanical properties of the soil and concluded that the area was not suitable for settlement

Rusydy, I. *et al.* (2019) conducted rock mass classification and kinematic analysis along the United States Agency for International Development highway in Indonesia aiming to examine the quality of rock mass and possible rock failure. From

the slope kinematic analysis, wedge failure and toppling failure are possible in the study area. RMR ratings revealed that the area falls under Fair to Good rock and ranges from 57 to 64 in RMR.

Alkhamaiseh T. *et al*. (2018) performed a geotechnical, geological, and geophysical investigation in a landslide-prone area. coring was done for the determination of lithology and a geophysical survey was carried out to study the hydrogeological condition of subsurface materials. They revealed that all the result of the investigation shows fairly weak and loose materials below the bedrock that trigger planar failure.

Froude & Perley (2018) did slope stability analysis using the limit equilibrium method (LEM) on a hill slope of Iasi City. The variation in water table location was taken into consideration. The main objective is the calculation of the factor of safety and probability of slope failure. They concluded that for hillslope, the pseudo-static case is critical.

Deshpande *et al*. (2018) carried out geophysical surveys using vertical electrical sounding to investigate the subsurface fracture zone in Ganori village of Aurangabad district to identify the presence of groundwater. Four layers with 50 ohm-m to 105 ohm-m were observed in the study area.

Laldinpuia *(2018)* using the limit equilibrium method, performed slope stability analysis to determine the factor of safety in Rangvamual landslide along Aizawl airport. He used Slide 6.0 software, which is based on the Mohr-Coulomb criterion after various methods, such as the Ordinary/Fellenius method, Bishop simplified method, Janbu simplified method, Spencer method, US Corps of Engineer method, GLE/Morgenstern Price method, respectively. He designed and suggested mitigation measures on his findings.

Khan, M, A., *et al.* (2017), performed a cycle of wetting and drying of shales and clay to study the change in their strength. They found out that the angle of internal friction and cohesion value of soil decreases because of the wetting and drying cycle.

Senthikumar, V., *et al* (2017) carried out a geotechnical investigation and analysis of slope stability in the Marappalam location of the Nilgiris district. The study revealed that a landslide had occurred in the study area due to heavy rainfall that saturated the soil in the study area.

Laldintluanga *et al.* (2016) A study was conducted to map landslide zonation along the state highway between Aizawl and Aibawk town, employing five thematic layers to assess factors contributing to landslides. The study yielded a landslide zonation map categorized into five classes: very high, high, moderate, low, and very low susceptibility. Additionally, a comprehensive landslide inventory was conducted to document existing landslide occurrences along the highway. Based on the findings, mitigation measures were recommended to address the identified landslide hazards and improve road safety and stability in the area. This study provides valuable insights for land use planning, infrastructure development, and disaster risk reduction efforts along the highway corridor

Chitra and Gupta (2016) carried out a geotechnical investigation and slope stability analysis in the Pomendi landslide due to slope cutting. From the study, he reveals that the sections were unsafe and liable to slope failure during monsoon due to slope modification. Also, he identified that most of the slope failures in the study area are human-induced along with the slope and bed relationship.

Pal, R. *et al* (2016) studied ground movement in Darjeeling, Himalaya in a hilly area of the basin, and flood that occurs in the plain portion of the basin in the district of Jalpaiguri. They observed that the occurrence of a landslide after floods is due to the steep topographic slope. Torrential rainfall, deforestation, weak geology, and torrential rainfall are the main cause of landslides that brings severe destruction to the basin. construction. The record of the consequences of these two disasters brings into focus the severe impact caused on the basin dynamics

Siddique, T. e*t al*. (2015) slope mass rating (SMR) and kinematic analysis were carried out along the slopes of NH-58 in Himalayan terrain which have an important role in socio-economic development for the people. The study area falls under the stable class in slope mass rating (SMR) and is under a range between low

to moderate vulnerability to the landslide based on landslide susceptibility score (LSS)

Laldinpuia (2013) investigated Saiha slumping area. He carried out a geological and geotechnical investigation and explained the structure of the slump area and the nature of transverse cracks. Suggestions and mitigation measures were given from his findings.

Siddiqui's (2012) correlation was carried out between the geotechnical properties of soil and the electrical resistivity of subsurface lithology. From the investigation, a weak correlation was observed between the unit weight of soil and cohesion value.

Yalcin, A.,(2011) studied a large landslide area Trabzon province region. He compared the geotechnical properties of the soil in landslide areas and stable areas. He observed that with an increase in the moisture content, the shear strength decreases.

Kumar and Sanoujam(2007), used kinematics and slope stability analysis to understand the causes of slope failure in NH-39 Assam- Manipur to Myanmar. Kinematic analysis revealed that wedge failure is high for slope instability

Stark T.D. *et al* . (2005) provide a recommendation about the magnitude and type of shear strength parameters to be used for the analysis of landslides. They present that with an increase in soil plasticity, the healing magnitude increases and this could affect the time, cost, and remediation of landslides.

Singh, T.N. *et al* (2005) a study was carried out to asses and understand the behavior and the kinematics of rock in Batseri Village of Sangla Valley where a rock fall occurred on 21st July 2021. The rotational motion of the rock was observed with three prominent sets of joints. From the analysis, they revealed that the joints are weakened especially during the monsoon season. The protective measures were designed from the result of the analysis of kinematic energy and the height or jump of the rock displaced.

Tsiambaos and Sabatakakis (2004) conducted a study that evaluated the feasibility of using point load testing as an alternative to triaxial testing for assessing the strength characteristics of sedimentary rocks. Several laboratory experiments were conducted to investigate the effectiveness of point load testing when triaxial tests were not available. Through these tests, the study aimed to establish the competence and reliability of point load testing as a practical and accessible method for determining rock strength properties in situations where conducting triaxial tests may not be feasible or practical. The results obtained from these laboratory investigations provided valuable insights into the suitability and accuracy of point load testing in assessing the strength and durability of sedimentary rocks, offering a viable alternative approach for geotechnical analysis and rock mechanics studies

Parkash, S., *et al*. (2003) conducted a study to assess slope stability along SH-53 using Slope Mass Rating (SMR) and kinematic analysis techniques at eight selected sites. The analysis revealed planar-type failures at these sites, indicating potential instability. Based on rock classification, most sites were categorized as unstable rock slopes. These findings highlight the need for proactive slope management and engineering interventions to mitigate risks and ensure the safety of the transportation infrastructure along SH-53. The use of SMR and kinematic analysis provided valuable insights for informed decision-making and slope stabilization efforts.

Schepers, R., *et al.* (2001) subsurface lithology was determined using a different geophysical method like geophysical well logs data. Also, the subsurface rock strength and weak zone of the study area were determined using borehole data.

Duncan, J, M., (1996) explained the LEM of slope stability, strength, and deformation properties of soil and the FEM of soil-structure interaction. He illustrated a manual calculation of soil slope stability analysis.

CHAPTER 4

METHODOLOGY

4.1: ATTERBERG LIMIT TEST

The Attreberg limit test is performed according to IS: 2720 (Part 5). It is used in the determination of the moisture content of the soil at which clay and silt soil transit in different phases. It is used for finding the plastic limit(PL), liquid limit(LL), and shrinkage limit(SL) of the soil sample.

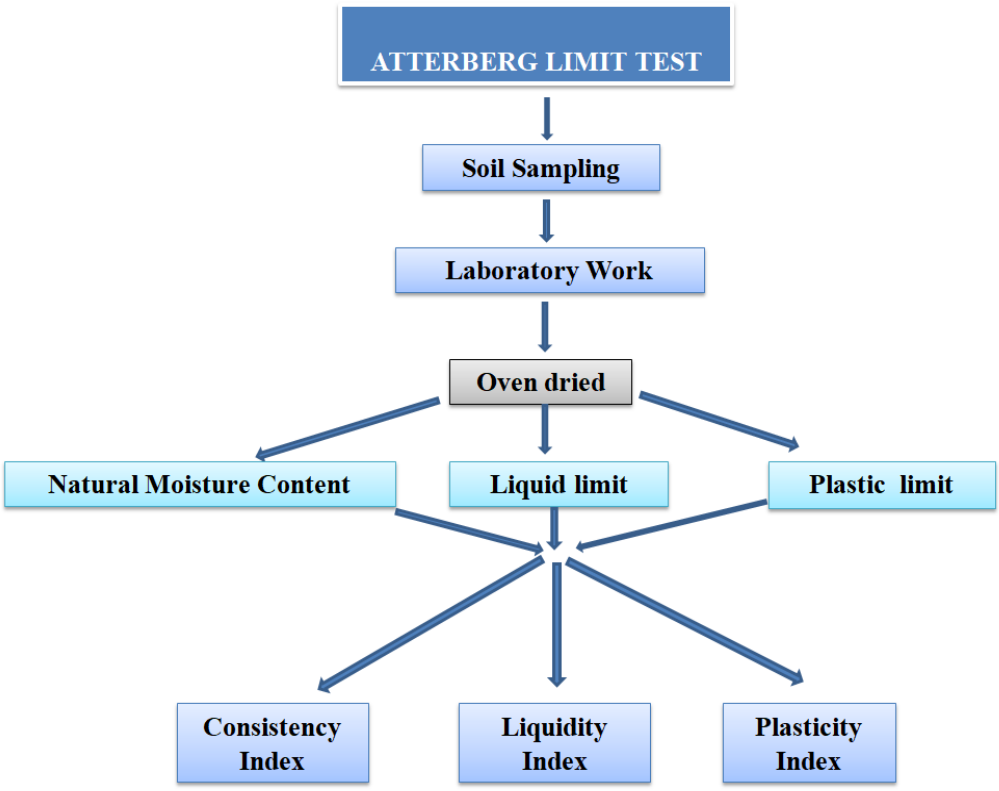

Figure 4.1. Atterberg limit methods flowchart

4.1.1 Soil Sampling

Undisturbed soil samples were collected at a depth of 5ft (Figure 4.2) using a core sampler and placed in a sample bag so that there was no loss in the moisture content.

Figure 4.2. Soil sample pit

4.1.2 Determination of Natural Water Content of Soil (Oven-drying method)

The natural water content of the soil is determined by the amount of water present in the soil expressed as a percentage of the oven dry weight.

The weight of the container (W_1) is taken after it is cleaned and dried. The soil specimen of the required quantity is taken in the container, crumbled, and placed loosely and the weight of the container with the soil sample (W_2) is taken. It is kept in an oven for 24 hours where the temperature is maintained at (110 ± 5) ºC. Then

the new weight (W_3) of the container with the dried specimen is taken. The observed data is given in Table 4.1.

Calculation:

The water content of the representative soil specimen 'W' as a percentage can be calculated by using the formula (Equation- 1).

$$\boldsymbol{W = \frac{W_2 - W_3}{W_3 - W_1} \times 100} \quad (Equation - 4.1)$$

Where,

Percentage of water content

W_1=weight of the empty container in g

W_2=weight of the container with wet soil in g

W_3=weight of the container with dry soil in g

Table 4.1: Datasheet for natural moisture content of the soil

Container no.	*Wt. of empty container (in g)*	*Wt. of container + wet sample (in g)*	*Wt. of container + dry sample (in g)*	*Moisture Content (%)*	*Average Moisture content (%)*

4.1.3 Test for determination of Liquid Limit (Using Casagrande apparatus)

Apparatus:

- The equipment necessary for the test includes:
- Mechanical liquid limit device (Fig. 4.3): It must adhere to the standards outlined in IS:9259-1979.

- Grooving tool: It should comply with the specifications set forth in IS:9259-1979.
- Porcelain evaporating dish: Approximately 12-15 cm in diameter.
- Flat glass plate: This alternative to the porcelain evaporating dish should be 10mm thick and approximately 45 cm^2 or larger.
- Spatula: A flexible blade measuring about 20 cm long and 3 cm wide, used for mixing soil and water in the porcelain evaporating dish.Palette Knives – about 20 cm long and 3cm wide (for mixing soil and water on the flat glass plate).
- Balance- Sensitive to 0.01g.
- Oven-Thermostatically controlled with the interior of non-corroding material to maintain the temperature between 105 to 110℃
- Wash bottle or beaker- Containing distilled water
- Containers-air is tight and non-corrodible for determination of moisture content.

Figure 4.3. Casagrande Apparatus

Soil sample:

A soil sample of 120g which is passing through the sieve of 425-micron IS sieve obtained per IS: 2720 – 1983 is taken. The required amount of soil sample passing through the sieve can be obtained by rubbing the wet soil through the sieve.

Procedure:

About 120g of the soil sample passing through a 425-micron IS Sieve should be thoroughly mixed with distilled water either in the evaporating dish or on the flat glass plate until it forms a uniform paste. This paste should exhibit a consistency that necessitates 30 to 35 drops of the cup to achieve the required closure of the standard groove. In the instance of clayey soils, allow the soil paste to stand for a minimum of 24 hours to ensure even moisture distribution throughout the soil mass. Before the test, thoroughly remix the soil. A portion of the paste should be placed in the cup above the spot where the cup rests on the base, compressed down, and spread into position with as few strokes of the spatula as possible while simultaneously trimming it to a depth of one centimeter at the point of maximum thickness, returning any excess soil to the dish. The soil in the cup should then be smoothed by firm strokes of the grooving tool along the diameter through the center line of the cam follower to create a clean, sharp groove of the proper dimensions. Fit the cup and drop it by turning the crank at a rate of two revolutions per second until the two halves of the soil cake come into contact with the bottom of the groove over a distance of approximately 12mm, which should be measured with the end of the grooving tool or a ruler. Record the number of drops required to close the groove over this length. Add a little extra soil mixture to the cup, mix it with the soil already in the cup, and repeat the test. Under no circumstances should dried soil be added to the thoroughly mixed soil being tested. A representative slice of soil, approximately the width of the spatula, extending from about the edge of the soil cake at a right angle to the groove and including the portion of the groove in which the soil flowed together, should be taken in a suitable container. Express its moisture content as a percentage of the oven dry weight determined as described in IS: 2720 (Part 2)– 1973. Repeat the operations

specified above for at least three additional trials, each time adding sufficient water to the soil collected in the evaporating dish or flat glass plate to achieve a more fluid condition. Record the number of blows and determine the moisture content as before. The specimen should have a consistency such that the number of drops required to close the groove falls between 5 and 35, with the points on the flow curve evenly distributed within this range. Proceed with the test from the drier (more drops) to the wetter (fewer drops) condition of the soil, or vice versa, provided that drying is accomplished by kneading the wet soil rather than adding dry soil. A 'flow curve' shall be plotted on a semi-logarithmic graph representing water content on the arithmetic scale and the number of drops on the logarithmic scale. The flow curve is a straight line drawn as nearly as possible through the four or more plotted points. The moisture content corresponding to 25 drops as read from the curve shall be rounded off to the nearest whole number and reported as the liquid limit of the soil (Table 4.2).

Table 4.2: Datasheet for liquid limit

Container no.	*No. of revolution*	*Weight of beaker + wet sample (g)*	*Weight of beaker + dry sample (g)*	*Weight of beaker (g)*	*Moisture content (%)*

4.1.4. Determination of Plastic Limit

Apparatus:

- Porcelain evaporating dish: Approximately 12cm in diameter, or a flat glass plate: 10 mm thick and around 45cm square or larger.
- Spatula: Flexible, with a blade about 8 cm long and 2 cm wide.
- Palette Knives: Two, featuring a blade approximately 20 cm long and 3 cm wide. These are intended for use with a flat glass plate for mixing soil and water.

- Surface for rolling: A ground-glass plate measuring about 20 cm x 15 cm.
- Containers: Must be airtight for determining moisture content.
- Electronic balance: Sensitive to 0.01g for precise measurements.
- Oven: Must be thermostatically controlled with a non-corroding interior, maintaining a temperature range between 105°C and 110°C.
- Rod: Approximately 3 mm in diameter and around 10 cm long.

Soil sample:

A soil sample weighing about 20g from the thoroughly mixed portion of the material passing 425 microns IS Sieve, obtained per IS: 2720 (Part 1)– 1983 shall be taken.

Procedure:

To properly prepare the soil sample for testing, first, mix it thoroughly with distilled water until it reaches a plastic consistency suitable for molding. Clayey soils should be left to stand for 21 hours to ensure even moisture distribution. Next, shape approximately 8 grams of the plastic soil into a ball and roll it on a flat glass surface with enough pressure to form a thread of consistent diameter. Maintain a rolling rate of 80 to 90 strokes per minute, each stroke defined as one complete motion forward and back. Continue rolling until the thread reaches a 3 mm diameter. Then, knead the soil back into a uniform mass and repeat the rolling process. Alternate rolling and kneading until the thread crumbles under pressure, typically occurring at a diameter exceeding 3 mm. Consider this point as the endpoint, without attempting to manipulate the thread's diameter precisely. Collect the crumbled soil in an airtight container for further analysis of its moisture content following the method outlined in IS: 2720 (Part 2) – 1973.

Observations from the test must be diligently documented. The moisture content obtained signifies the plastic limit of the soil. To determine the plastic limit, a minimum of three portions of the soil passing through a 425-micron IS Sieve should undergo testing. The average value of these results, rounded to the nearest whole number, shall be reported as the plastic limit of the soil (refer to Table 4.3)

Table 4.3: Datasheet for plastic limit

Container no.	*Weight of empty beaker (g)*	*Weight of empty beaker + wet sample (g)*	*Weight of empty beaker + dry sample (g)*	*Moisture content (%)*	*Plastic limit (Wp)*

4.1.5. Determination of Plasticity Index

The Plasticity Index is calculated as the difference between its liquid limit and plastic limit:

$$Plasticity\ Index\ (I_p) = Liquid\ Limit\ (w_L) - Plastic\ Limit\ (w_p) \quad (Equation4.\ 2)$$

The difference calculated shall be reported as the plasticity Index, except under the following conditions:

a) In the case of sandy soils plastic limit should be determined first. When the plastic limit cannot be determined, the plasticity index should be reported as N_p (non-plastic).
b) When the plastic limit is equal to or greater than the liquid limit, the plasticity index shall be reported as zero. The plasticity index can also be known approximately from equation 2 (Nagaraj and Jayadeva, 1983).

$$I_p = 0.74\ (w_L - 8) \quad (Equation4.\ 3)$$

A soil is termed ‘non-plastic’ (N.P) if it cannot be rolled into threads to determine the plastic limit or if its plasticity index is zero.

4.1.6. Liquidity Index

The liquidity index can be calculated as follows:-

$$\frac{Natural\ moisture\ content\ of\ the\ soil - Plastic\ limit\ of\ the\ soil}{Plasticity\ index\ of\ the\ soil} \quad (Equation\ 4.4)$$

4.1.7. Consistency Index

The consistency index (CI) can be calculated as follows:-

$$CI = \frac{(LL-W)}{(LL-PL)} \quad (Equation\ 4.5)$$

Where,

CI= Consistency Index

LL= Liquid Limit

W= Natural Moisture Content

PL= Plastic Limit

4.2 STANDARD PROCTOR COMPACTION TEST

The Standard Proctor Compaction test is performed as per IS: 2720 Part VII-1980

Apparatus

- Oven

- Seive size of 4.75mm
- Balance
- Mixer tools
- Container
- Cylindrical metal mold
- Steel straightedge
- Metal rammer

Figure 4.4: ProctorCompaction test apparatus

Procedures

A 2kg oven-dried soil sample was placed in a container. The mass of an empty mold was measured and recorded. The sample was then mixed with water and compacted in a cylindrical metal mold using 25 blows. Subsequently, the compacted sample, along with the mold, was weighed and recorded. This process was repeated

with an increase in the amount of water. Calculations were performed using the following formula:

$$\gamma_m = \frac{m_2 - m_1}{v_m} \qquad \text{(Equation 4.6)}$$

Where, Vm=Bulk density

m_1 = Mass of mould and base in gm

m_2 = Mass of mould, base and soil

v_m = Volume of mould

$$\gamma_d = \frac{100\gamma_m}{100+w} \qquad \text{(Equation 4.7)}$$

Where , Vd= Dry density

4.3 Direct Shear Test

The direct shear test is performed as per IS: 2720 (Part 13)-1986

Apparatus:

- Loading pad, base plates, shear box grid plats, water jacket, and porous stone should conform to IS: 11229-1985
- Weights are for applying normal loads if required
- Proving Ring
- Micrometer Dial Gauges-two micrometer dial gauges with one suitably mounted for measuring vertical compression and the other mounted to measure the horizontal movement of the specimen
- Spatula and straight-edge
- Loading Frame
- Stop Clock
- Balance
- Sample Trimmer or Core Cutter

Figure 4.5: Direct shear test apparatus

Preparation of specimen

- Undisturbed Specimens: The required size of the specimen is prepared as per IS: 2720 (Part 1)-1983.
- Remoulded Specimen: The soil in the shear box is tamped in the box itself. A base plate and porous stone or grid plate are placed at the bottom of the shear box.
- Moisture content is observed from the trimming obtained during cutting and the cut specimen is weighed. The bulk dry density in the shear box is determined using this information

Procedure

In a Consolidated Drained (CD) test, the prepared specimen undergoes a series of steps. Initially, the specimen is placed within the shear box alongside porous stones, and perforated grid plates are fitted into the load frame. Following this, normal stress is applied, allowing the sample to consolidate. Once consolidation is complete, the shear test is conducted at a slow rate. Subsequently, the shear box is

removed, and the sample is extracted from it. Finally, the moisture content of the sample is measured. This test procedure is repeated three times on separate specimens, each subjected to different normal stresses but with consistent density

4.4 SOIL TRIAXIAL TEST

Soil triaxial test was performed as per IS 2720(Part 12): 1993. Determination of Shear Strength Parameters Of Soil From Consolidated Undrained Triaxial Compression Test.

Apparatus

- Triaxial cell
- Triaxial control panels
- Triaxial load frames
- Load and displacement measurement
- Triaxial cell accessories

Procedure

In the laboratory, remolded samples are meticulously prepared to achieve the desired density and moisture content using both static and dynamic compaction methods. Once prepared, the specimen is positioned on the pedestal cell within the triaxial cell, ensuring central alignment. The cell is then assembled with the loading ram affixed to the top cap of the specimen, and the entire setup is placed in the loading machine. Initially, the loading ram is adjusted to bring it a short distance from the seat, with the value of the load measuring gauge duly recorded. Subsequently, further adjustments are made to the loading machine to ensure the loading ram makes contact with the seat of the specimen. The axial compression of the specimen is then recorded. To induce failure within a controlled timeframe of 5 to 10 minutes, an appropriate rate of axial compression is selected. Throughout the test, a series of readings of the load are taken to delineate the stress-strain curve. The test is continued until either the maximum stress has been surpassed or until a 20% axial strain is reached. Finally, the final reading of the load is recorded after unloading the specimen. *Calculations*

The area at any strain, $A=A_O/(1-e)$ (*Equation 4.8*)

Where, A_o = Initial area of the specimen

$1-e= (L_o - L)/ L_o$ (*Equation 4.9*)

Deviatoric stress = L/A_c (*Equation 4.10*)

Where, L=Load

A_c = corrected area

Figure.4.6. Soil Triaxial Apparatus

4.5 SLOPE STABILITY ANALYSIS USING LIMIT EQUILIBRIUM METHOD

The study area was analyzed in SLIDE 6.0, using the Bishop simplified method, GLE/Morgenstern method, Ordinary/Fellenius method, Janbu simplified method, Janbu corrected method, and Spencer method. These methods are based on several parameters such as the geometry of the slope, cohesion of the soil (c) and angle of internal firction (φ). The mode of failure is pre-assumed where the failure occurs when the driving force exceeds the resisting force. Only the equilibrium of forces is satisfied in the simplest form of limit equilibrium analysis. The sum of the forces triggering the sliding of the slope is compared with the sum of the forces resisting the failure along an assumed plan. The ratio of the resisting force and the driving force is called a factor of safety FoS, which can be given by

$$FoS = \frac{\sum \text{Resisting forces}}{\sum \text{Driving forces}} \qquad (\textit{Equation 4.11})$$

A factor of safety less than 1.0 indicates slope instability and the slope is liable to failure.

Procedure

- Side 6.0 software is used for slope stability analysis using the limit equilibrium method (LEM).
- The external boundary was made and the geometry of the study area was plotted.
- A material boundary was made and project settings were done selecting the direction of slope failure, methods to be employed, and addition of parameters was done.

- The material was defined by adding parameters like cohesion value, angle of internal friction, and dry density value. Grid was set up and computation was done.
- The file was saved and then interpretation was done giving a model showing a slip circle and factor of safety.

4.6 Slake Durability Test

Slake Durability Index

The slake durability test is to be carried out as per IS: 10050 -1981 guidelines to assess the rock resistance to disintegration under drying and wetting in a slaking fluid.

Procedures

1. Begin by selecting a sample containing 10 rock lumps, each with a weight falling within the range of 40-60 g, resulting in a total sample weight of 400-600 g. Preferably, choose rough spherical rocks with rounded corners.

2. Next, place the sample in a clean drum and subject it to a temperature of 105±5°C until it reaches constant weight. Record the weight of the drum and the sample. Once done, secure the lid onto the drum, mount it in the trough, and couple it to the motor.

3. Fill the trough with slaking fluid. Then, fill it with tap water at a temperature of 20°C up to a level 20 mm below the drum axis. Rotate the drum at a speed of 20 rev/min for 10 minutes.

4. Following the rotation, remove the drum from the trough and take off the lid. Dry both the drum and the retained portion of the sample until reaching a constant weight at 105±5°C. Record the weight of the drum plus the retained portion of the sample as weight B.

5. Repeat the test to obtain the weight of C. Record the weight of the drum plus the retained portion of the sample as weight C.

Slake durability Index (first cycle) $I_{d1} = \frac{B-D}{A-D}\ 100$ (*Equation 4.12*)

Slake Durability Index (second cycle) $I_{d2} = \frac{C-D}{A-D}100$ (*Equation 4.13*)

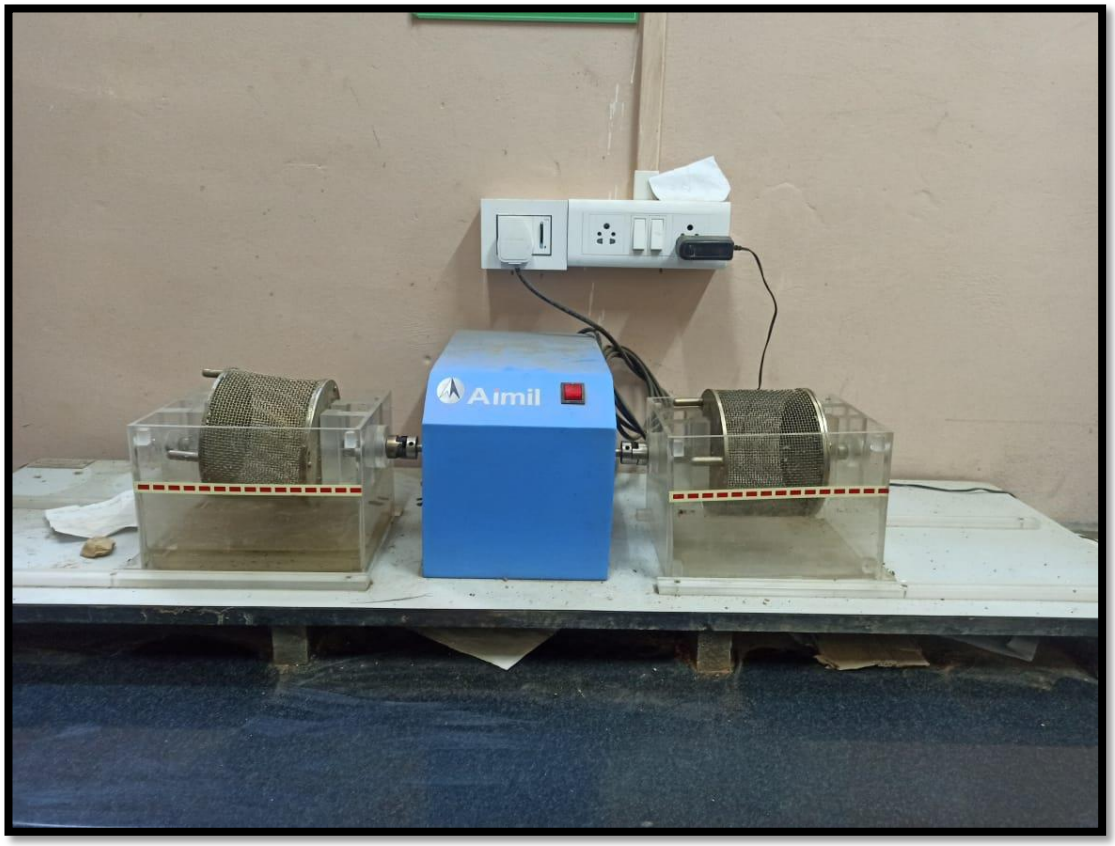

Figure.4.7. Slake Durability Test Apparatus

Table 4.4: Classification of rocks based on the Slake Durability Index (After Franklin and Chandra, 1972)

Slake-Durability I_d percentage	**Classification**
0-25	Very low
Over 25-50	Low
Over 50-75	Medium
Over 75-90	High
Over 90-95	Very high
Over 95-100	Extremely high

4.7 Point Load Strength Index Test

Block and Irregular Lump Test

The determination of rock strength using the Point Load test was conducted in the study area using the Point Load Strength Index apparatus according to IS 8764:1998. The following procedures were adhered to for the Irregular Lump test:

a) Lumps and blocks of rock samples measuring 50 + 35 mm were prepared, ensuring that the ratio between diameter (D) and width (W) fell within the range of 0.3 to 1. A ratio close to 1, or preferably equal to 1, was sought for the irregular lump test.
b) For heterogeneous and anisotropic rock samples, it was preferable to conduct tests on ten or more specimens to achieve optimal results.
c) The lump rock sample was then placed in the testing machine, ensuring contact with the platen and the sample with the smallest dimensions.
d) The mean width (W) of samples that are not parallel was calculated by

$$.W = \frac{W1+W2+W3}{3} \qquad \textit{(Equation 4.14)}$$

The load at failure 'P' is recorded after the load has been applied for 10 to 16 seconds.

The point load lump strength index is calculated by the formula

$$\boldsymbol{I_L\,(50) = P/\,(DW)^{0.75}\sqrt{D^*}} \qquad \textit{(Equation 4.15)}$$

Where,

P = Peak load in N at failure

(DW) = the minimum cross sectional area passing through point loads in mm^2.

*I*L(50) = Point load lump strength index in kgf/cm^2.

D*= Standard size of lump 50mm or 5cm .

Figure 4.8: Point Load Index Apparatus

4.8 ROCK MASS RATING (RMR) SYSTEM

The RMR, developed by Bieniawski in South Africa during 1972-1973, is a quantitative rock mass classification system or Geomechanics Classification system. Its primary purpose is to assess the stability and support requirements of tunnels (Bieniawski, 1973b). Moreover, the RMR method extends its applicability beyond tunnels, serving to evaluate the stability conditions of rock slopes and critical sections of rock masses susceptible to slope failure.

The RMR system comprises five basic parameters for the classification of a rock mass (Bieniawski 1989) and classification based on rock mass properties given in Table 2.4.

1. Uniaxial compressive strength (UCS) of intact rock material.
2. Rock quality designation (RQD)
3. Joint or discontinuity spacing
4. Joint condition/ condition of discontinuities
5. Ground water condition

Table 4.5: RMR classification based on properties of rock mass(Bieniawski, 1989)

Parameters									
1	Strength of intact rock material	PLI	>10MPa	4-10 MPa	2-4 MPa	1-2 MPa	For this low range, UCS test is preferred		
		UCS	>250MPa	100-250MPa	20-100 MPa	25-50MPa	5-25 MPa	1-2 MPa	<1 MPa
	Ratings		15	12	7	4	2	1	0
2	RQD		90%-100%	75%-90%	50%-75%	25%-50%	<25%		
	Ratings		20	17	13	8	3		
	Spacing of Discontinuities		>2	0.6-2m	200-600	60-200	<60mm		

3				mm	mm		
	Ratings	20	15	10	8	5	
4	Condition of discontinuties	Very rough surfaces not continuous no separation, unweathered wall rock	Slightly rough surfaces, seperation <1mm, slightly weathered walls	Slightly rough surfaces, seperation <1mm, highly weathered walls	Slickenside surfaces of gouge <5mm thick or seperation 1-5mm continuous	Soft gouge >2mm thick or separation >5mm continuous	
	Ratings	30	25	20	10	0	
5	Groundwater	Inflow per 10m tunnel length(1/m)	None	<10	10-25	25-125	>125
		Joint water press/major principal σ	0	<0.1	0.1-0.2	0.2-0.5	>0.5
		General conditions	Completely dry	Damp	Wet	Dripping	Flowing
	Ratings		15	10	7	4	0
	GUIDELINES FOR CLASSIFICATION OF DISCONTINUITY						
Discontinuity length(persistence)			>1	1-3m	3-10m	10-20m	>20m
Ratings			6	4	2	1	0
Seperation(aperture)			none	<0.1mm	0.1-1.0mm	1-5mm	5mm
Ratings			6	5	4	1	0
Roughness			Very Rough	Rough	SlightlyRough	Smooth	slickenside
Ratings			6	5	3	1	0
Infillings (Gouge)			None	Hard fillings >5mm	Hard fillings <5mm	Soft fillings <5mm	Soft fillings >5mm

Ratings	6	4	2	2	0
Weathering	Unweathered	Slightly weathered	Moderately weathered	Highly weathered	Decomposed
Ratings	6	5	3	1	0

Table 4.6: Classification of rock class(Bieniawski 1989)

S. No.	***Parameter/ properties of rock mass***	***RMR (Rock class)***				
		100-81 (I)	***80- 61 (II)***	***60- 41 (III)***	***40-21 (IV)***	***<20 (V)***
1	Classification of rock mass	Very good	Good	Fair	Poor	Very poor
2	Average stand-up time	20 years for a 15m span	1 year for 10m span	1 week for 5m span	10 hours for 2.5m span	30 minutes for 1m span
3	Cohesion of rock mass (MPa)	>0.4	0.3- 0.4	0.2- 0.3	0.1- 0.2	<0.1
4.	Angle of internal friction of rock mass	$>45^o$	35^o- 45^o	25^o- 35^o	15^o- 25^o	$<15^o$
5	Allowable bearing pressure (T/m^2)	600- 440	440- 280	280- 135	135- 45	45- 30
6	Safe cut slope (^{o}) (Waltham, 2002)	>70	65	55	45	<40

4.8.1 Uniaxial Compressive Strength (UCS)

The UCS of an intact rock material can be determined by the point load strength index test of rock cores and lumps (Table 4.7).

Table 4.7: UCS & Point Load Strengths relation (Bieniawski, 1979 & 1984)

Compressive strength (Mpa)	***Point load strength (Mpa)***	***Qualitative description***	***Rating***
>250	8	Extremely strong	**15**
100 to 250	4 to 8	Very strong	**12**
50 to 100	2 to 4	Strong	**7**
25 to 50	1 to 2	Medium strong	**4**
5 to 25	Use of UCS is preferred	Weak	**2**
1 to 5	-do-	Very weak	**1**
<1	-do-	Extremely weak	**0**

4.8.2 Rock Quality Designation (RQD)

Rock quality designation (RQD) is a quantitative assessment of rock quality (Deere 1964; Table 4.8). RQD can be determined by using a Volumetric Joint count (J_v) where coring cannot be taken, for clay-free rock masses $J_v$can be converted into RQD by equation 3 (Table 4.7; Palmstrom, 1982).

$$RQD = 115 - 3.3\,J_v \qquad \text{(}\textit{Equation 4.16}\text{)}$$

This equation is best applied for flat and long blocks (Palmstrom, 2005).$J_v\ is\ the$ total number of joints per cubic meter or the volumetric joint count.

Palmstrom (2005) developed a new relationship between RQD and J_v , which is for cubic-shaped blocks and gives a better correlation (Equation 4).

$$RQD = 110 - 2.5J_v \qquad (Equation\ 4.17)$$

The total number of joints within a representative unit volume of a rock mass is defined as a Volumetric joint count J_v (Palmstrom, 1982, 1985, 1986; Sen *et al*.1992) and is given in equation 5.

$$J_{v=} \sum_{i=1}^{J} \left(\frac{1}{S_i}\right) \qquad (Equation\ 4.18)$$

Where,

S_I = the average joint spacing in meters for the i^{th}joint set

J= total number of joint sets excluding random joint set

Palmstrom adopted a new equation including the spacing of the random joints and a correction of 5m for each random joint (Equation 6; Palmstrom, 2005). The volumetric joint count can be estimated by counting all discontinuities present in the area.

$$J_{v=} \sum_{i=1}^{J} \left(\frac{1}{S_i}\right) \frac{N_r}{5\sqrt{A}} \qquad (Equation\ 4.19)$$

Where, N_r = number of random joints in the area considered

A= area in m^2

S_i = the average joint spacing in meters for the i^{th}joint set

Table 4.8: RQD classification and rating (Bieniawski, 1979)

RQD (%)	***Qualitative description***	***Rating***
90 to 100	Excellent	**20**
75 to 90	Good	**17**
50 to 75	Fair	**13**
25 to 50	Poor	**8**
<25	Very poor	**3**

Table 4.9: Classification of Volumetric Joint Count (J_v)

Degree of jointing	J_v
Very low	<1
Low	1-3
Moderate	3- 10
High	10-30
Very high	30- 60
Crushed	>60

4.8.3 Joint or Discontinuity Spacing

Joint spacing or discontinuity spacing can be defined as the perpendicular distance between the adjacent discontinuities or between the joints of the same joint set (Palmstrom, 2005; Table 4.10). It is widely accepted that the spacing of joints is of great importance in appraising a rock mass structure. The very presence of joints reduces the strength of a rock mass and their spacing governs the degree of such a reduction(Bieniawski, 1973).

Table 4.10: Discontinuity spacing classification (Bieniawski, 1979)

Spacing (m)	***Description***	***Rating***
>2	Very wide	**20**
0.6- 2	Wide	**15**
0.2- 0.6	Moderate	**10**
0.06- 0.2	Close	**8**
<0.06	Very close	**5**

4.8.4 Joint or discontinuity conditions

These parameters encompass the roughness of the discontinuity surfaces, their separation length of the discontinuity and continuity of the joints, weathering of the joints surface, slickenside, and infillings or gouge (Table 4.11).

Table 4.11: Joint separation and rating (Bieniawski, 1979)

Description	***Joint separation(mm)***	***Rating***
Very rough, un-weathered, wall rock tight and discontinuous, no separation	0	**30**
Rough, slightly weathered, wall rock surface separation <1	<1	**25**
Slightly rough, moderately to highly weathered, wall rock surface separation <1mm	<1	**20**
Slickenside's wall rock surface, 1-5 mm thick gouge, or 1-5 mm wide continuous discontinuity	1 - 5	**10**
Soft gouge of >5mm thick or continuous discontinuity > 5mm	>5	**0**

4.8.5 Groundwater conditions

Table 4.12: Groundwater condition and rating (Bieniawski, 1979)

Inflow per 10 m tunnel length (L/min)	None	<10	10 - 25	25 - 125	>125
The ratio of joint water pressure to major principal stress	0	0 - 0.1	0.1 - 0.2	0.2 -0.5	>0.5
General description	Completely dry	Damp	Wet	Dripping	Flowing
Rating	**15**	**10**	**7**	**4**	**0**

4.9 KINEMATIC ANALYSIS

Kinematic analysis is the determination of the possible modes of slope failure such as planar, wedge, and toppling based on the dip amount and dip direction of the discontinuities in a stereographic projection. Rocscience software Dips 6.0 is used for the present study and provides the condition of stability and direction of possible sliding(Wyllie and Mah, 2004).

The structural data plotted shows the concentration of poles, which is very significant in identifying the planes of failure and planes that are unlikely for slope failure (Markland, 1972; Hocking, 1976).

Conditions that must be satisfied during stereographic projection in kinematic analysis in different types of slope failure such as planar failure, wedge failure, and toppling failure.

4.9.1 Planar failure

The plane on which sliding occurs must strike parallel or nearly parallel (Approximately ±20º) to the slope face, the sliding plane must be 'daylight ' in the slope face, which means that the dip of the plane must be less than the dip of the slope face. The dip of the sliding plane must be greater than the angle of a plane or

the intersection of the discontinuity with the slope must be outside the friction circle (Fig. 4.9.a).

4.9.2 Wedge failure

Wedge failure occurs when two or more discontinuities intersect. Certain geometrical conditions must be satisfied for a wedge failure to occur. On the stereonet, the line of the two great circles of the planes intersect and the orientation of the line is defined by its trend and plunge, the plunge of the line must be less than the slope angle and steeper than the average friction angle of the two slide planes. The line of intersection must dip in the direction out of the face for sliding to be feasible (Fig. 4.9.b).

4.9.3 Toppling failure

Toppling failure occurs when the discontinuity or joints are at a high angle (~ 70º) and the dip of the discontinuity must be within 10º in the direction of the face such that several slabs formed in the same trend with the face (Fig. 4.9.c).

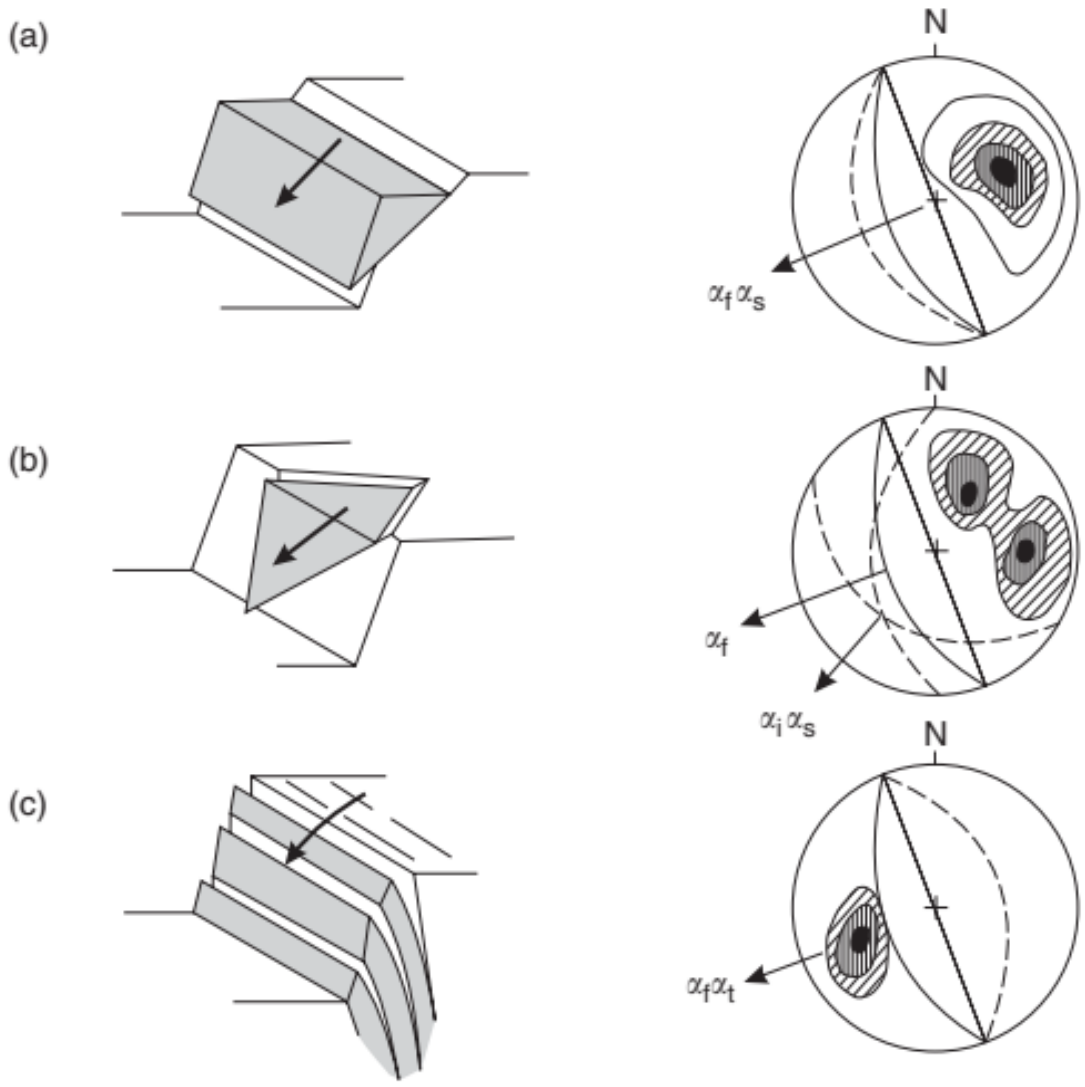

Fig 4.9: a) Planar failure, b) Wedge failure c)Toppling

4.10 ELECTRICAL RESISTIVITY SURVEY

The electrical resistivity method using the Vertical Electrical Sounding (VES) technique was used in the study area for determining the relation between the resistivity of the subsurface rock and soil and their engineering properties. Signal Stacking Resistivity Metre (SSRMT-ATS) instrument was used for the survey. Schlumberger configuration is the most suitable configuration for Vertical Electrical Sounding (VES) and gives the best resolution compared to the other configurations.

The resistivity-sounding technique can be employed to study the vertical variations in resistivity of the subsurface materials. The different subsurface layers and the corresponding resistivities are estimated. In Schlumberger configuration(Figire.4.10), the center electrodes or the potential electrodes are kept fixed and the current or outer electrodes are progressively increasing. The spacing of the potential electrodes is at least one-fifth of the spacing of the current electrodes. The depth of investigation increases with an increase in the spacings of the current electrodes. The apparent resistance values obtained with increasing electrode separations are used to estimate the thicknesses and resistivities of the subsurface formations.

In Schlumberger configuration, the four electrodes ‘A, M, N, B’ are placed on the ground in a straight line with the center point ‘O’. The current ‘I’ is supplied through the outer electrodes or current electrodes and the potential across ‘MN’ is measured.

The formula for calculation of apparent resistivity using Schlumberger Configuration is:

$$\rho_{as} = \frac{\pi(L^2 - l^2)}{2l} \Delta V/I \qquad \textit{(Equation 4.20)}$$

Where ,

ρ_{as}= Apparent resistivity

$\frac{\Pi(L^2 - l^2)}{2l}$ = configuration factor for Schlumberger array,

$\Delta V/I$= the resistance R.

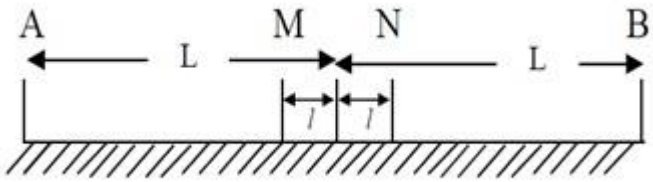

Figure 4.10: Schlumberger Configuration

4.11 GROUND MONITORING USING TOTAL STATION

The total station is an electronic theodolite integrated with an electronic distance meter (EDM) for reading distances from the instrument to a particular point. It is used for measuring angles, heights, and distances. N6 series total station is used for monitoring the ground movement in the study area

Procedure for ground monitoring

- Instrument setup- The instrument is mounted on the tripod stand and leveling is done by centering the bubbles using leveling screw and adjusting the tripod stands.
- The height of the instrument is measured and recorded in the instrument
- An occupied point is taken which is a fixed point below the instrument on the ground.
- A stable permanent point is taken as a backsight point in the stable area
- The front sight point is then taken focusing on the target/observed point in an unstable area (Figure 4.11)
- The number of the front sight points depends on the requirement and area of the monitored site.
- The coordinates and elevation of each point are recorded and are used for monitoring the ground movement

- This monitoring was done monthly in two locations of the study area(Figure 4.12)
- The data collected was plotted in Microsoft Excel in order to show the rate of ground movement

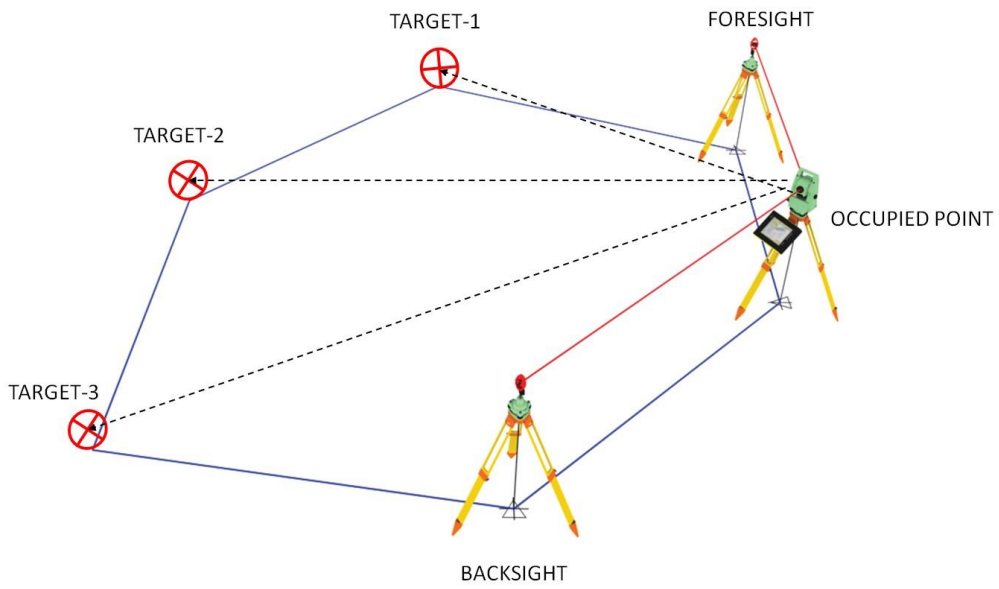

Figure 4.11: Total Station Monitoring station and reading points

Figure 4.12: Field photograph of ground movement monitoring in location-2

4.12 CORE DRILLING

A core drilling was performed at location-2 using the Diamond Core Drill TRD 80s Model. A 28m depth was reached. NX(types of core barrel) casing pipe of 3.4m and BX casing pipe of 8.20m were introduced in the borehole(Figure 4.13). The core samples were identified(Figure 4.14) and litholog was prepared in comparison with the resistivity data.

Figure 4.13: Core Drilling at Location-2

Figure 4.14: Core samples

CHAPTER 5

RESULTS AND DISCUSSION

5.1 RESULTS

5.1.1 FIELD DATA

The study area Zuangtui falls under the Survey of India toposheet 84 A/9. It is 965m above the sea level and lies between 23°44’54.54” N to 23°44’53.16” N latitudes and 92°44’14.82” E to 92°44’18.6” E longitudes.

The study area is geographically divided into two distinct locations. The first location, referred to as Location 1, is positioned on the boundary between the Zuangtui and Thuampui local councils (Figure 5.1). Location 2 is situated within the confines of the P&E (Power and Electricity) and PWD (Public Works Department) complex.

5.1.1.1 LOCATION-1 (ZUANGTUI THUAMPUI LOCAL COUNCIL BORDER)

Ground subsidence has occurred since 1987 in Zuangtui-Thuampui local council border. A road connecting Zuangtui Power Station (132KV), Industrial estate, PHE store room, Food & Civil Supply, and PWD laboratory passes through this area.

The road in the study area experiences frequent reconstruction as a result of active slope movement. A 6-foot high gabion wall and masonry wall along a road section were observed to bulge due to active ground motion (Figure 5.2) In the lower section of this affected area, a 15-foot high gabion wall (Figure 5.3) has been constructed to manage the slope, although it is currently in an unstable condition. To help control subsidence, a check dam was installed at the base of the slope. These measures reflect the efforts undertaken to mitigate the impacts of slope instability and ground movement on the road infrastructure in this location.

A ground displacement of 1ft was observed in September 2022 (Figure 5.4). The lower portion of the public steps was detached and the foundations of Assam-type pillars were displaced (Figure 5.5). Two houses were vacant and demolished due to the collapse of the retaining wall (Figure 5.6). The area is covered by loose sediments. The average slope angle is 37° with a slope aspect of N183°. An outcrop was observed on the southern portion of the study area. A soft friable Silty shale bed with a dip amount of 26° dipping towards N76° was observed in the study area.

Figure 5.1 Subsidence area of location-1(zuangtui-Thuampui local council border)

Figure 5.2. 6ft high gabion and masonry wall constructed in the upper portion of the study area

Figure 5.3. Gabion wall constructed in the road section of the middle area

Figure 5.4. 1ft ground subsidence in location 1

Figure 5.5. Collapsed of steps and building foundation

Figure 5.6. Collapsed of retaining wall

5.1.1.2 LOCATION-2 (P&E AND PWD COMPLEX ZUANGTUI)

Location 2 in the study area lies to the east of Zuangtui (Figure 5.7), with an active river flowing on its southeastern side in a northeast direction, cutting the toe of the study area. Following a significant subsidence event, an average ground displacement of approximately 1 foot was recorded in September 2022. This displacement resulted in several consequences: buildings belonging to the Power & Electricity department were vacated, and government quarters stood abandoned. Structural damage became evident across various sites. The Thuampui Presbyterian church exhibited fractures and cracks (Figure 5.8). Tensional cracks appeared along the middle section of the slope adjacent to the link road (Figure 5.9). Additionally, the masonry retaining wall, part of the Zunagtui Presbyterian church pathway, succumbed to multiple subsidence events and collapsed (Figure 5.10). The impact of the 2015 subsidence was also felt by the Zuangtui power station (132KV) (Figure 5.11), prompting its relocation by 2020. The area is covered by thin loose sediments underlain by intercalation of silty shale and clay shale.

The average slope angle is 32° towards South East. An outcrop is observed in 5 different spots. On the North Eastern side of the area, a shale bed is observed with an attitude of N175°/40° dipping towards the northeast marking a boundary between stable and unstable areas(Figure 5.12 a). In the northern part of the area, a 5ft thick shale bed of 34° dip amount, dipping towards the northeast with two prominent joint sets associated with random joints was observed (Figure 5.12 b). In the lower portion, on the southwestern side, a shale bed with an attitude of N150°/32° dipping towards the northeast which is a continuation of the outcrop observed in the northeastern side of the study area was observed (Figure 5.12 c). This bed marks the boundary between the stable and unstable areas. Another outcrop with an attitude of N135°/55° was found in the southeast along the stream within the slide area (Figure 5.12 d). All the outcrops in the northeast, northern, and southeast showed the same dip direction i.e. towards the northeast.

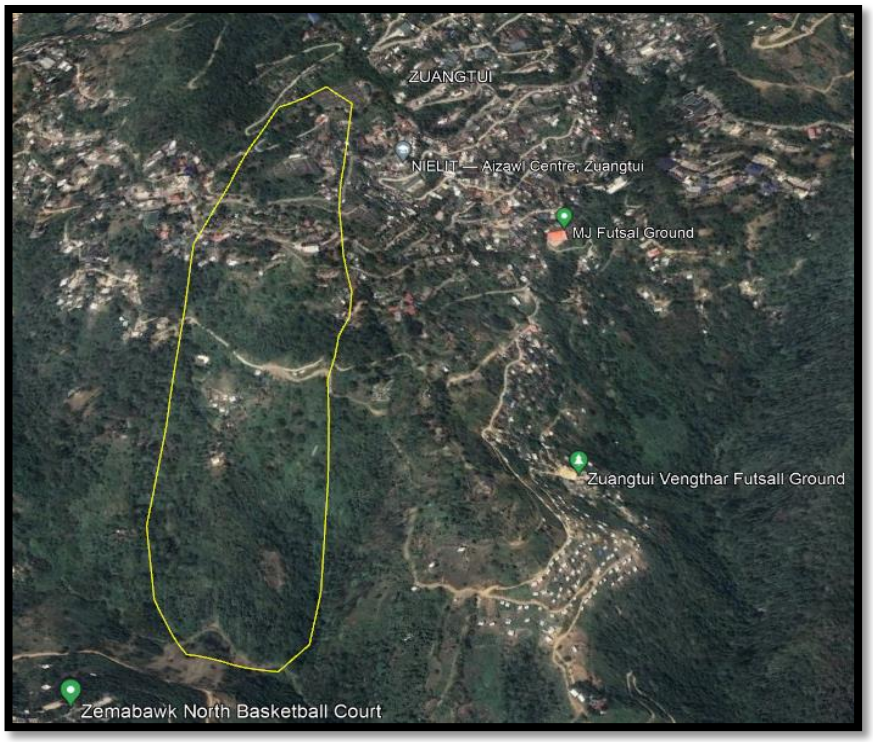

Figure 5.7 .Location 2 of the Study Area

Figure 5.8. Cracks and fractures observed on the wall of Zuangtui Presbyterian Church

Figure 5.9. Tensional cracks observed in location-2

Figure 5.10. Collapsed Masonry retaining wall near Zuangtui Presbyterian Church

Figure 5.11. Zuangtui 132KV power substation

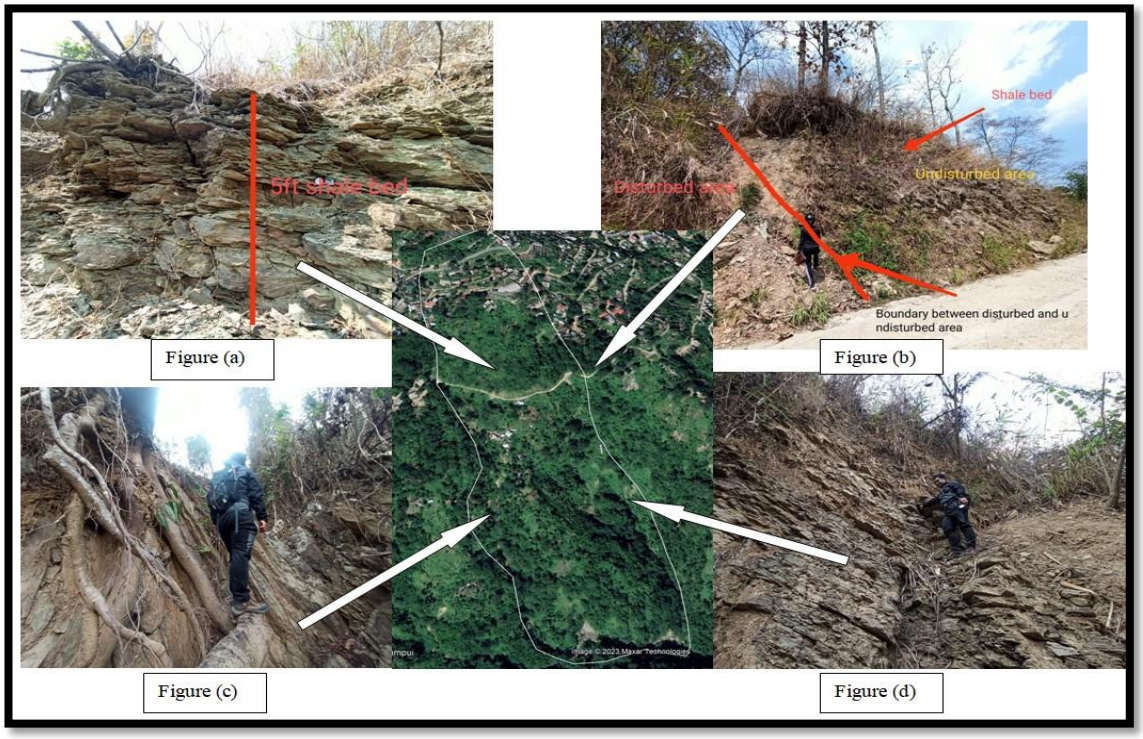

Figure 5.12. Photographs of an outcrop in Location-2

5.1.2 GEOTECHNICAL DATA OF SOIL

The geotechnical properties of the soil were studied using different geotechnical methods. Atterberg limit test where liquid limit, plastic limit, consistency index, liquidity index, plasticity index, and natural moisture content test were performed to understand the characteristics of soil when in contact with moisture. Direct shear tests and triaxial tests were performed to understand the shear strength of the soil.

Three soil samples ZS1,ZS2 & ZS3 were collected from location-1(Figure 5.13) and five soil samples ZS4,ZS5,ZS6,ZS7,& ZS8 were collected from location-2 (Figure 5.14)

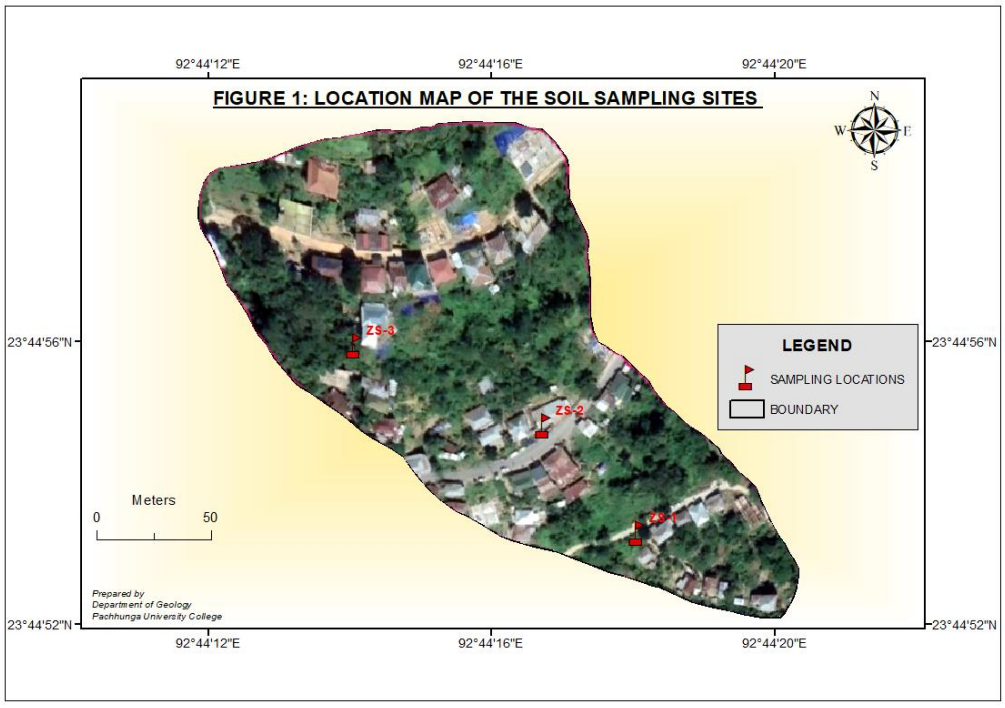

Figure 5.13. Soil sample location map for location-1

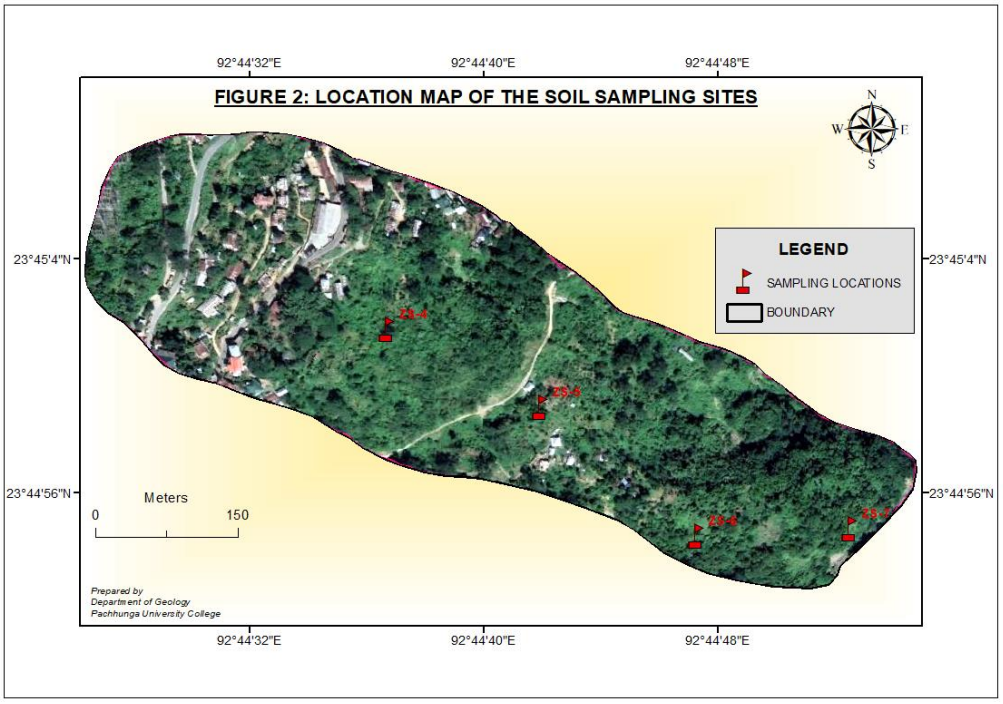

Figure 5.14. Soil sample location map for location-2

5.1.2.1 Atterberg Limit

For the Atterberg limit test, liquid limit, plastic limit, and natural moisture content were performed from which liquidity index, plasticity index, and consistency index are obtained.

5.1.2.1.1 *Natural Moisture Content*

Soil samples collected from each location were prepared for finding the natural moisture content and the results are given in Table 5.1. The natural moisture content (NMC) of soil is defined as the ratio of the weight of moisture to the weight of the solid particles in a given mass of soil. Among the soil samples tested, ZS3 exhibits the highest moisture content with an NMC of 30.23%, indicating that a significant proportion of its total weight is attributed to moisture. Conversely, ZS7 has the lowest moisture content among the samples, with an NMC value of 8.06%, signifying that it contains relatively less moisture compared to the other samples

tested. This variation in natural moisture content can influence the engineering properties and behavior of the soil, such as its compaction, strength, and susceptibility to volume changes.

Table 5.1*:* Natural moisture content of the soil for location-1 and location-2

Sample No	Beaker Wt	Beaker +Wet soil	Beaker+ dry soil	Moisture	NMC
	11.747	40.32	34.33	26.52438	
	11.18	41.56	36.24	21.22905	
ZS1	11.006	43.52	37.32	23.5616	23.77
	11.747	43.29	37.75	21.30523	
	11.18	44.32	36.67	30.01177	
ZS2	11.006	42.01	36.71	20.61936	23.97
	11.747	45.93	36.65	37.26459	
	11.18	49.26	42.21	22.71995	
ZS3	11.006	47.754	39.12	30.71068	30.23
	11.747	45.8	39.734	21.67435	
	11.18	48.396	43.283	15.92686	
ZS4	11.006	42.996	36.401	25.96968	21.19
	11.747	46.283	39.38	24.981	
	11.18	49.064	41.028	26.92308	
ZS5	11.006	48.165	42.166	19.25225	23.71
	11.747	49.04	42.01	23.22969	
	11.18	47.56	41.54	19.82872	
ZS6	11.006	52.94	45.56	21.35787	21.47
	11.00	39.04	37.01	7.8	
	10.90	37.56	35.54	8.19	
ZS7	11.51	42.94	40.56	8.19	8.06
	11.747	47.93	41.78	20.47747	
	11.18	43.6	37.62	22.61725	
ZS8	11.006	45.96	39.71	21.77397	21.622

5.1.2.1.2 *Liquid Limit*

The liquid limit test was carried out for the soil samples collected from both locations. 3 samples (ZS1, ZS2 & ZS3) were collected from location-1 and five samples (ZS4, ZS5, ZS6, ZS7 & ZS8) were collected from location-2. The results of the liquid limit are given in Table 5.2 and the liquid limit graph from Figure 5.15 to 5.22

Since the liquid limit is the minimum water content where the soil starts to behave as a liquid, the ZS4 site is observed as the lowest liquid limit having 29.17%. In contrast, ZS2 has the highest values among the eight samples, with a liquid limit having 40.95%.Three points of moisture content was taken for each sample to determine the liquid limit, these points were sufficient enough to have the best fit curve which was also recommended by the ASTM (American Society for Testing and Materials) and other standard testing procedures typically recommend using three points to determine the liquid limit and plastic limit. This methodology has been established through empirical testing and statistical analysis to provide reliable results.

Table 5.2: Results of Liquid Limit for different soil samples

Sample No.	No of blows	Wt of Container	Container + Wet Soil	Container + Dry Soil	Wt of Dry Soil	Moisture Content	Liquid Limit (%)
ZS1	34	15.571	26.222	23.208	7.637	39.466	40.22
	21	21.653	30.614	28.043	6.390	40.235	
	12	16.305	25.036	22.462	6.157	41.806	
ZS2	33	17.56	25.81	23.431	5.871	40.521	40.95
	26	18.810	26.959	24.599	5.789	40.767	
	13	15.255	23.54	21.101	5.846	41.721	
ZS3	33	11.178	18.635	16.511	5.333	39.827	40.67
	27	10.423	15.114	13.761	3.338	40.533	
	17	11.221	29.922	19.494	8.273	41.436	
ZS4	17	18.525	28.001	25.810	7.285	30.073	29.17
	29	15.225	24.919	22.758	7.533	28.687	
	9	16.249	26.583	24.085	7.836	31.879	
ZS5	40	18.112	29.835	26.904	8.792	33.337	34.82
	26	18.560	27.958	25.557	6.997	34.315	
	8	18.520	31.025	27.652	9.132	36.936	
ZS6	33	11.178	18.635	16.511	5.333	39.827	40.60
	27	10.423	15.114	13.761	3.338	40.533	
	17	11.221	22.922	19.494	8.273	41.436	
ZS7	38	16.303	27.621	24.873	8.570	32.065	33.41
	23	21.653	31.867	29.305	7.652	33.481	
	17	15.573	23.938	21.798	6.225	34.378	
ZS8	40	15.57	22.693	20.814	5.244	35.831	37.43
	27	21.653	26.003	24.822	3.169	37.267	
	11	16.303	23.916	21.787	5.484	38.822	

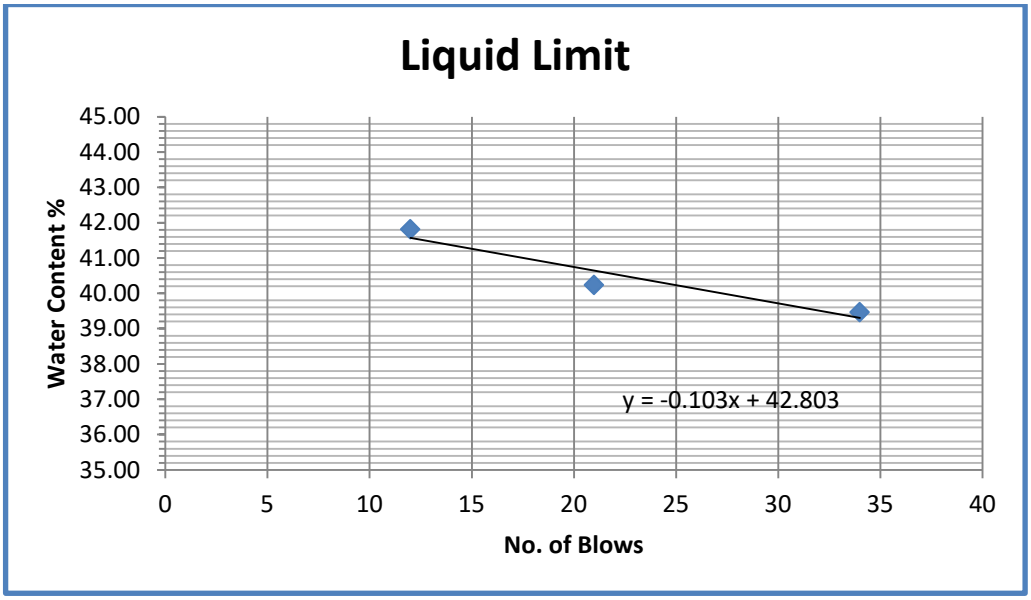

Figure 5.15. Graph of liquid Limit test for ZS1

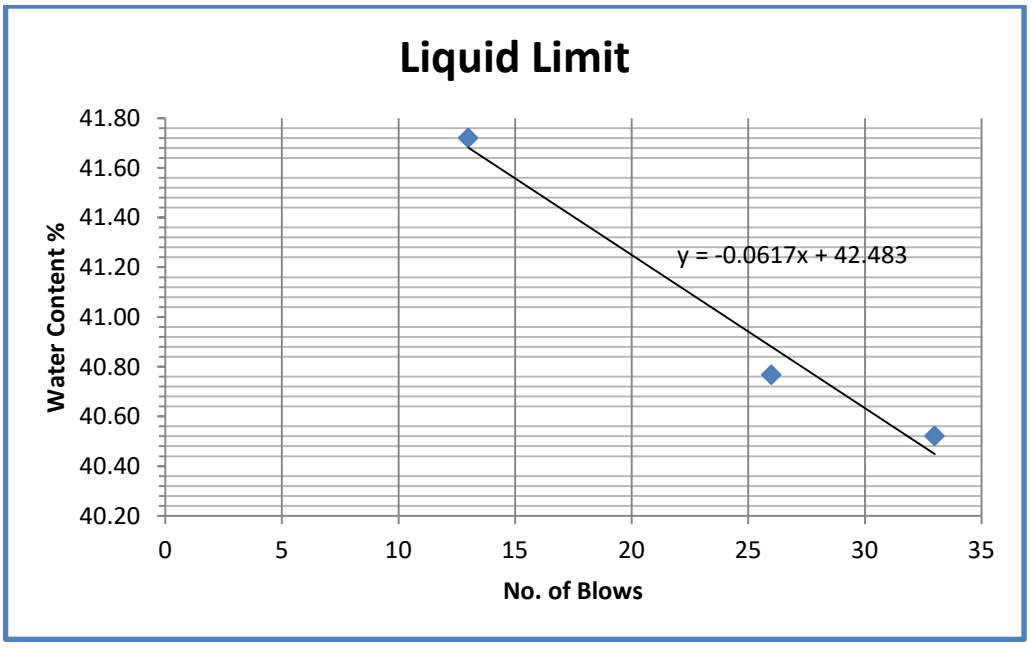

Figure 5.16. Graph of liquid Limit test for ZS2

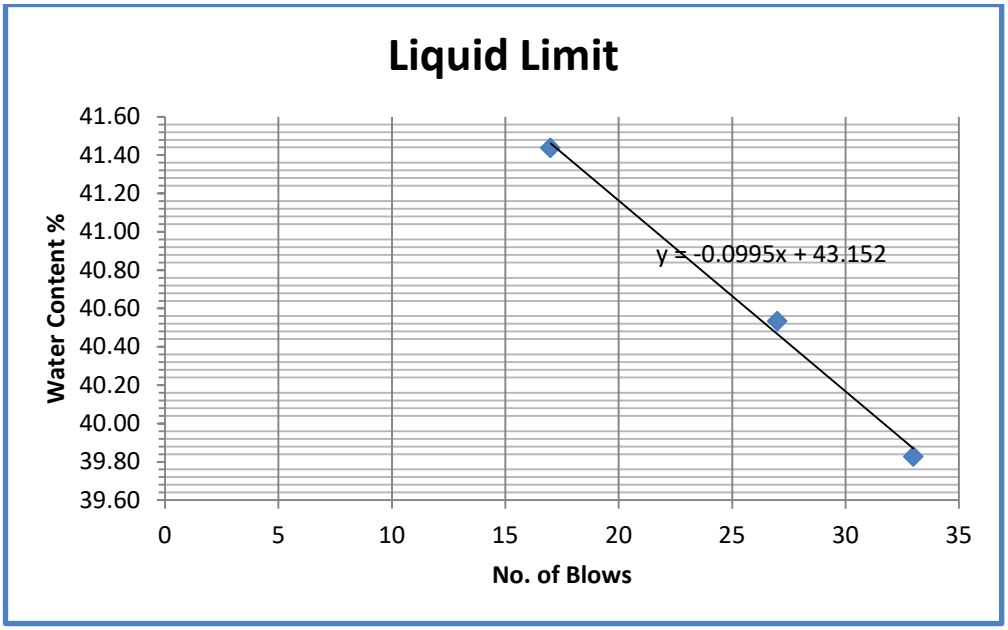

Figure 5.17. Graph of liquid Limit test for ZS3

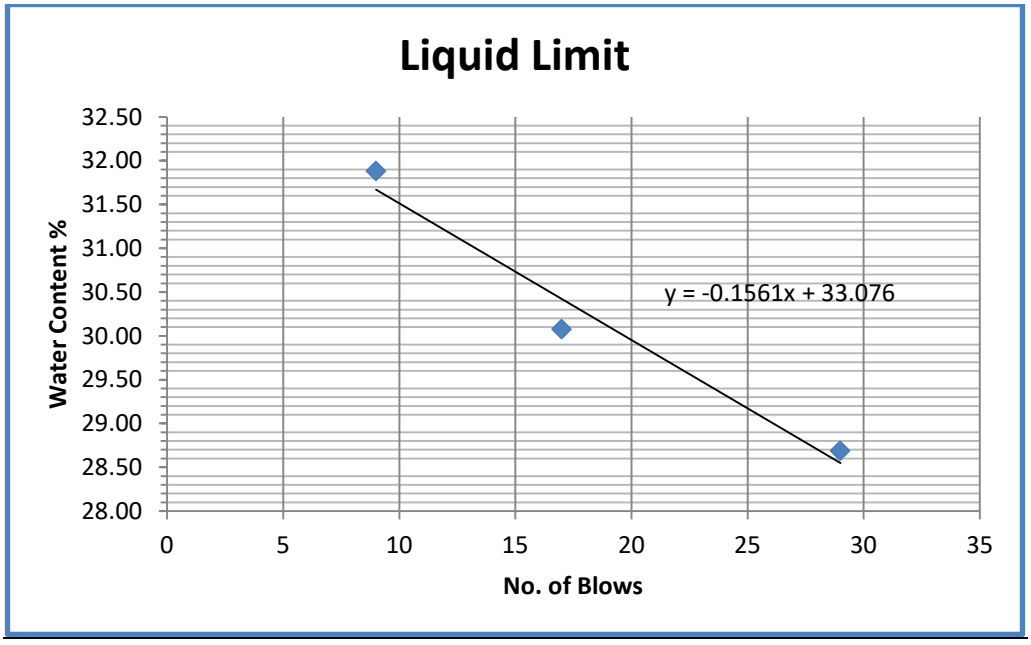

Figure 5.18. Graph of liquid Limit test for ZS4

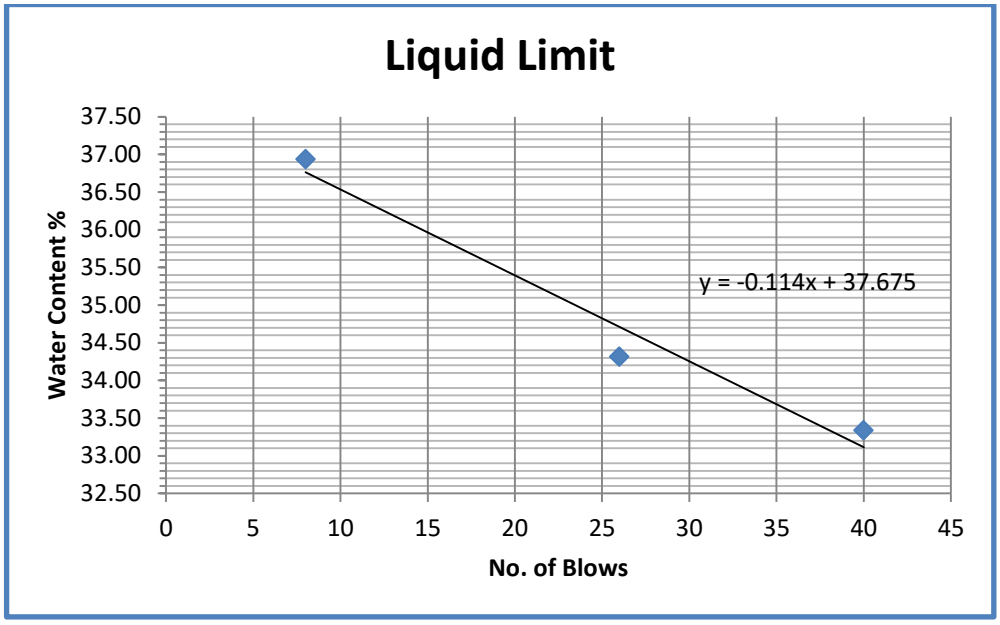

Figure 5.19. Graph of Liquid Limit test for ZS5

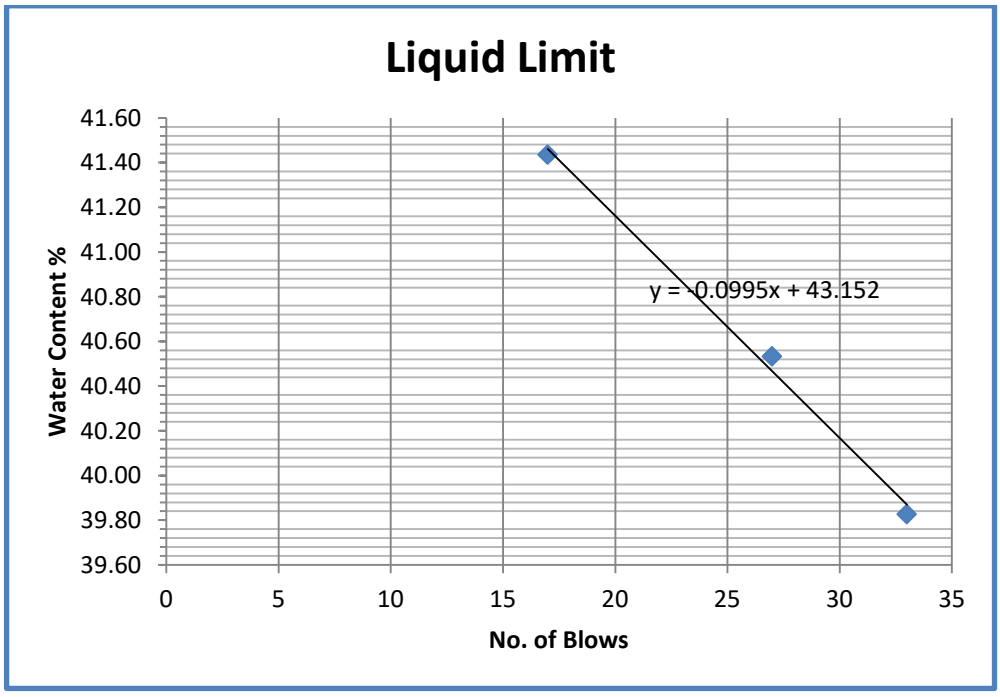

Figure 5.20. Graph of Liquid Limit test for ZS6

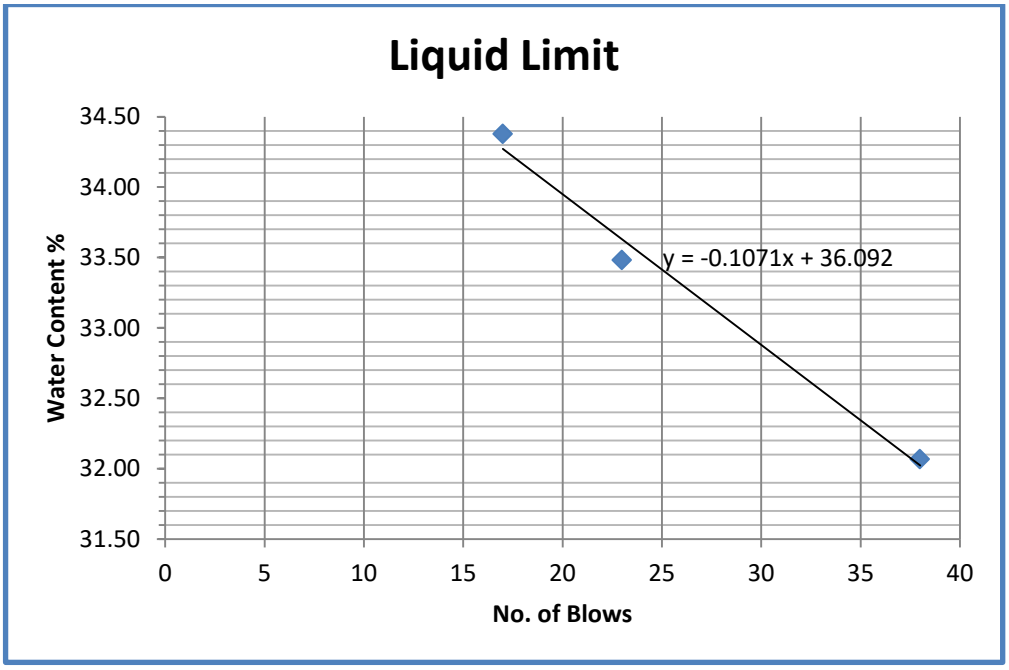

Figure 5.21. Graph of Liquid Limit test for ZS7

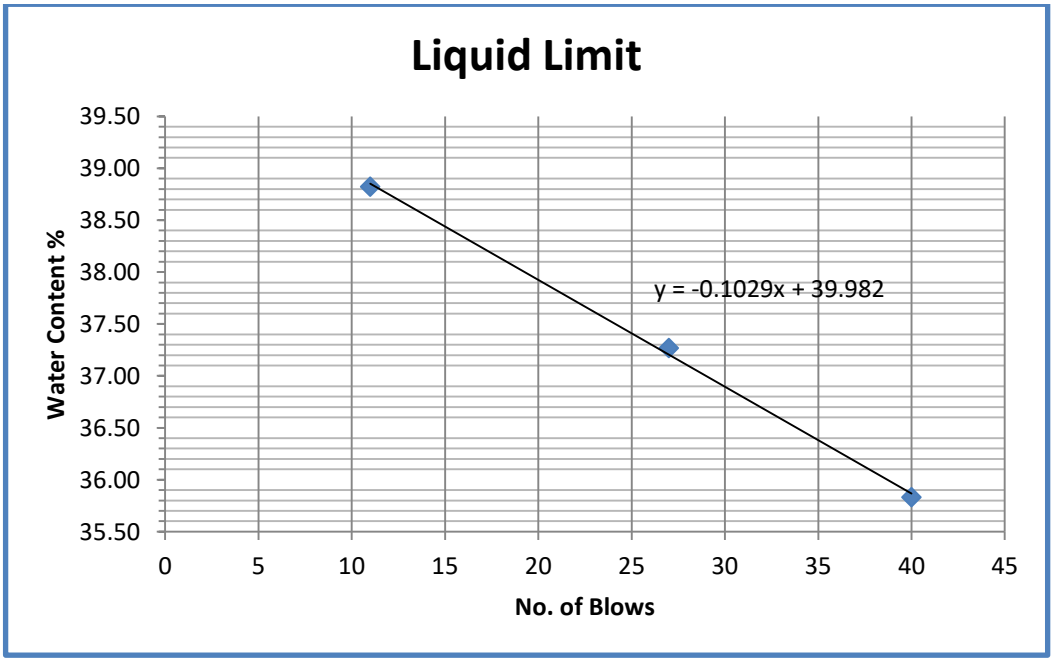

Figure 5.22. Graph of Liquid Limit test for ZS8

5.1.2.1.3 *Plastic Limit*

The results of the plastic limit for different locations are given in Table 5.3

Table 5.3: Plastic Limit for different soil samples

Sample No.	**Weight of Container with Lid, W1 (gm)**	**Weight of Container with Lid + wet soil, W2 (gm)**	**Weight of Container with Lid + dry soil, W3 (gm)**	**Weight of dry soil**	**Weight of water in the soil**	**Moisture content, w (%)**	**Plastic Limit**
ZS1	4.121	7.047	6.448	2.327	0.599	25.741	
	11	13.507	13.001	2.001	0.506	25.287	
	11.445	13.311	12.921	1.476	0.390	26.423	25.82
ZS2	11.518	18.537	17.008	5.490	1.529	27.851	
	10.916	14.717	13.899	2.983	0.818	27.422	
	11.525	14.182	13.624	2.099	0.558	26.584	27.29
ZS3	11.003	13.988	13.408	2.405	0.580	24.116	
	10.916	12.910	12.516	1.600	0.394	24.625	
	11.525	14.499	13.917	2.392	0.582	24.331	24.36
ZS4	9.502	11.657	11.287	1.785	0.370	20.728	
	10.764	13.860	13.330	2.566	0.530	20.655	
	10.523	12.334	12.030	1.507	0.304	20.173	20.52
ZS5	4.369	6.374	5.986	1.617	0.388	23.995	
	4.120	5.504	5.238	1.118	0.266	23.792	
	4.383	5.532	5.310	0.927	0.222	23.948	23.91
ZS6	6.968	8.366	8.026	1.058	0.340	32.136	
	4.753	7.874	7.111	2.358	0.763	32.358	
	6.599	9.922	9.120	2.521	0.802	31.813	32.10
ZS7	10.912	13.241	12.787	1.875	0.454	24.213	
	11.006	14.242	13.637	2.631	0.605	22.995	
	11.521	14.064	13.594	2.073	0.470	22.672	23.29
ZS8	11.003	13.099	12.700	1.697	0.399	23.512	
	10.916	13.060	12.645	1.729	0.415	24.002	
	11.525	13.217	12.894	1.369	0.323	23.594	23.70

The minimum moisture content at which the soil behaves as plastic is the plastic limit of the soil. The plastic limit of the soil samples in the study area ranges between 20.52(ZS4) and 27.29 (ZS2).

5.1.2.1.4 *Plasticity Index, Liquidity Index, and Consistency Index*

The value obtained from natural moisture content, liquid limit, and plastic limits is used for the calculation of the plasticity index, liquidity index, and consistency index of the soil. The classification was carried out according to Coduto 1999 modified after Sower's 1979. The obtained value for each sample is given in Table 5.4

Table 5.4:Value of Plasticity Index, Liquidity Index, and Consistency Index and their Classification after Coduto,1999 modified after Sowers, 1979

Sample No.	Plasticity Index	Classification	Liquidity Index	Classification	Consistency Index	Classification
ZS1	14.4	Slightly plastic	-0.14	Semi-solid	1.14	Semi-solid
ZS2	13.66	Slightly plastic	-0.24	Semi-solid	1.24	Semi-solid
ZS3	16.31	Medium Plastic	-0.18	Semi-solid	1.18	Semi-solid
ZS4	8.65	Slightly plastic	0.07	Semi-solid	0.92	Semi-solid
ZS5	10.91	Slightly plastic	-0.01	Semi-solid	1.01	Semi-solid
ZS6	8.57	Slightly plastic	-0.21	Semi-solid	1.21	Semi-solid
ZS7	10.12	Slightly plastic	-1.17	Semi-solid	1.18	Semi-solid
ZS8	13.73	Slightly plastic	-0.15	Semi-solid	1.15	Semi-solid

The lowest plasticity index is shown by ZS6 with a PI of 8.57. A liquidity index of 0.07 in ZS5 is the highest among the samples. All the samples range between 0.92 to 1.24 in the consistency index. From the plasticity index, liquidity index, and consistency index, we can interpret that the soils have semi-solid and slightly plastic characters.

5.1.2.2 STANDARD PROCTOR COMPACTION

The value of dry density for each sample prepared as per IS: 2720 Part VII-1980 is given in the table and figure from Table 5.5 to Table 5.12 and Figure 5.23 to Figure 5.30 respectively.

Table 5.5: Standard Proctor Compaction Test for ZS1

SL NO	**PARTICULARS**	**Unit**	**TRIAL**			
			1	**2**	**3**	**4**
1	Mass of empty mould (M1)	gm	4679	4679	4679	4679
2	Volume of mould (V)	cc	989.6	989.6	989.6	989.6
3	Mass of mould + Soil sample (M2)	gm	6556	6650	6678	6668
4	Mass of wet soil (M)	gm	1877	1971	1999	1989
5	Wet/Bulk Density (ϒwet)	g/cc	1.90	1.99	2.02	2.01
6	Water content (w)	%	18	20	22	24
7	Dry density (ϒd)	g/cc	1.61	1.66	1.66	1.62

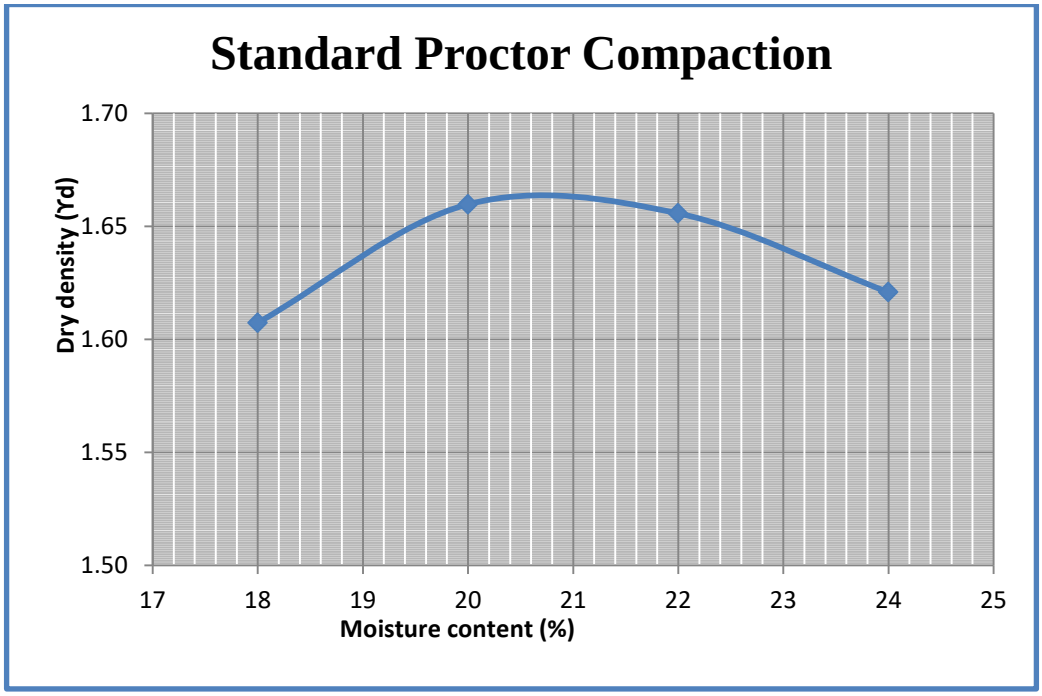

Figure 5.23. Proctor Compaction Curve for ZS1

Table5.6: Standard Proctor Compaction Test for ZS2

SL NO	**PARTICULARS**	**Unit**	**TRIAL**			
			1	**2**	**3**	**4**
1	Mass of empty mould (M1)	gm	4679	4679	4679	4679
2	Volume of mould (V)	cc	989.6	989.6	989.6	989.6
3	Mass of mould + Soil sample (M2)	gm	6497	6547	6648	6651
4	Mass of wet soil (M)	gm	1818	1868	1969	1972
5	Wet/Bulk Density (Ɣ wet)	g/cc	1.84	1.89	1.99	1.99
6	Water content (w)	%	15	17	19	21
7	Dry density (Ɣd)	g/cc	1.60	1.61	1.67	1.65

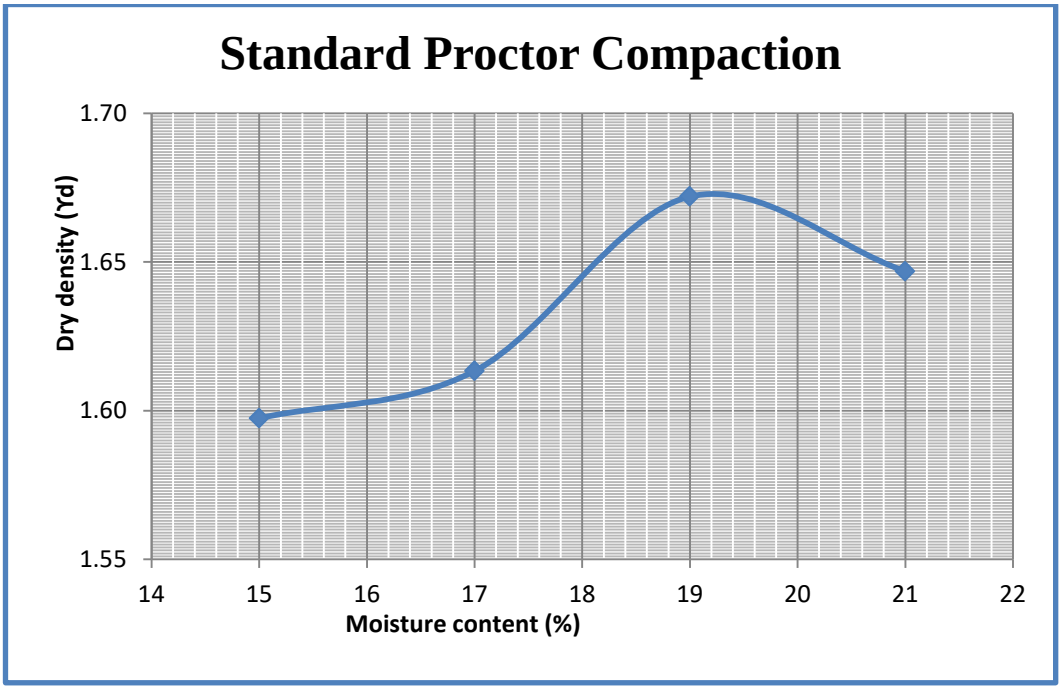

Figure 5.24. Standard Proctor Compaction Curve for ZS2

Table 5.7 Standard Proctor Compaction Test for ZS3

SL NO	**PARTICULARS**	**Unit**	**TRIAL**			
			1	**2**	**3**	**4**
1	Mass of empty mould (M1)	gm	4679	4679	4679	4679
2	Volume of mould (V)	cc	989.6	989.6	989.6	989.6
3	Mass of mould + Soil sample (M2)	gm	6647	6701	6740	6747
4	Mass of wet soil (M)	gm	1968	2022	2061	2068
5	Wet/Bulk Density (Ɣwet)	g/cc	1.99	2.04	2.08	2.09
6	Water content (w)	%	13	15	17	19
7	Dry density (Ɣd)	g/cc	1.76	1.78	1.78	1.76

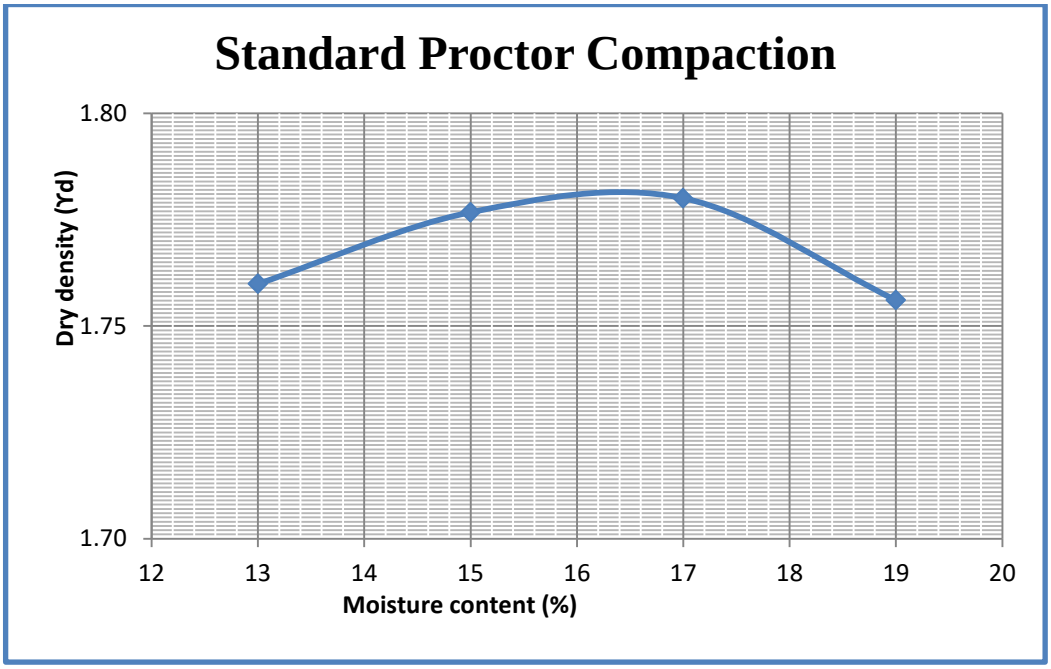

Figure 5.25.Standard Proctor Compaction Curve for ZS3

Table 5.8: Standard Proctor Compaction Test for ZS4

SL NO	**PARTICULARS**	**Unit**	**TRIAL**			
			1	**2**	**3**	**4**
1	Mass of empty mould (M1)	gm	4679	4679	4679	4679
2	Volume of mould (V)	cc	989.6	989.6	989.6	989.6
3	Mass of mould + Soil sample (M2)	gm	6730	6798	6821	6807
4	Mass of wet soil (M)	gm	2051	2119	2142	2128
5	Wet/Bulk Density (Ƴwet)	g/cc	2.07	2.14	2.16	2.15
6	Water content (w)	%	13	14	15	16
7	Dry density (Ƴd)	g/cc	1.83	1.88	1.88	1.85

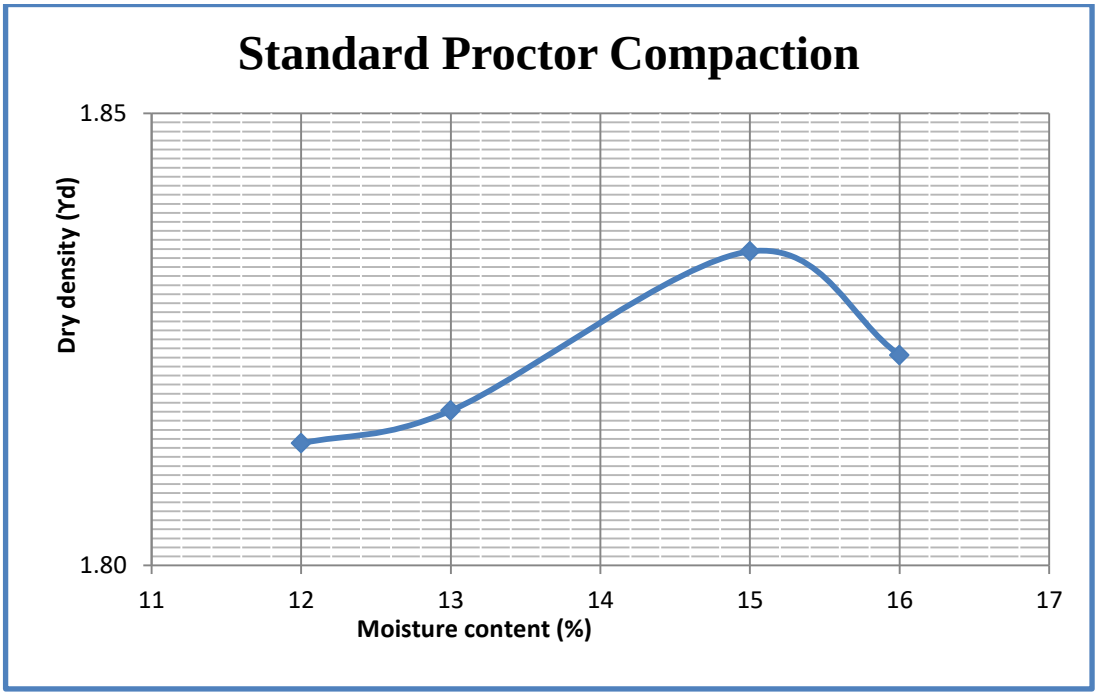

Figure 5.26. Standard Proctor Compaction Curve for ZS4

Table 5.9: Standard Proctor Compaction Test for ZS5

SL NO	**PARTICULARS**	**Unit**	**TRIAL**			
			1	**2**	**3**	**4**
1	Mass of empty mould (M1)	gm	4679	4679	4679	4679
2	Volume of mould (V)	cc	989.6	989.6	989.6	989.6
3	Mass of mould + Soil sample (M2)	gm	6689	6711	6767	6772
4	Mass of wet soil (M)	gm	2010	2032	2088	2093
5	Wet/Bulk Density (Ɣwet)	g/cc	2.03	2.05	2.11	2.11
6	Water content (w)	%	12	13	15	16
7	Dry density (Ɣd)	g/cc	1.81	1.82	1.83	1.82

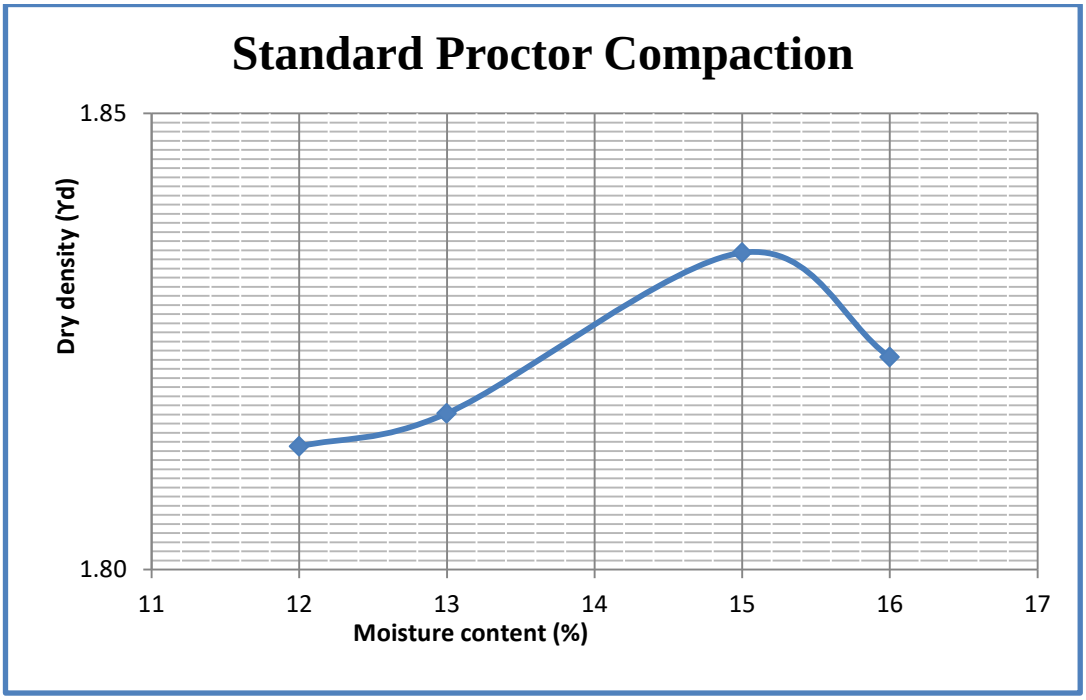

Figure 5.27. Standard Proctor Compaction Curve for ZS5

Table 5.10: Standard Proctor Compaction Test for ZS6

SL NO	**PARTICULARS**	**Unit**	**TRIAL**			
			1	**2**	**3**	**4**
1	Mass of empty mould (M1)	gm	4679	4679	4679	4679
2	Volume of mould (V)	cc	989.6	989.6	989.6	989.6
3	Mass of mould + Soil sample (M2)	gm	6340	6426	6449	6415
4	Mass of wet soil (M)	gm	1661	1747	1770	1736
5	Wet/Bulk Density (Ɣwet)	g/cc	1.68	1.77	1.79	1.75
6	Water content (w)	%	13	15	17	18
7	Dry density (Ɣd)	g/cc	1.49	1.54	1.53	1.49

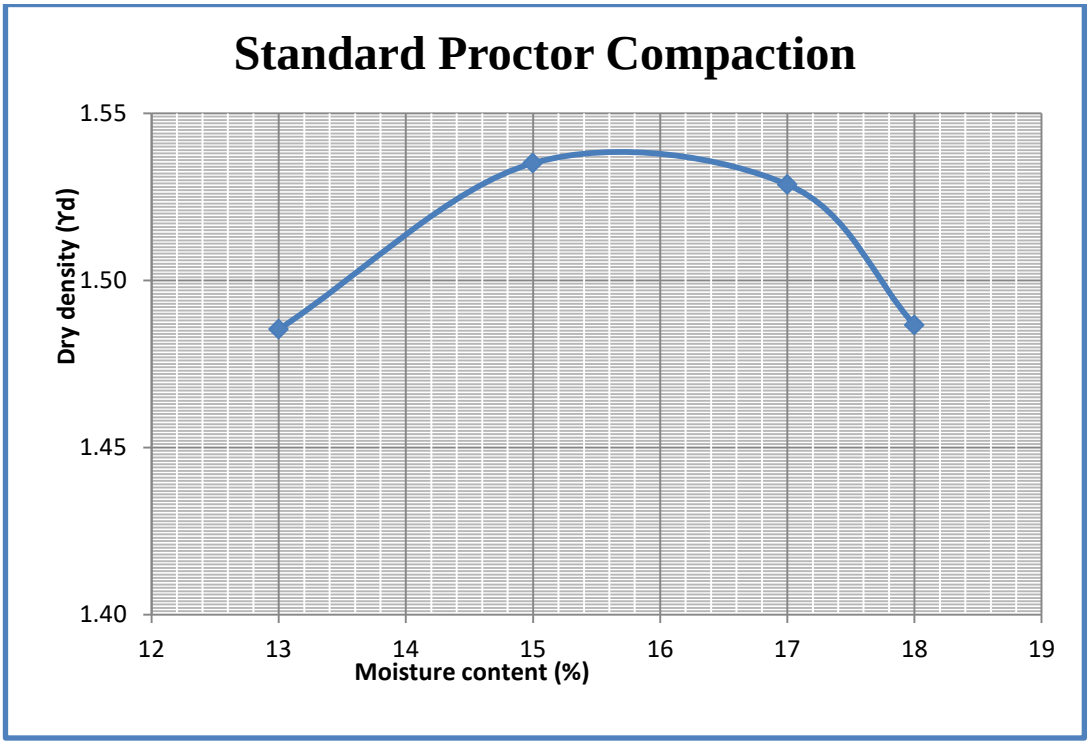

Figure 5.28. Standard Proctor Compaction Curve for ZS6

Table 5.11:Standard Proctor Compaction Test for ZS7

SL NO	**PARTICULARS**	**Unit**	**TRIAL**			
			1	**2**	**3**	**4**
1	Mass of empty mould (M1)	gm	4679	4679	4679	4679
2	Volume of mould (V)	cc	989.6	989.6	989.6	989.6
3	Mass of mould + Soil sample (M2)	gm	6603	6662	6778	6738
4	Mass of wet soil (M)	gm	1924	1983	2099	2059
5	Wet/Bulk Density (Ɣwet)	g/cc	1.94	2.00	2.12	2.08
6	Water content (w)	%	12	14	16	18
7	Dry density (Ɣd)	g/cc	1.74	1.76	1.83	1.76

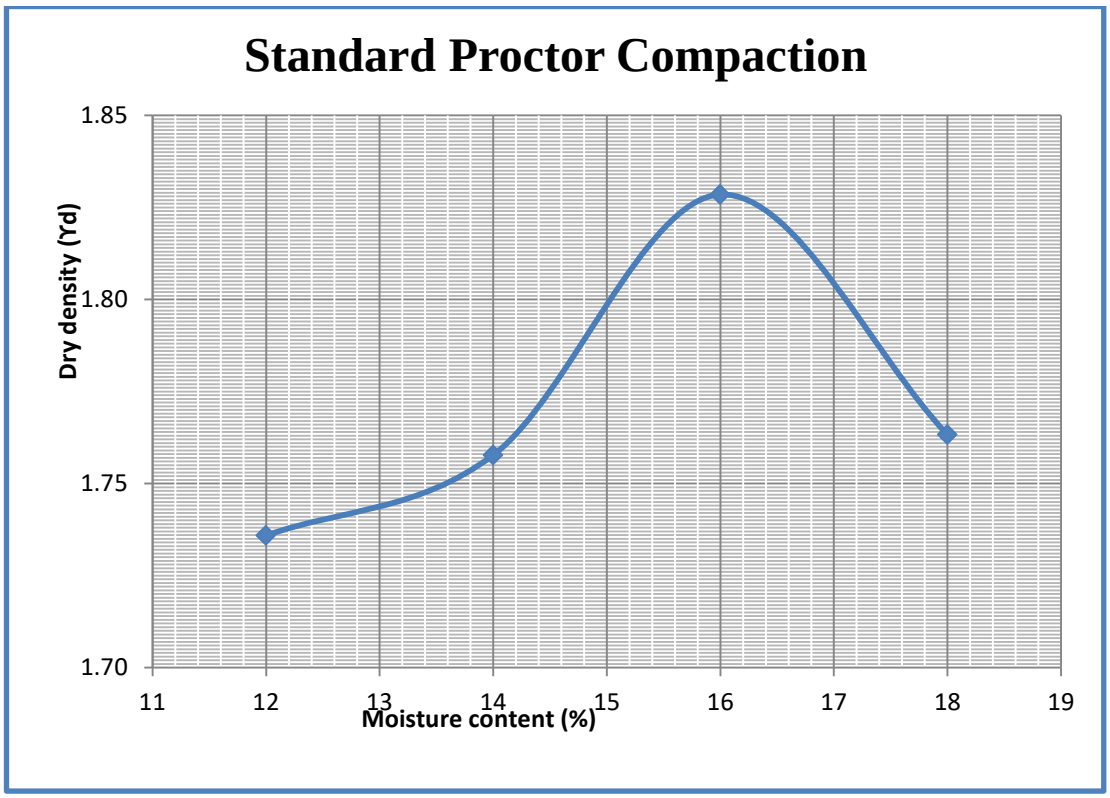

Figure 5.29. Standard Proctor Compaction Curve for ZS7

Table 5.12: Standard Proctor Compaction Test for ZS8

SL NO	PARTICULARS	Unit	TRIAL				
			1	**2**	**3**	**4**	**5**
1	Mass of empty mould (M1)	gm	4679	4679	4679	4679	4679
2	Volume of mould (V)	cc	989.6	989.6	989.6	989.6	989.6
3	Mass of mould + Soil sample (M2)	gm	6493	6559	6640	6686	6672
4	Mass of wet soil (M)	gm	1814	1880	1961	2007	1993
5	Wet/Bulk Density (Ɣwet)	g/cc	1.83	1.90	1.98	2.03	2.01
6	Water content (w)	%	15	17	19	21	23
7	Dry density (Ɣd)	g/cc	1.59	1.62	1.67	1.68	1.64

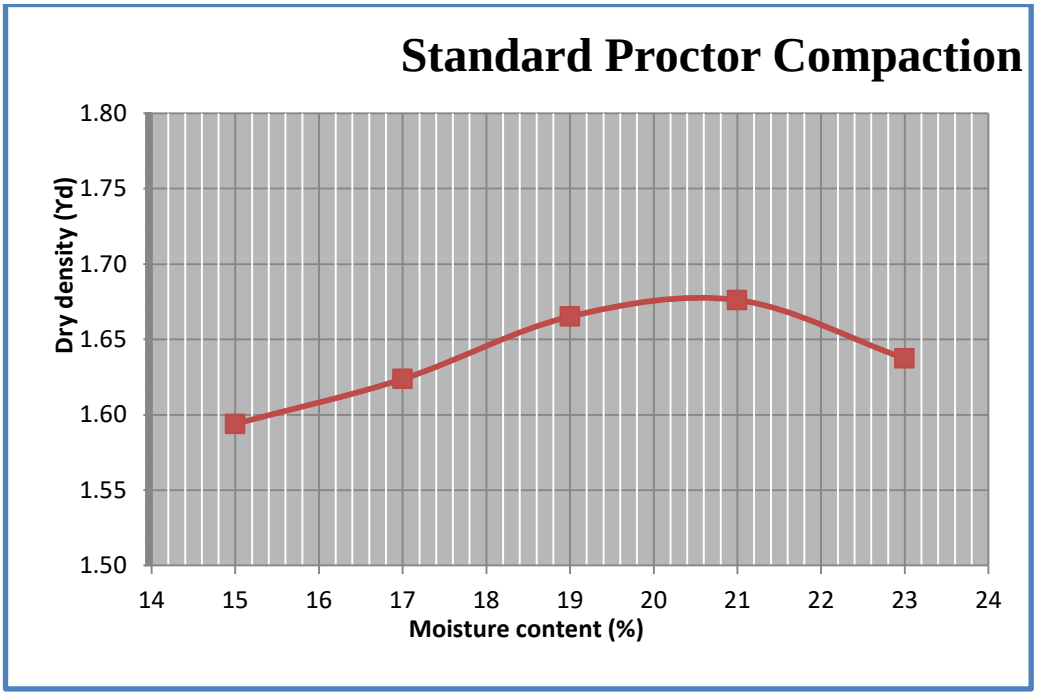

Figure 5.30. Standard Proctor Compaction Curve for ZS8

The lowest dry density 1.52g/cc was shown by ZS6 with an optimum moisture content of 16%.

5.1.2.3 DIRECT SHEAR TEST

The direct shear test was performed as per IS: 2720 (Part 13)-1986 and the value is given in Table 5.13 and the shear stress failure is given in figure from Figure 5.31 to Figure 5.38. It is the maximum stress at which the soil failure occurs.

Table 5.13: Direct Shear value for different samples in both locations

Sample No	Normal stress τ(kg/cm2)	Shear stress at failure τ(kg/cm2)	Cohesion (kg/cm2)	Angle of internal friction (°)
ZS1	0.5	0.58704	0.326	27.95
	1	0.86582		
	1.5	1.11779		
ZS2	0.5	0.57364	0.127	29.72
	1	0.82025		
	1.5	1.1446		
ZS3	0.5	0.51199	0.23	29.02
	1	0.77736		
	1.5	1.06686		
ZS4	0.5	0.4691	0.202	28.67
	1	0.76396		
	1.5	1.01593		
ZS5	0.5	0.4959	0.242	26.99
	1	0.75324		
	1.5	1.00521		
ZS6	0.5	0.42353	0.146	29.02
	1	0.70231		
	1.5	0.9784		
ZS7	0.5	0.51199	0.241	27.59
	1	0.74519		
	1.5	1.03469		
ZS8	0.5	0.4825	0.209	28.9
	1	0.76664		
	1.5	1.03469		

Direct shear test performed for 8 different samples at a depth of 5ft in locations 1 & 2 shows that the cohesion value ranges between 0.12 kg/cm^2 in ZS2 to 0.326 kg/cm^2 in ZS1. The angle of internal friction is maximum in ZS2 (29.71°)

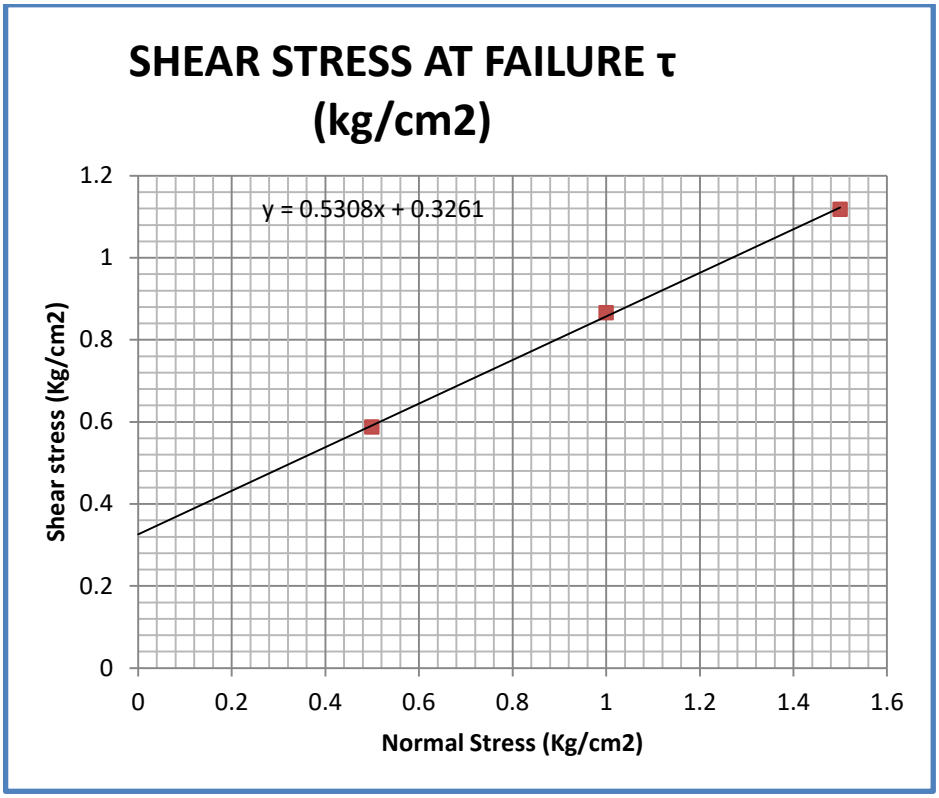

Figure 5.31. Shear stress at failure for ZS1

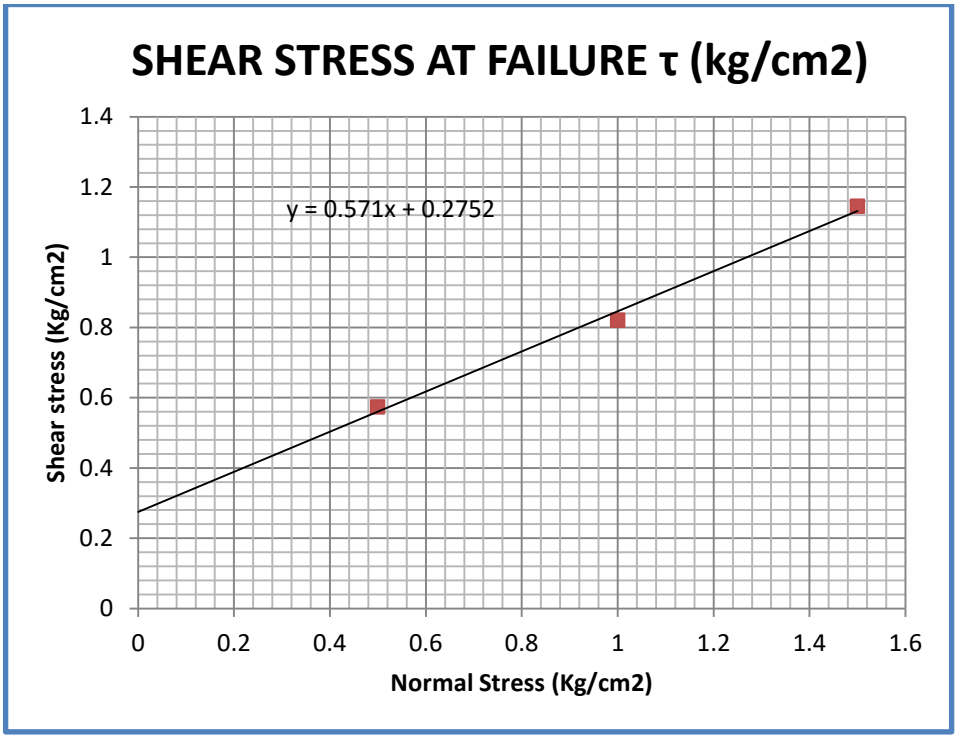

Figure 5.32. Shear Stress at Failure for ZS2

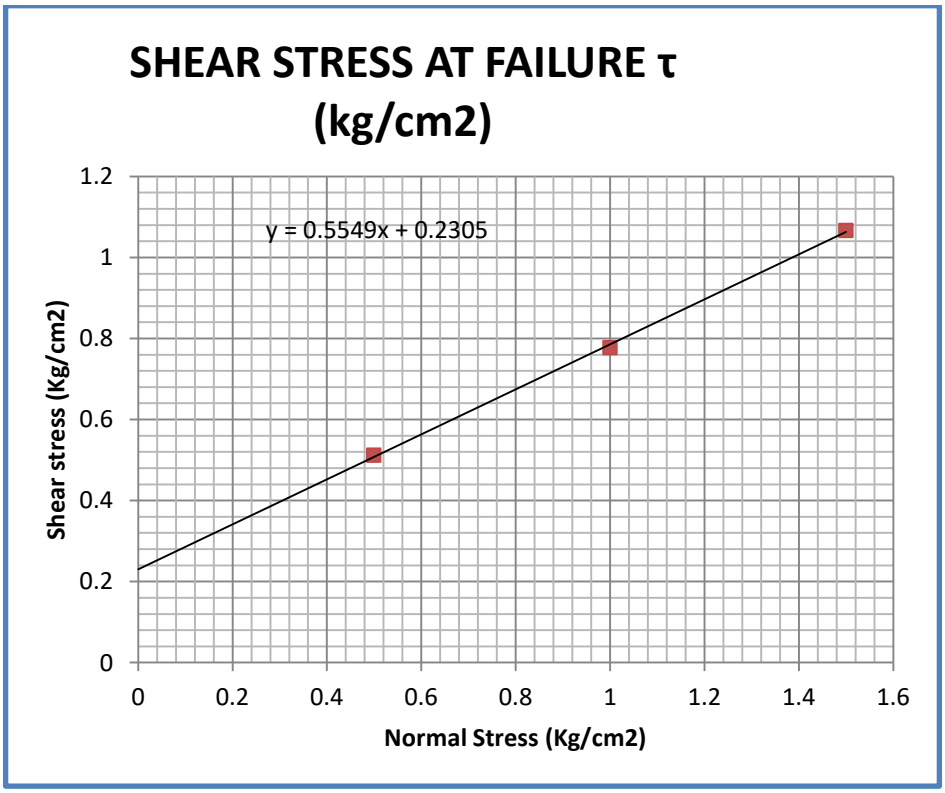

Figure 5.33. Shear Stress at Failure for ZS3

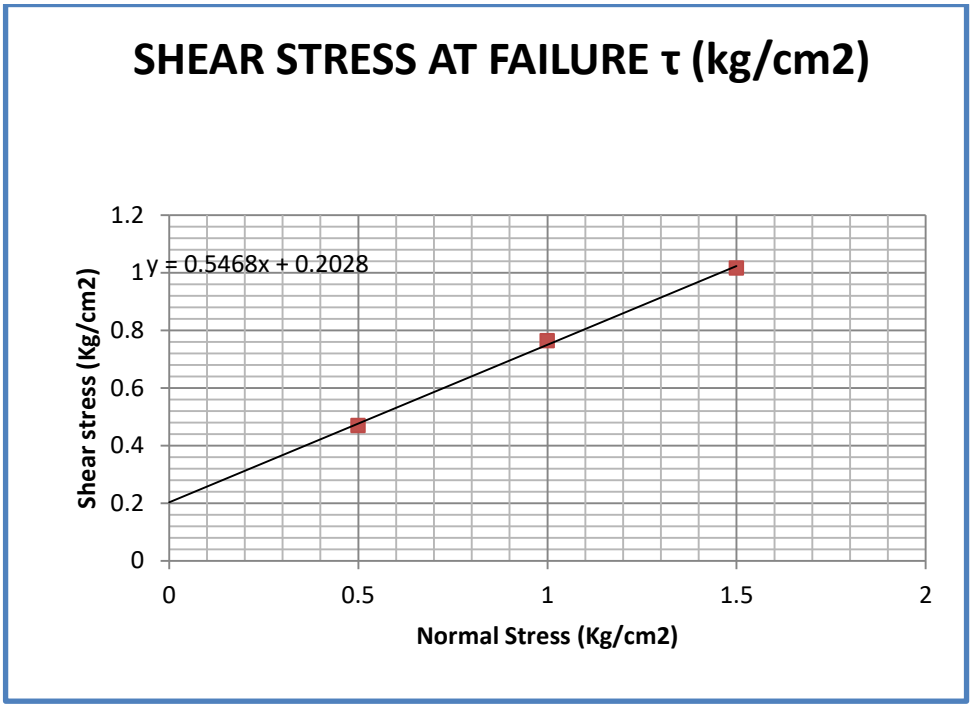

Figure 5.34. Shear Stress at Failure for ZS4

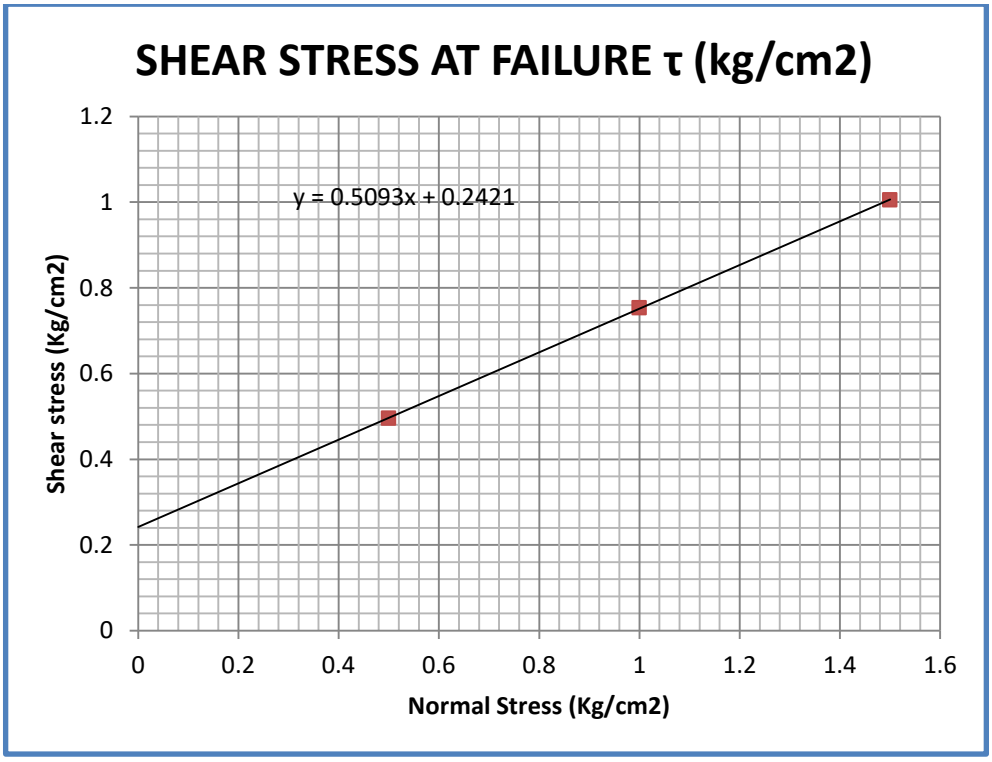

Figure 5.35. Shear Stress at Failure for ZS5

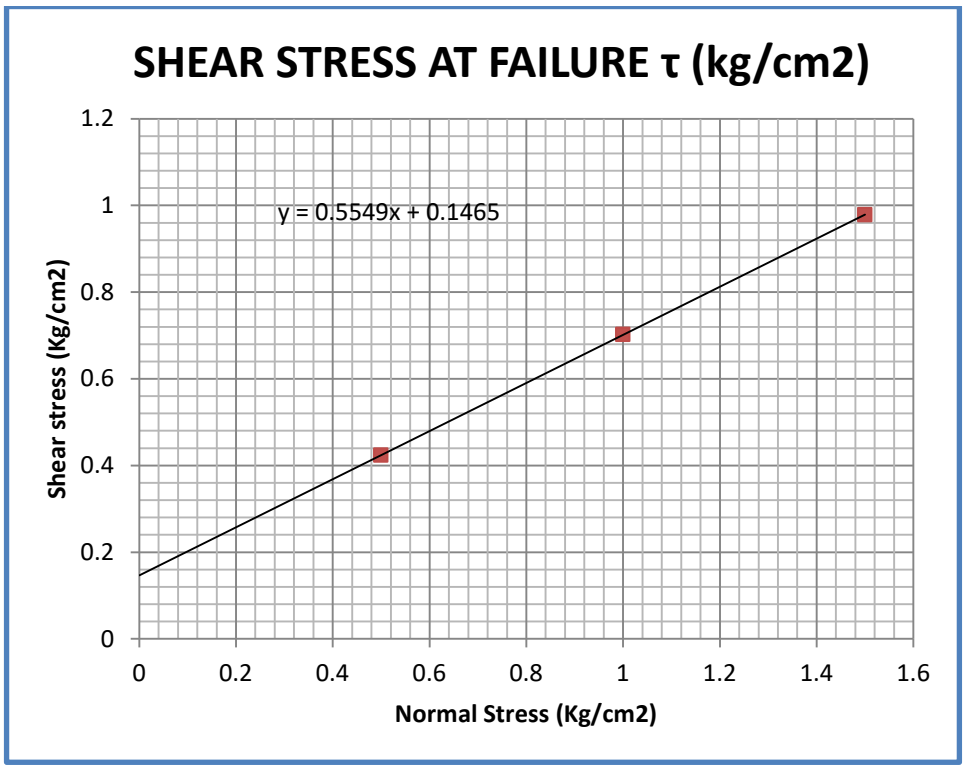

Figure 5.36. Shear Stress at Failure for ZS6

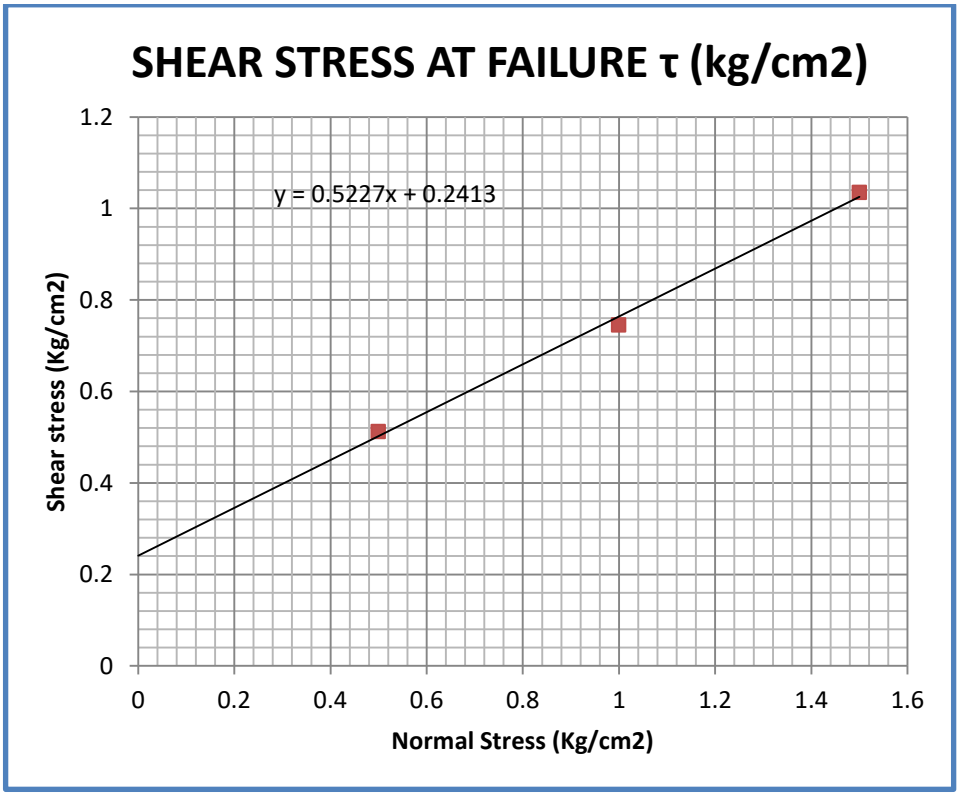

Figure 5.37. Shear Stress at Failure for ZS7

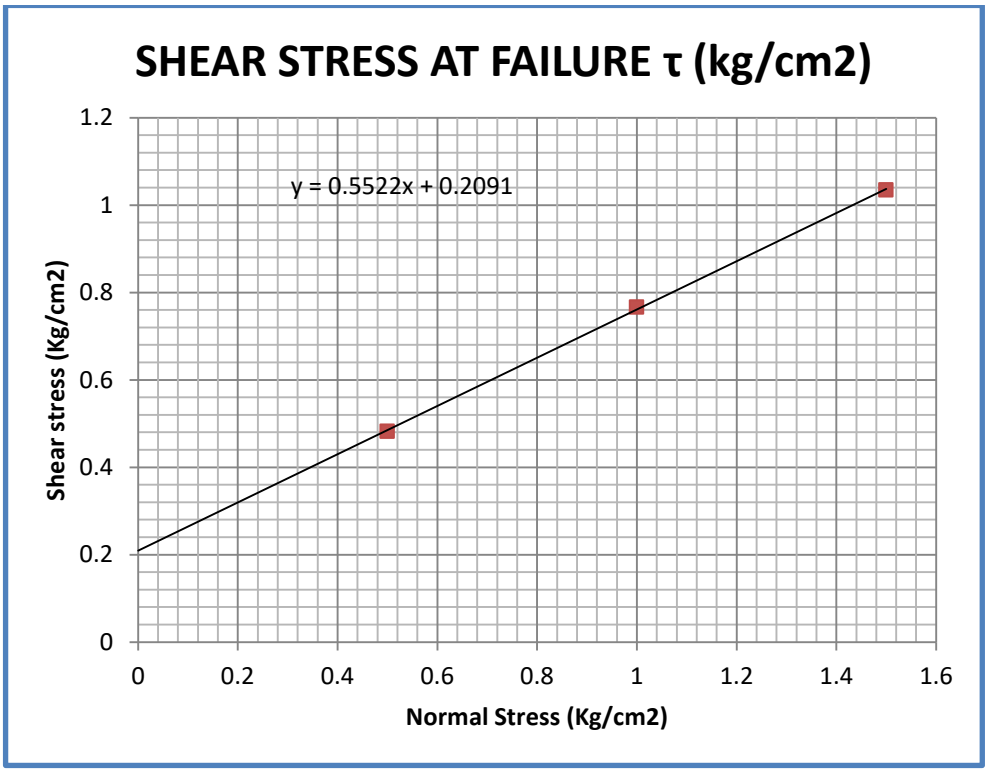

Figure 5.38. Shear Stress at Failure for ZS8

5.1.2.4 SOIL TRIAXIAL TEST

Soil triaxial test was performed in two locations at a depth of 5ft L1S1 and L2S4 as per IS 2720(Part 11): 1993(Consolidated Undrained Triaxial Compression Test). The parameters are given in Table 5.14 and the failure envelope is given in Figure 5.39 & 5.40

Table 5.14: Results of Soil Triaxial Test for ZS1 and ZS7

Parameters	**ZS1**			**ZS7**		
	1	2	3	1	2	3
Cell Pressure (KPa), σ3	36	72	144	84	168	336
Deviator stress at failure(KPa) Δσd	104	133	197	174	243	374
Axial stress(KPa), σ 1	140	205	341	260	411	710
Radius (KPa)	52	66.5	98.5	88	121.5	187
σ Average (KPa)	88	138.5	242.5	172	289.5	523
Cohesion(KPa)	26			39		
Angle of internal friction(°)	18			20		

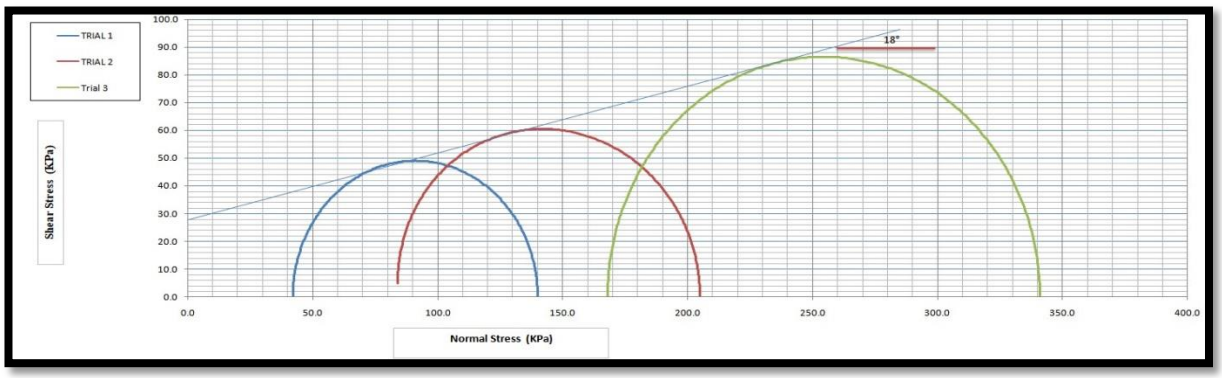

Figure 5.39. Failure envelope for ZS1

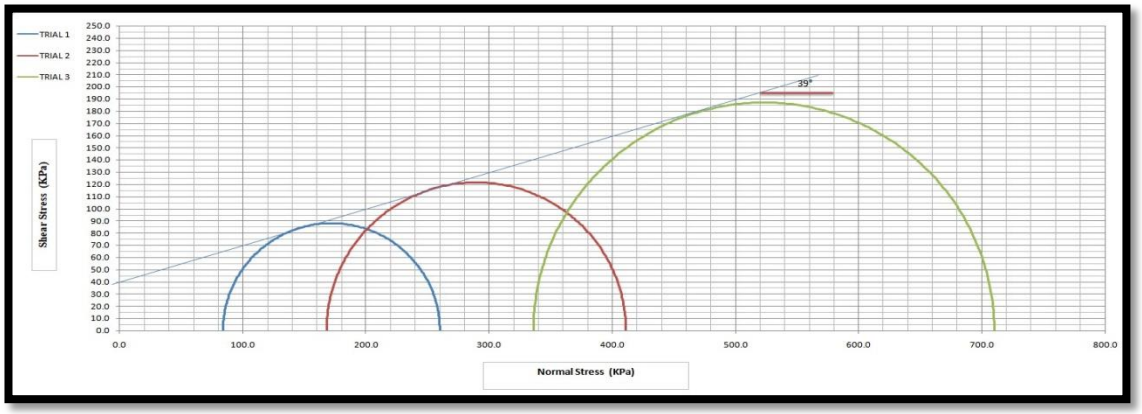

Figure 5.40. Failure envelope for ZS7

From the result of the soil triaxial test carried out for ZS1 and ZS7, the angle of internal friction and the cohesion values are 18° & 20° and 26 & 39 respectively.

5.1.3 SLOPE STABILITY ANALYSIS USING LIMIT EQUILIBRIUM METHOD (LEM)

Using the limit equilibrium method**,** Slope stability analysis was done for ZS1, ZS3, ZS7 & ZS8, and ZS4 & ZS5 & ZS6. Different methods like Bishop Simplified, GLE/ Morgenstern-Price, Janbu Corrected, Janbu Simplified, Ordinary/Fellenius, and Spencer methods were employed.

5.1.3.1 Slope Stability Analysis from Direct Shear Parameters

The parameters obtained from the direct shear test like the angle of internal friction and cohesion of the soil and proctor compaction test like the dry unit weight of the soil are utilized for slope stability analysis using LEM methods. The Factor of Safety obtained from the analysis by different methods and the slip circle in the model are given in Table 5.15 and Figure 5.41 to 5.64 respectively.

Table 5.15: Factor of Safety (FoS) shown by different methods

Method	**ZS1**	**ZS3**	**ZS7 & ZS8**	**ZS4,ZS5& ZS6**
Bishop Simplified	0.82	0.78	0.56	0.61
GLE/ Morgenstern-Price	1.33	0.77	0.55	0.59
Janbu Corrected	0.92	0.78	0.56	0.58
Janbu Simplified	0.86	0.73	0.54	0.54
Ordinary/Fellenius	0.83	0.74	0.54	0.53

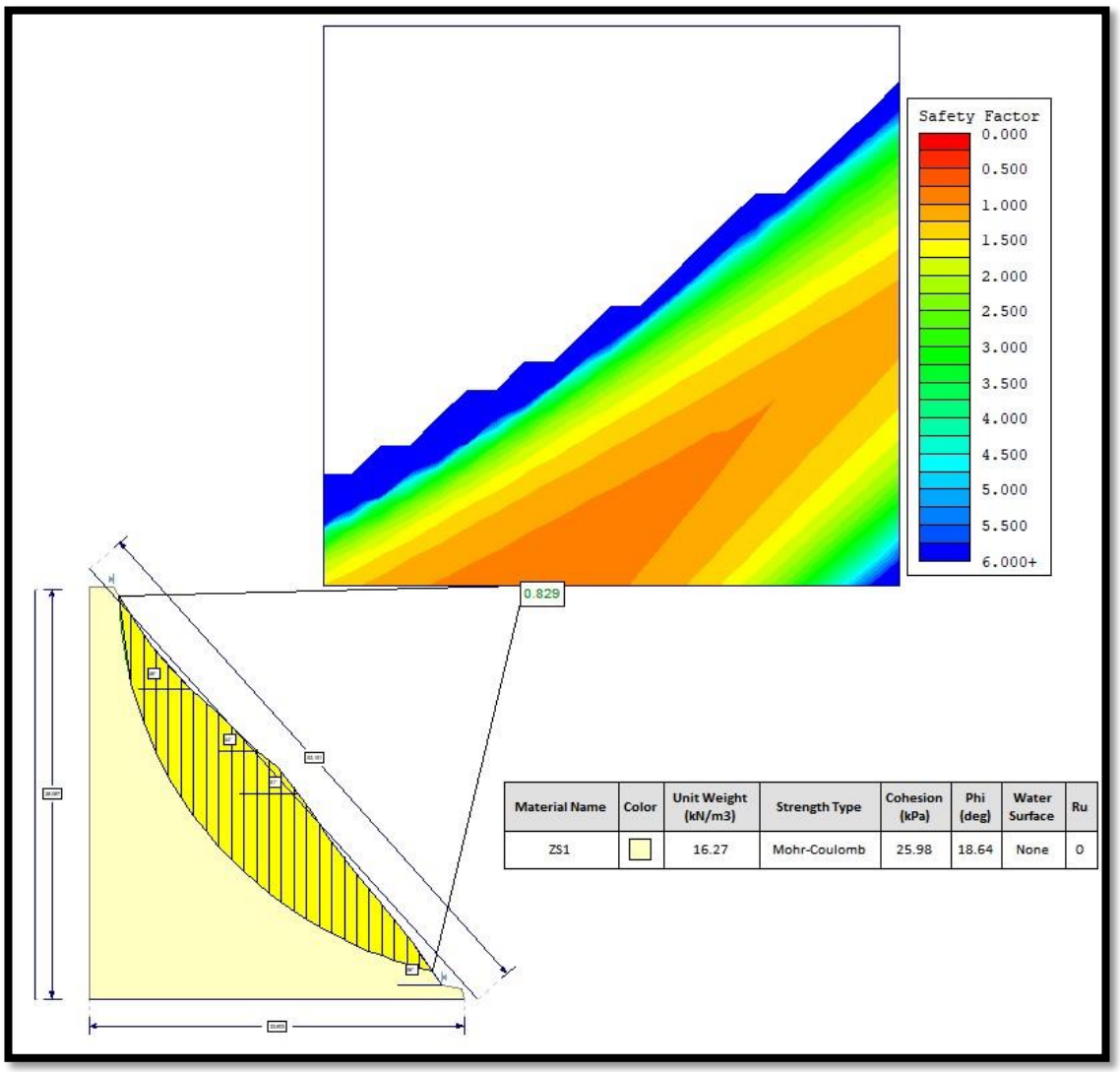

Figure 5.41. LEM plot for ZS1 (Bishop Simplified Method)

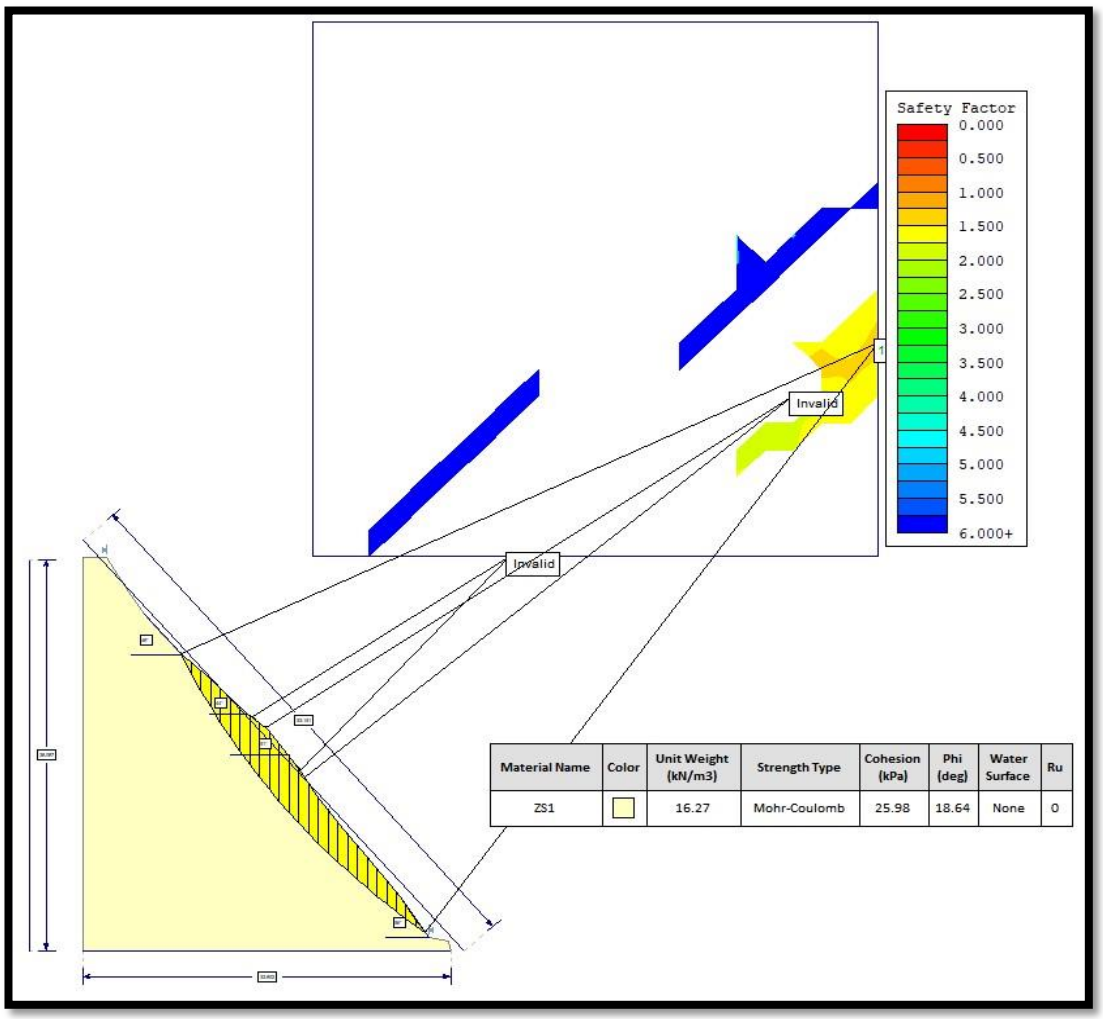

Figure 5.42. LEM plot for ZS1(GLE/Morgenstren-price Method)

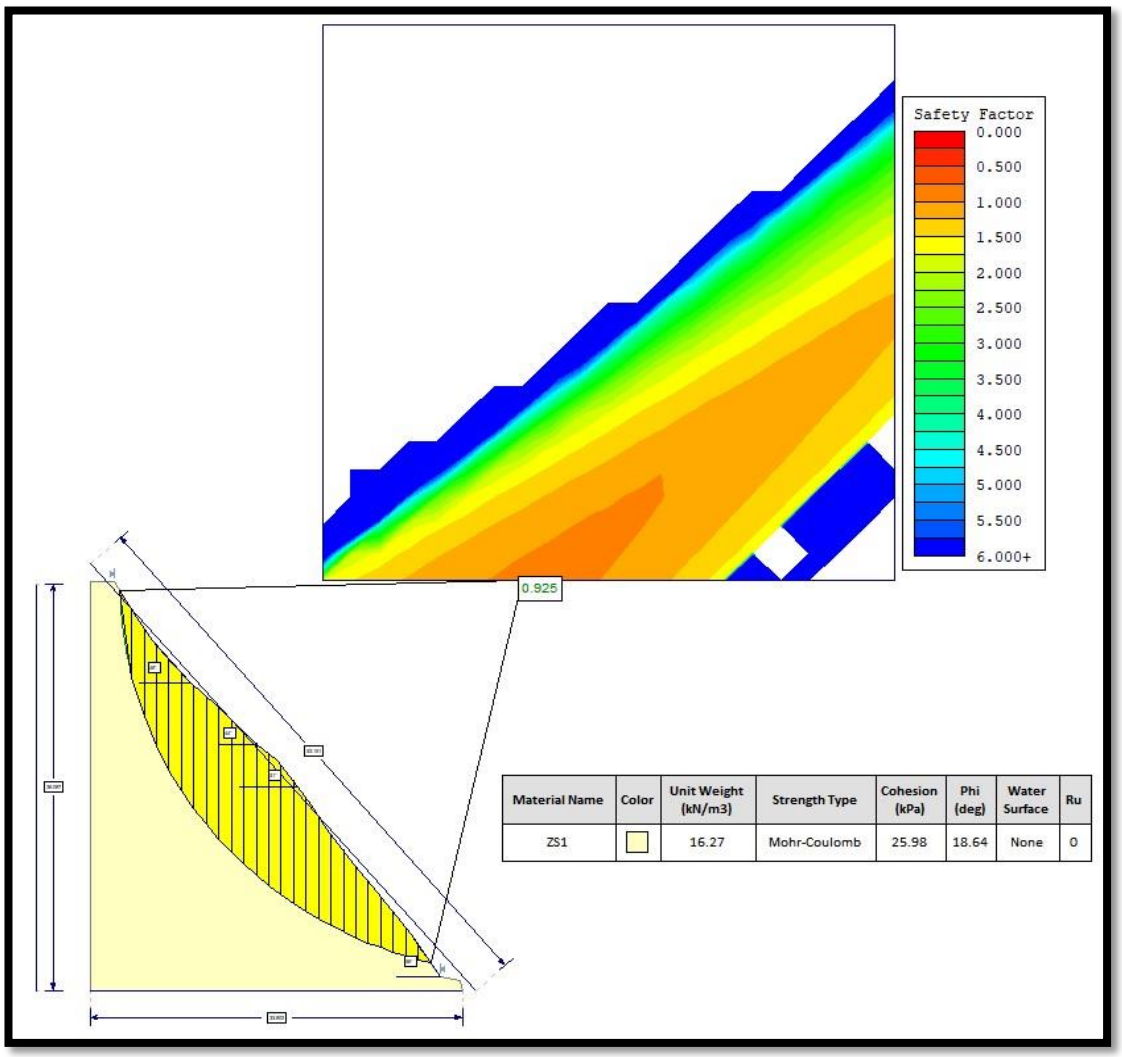

Figure 5.43. LEM plot for ZS1(Janbu corrected Method)

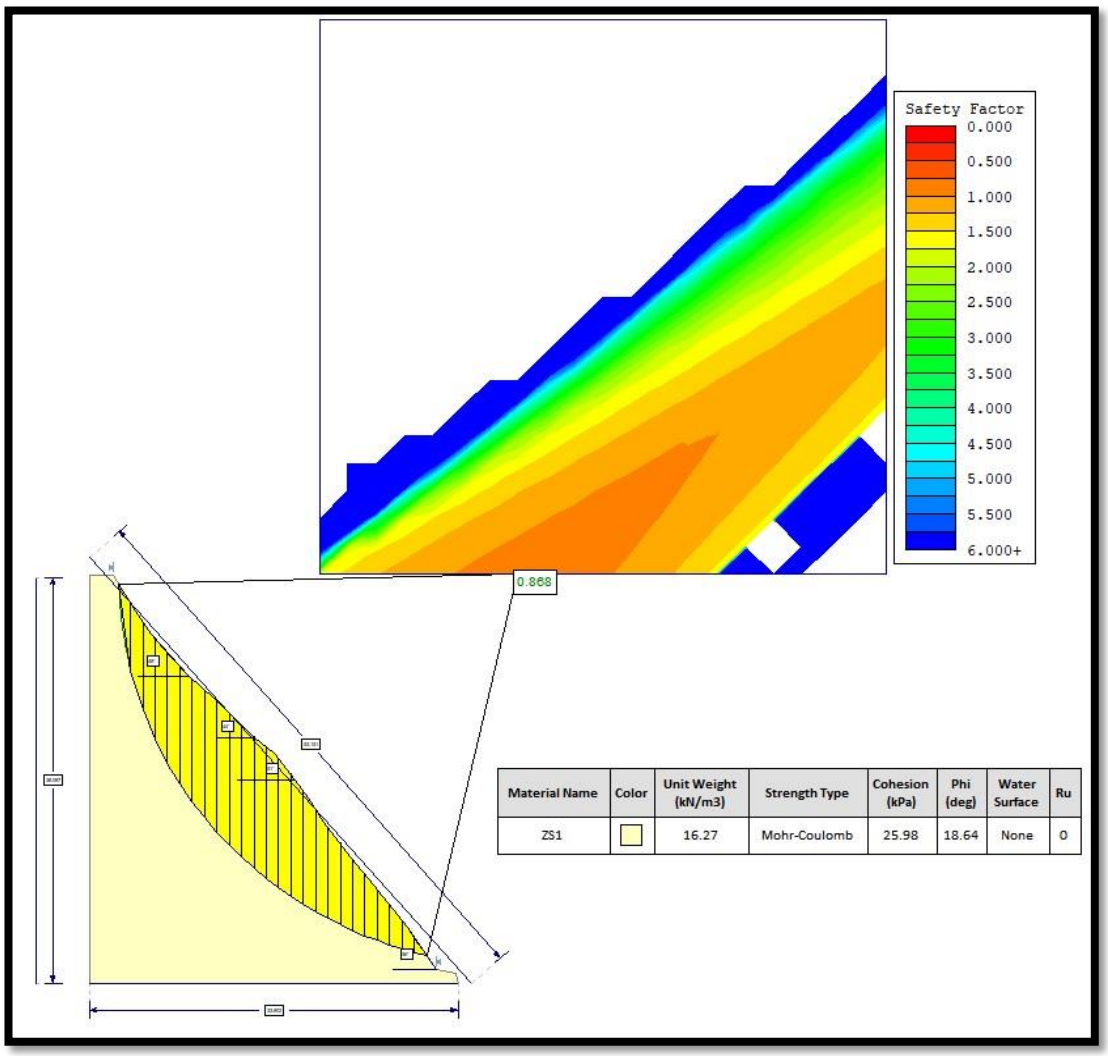

Figure 5.44. LEM plot for ZS1(Janbu simplified Method)

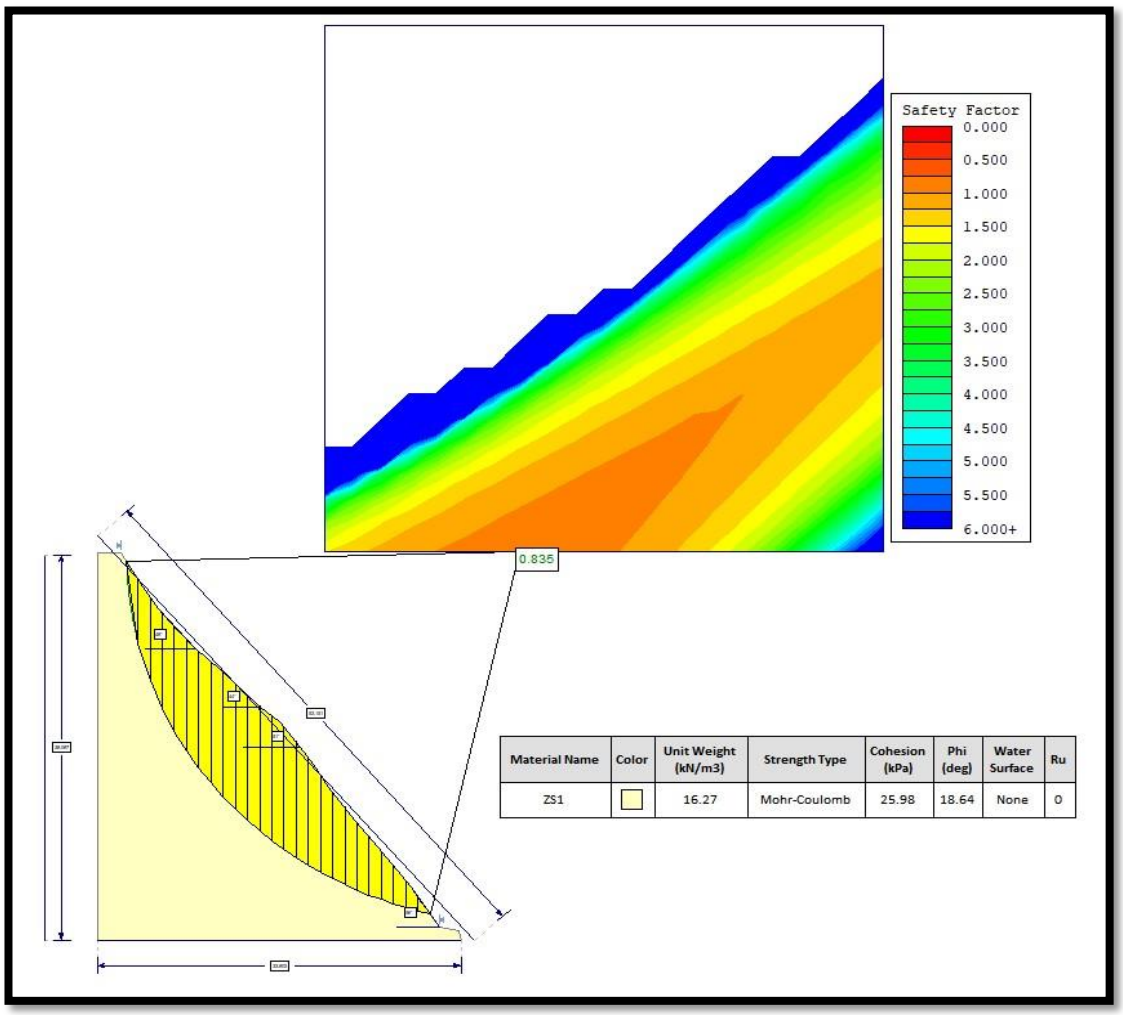

Figure 5.45. LEM plot for ZS1(Ordinary/Fellenius Method)

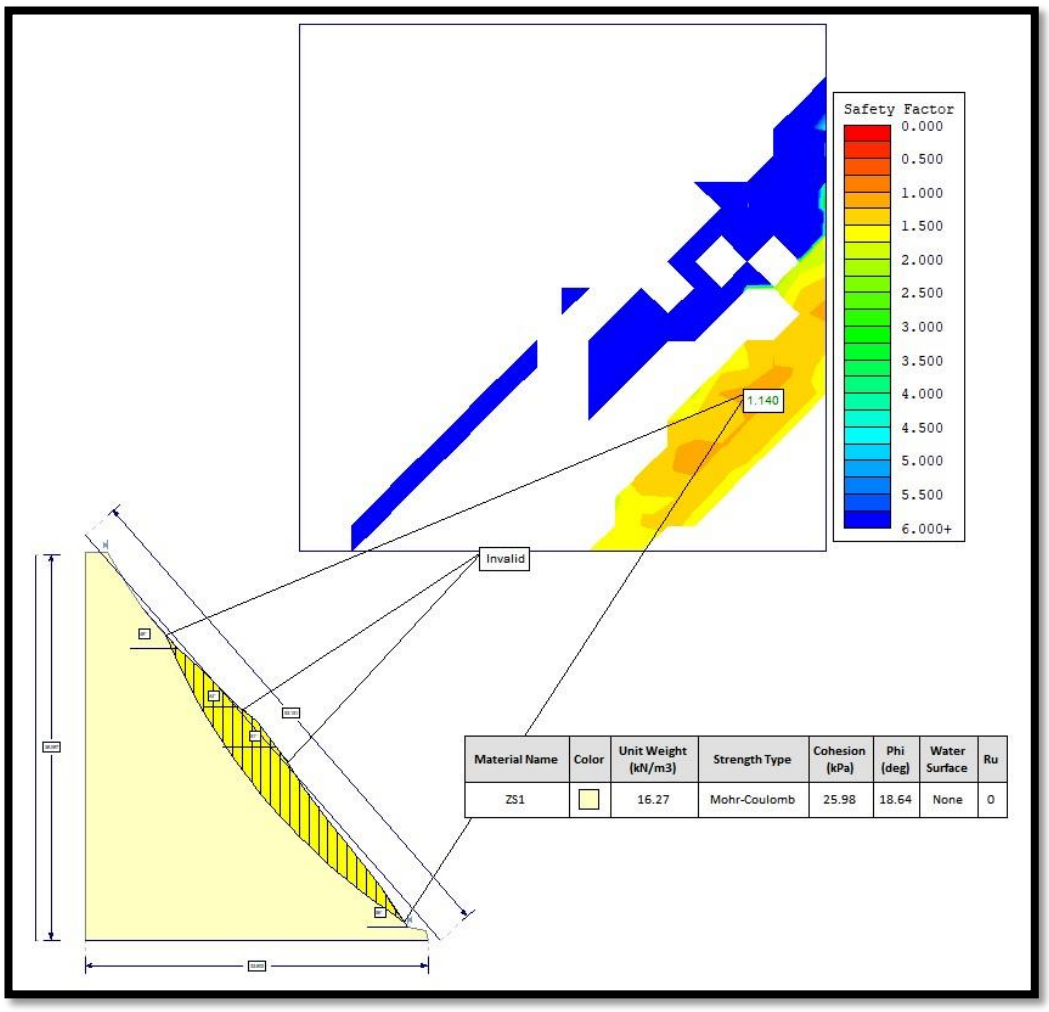

Figure 5.46. LEM plot for ZS1(Spencer Method)

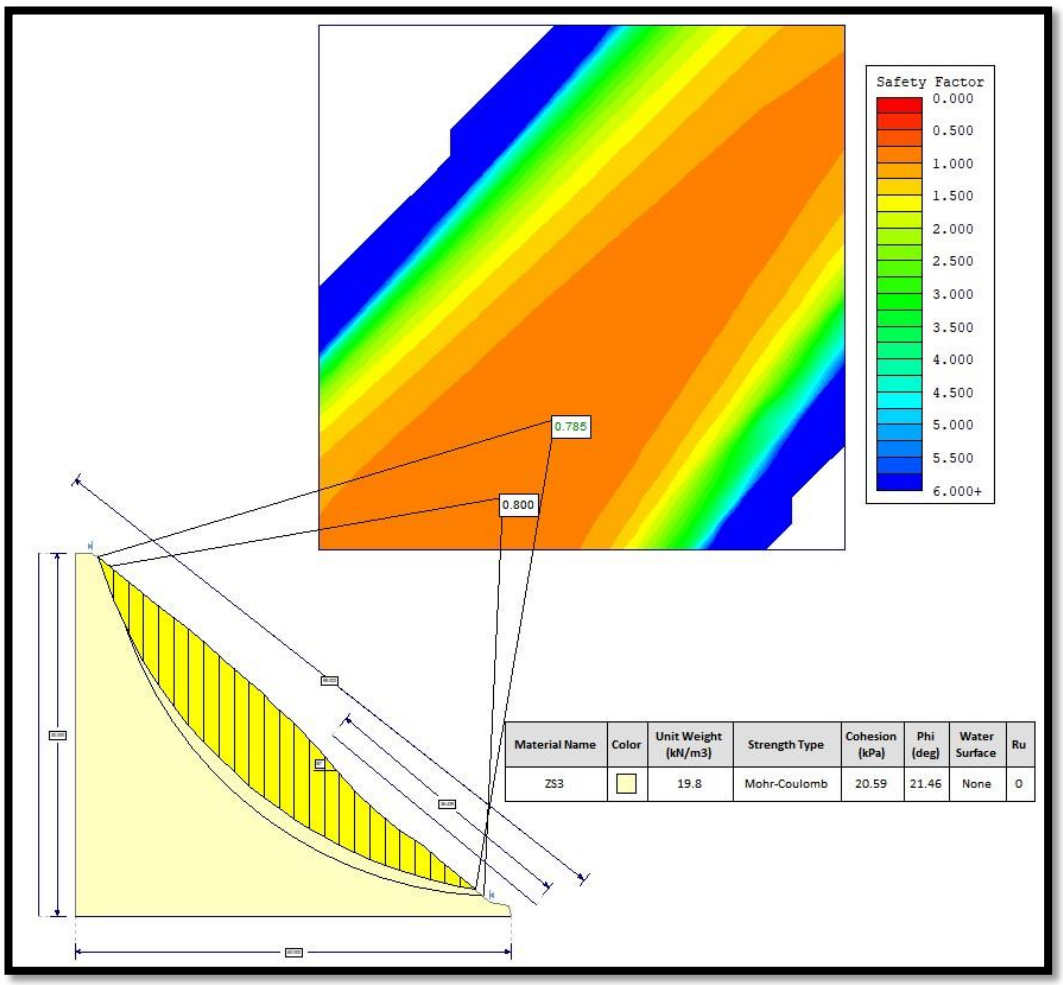

Figure 5.47. LEM plot for ZS3 (Bishop simplified Method)

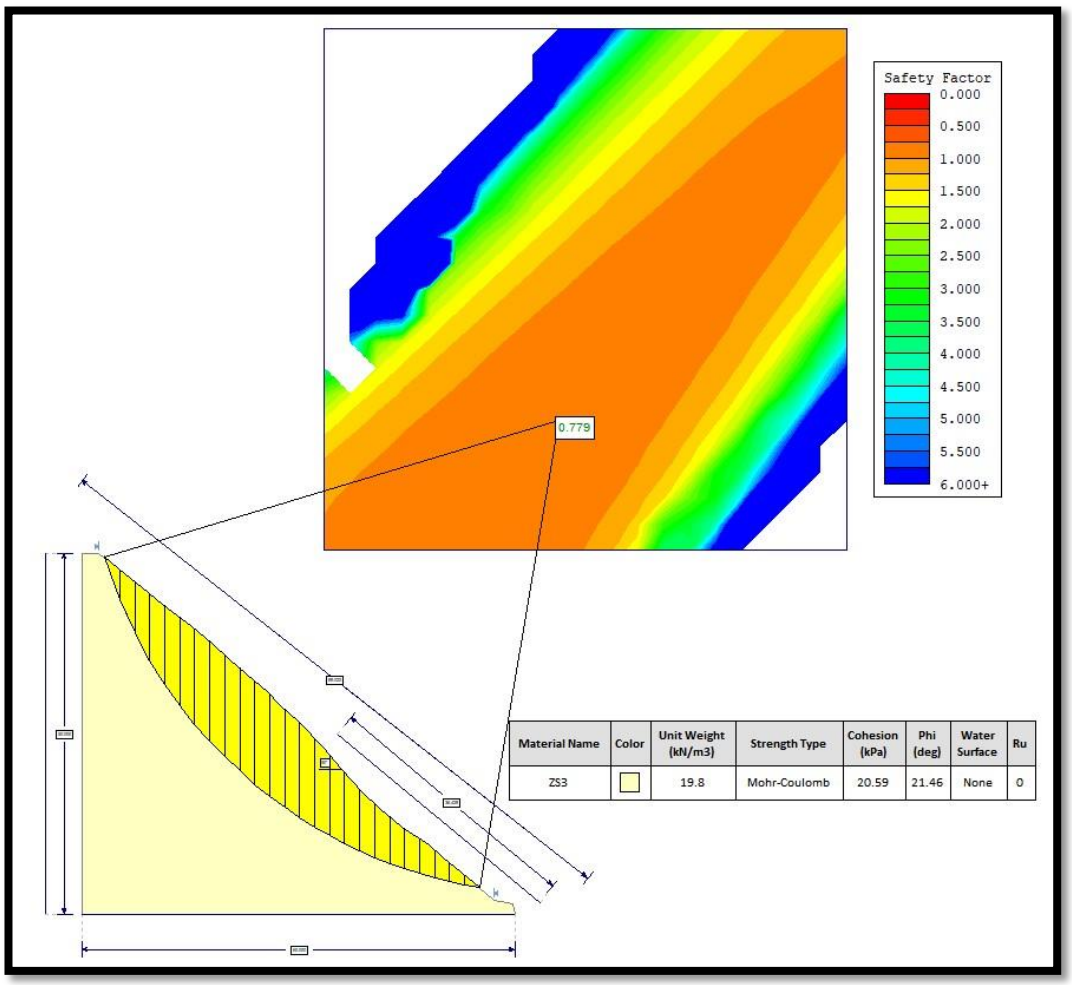

Figure 5.48. LEM plot for ZS3 (GLE/Morgenstren-price Method)

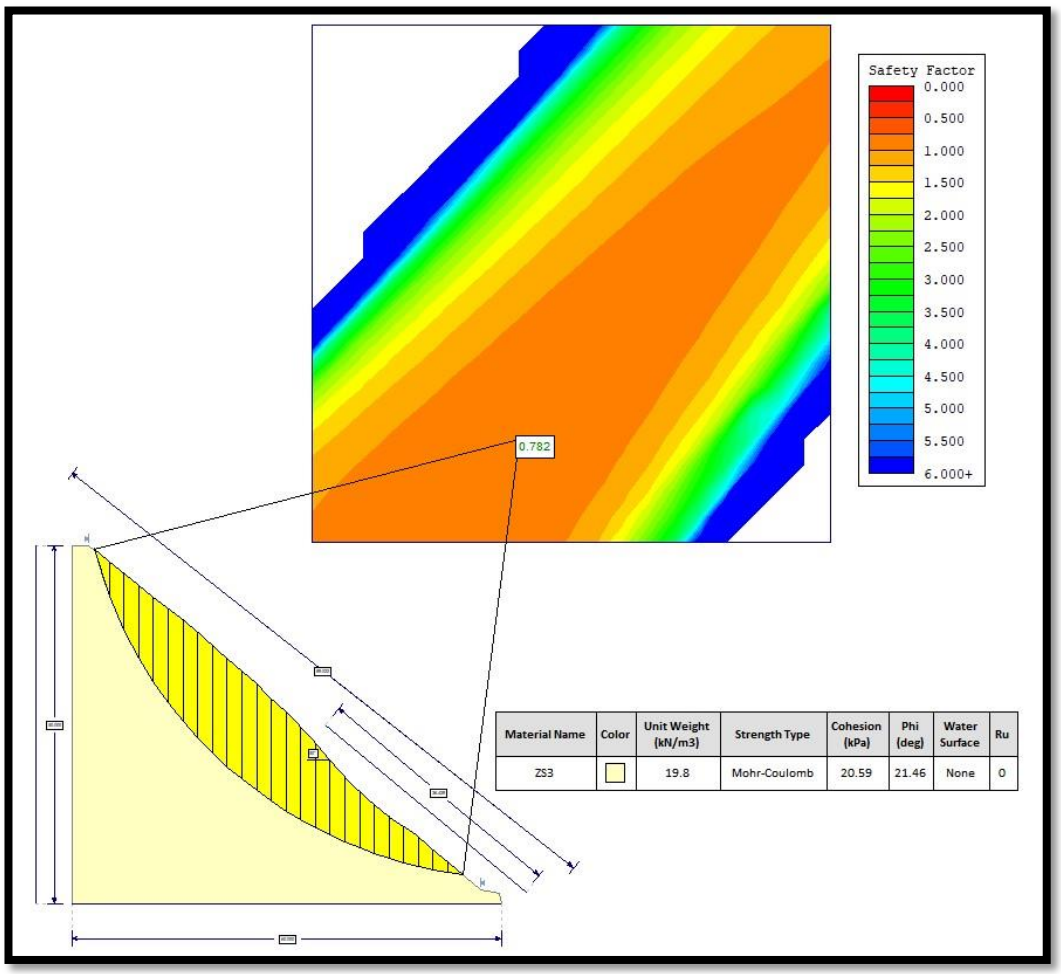

Figure 5.49. LEM plot for ZS3(Janbu corrected Method)

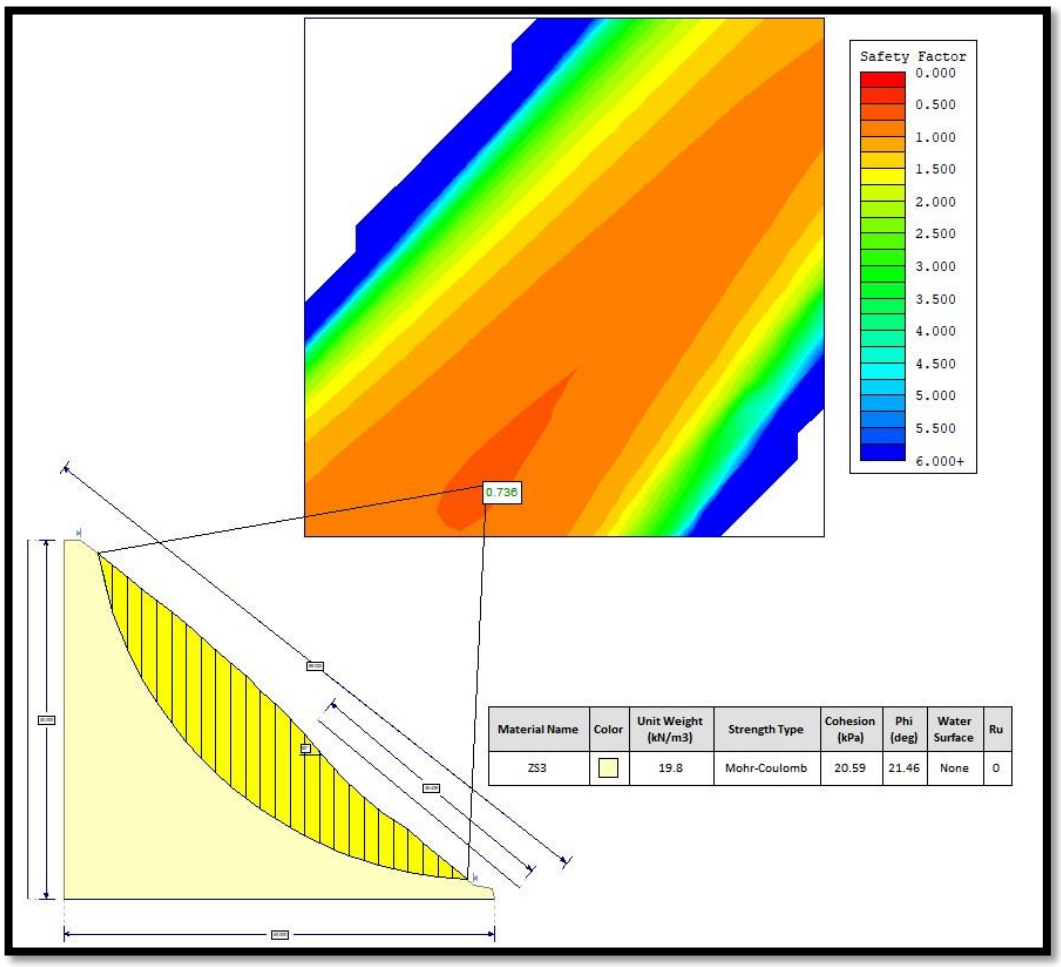

Figure 5.50. LEM plot for ZS3(Janbu simplified Method)

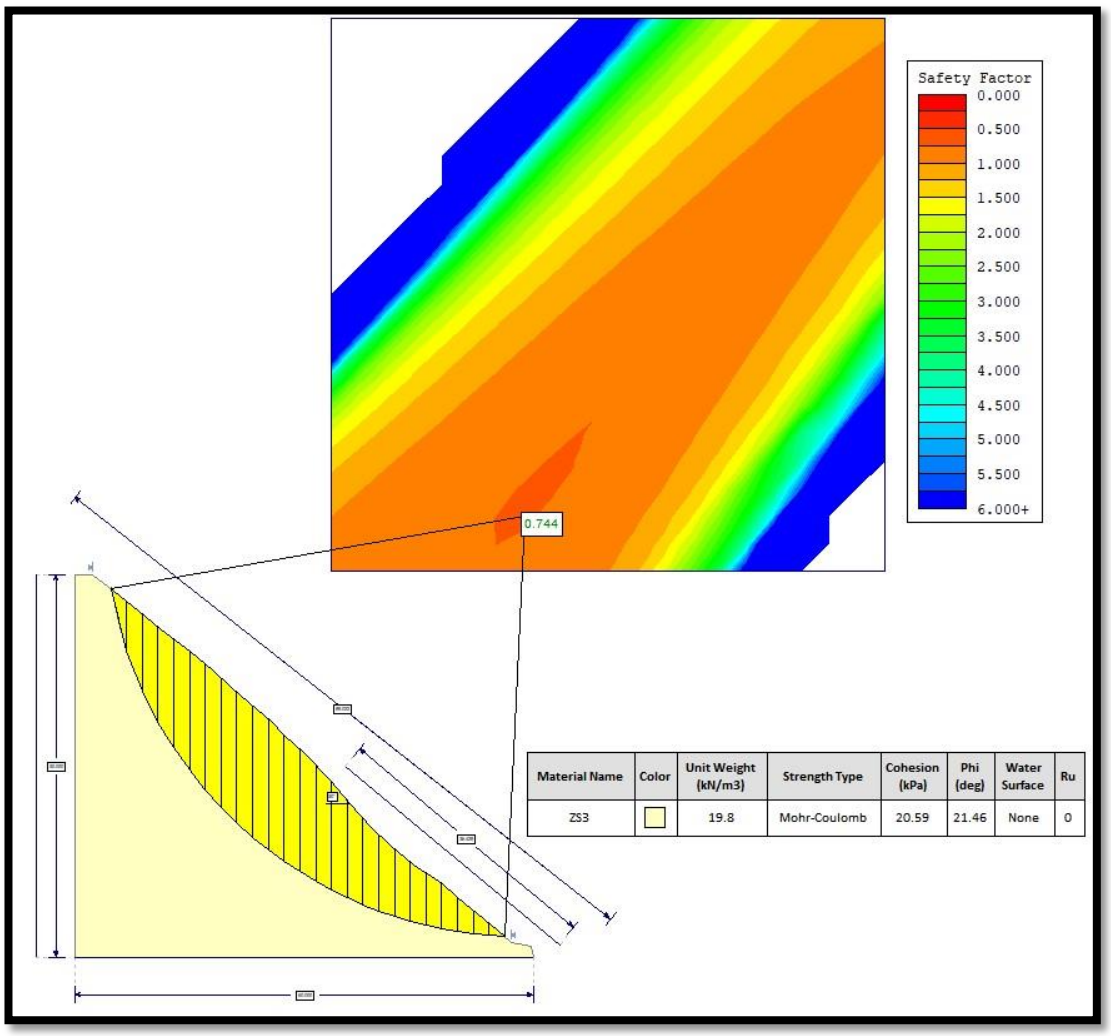

Figure 5.51. LEM plot for ZS3(Ordinary/Fellenius Method)

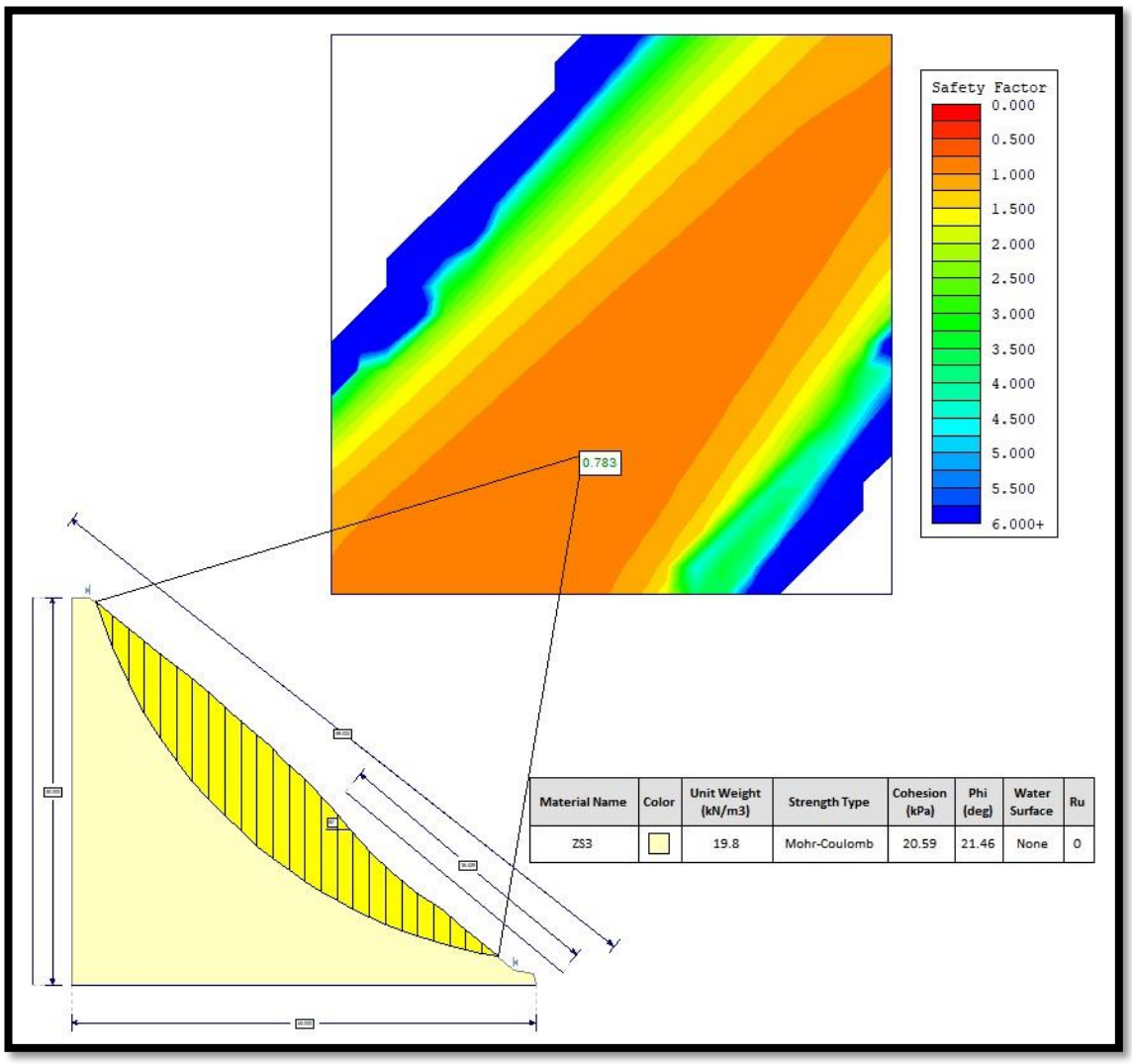

Figure 5.52. LEM plot for ZS3(Spencer Method)

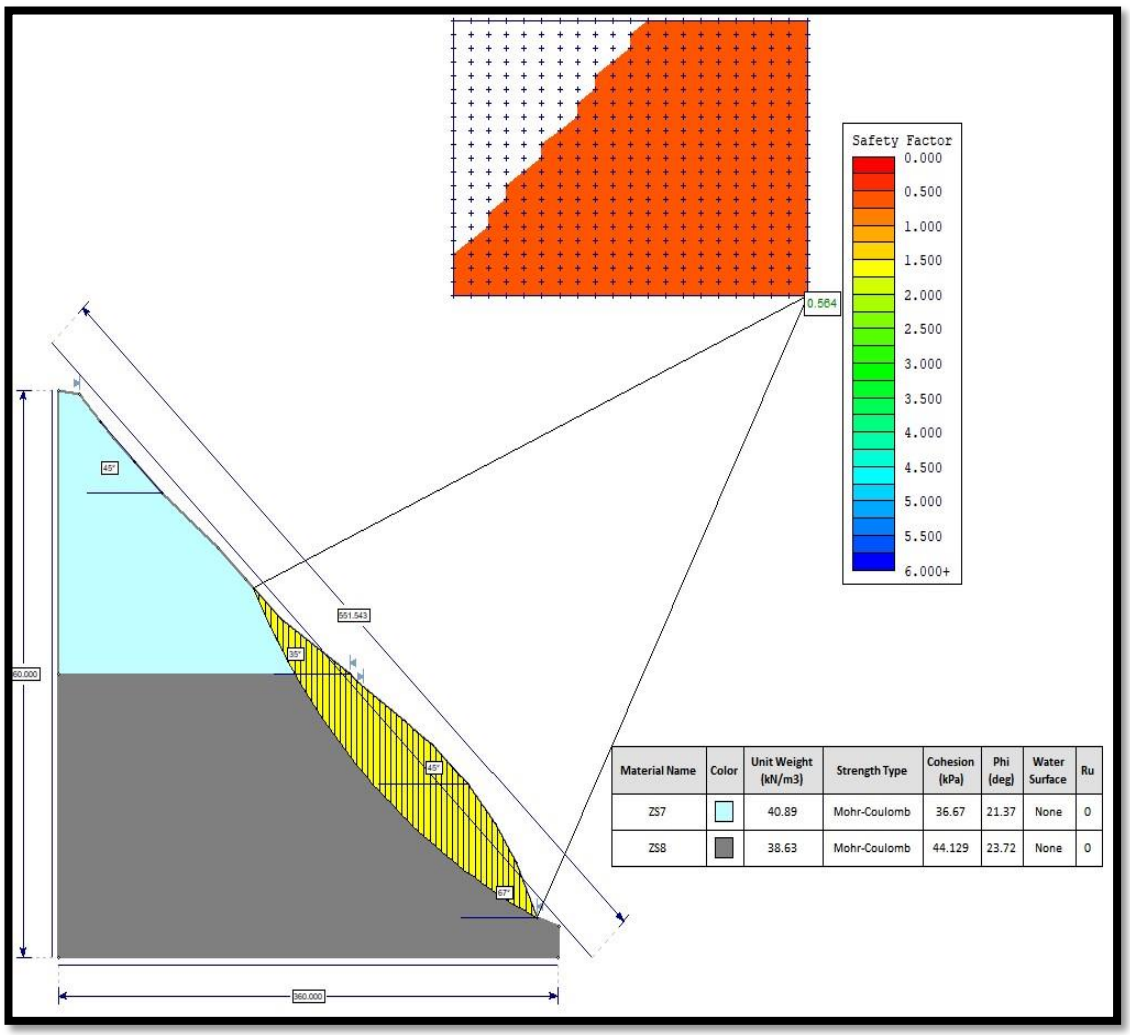

Figure 5.53. LEM plot for ZS7 & ZS8 (Bishop simplified Method)

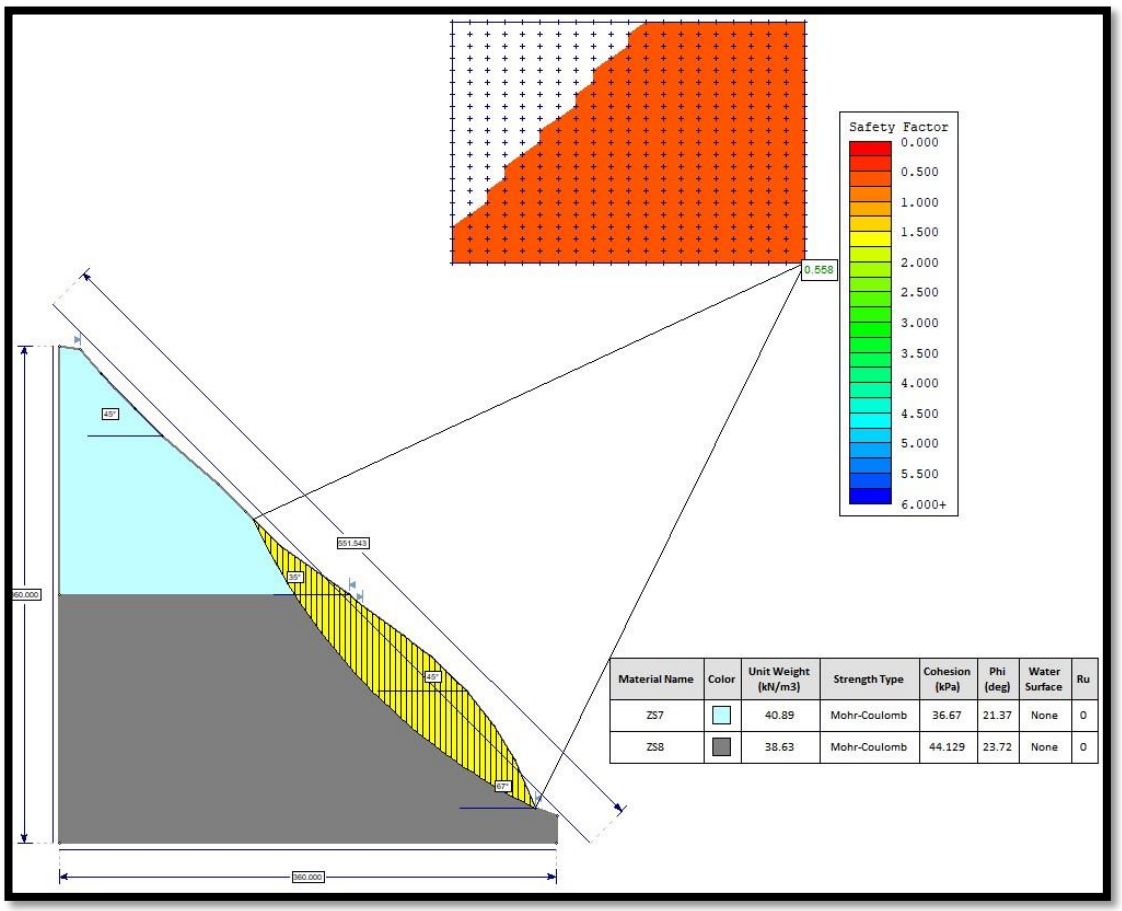

Figure 5.54. LEM plot for ZS7 & ZS8 (GLE/Morgenstren-price Method)

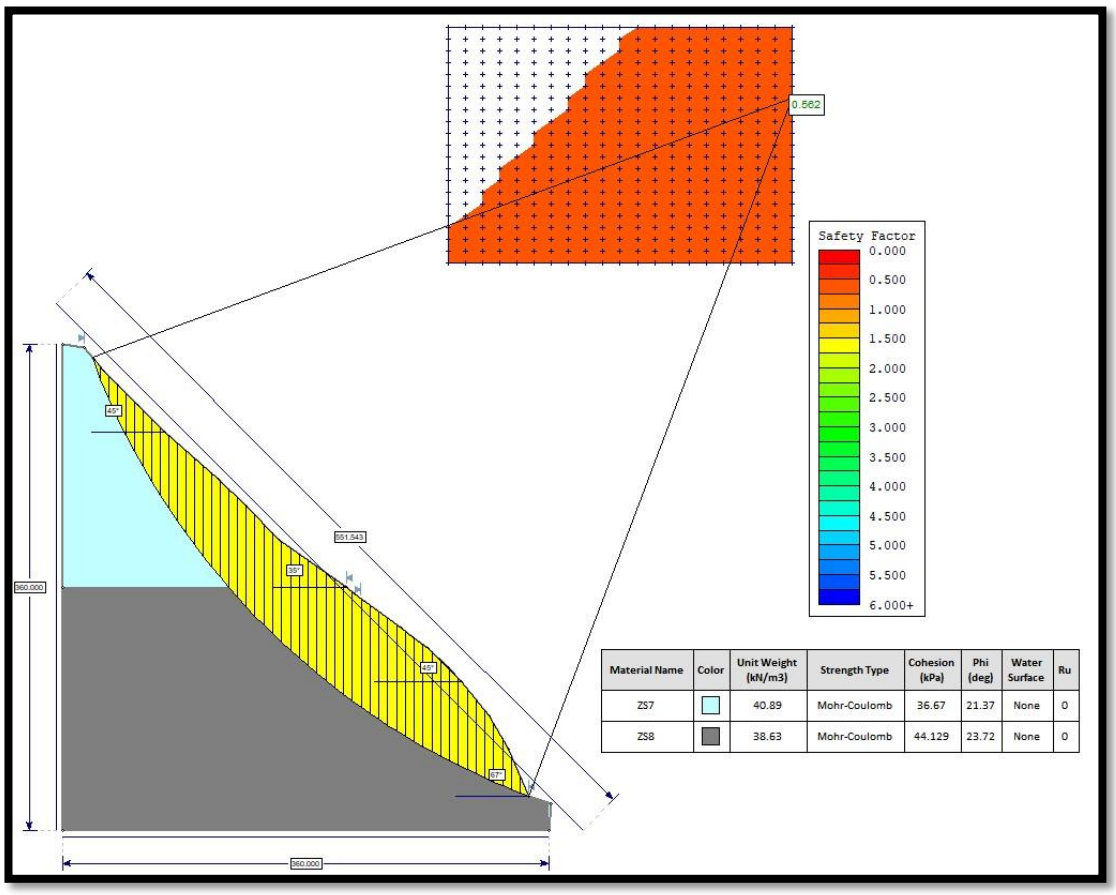

Figure 5.55. LEM plot for ZS7 & ZS8 (Janbu corrected Method)

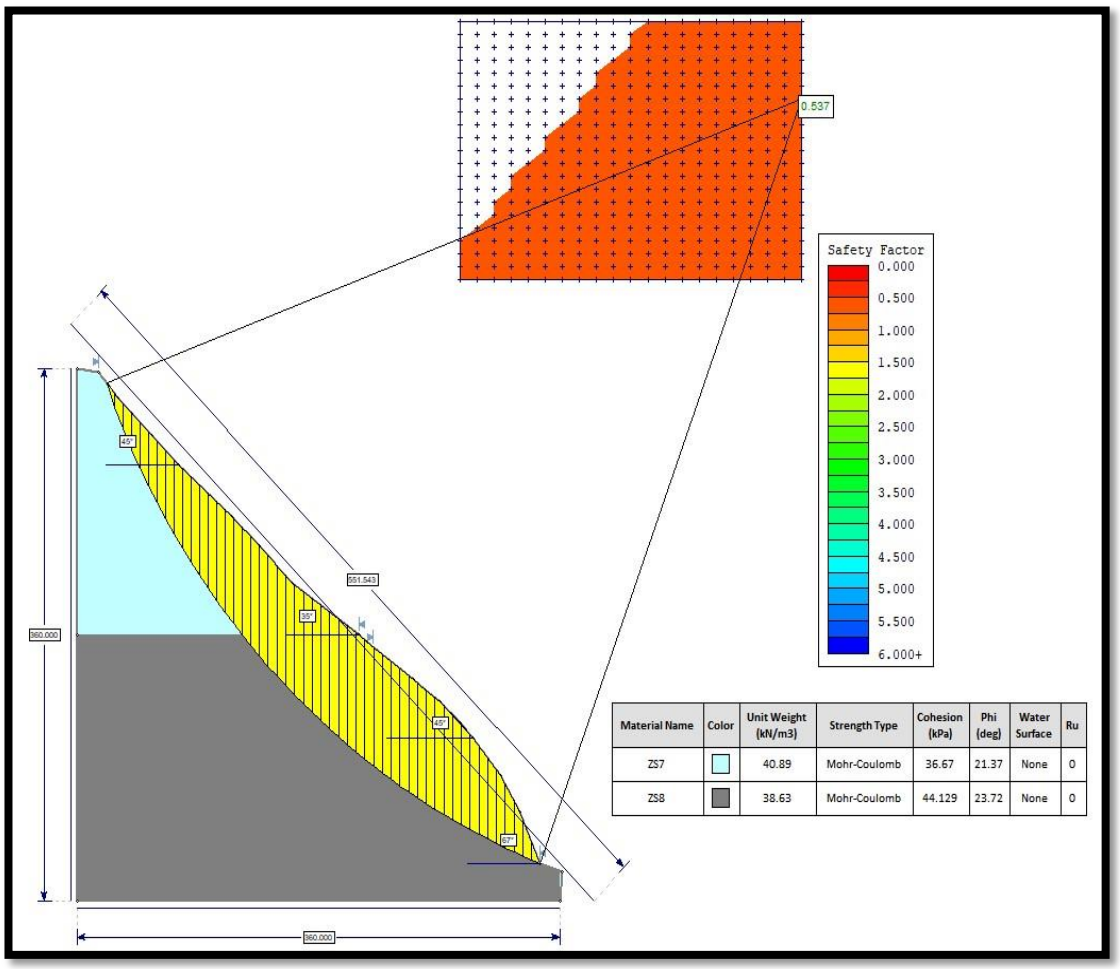

Figure 5.56. LEM plot for ZS7 & ZS8 (Janbu simplified Method)

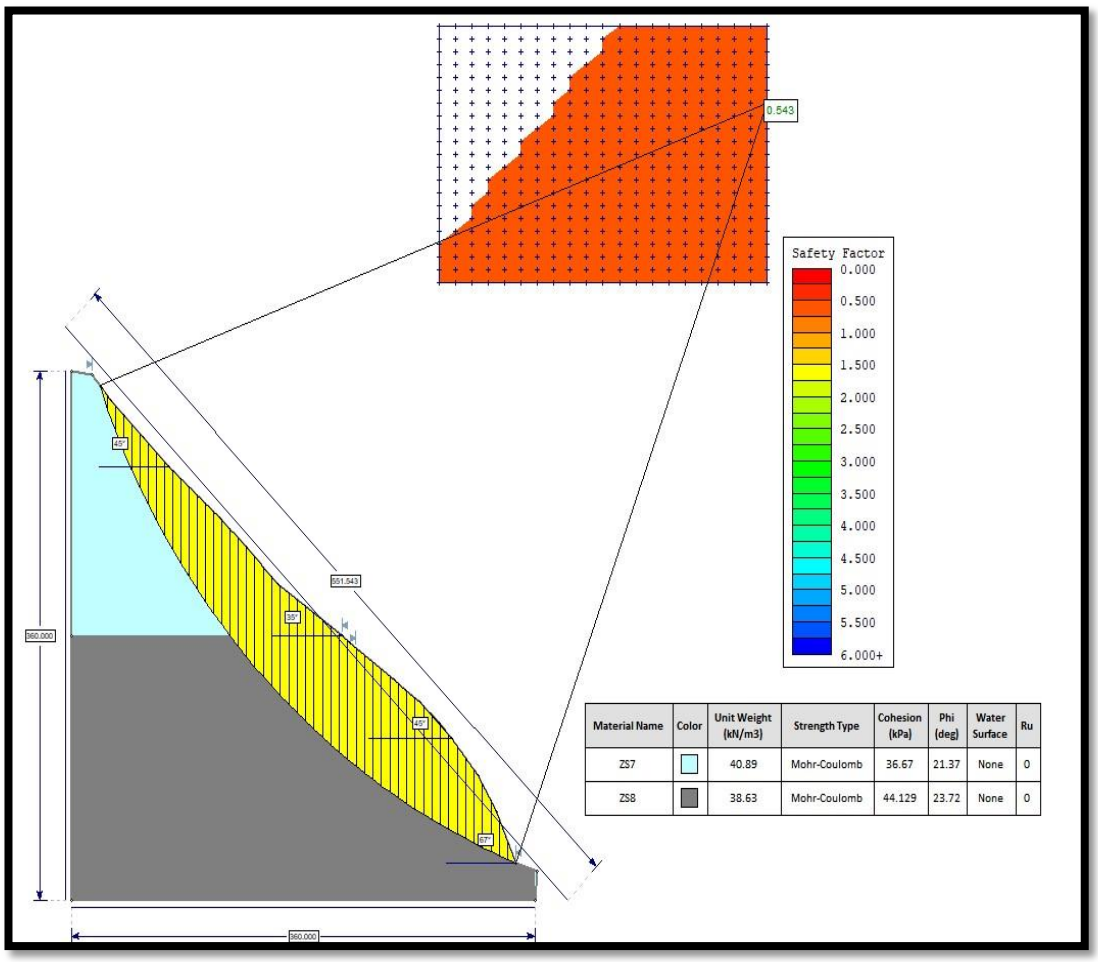

Material Name	Color	Unit Weight (kN/m3)	Strength Type	Cohesion (kPa)	Phi (deg)	Water Surface	Ru
ZS7		40.89	Mohr-Coulomb	36.67	21.37	None	0
ZS8		38.63	Mohr-Coulomb	44.129	23.72	None	0

Figure 5.57. LEM plot for ZS7 & ZS8 (Ordinary Method)

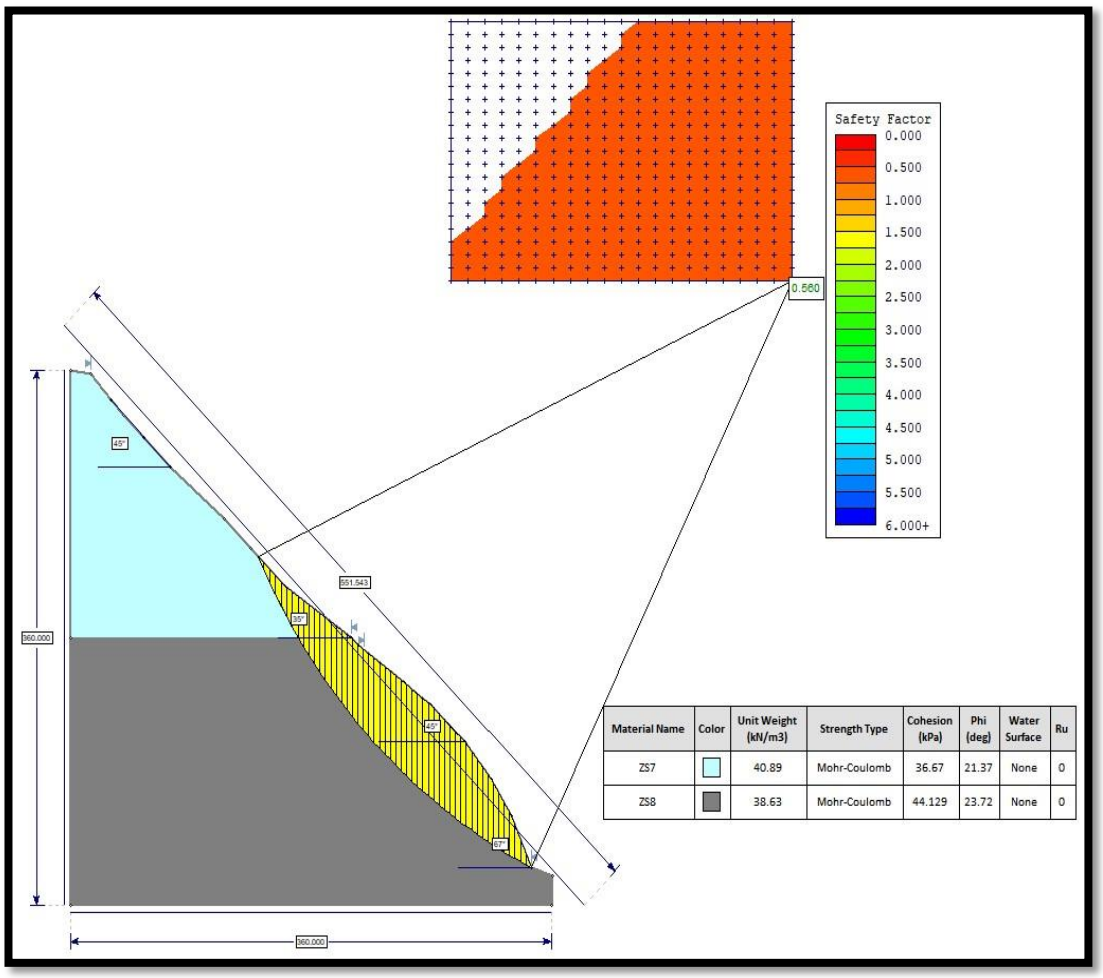

Figure 5.58. LEM plot for ZS7 & ZS8 (Spencer Method)

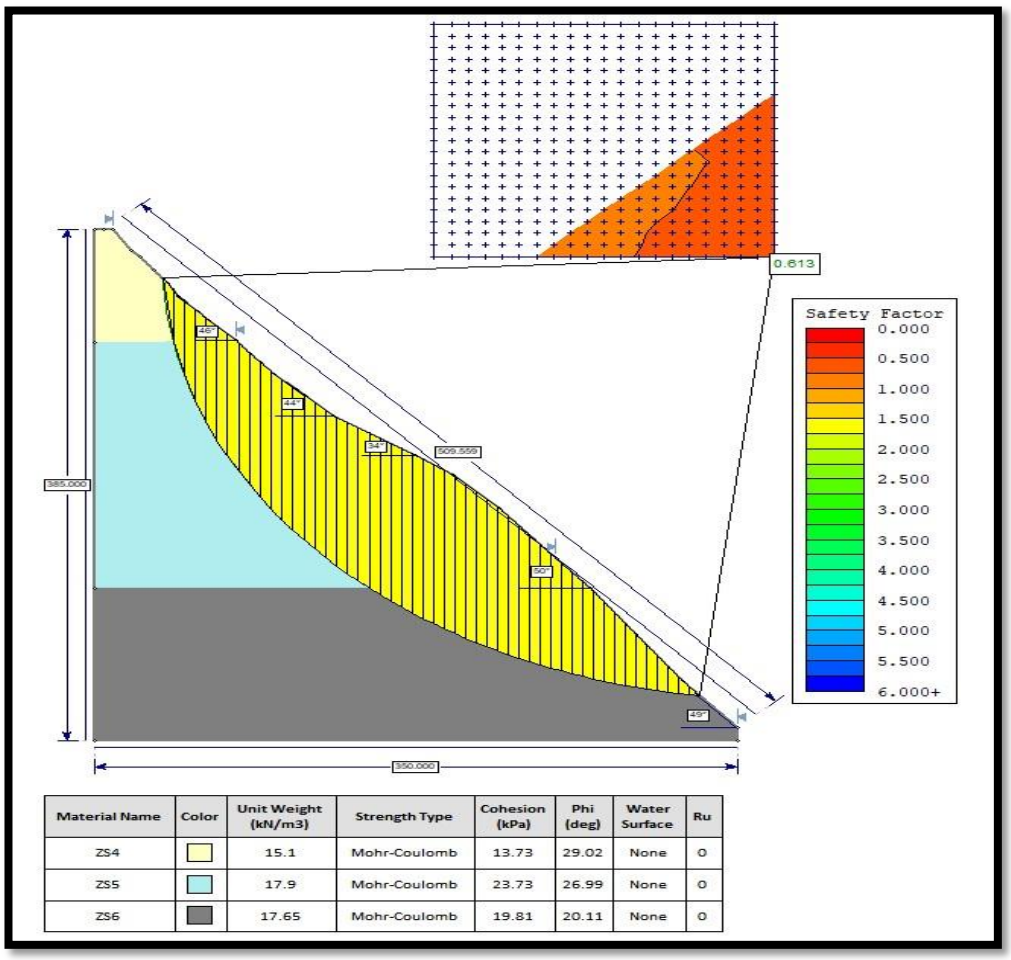

Material Name	Color	Unit Weight (kN/m3)	Strength Type	Cohesion (kPa)	Phi (deg)	Water Surface	Ru
ZS4		15.1	Mohr-Coulomb	13.73	29.02	None	0
ZS5		17.9	Mohr-Coulomb	23.73	26.99	None	0
ZS6		17.65	Mohr-Coulomb	19.81	20.11	None	0

Figure 5.59. LEM plot for ZS4,ZS5 & ZS6 (Bishop simplified Method)

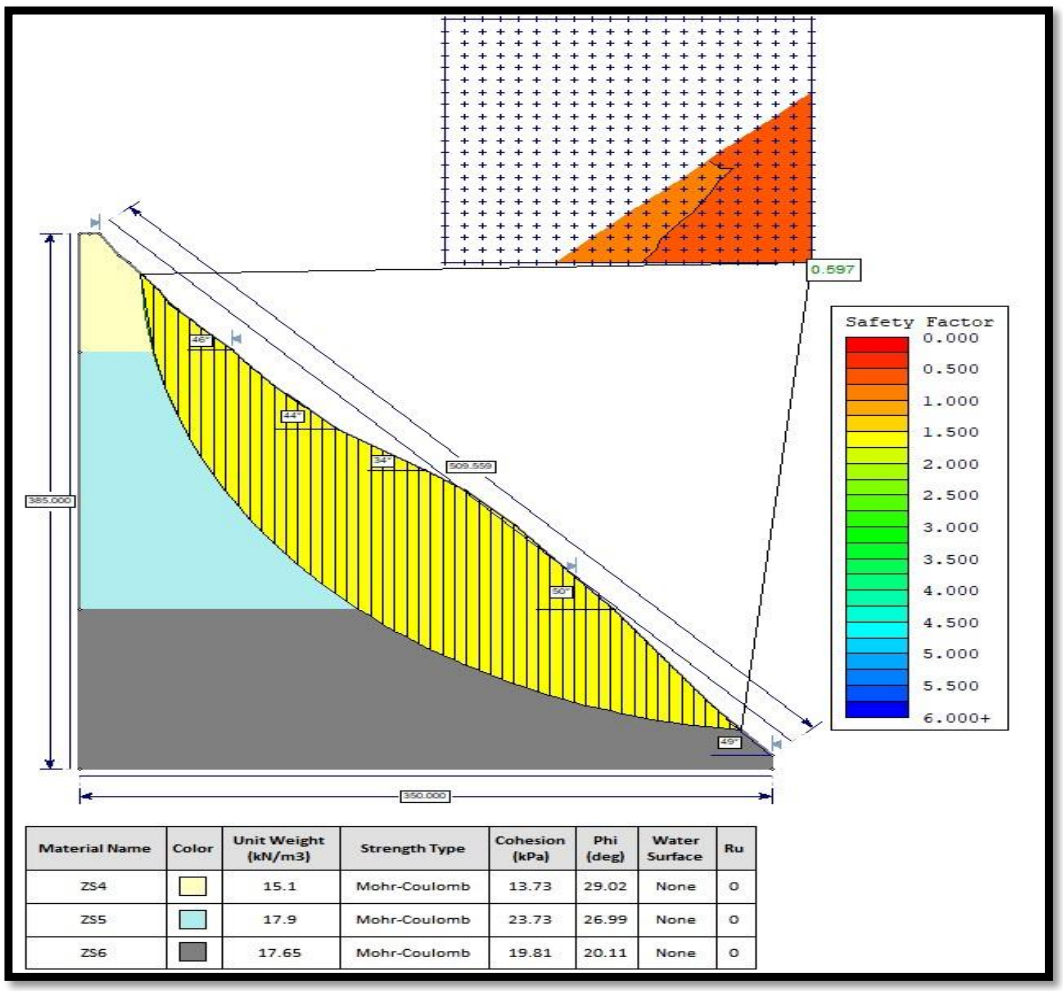

Material Name	Color	Unit Weight (kN/m3)	Strength Type	Cohesion (kPa)	Phi (deg)	Water Surface	Ru
ZS4		15.1	Mohr-Coulomb	13.73	29.02	None	0
ZS5		17.9	Mohr-Coulomb	23.73	26.99	None	0
ZS6		17.65	Mohr-Coulomb	19.81	20.11	None	0

Figure 5.60. LEM plot for ZS4,ZS5 & ZS6 (GLE/Morgenstren-price Method)

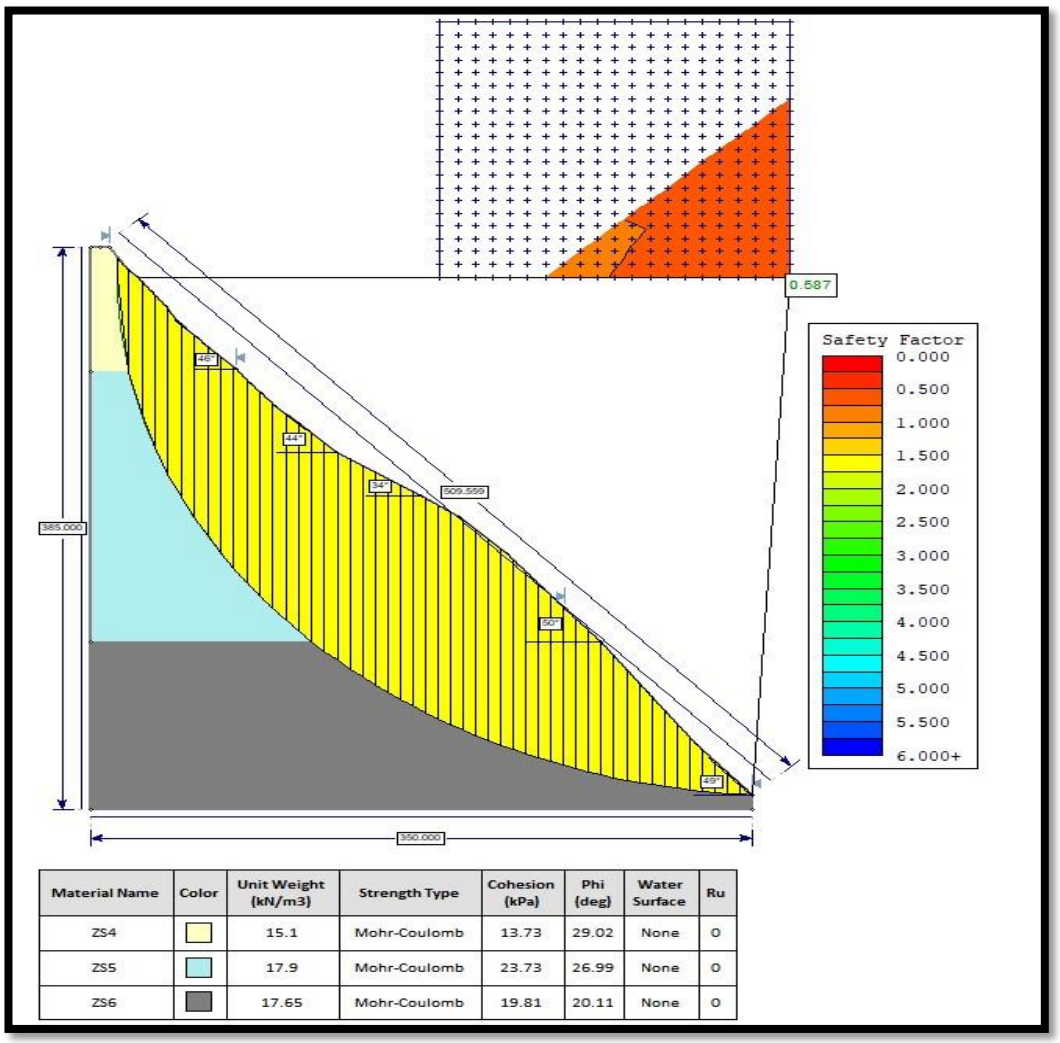

Material Name	Color	Unit Weight (kN/m3)	Strength Type	Cohesion (kPa)	Phi (deg)	Water Surface	Ru
ZS4		15.1	Mohr-Coulomb	13.73	29.02	None	0
ZS5		17.9	Mohr-Coulomb	23.73	26.99	None	0
ZS6		17.65	Mohr-Coulomb	19.81	20.11	None	0

Figure 5.61. LEM plot for ZS4,ZS5 & ZS6 (Janbu corrected Method)

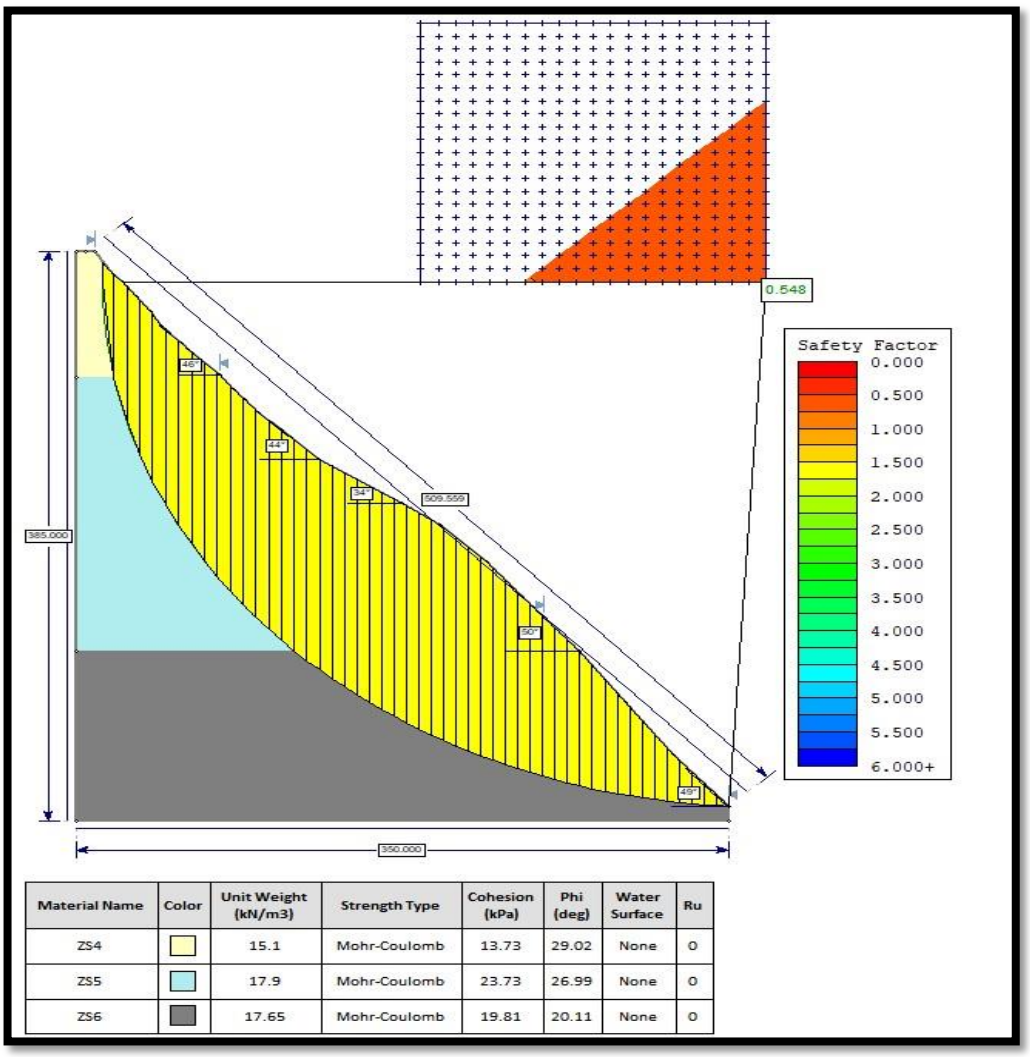

Material Name	Color	Unit Weight (kN/m3)	Strength Type	Cohesion (kPa)	Phi (deg)	Water Surface	Ru
ZS4		15.1	Mohr-Coulomb	13.73	29.02	None	0
ZS5		17.9	Mohr-Coulomb	23.73	26.99	None	0
ZS6		17.65	Mohr-Coulomb	19.81	20.11	None	0

Figure 5.62. LEM plot for ZS4,ZS5 & ZS6 (Janbu simplified Method)

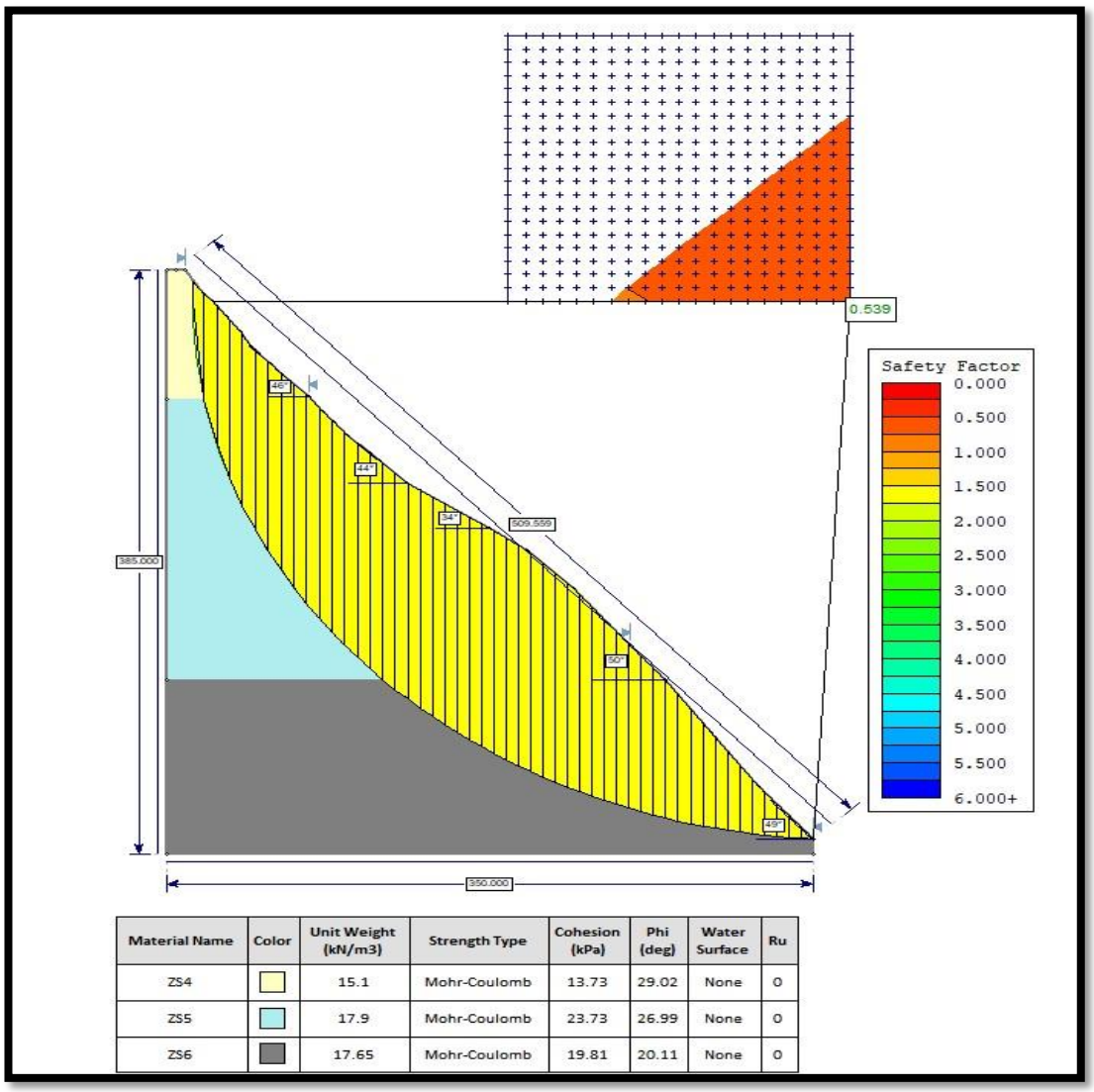

Material Name	Color	Unit Weight (kN/m3)	Strength Type	Cohesion (kPa)	Phi (deg)	Water Surface	Ru
ZS4		15.1	Mohr-Coulomb	13.73	29.02	None	0
ZS5		17.9	Mohr-Coulomb	23.73	26.99	None	0
ZS6		17.65	Mohr-Coulomb	19.81	20.11	None	0

Figure 5.63. LEM plot for ZS4,ZS5 & ZS6 (Ordinary Method)

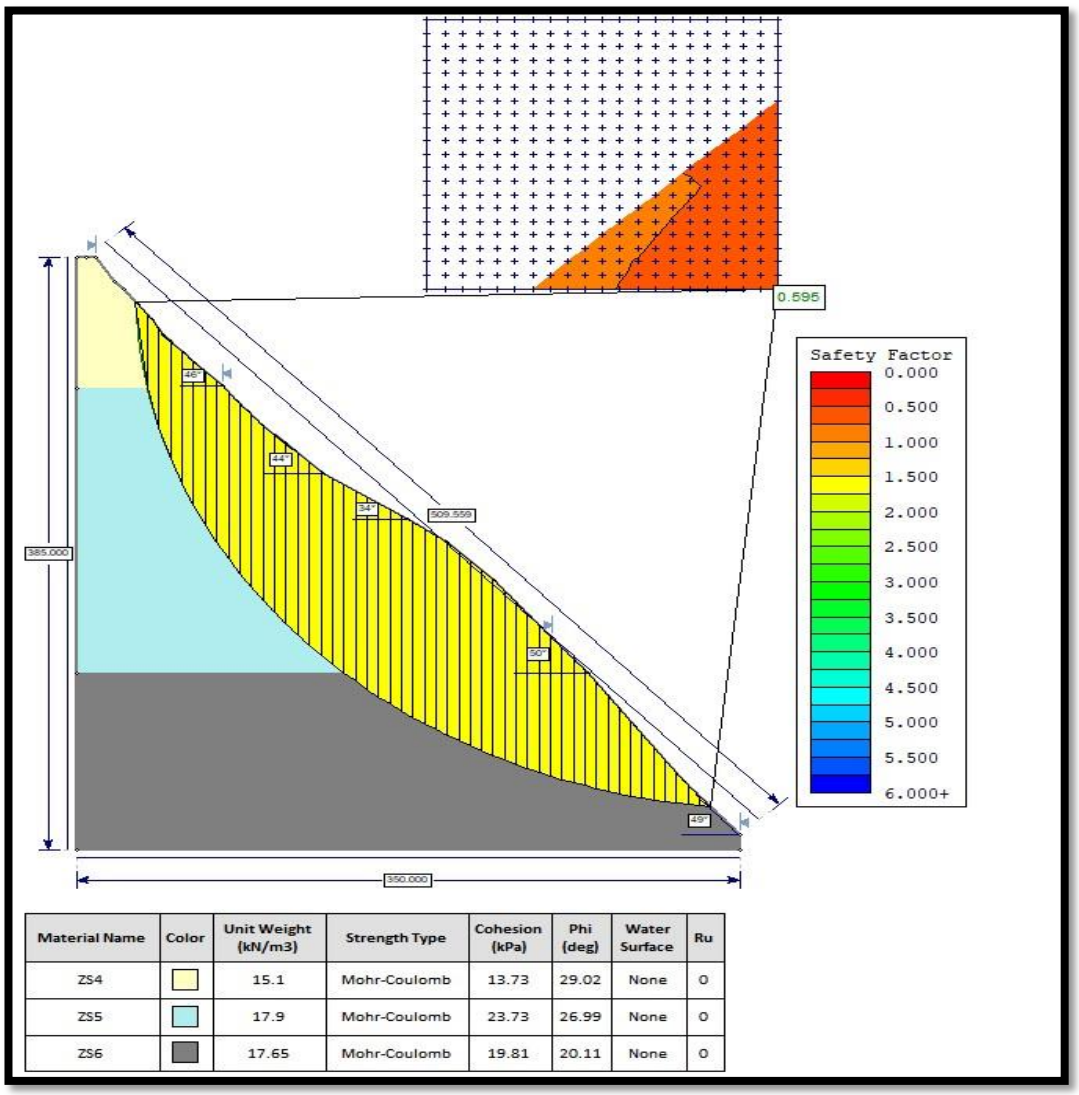

Material Name	Color	Unit Weight (kN/m3)	Strength Type	Cohesion (kPa)	Phi (deg)	Water Surface	Ru
ZS4		15.1	Mohr-Coulomb	13.73	29.02	None	0
ZS5		17.9	Mohr-Coulomb	23.73	26.99	None	0
ZS6		17.65	Mohr-Coulomb	19.81	20.11	None	0

Figure 5.64. LEM plot for ZS4,ZS5 & ZS6 (Spencer Method)

The slope stability analysis conducted using the Limit Equilibrium Method (LEM) at both locations 1 and 2 indicates that the calculated factor of safety (FoS) is below 1. This finding implies that the slopes at these locations are susceptible to failure under the existing conditions. A factor of safety below 1 suggests that the resisting forces within the slope (such as soil shear strength) are insufficient to counterbalance the destabilizing forces (such as gravity and external loads), increasing the risk of slope instability and potential failure.

5.1.3.2 Slope Stability Analysis from Direct Shear and Triaxial Test Parameters

From the direct shear and soil triaxial parameters obtained from ZS1 and ZS7, slope stability analysis was carried out using the Limit Equilibrium Method for finding the Factor of Safety.Since, the study consists of bedrock and slope failure occurred at a shallow depth above the bedrock which shows a characteristics of Infinite slope instability.Therefore, Direct shear test of soil in the study area was sufficient to determine the characteristics of soil and hence their shear strength. The FoS value obtained from direct shear and triaxial parameters are given in Table 5.16 and Figure 5.65 to 5.70.

Table 5.16: Factors of Safety obtained from direct shear and soil triaxial parameters

Method	**ZS1**		**ZS7**	
	Direct Shear (FoS)	Triaxial (FoS)	Direct Shear (FoS)	Triaxial (FoS)
Bishop Simplified	0.82	0.81	0.62	0.56
GLE/ Morgenstern-Price	1.33	1.2	0.62	0.56
Janbu Corrected	0.92	0.9	0.62	0.56
Janbu Simplified	0.86	0.85	0.59	0.53
Ordinary/Fellenius	0.83	0.82	0.59	0.54
Spencer	1.18	1.16	0.62	0.56

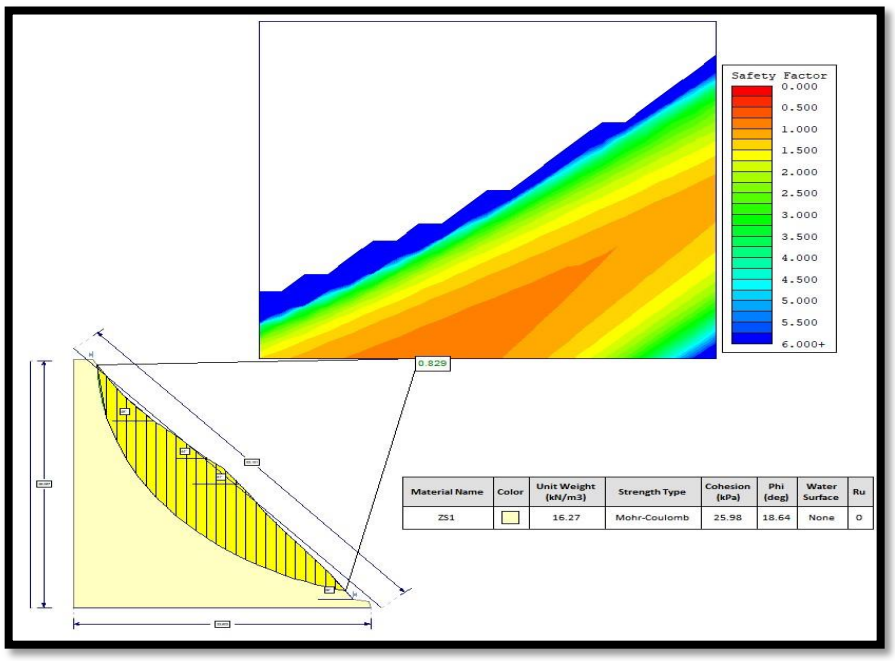

(a)

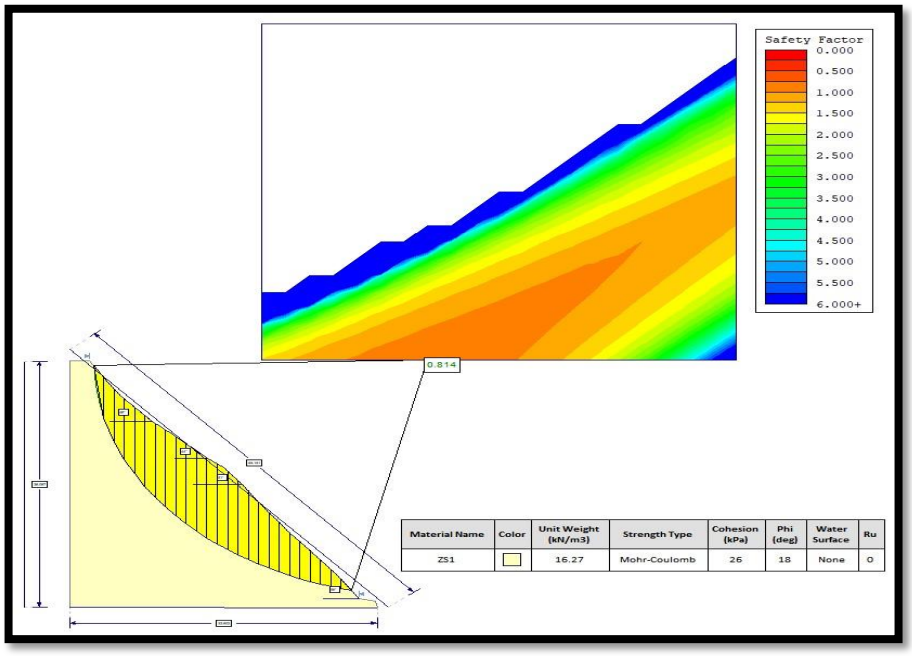

(b)

Figure 5.65. LEM plot for ZS1 (Bishop simplified method), (a) Direct Shear (b) Triaxial

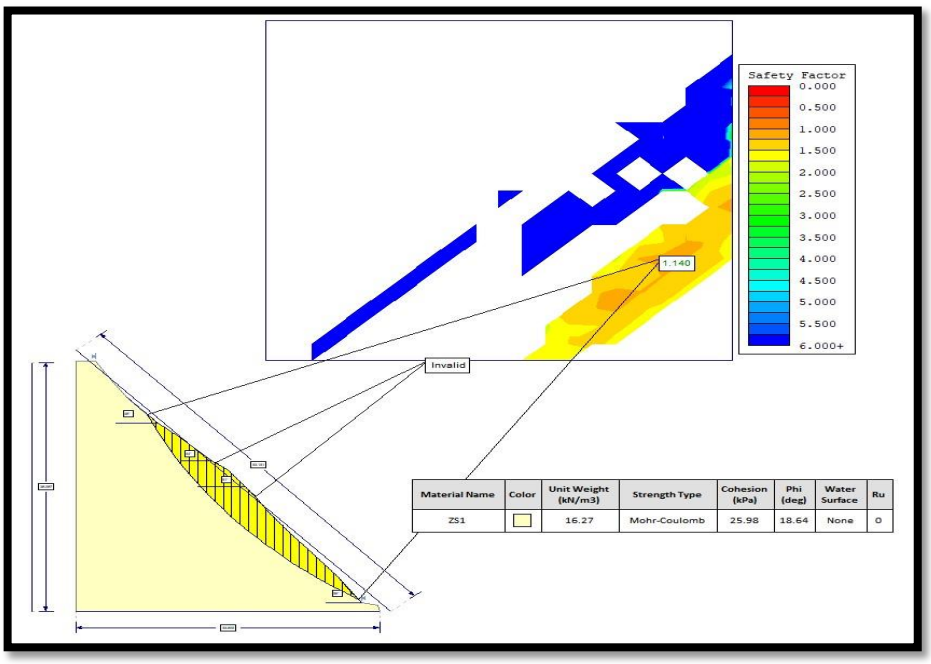

(2)

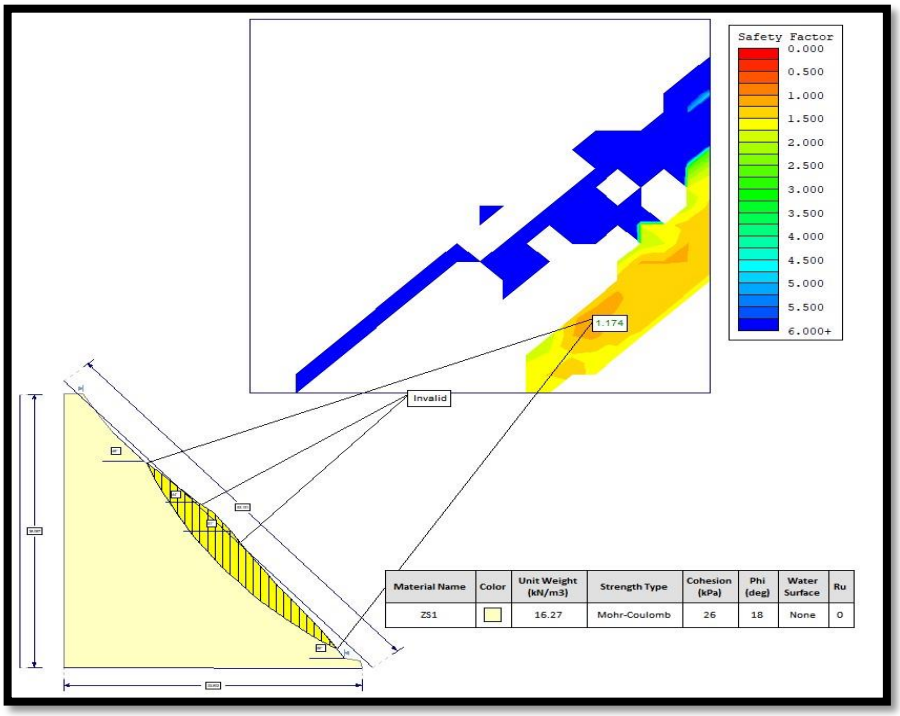

(b)

Figure 5.66. LEM plot for ZS1 (Spencer), (a) Direct Shear (b) Triaxial

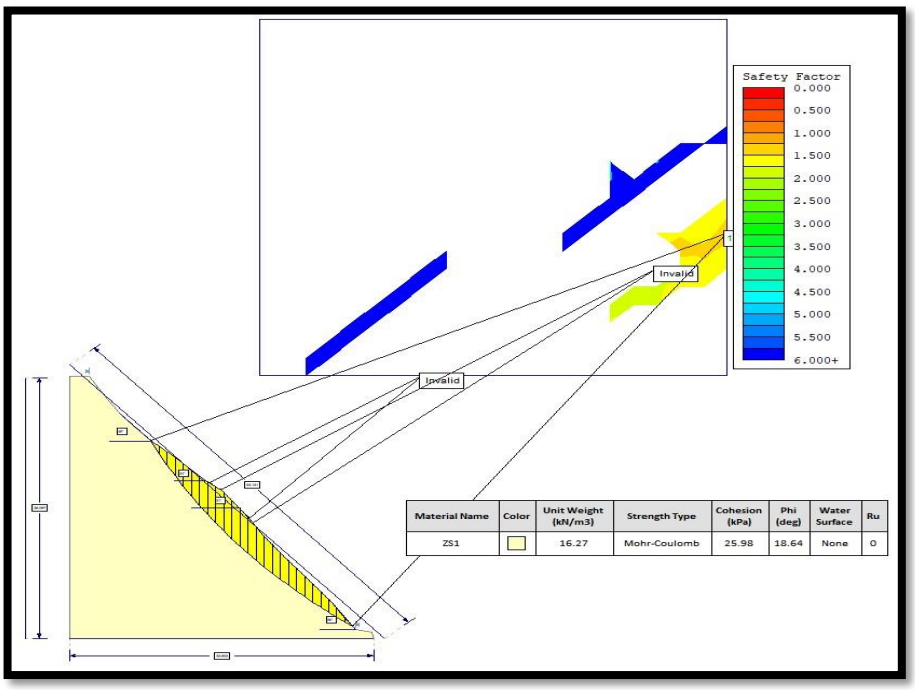

(a)

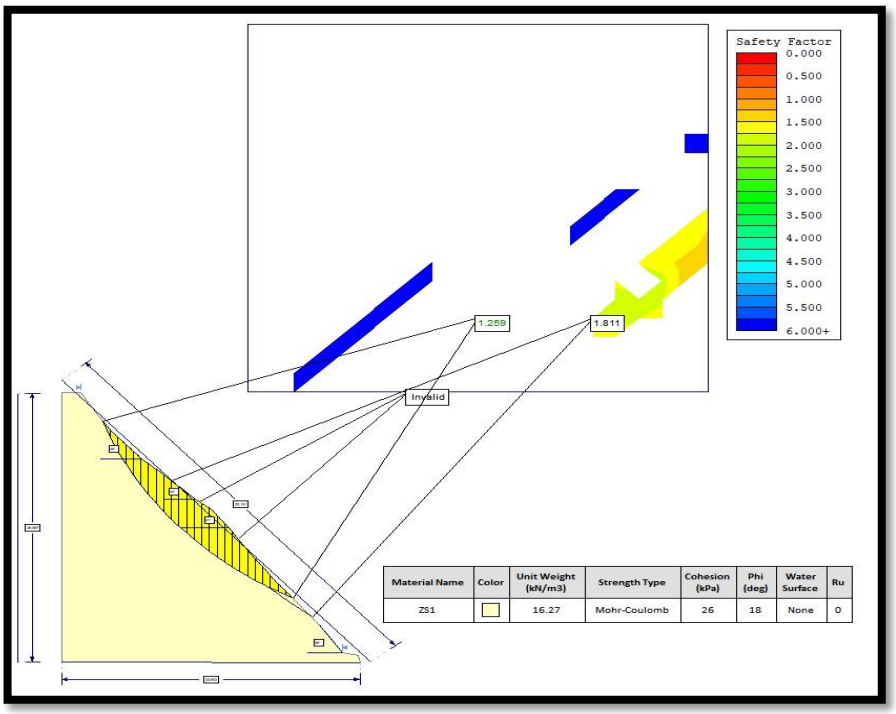

(b)

Figure 5.67. LEM plot for ZS1 (GLE/Morgenstren-price Method), (a) Direct Shear (b) Triaxial

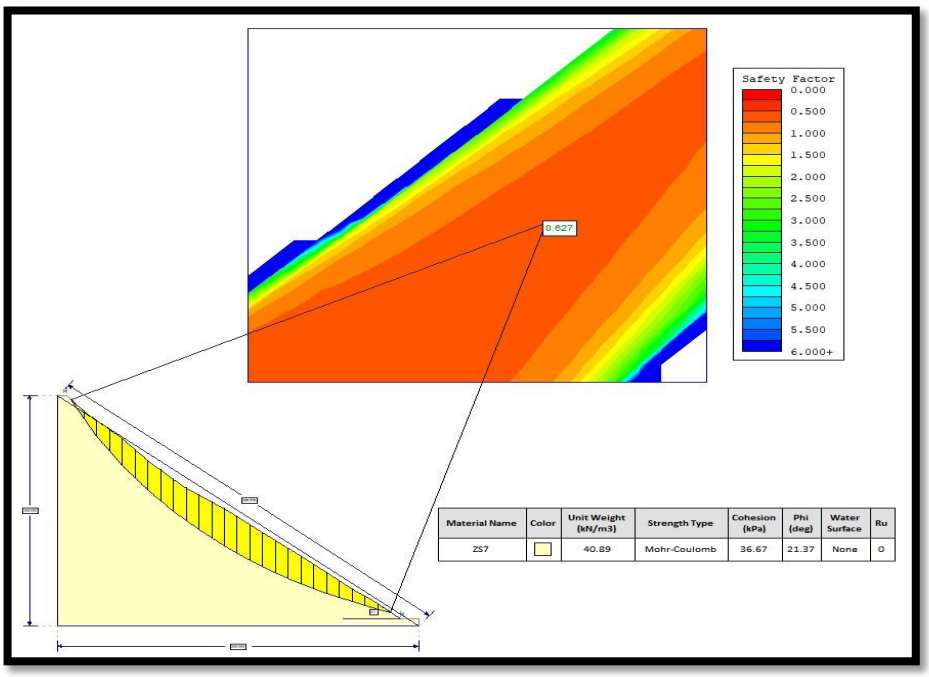

(a)

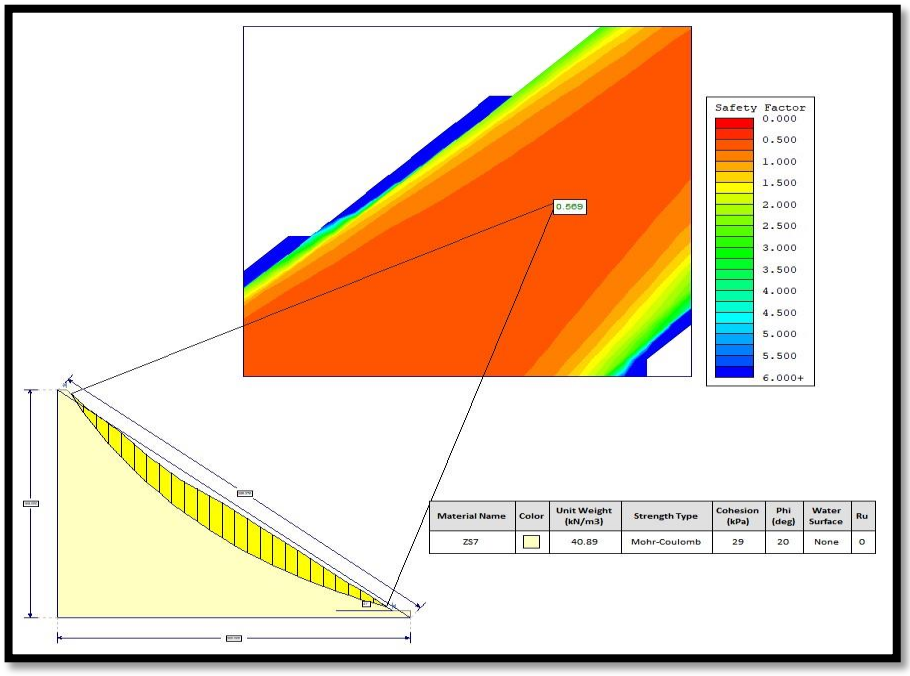

(b)

Figure 5.68. LEM plot for ZS7 (Bishop simplified method), (a) Direct Shear (b) Triaxial

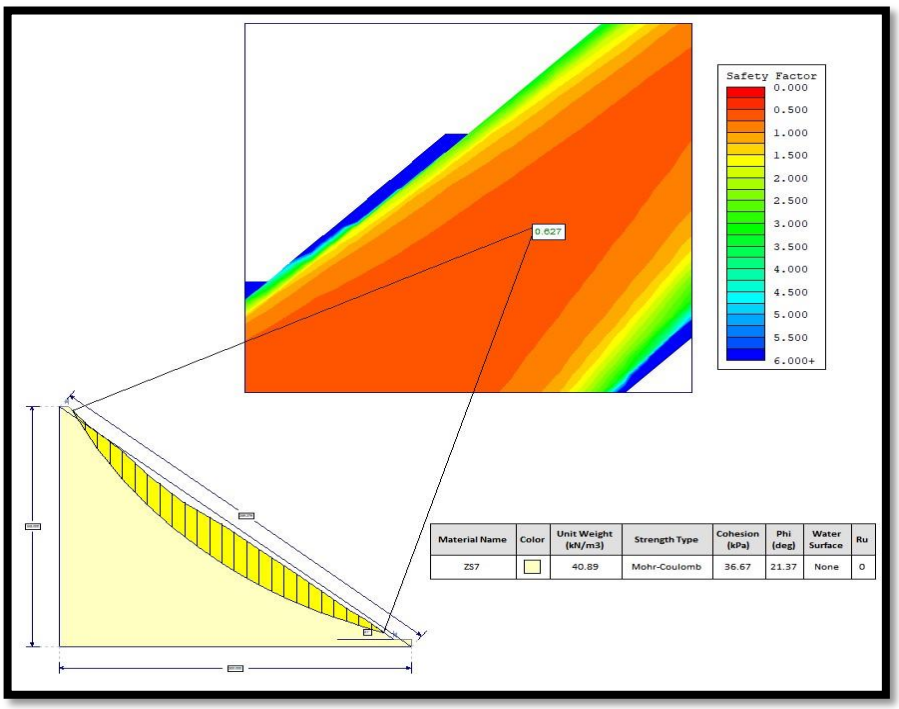

(a)

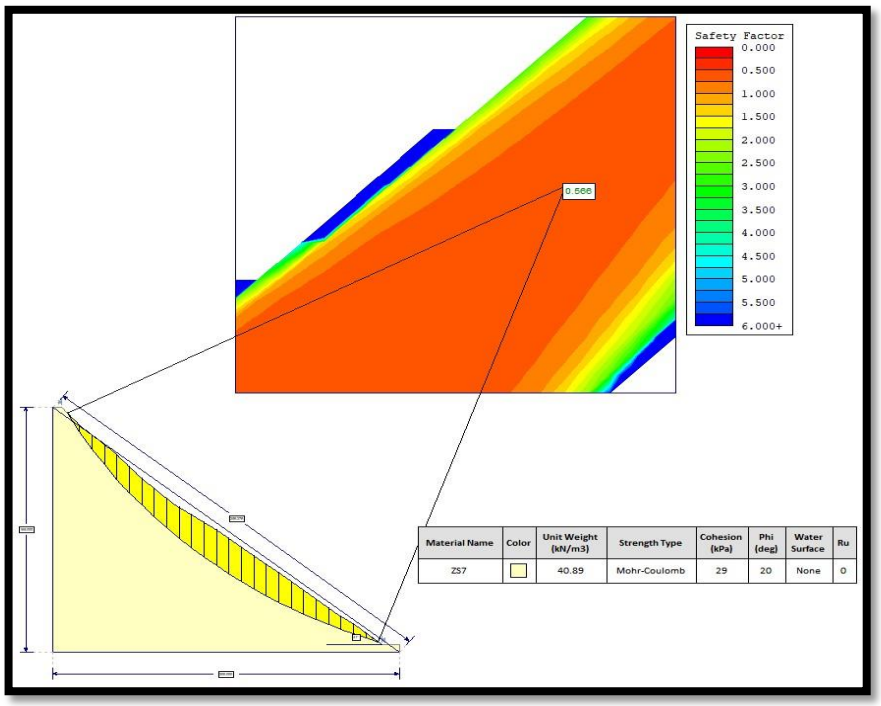

(b)

Figure 5.69. LEM plot for ZS7 (Spencer method), (a) Direct Shear (b) Triaxial

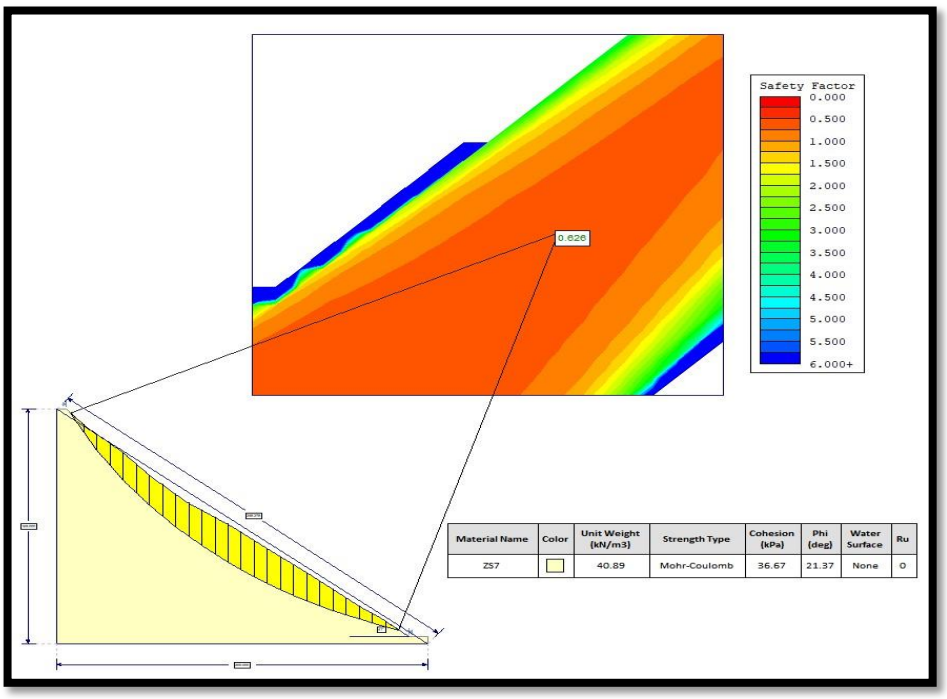

(a)

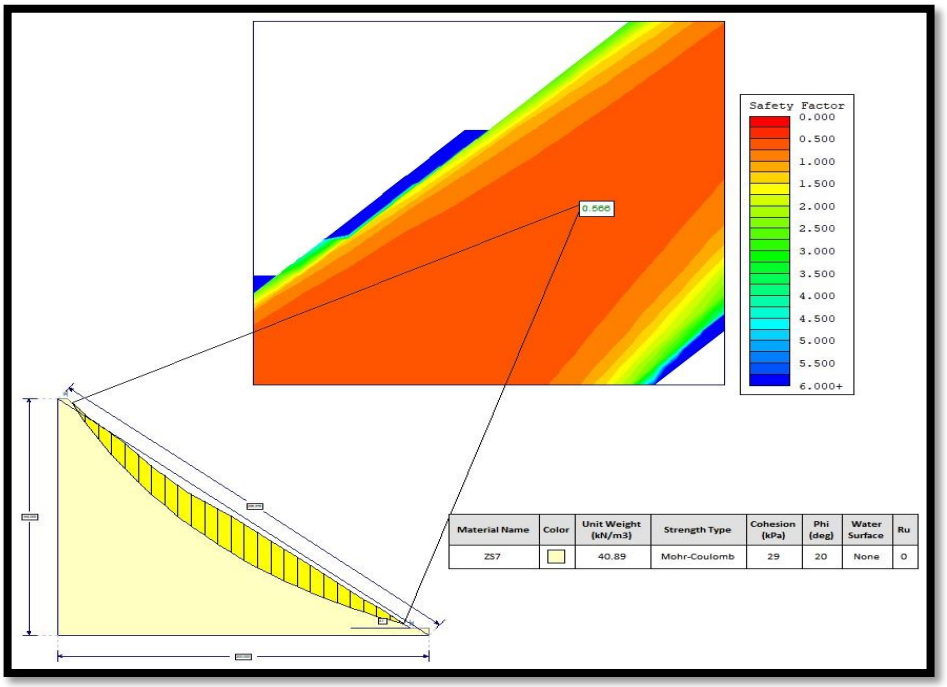

(b)

Figure 5.70. LEM plot for ZS7 (GLE/Morgenstern-price Method), (a) Direct Shear (b) Triaxial

The factor of safety for ZS1 and ZS7 obtained from the direct shear test is higher compared to the triaxial test in almost all the methods. There is a decimal difference in the FoS between the two tests.

5.1.4 ROCK ANALYSIS

Rock sampling was done in location 1 and location 2. Five rock samples were collected from L1(Figure 5.71) and ten samples from L2 (Figure 5.72). In rock analysis methods, slake durability test, point load strength index, rock mass rating, and kinematic analysis are performed.

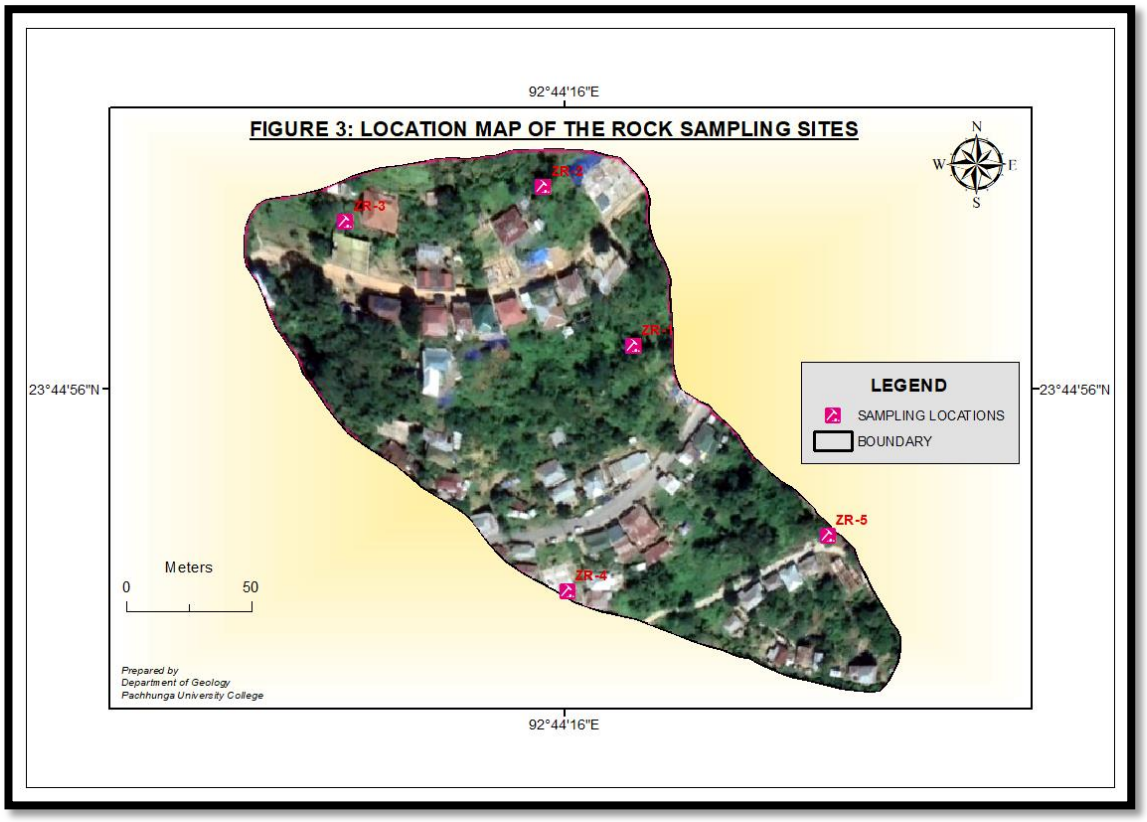

Figure 5.71. Rock sample location map for location-1

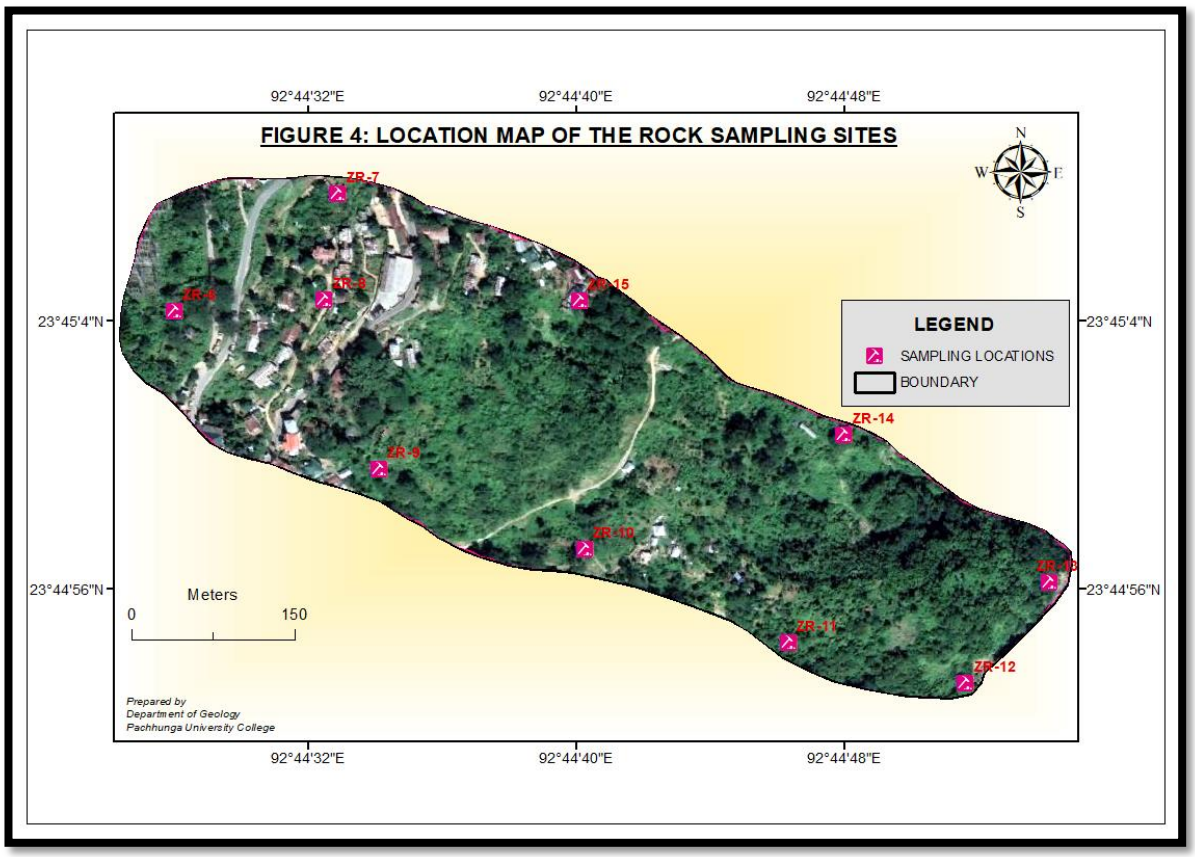

Figures 5.72. Rock sample location map for location-2

5.1.4.1 Slake Durability Test

The slake durability test assesses the ability of rock samples to withstand disintegration under repeated cycles of wetting and drying. The test was conducted according to the guidelines outlined in IS: 10050-1981. The results obtained for location 1 and location 2 are presented in Tables 5.17 and 5.18 respectively. Disintegrated samples in different cycles are given in Figures 5.73 and 5.74.

According to the findings, it was observed that the rock fragments increased in quantity with each successive cycle of the slake durability test, as illustrated in Figure 5.75. This trend suggests that the rock samples exhibited decreasing durability over multiple wetting and drying cycles. The increase in rock fragments indicates a progressive breakdown of the rock material, which is a critical factor to consider in assessing the long-term stability and durability of rock formations subjected to environmental conditions involving cyclic wetting and drying. The outcomes of the

slake durability test provide valuable insights into the susceptibility of the rock material to weathering and erosion, informing engineering decisions related to construction, infrastructure development, and slope stability in geological environments characterized by alternating moisture conditions.

Table 5.17: Slake Durability Test for Location 1 (After Franklin and Chandra, 1972)

SAMPLE LOCATION	**ROCK TYPES**	**SDI (%) FOR EACH CYCLE**				**ID_2** (%)	**DURABILITY**
		1	2	3	4		
ZR1	Shale with high clay content	95.28	84.97	75.12	60.72	84.97	High
ZR2	Silty Shale	97.82	97.63	83.81	66.33	97.63	Extremely High
ZR3	Shale with high clay content	90.94	82.74	80.26	69.37	82.74	High
ZR4	Clay-Shale	98.01	84.85	76.71	66.06	84.85	High
ZR5	Shale with high clay content	94.82	90.4	80.8	71.96	92.25	Very High

Table 5.18: Slake Durability Test for Location 2 (After Franklin and Chandra, 1972)

Sample No	Rock Types	SDI (%) for each cycle				ID_2 (%)	Durability
		1	2	3	4		
ZR6	Shale with high clay content	99.2	82.74	74.8	69.24	82.74	High
ZR7	Shale with high clay content	81.14	76.43	68.6	65.78	76.43	High
ZR8	Shale with high clay content	95.78	90	74	73	90	High
ZR9	Silty Shale	95	91	77	71	91	Very High
ZR10	Shale with high clay content	85.44	81.26	74.35	70.79	81.26	High
ZR11	Shale with high clay content	88.39	80.11	68.54	58.73	80.11	High
ZR12	Shale with high clay content	88.93	83.51	73.74	65.43	83.51	High
ZR13	Shale with high clay content	91.57	86.11	69.84	66.96	86.11	High
ZR14	Shale with high clay content	97	76.65	80.32	68.65	76.65	High
ZR15	Shale with high clay content	91.71	83.97	80.06	68.65	83.97	High

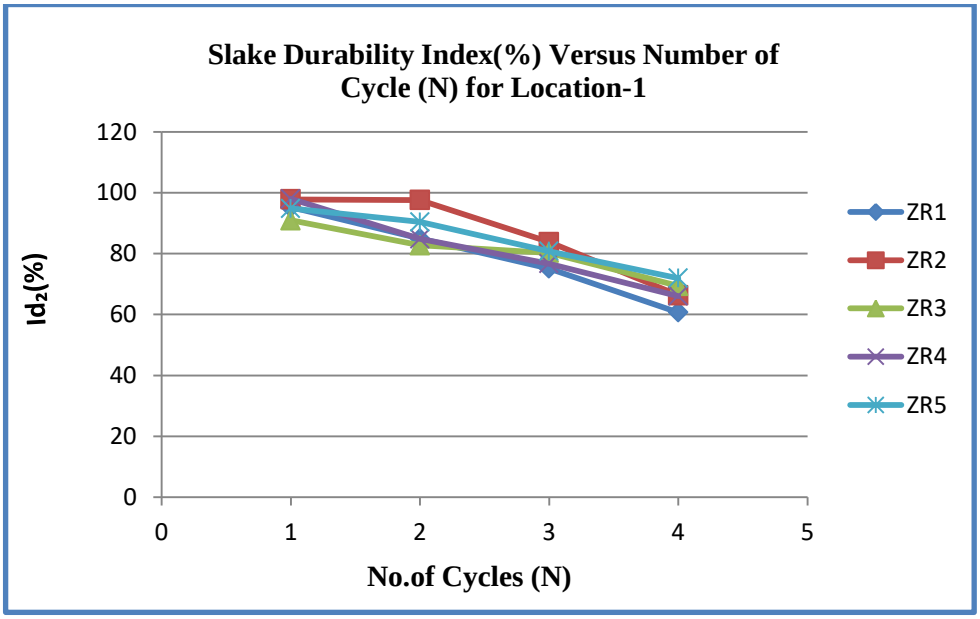

Figure 5.73. Slake Durability Index Vs Number of cycles for location-1

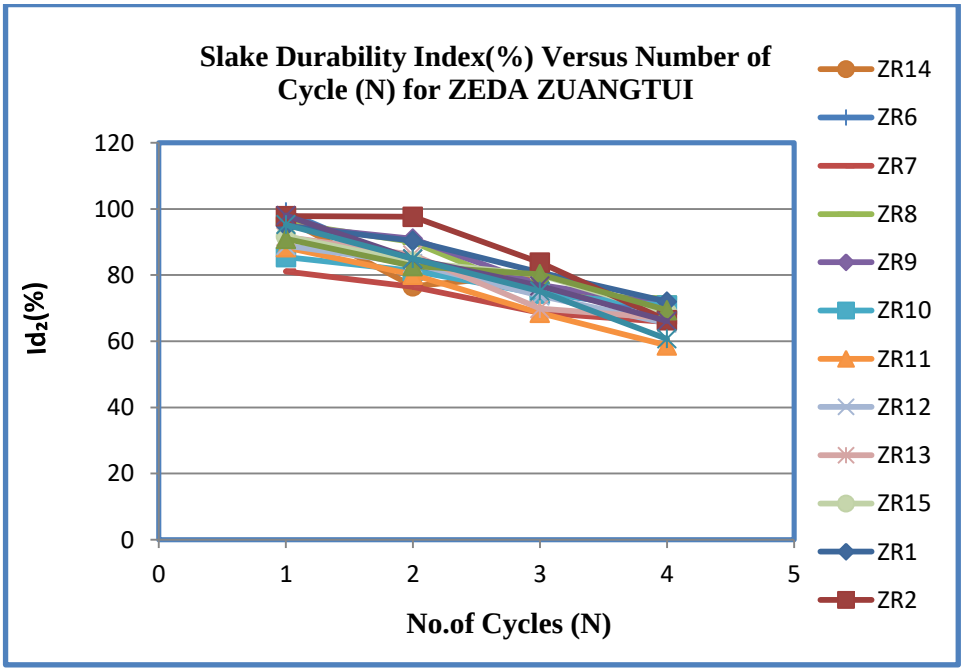

Figure 5.74. Slake Durability Index Vs Number of cycles for location-2

(a) First cycle

(b) Second cycle

(c) Third cycle

(d) fourth cycle

Figure 5.75. Rock fragments in different cycles of slake durability test

Four cycles of the slake durability test were carried out and the readings of the second cycle were taken. Most of the durability falls under high durability in the

second cycle. In location-1, ZR2 has the highest durability and ZR3 has the lowest durability. In location-2 ZR7 and ZR14 have the lowest durability in 2nd cycle of wetting and drying with an ID% of 76.43% and 76.65% respectively.

5.1.4.2 Point Load Index

Samples were collected from the same locations as the slake durability test sample point. The collected samples were prepared as per IS 8764: 1998 and the values are given in Tables 5.19 & 5.20 and Figures 5.76 & 5.77

Table 5.19: Point Load Test for Location 1

LOCATION	ROCK TYPES	PLI (kN)	PLI (kgf/cm^2)	PLI (MPa)	UCS (kgf/cm^2)	UCS (MPa)
ZR1	Shale with high clay content	0.789	18.89	1.8	283.35	27.78
ZR2	Silty Shale	0.97	23.49	2.3	352.41	34.55
ZR3	Silty Shale	0.58	14.04	1.3	210.6	20.65
ZR4	Shale with high clay content	0.43	10.43	1	156.59	16.35
ZR5	Silty Shale	0.89	21.55	2.1	323.35	31

Table 5.20: Point Load Test for Location 2

LOCATION	ROCK TYPE	P(kN)	PLI (kgf/cm^2)	PLI (MPa)	UCS (kgf/cm^2)	UCS (MPa)
ZR6	Clay-shale	0.45	10.89	1.06	163.49	16.03
ZR7	Silty Shale	0.5	12.11	1.18	181.65	17.81
ZR8	Clay-shale	0.4	9.68	0.94	145.2	14.23
ZR9	Clay-shale	0.67	16.22	1.59	243.3	23.85
ZR10	Clay-shale	0.35	8.47	0.83	127.05	12.45
ZR11	Clay-shale	0.45	10.89	1.06	163.35	16.01
ZR12	Clay-shale	0.35	8.47	0.83	127.05	12.45
ZR13	Clay-shale	0.4	9.68	0.94	145.2	14.23
ZR14	Clay-shale	0.5	12.11	1.18	181.65	17.81
ZR15	Clay-shale	0.6	14.53	1.42	217.95	21.37

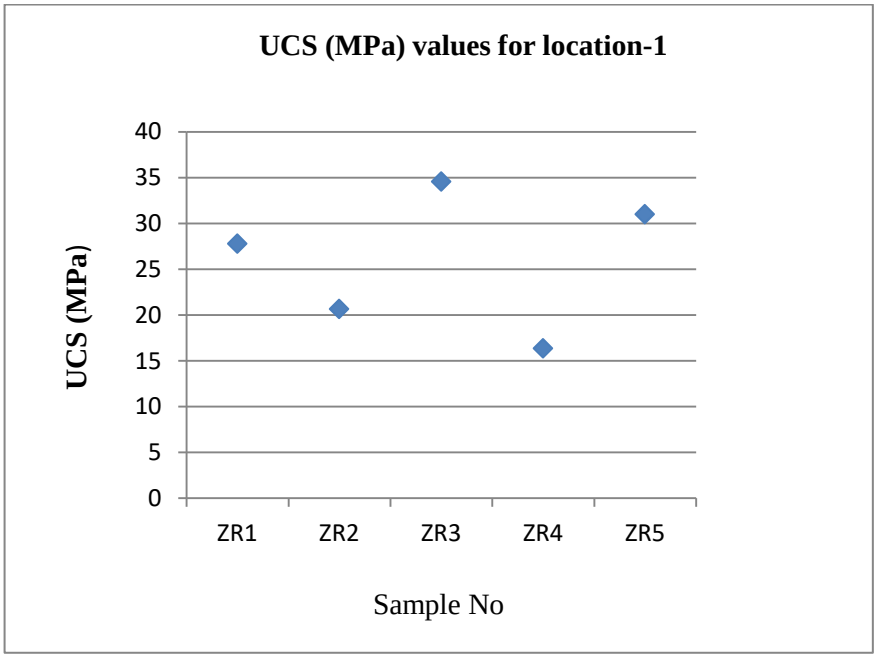

Figure 5.76. Uniaxial Compressive Strength curve for Location-1

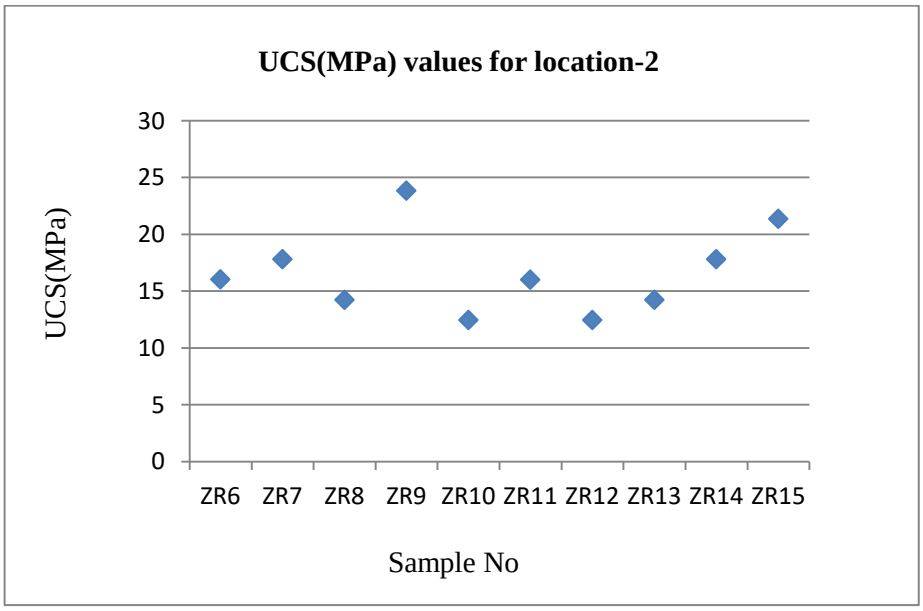

Figure 5.77. Uniaxial Compressive Strength curve for Location-2

The point load index for all the rock samples in both locations is below 2.5MPa. The Uniaxial Compressive Strength is below 20MPa in most of the sample points except in ZR9 and ZR15 in location 2 and below 30MPa except in ZR2 and ZR5 in location 1.

5.1.4.3.Rock Mass Rating

RMR is a quantitative rock mass classification system. It consists of six parameters of rock mass (Bieniawski 1989) such as Uniaxial compressive strength (UCS) of intact rock material, Rock quality designation (RQD), Joint or discontinuity spacing, Joint condition/ condition of discontinuities, Groundwater condition, and Joint Orientation**.** From the rock mass rating carried out in location-2, the rocks are classified as poor to fair rock. RMR value is maximum for Spot-4(RMR= 51,Fair) and minimum for Spot-5(RMR= 34, Poor) (Table 5.21)

Table 5.21: Parameters and Ratings for Rock classification for location 2 (Bieniawski 1989)

Spot No.	**UCS (MPa)**	**RQD**	**S.D (mm)**	**D.L (m)**	**Aperture (mm)**	**Roughness**	**Infillings (mm)**	**Weathering**	**Groundwater**	**RMR**
1	29.2	37	5	0.5	10 - 20	Slightly rough	Soft fillings <2mm	Moderately weathered	Damp	
Ratings	4	8	5	6	0	3	2	3	10	41 (Fair)
2	12	33.3	6	0.06	5-10	Rough	Soft fillings <5mm	Moderately weathered	Wet	
Ratings	2	8	5	6	0	5	2	3		38(Poor)
3	28	88	4.5	0.2	2 -5	Slightly rough	Soft fillings <5mm	Moderately weathered	Damp	
Ratings	4	17	5	6	1	3	2	3	10	51(Fair)
4	20	22	5	0.4	5 -12	Rough	None	Moderately weathered	Damp	
Ratings	2	3	5	6	0	5	6	3	10	40(Poor)
5	18	16	4.5	0.6	0.1 -2	Rough	Soft fillings <5mm	Moderately weathered	Wet	
Ratings	2	**3**	**5**	**6**	**1**	**5**	**2**	**3**	**7**	**34(Poor)**

5.1.4.4 KINEMATIC ANALYSIS

Rock attitude was collected from 5 different spots in location-2 and kinematic analysis was done using Dips 7 software. The attitude of rocks in different spots is given in Table 5.22 and the probable slope failure is given in the figure from Figures 5.78 to 5.97.

Table 5.22 : Rock Attitudes for Kinematic Analysis in location-2

Spot No.	**Rock Attitude**	**Spot 1**	**Spot 2**	**Spot 3**	**Spot 4**	**Spot 5**
Slope	Slope angle	51°	64°	46°	75°	51°
	Slope direction	N158(SE)	N154(SE)	N203(SW)	N130(SE)	N115(SE)
Bedding Plane	Dip Amount	39°	32°	32°	32°	53°
	Dip Direction	N84(NE)	N038(SE)	N64(NE)	N32(NE)	N46(NE)
Joint Set (J1)	Dip Amount	71°	71°	73°	56°	76°
	Dip Direction	N164(SE)	N182(SW)	N149(SE)	N213(SW)	N125(SE)
Joint Set (J2)	Dip Amount	60°	53°	54°	63°	56°
	Dip Direction	N243(SW)	N263(SW)	N244(SW)	N113(SE)	N215(SW)
Possible Planer Failure		0%	0%	0%	30%	0%
Possible Wedge Failure		1.10%	25.49	2.86	32%	1.90%
Possible Toppling Failure		0%	0.00%	0%	0%	0%
Possible Flexural Failure		0%	0.00%	0%	0%	0%

Coordinates of sample spot	3°45'6.18"N 92°44'40.20"E	23°45'0.66"N 92°44'35.90"E	23°44'57.11"N 92°44'31.60"E	23°44'59.75"N 92°44'46.44"E	23°44'56.47"N 92°44'41.59"E

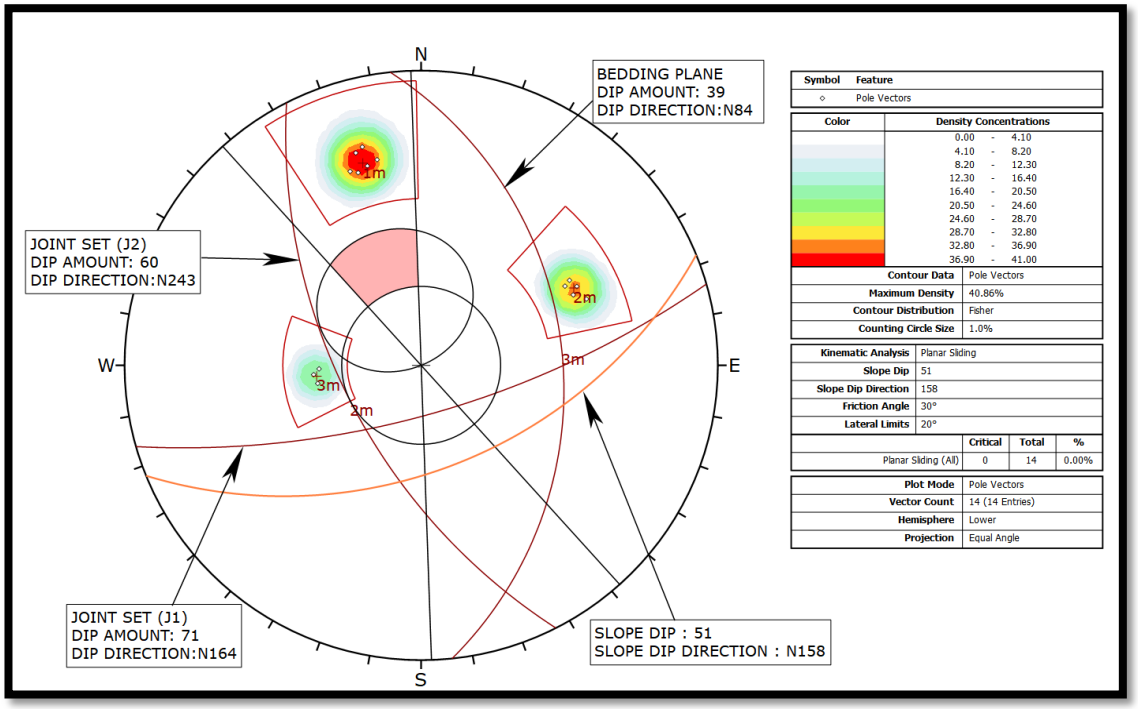

Figure 5.78. Probable Planar Failure for Spot 1

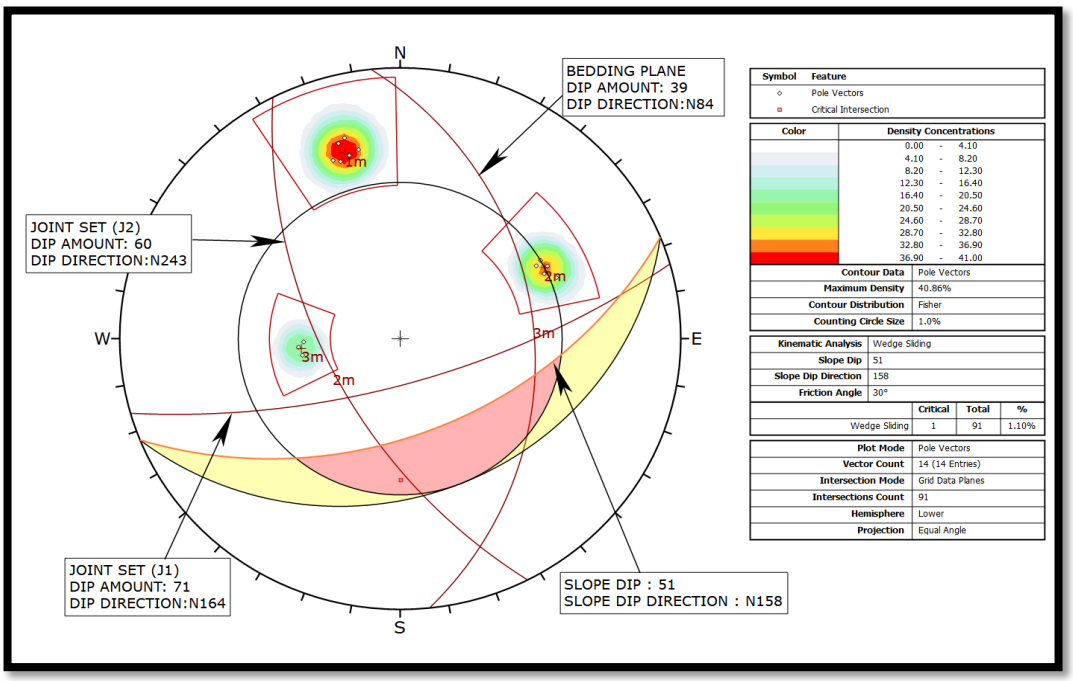

Figure 5.79. Probable Wedge failure for Spot 1

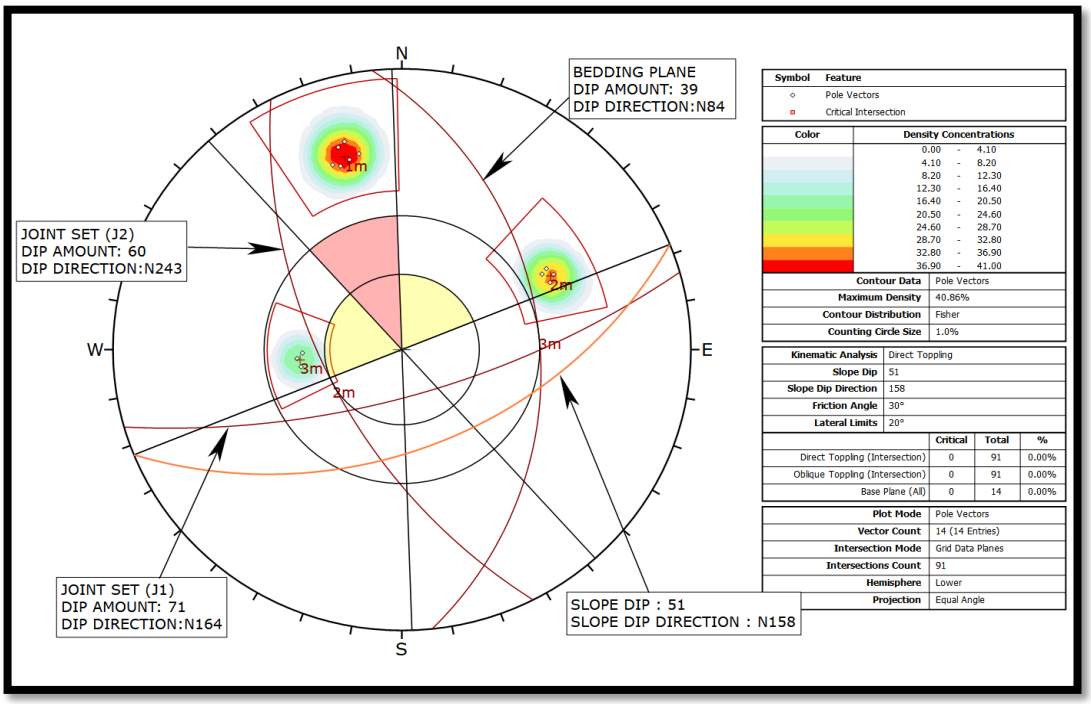

Figure 5.80. Probable Toppling Failure for Spot 1

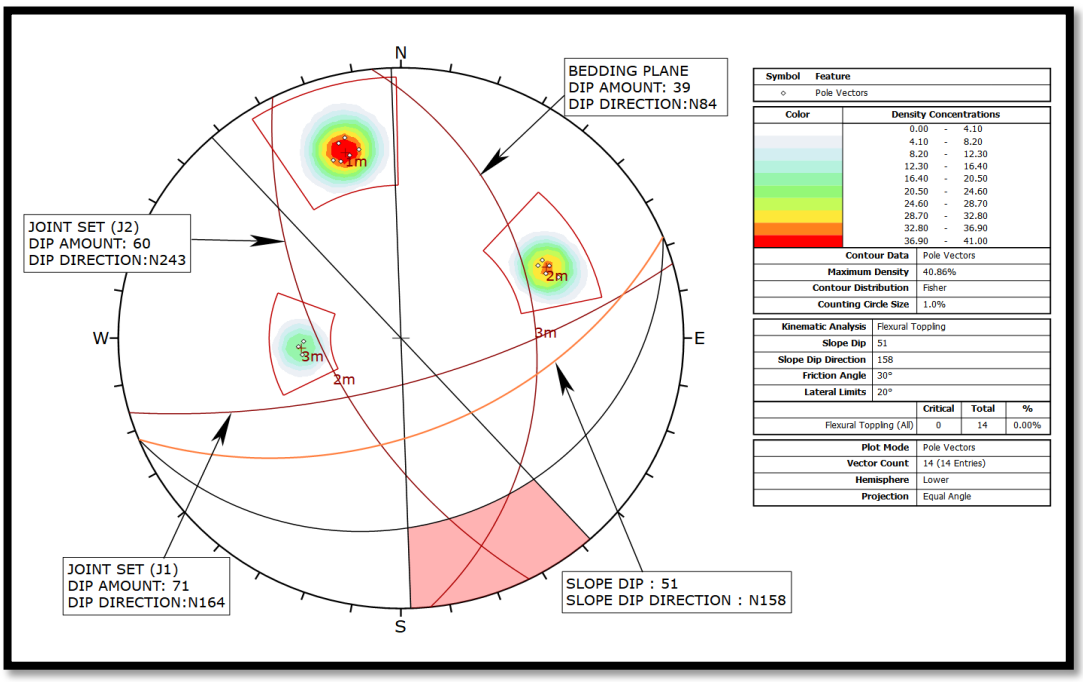

Figure 5.81. Probable Flexural Failure for Spot 1

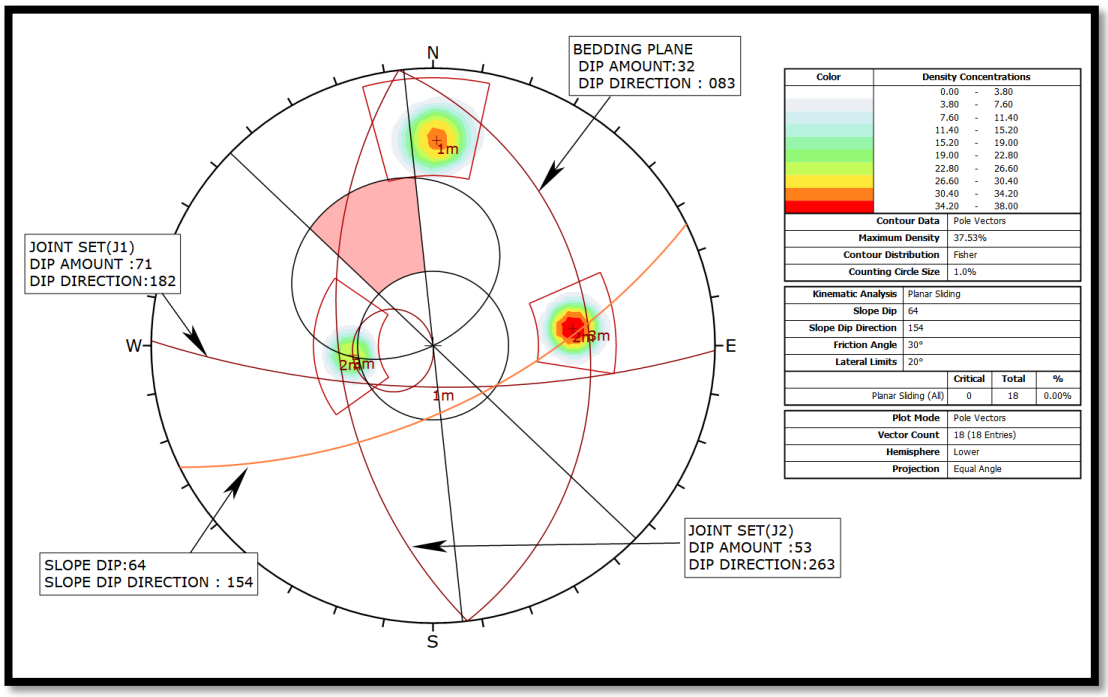

Figure 5.82. Probable Planer Failure for Spot 2

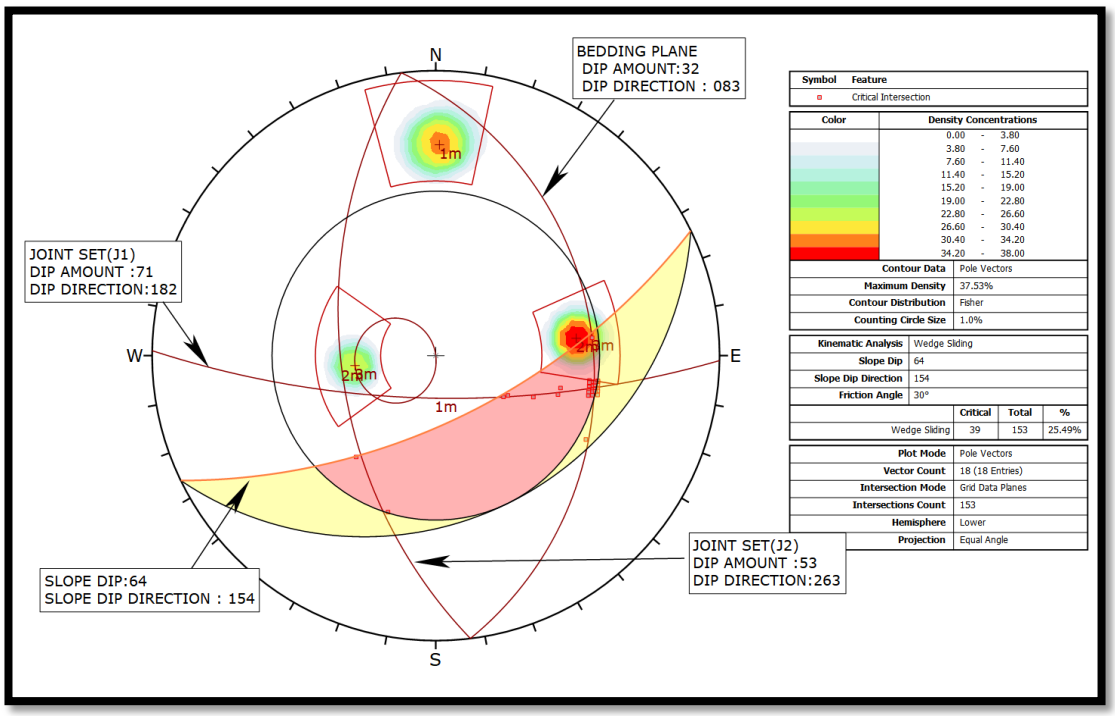

Figure 5.83. Probable Wedge failure for Spot 2

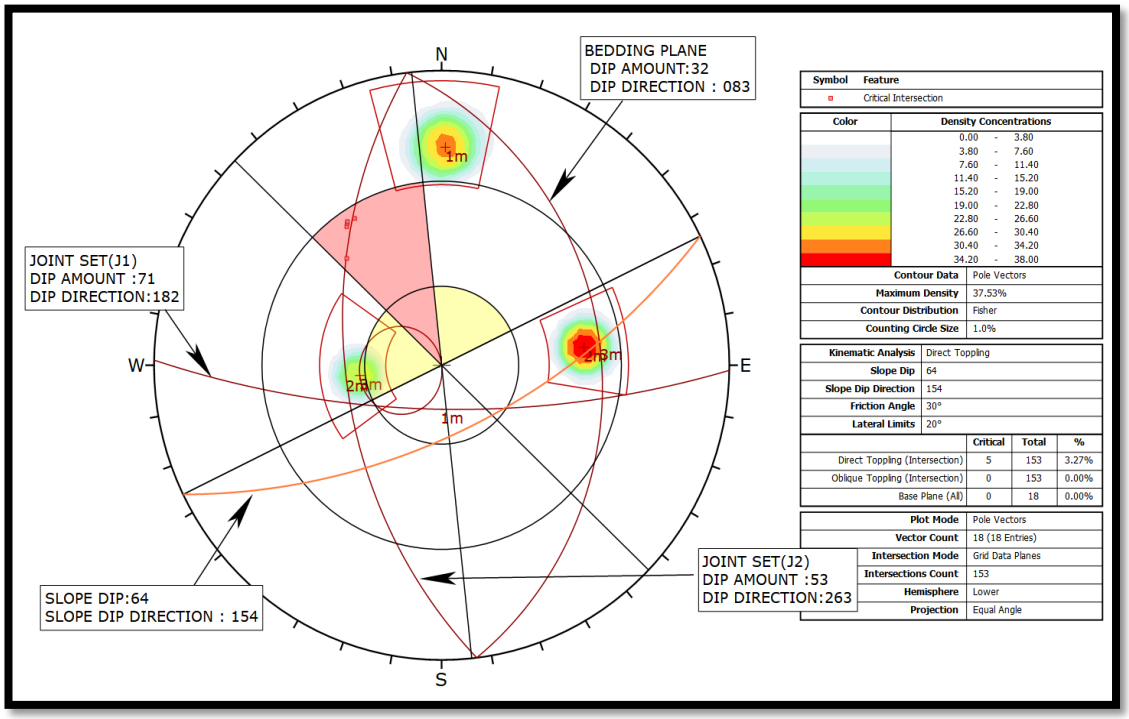

Figure 5.84. Probable Toppling Failure for Spot 2

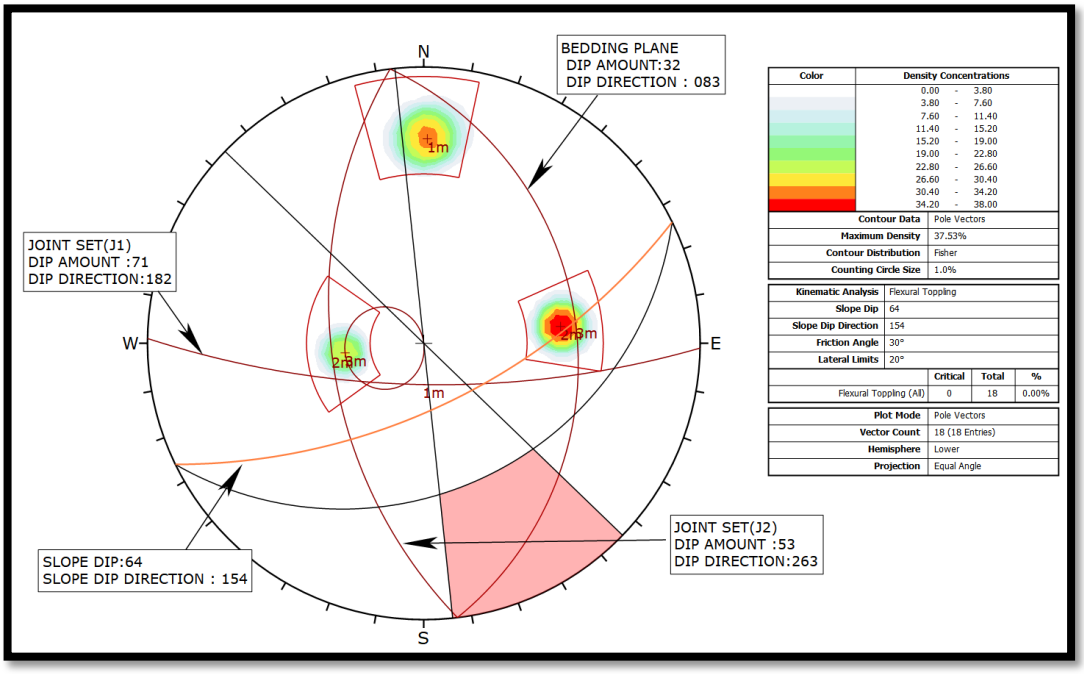

Figure 5.85. Probable Flexural Failure for Spot 2

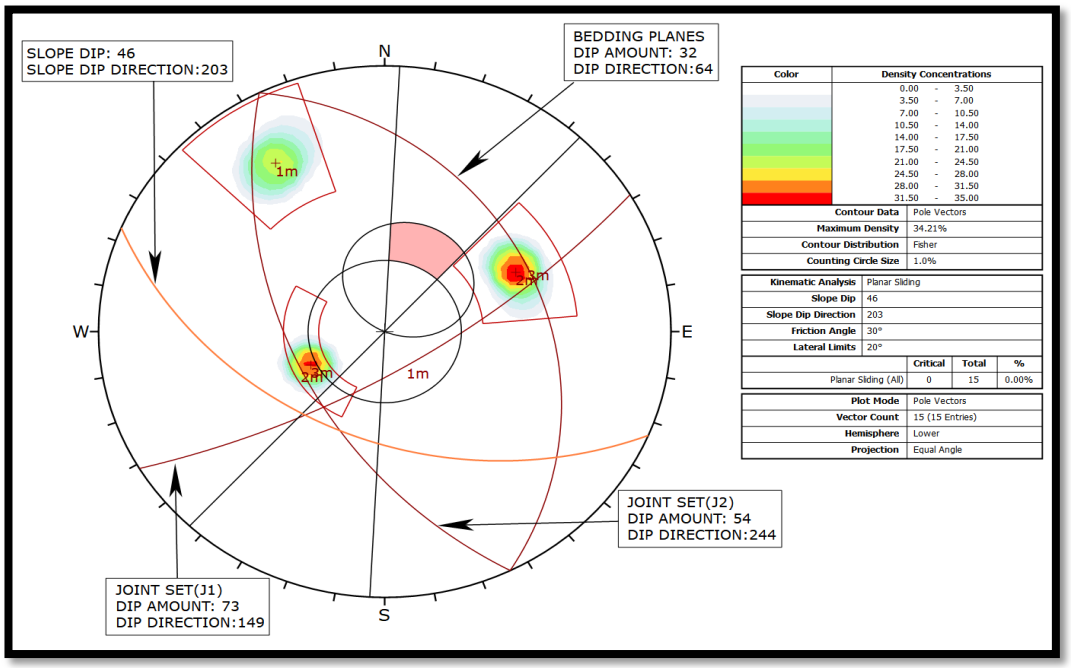

Figure 5.86. Probable Planer Failure for Spot 3

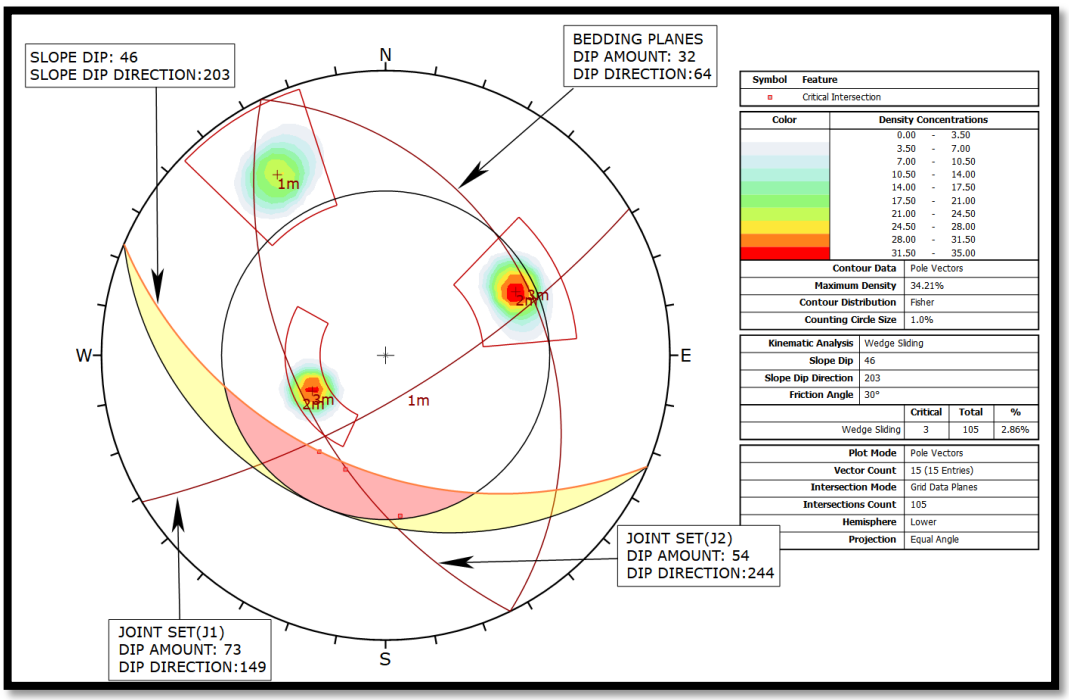

Figure 5.87. Probable Wedge failure for Spot 3

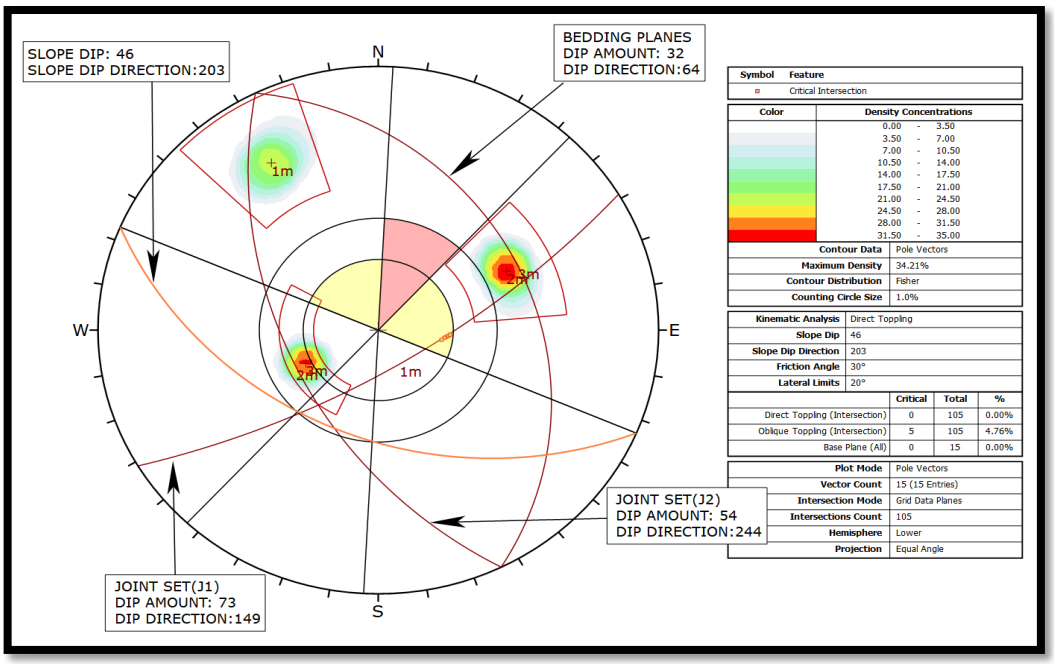

Figure 5.88. Probable Toppling Failure for Spot 3

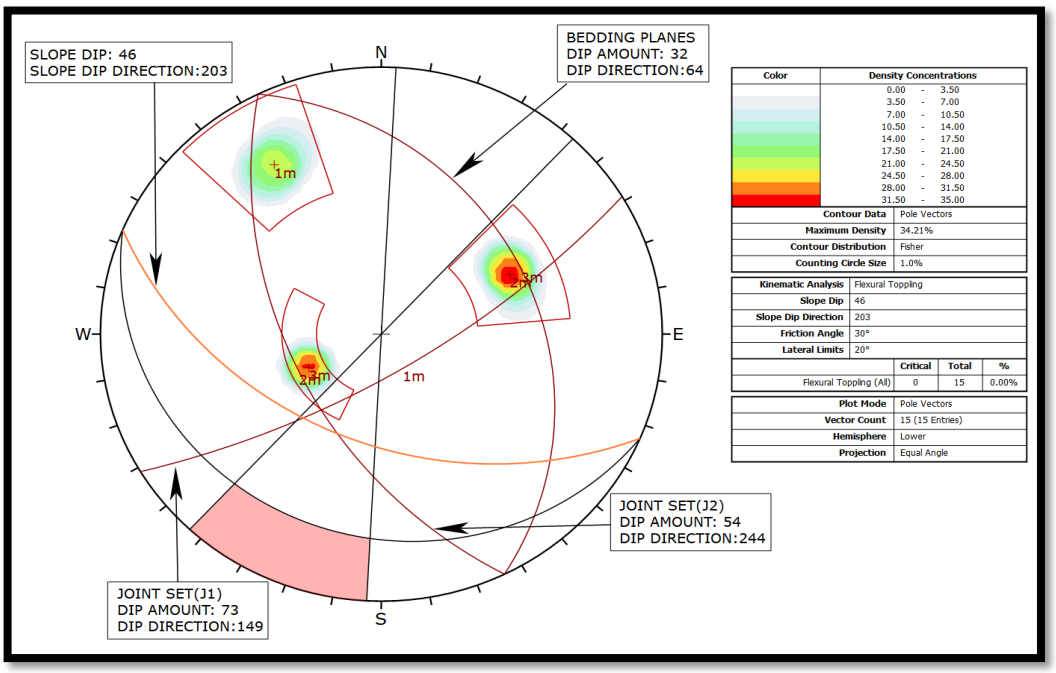

Figure 5.89. Probable Flexural Failure for Spot 3

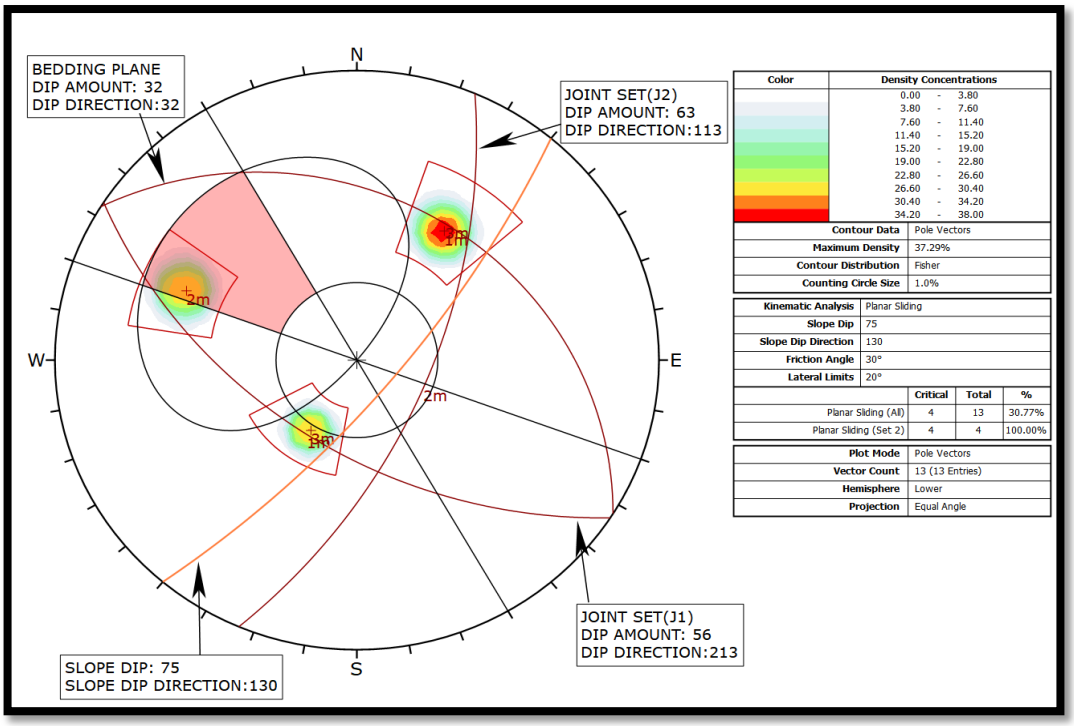

Figure 5.90. Probable Planer Failure for Spot 4

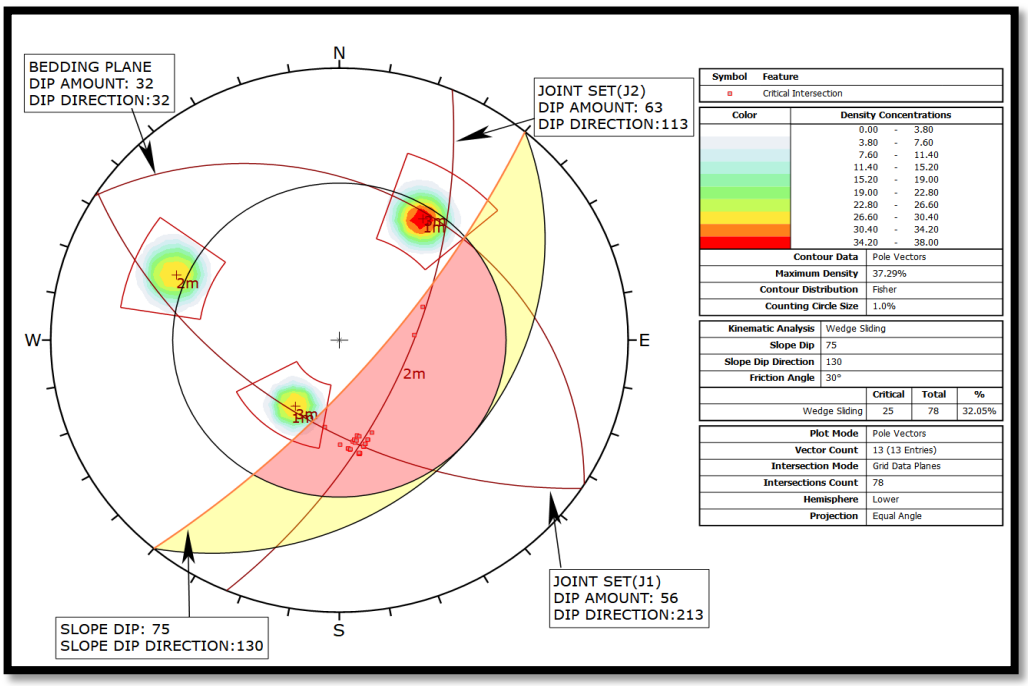

Figure 5.91. Probable Wedge failure for Spot 4

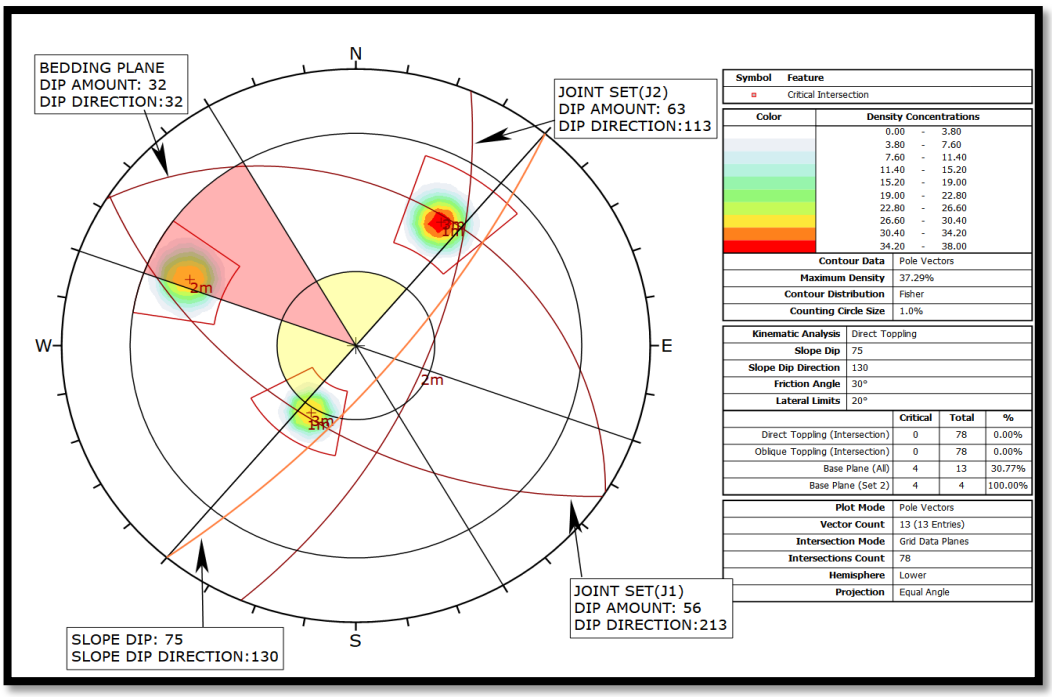

Figure 5.92. Probable Toppling Failure for Spot

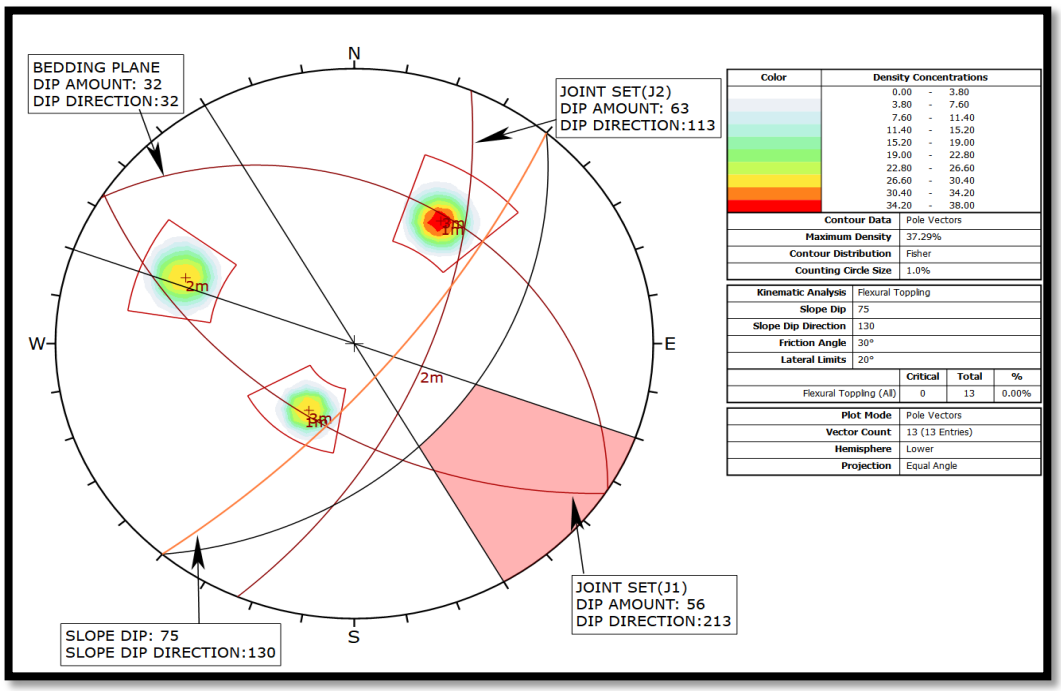

Figure 5.93. Probable Flexural Failure for Spot 4

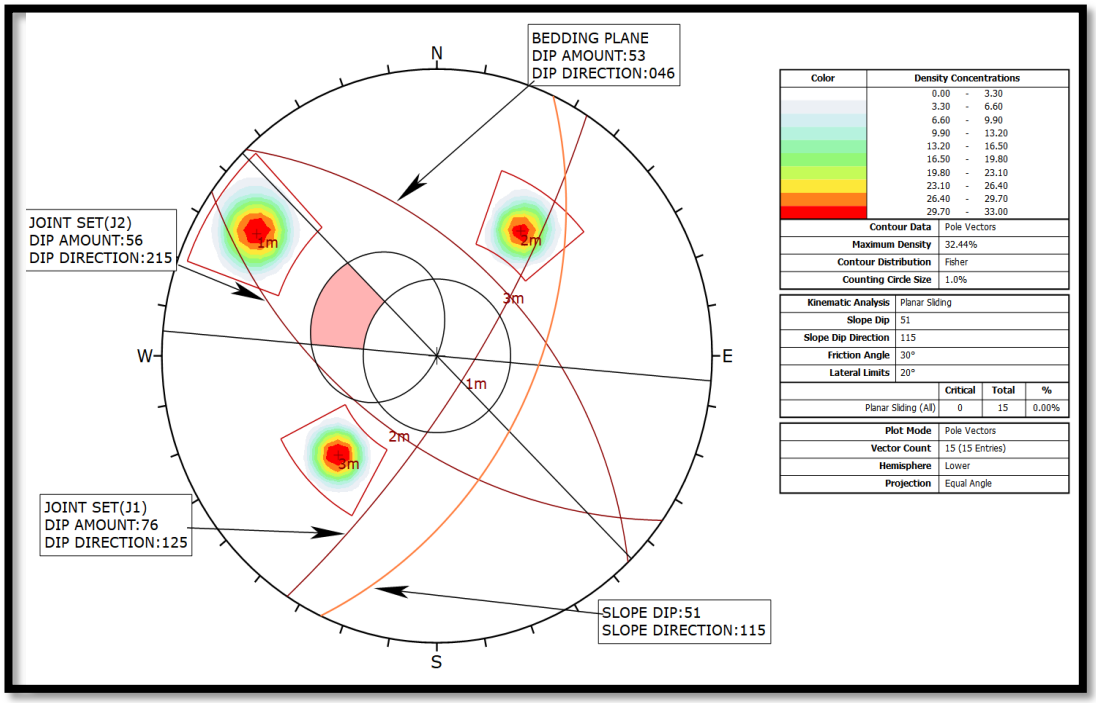

Figure 5.94. Probable Planer Failure for Spot 5

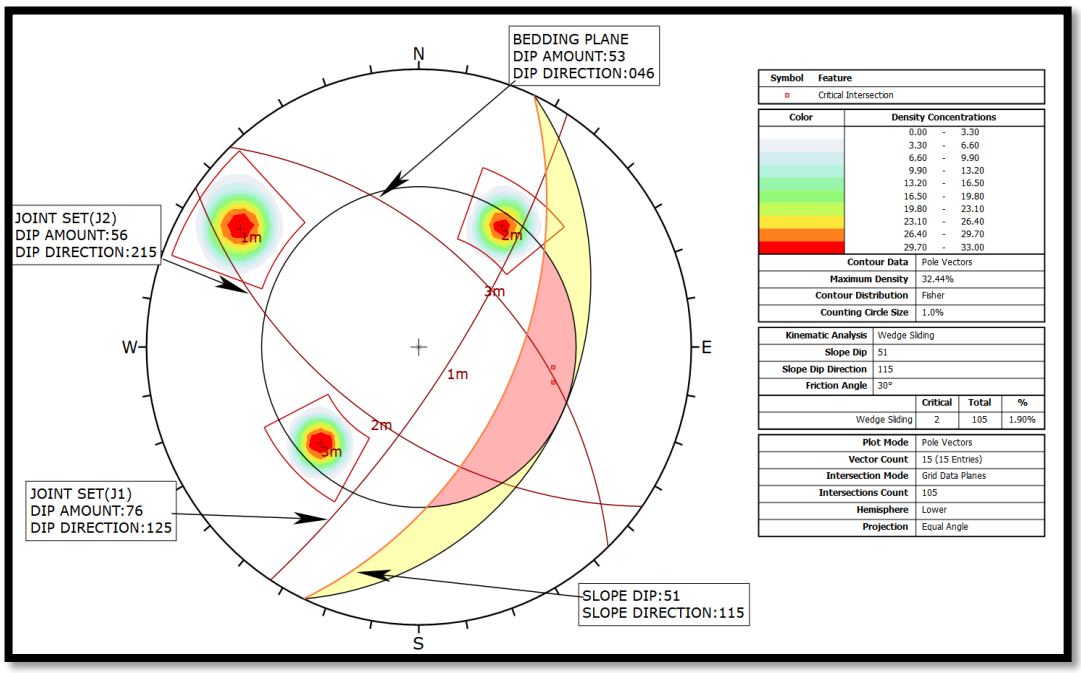

Figure 5.95. Probable Wedge failure for Spot 5

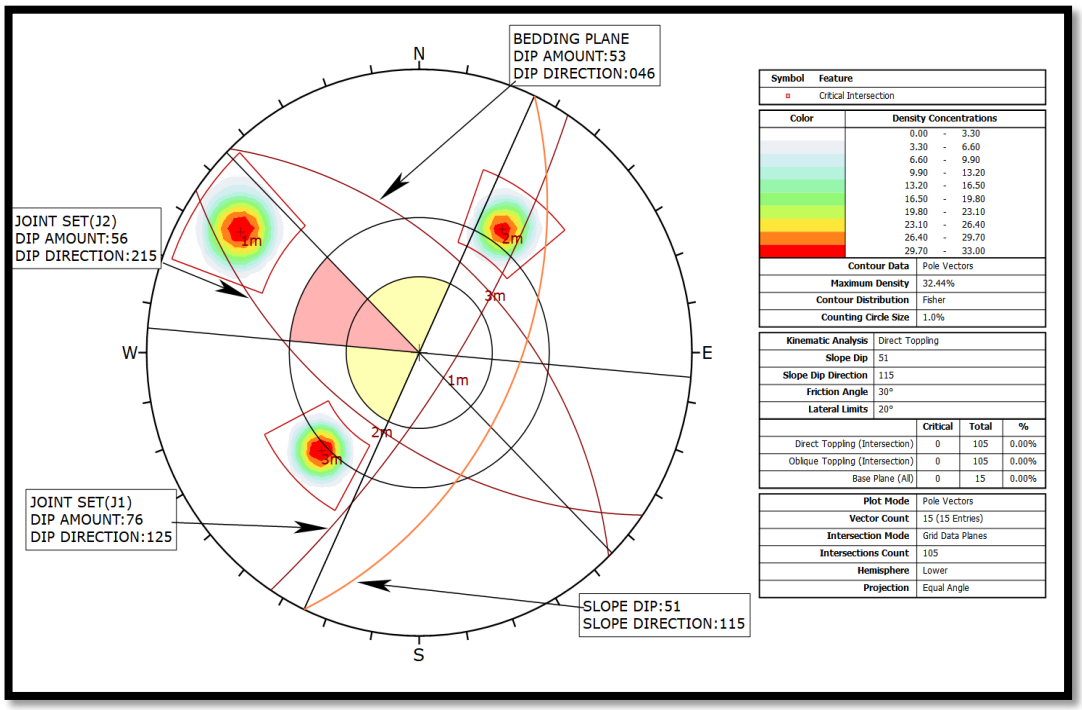

Figure 5.96. Probable Toppling Failure for Spot 5

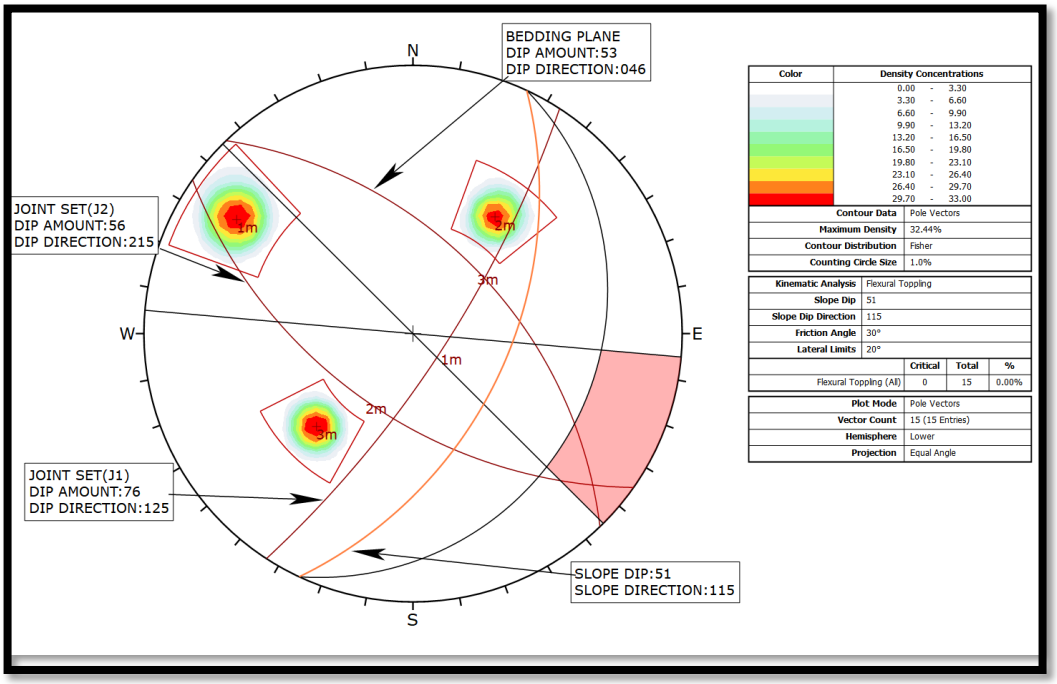

Figure 5.97. Probable Flexural Failure for Spot 5

The Kinematic Analysis performed for 5 different spots in Locattion-2 shows maximum probable wedge failure for all the spots. Other probable failure like a planer, toppling, and flexural failure are below 10%

5.1.5 ELECTRICAL RESISTIVITY SURVEY

A resistivity survey was carried out in three areas in location-2 using the Schlumberger configuration which gives the best resolution compared to another configuration. The resistivity curve was plotted and a pseudo-section was prepared using IPi2win software(Figure 5.98 to 5.100)

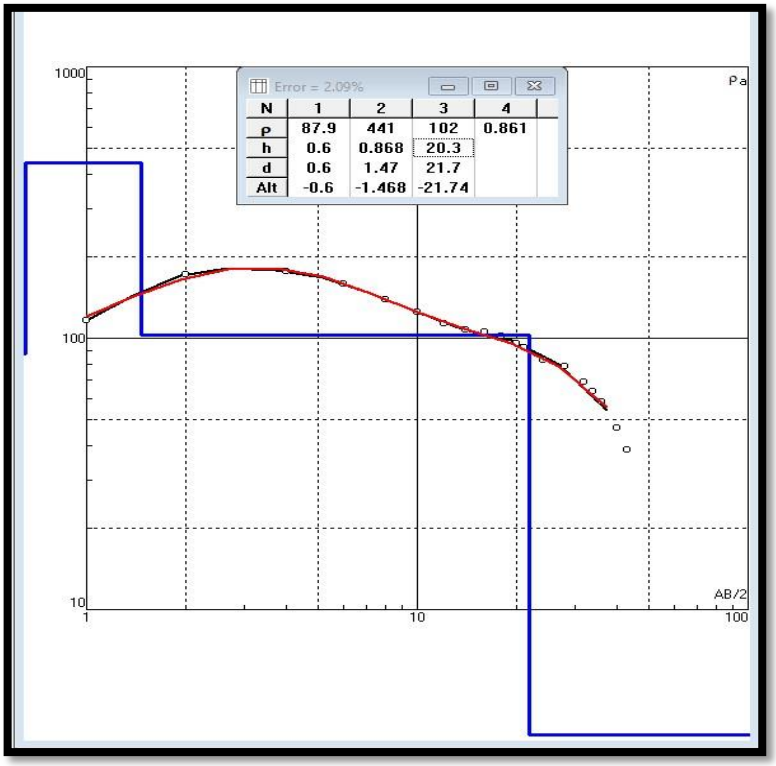

Figure 5.98. Vertical Electrical Sounding(VES)-1, red lines and blue lines indicate the observed and synthetic resistivity data respectively.

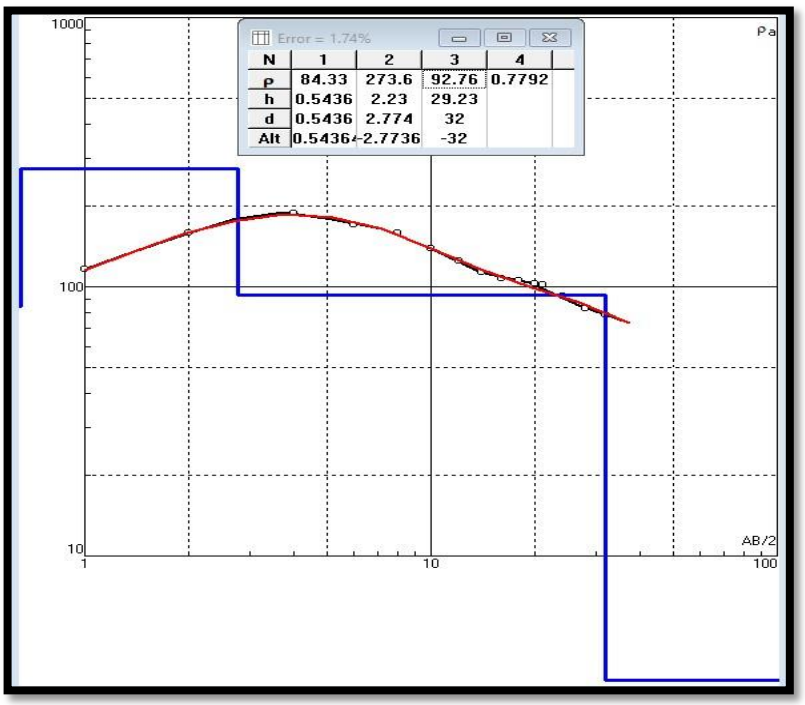

Figure 5.99. Vertical Electrical Sounding(VES)-2

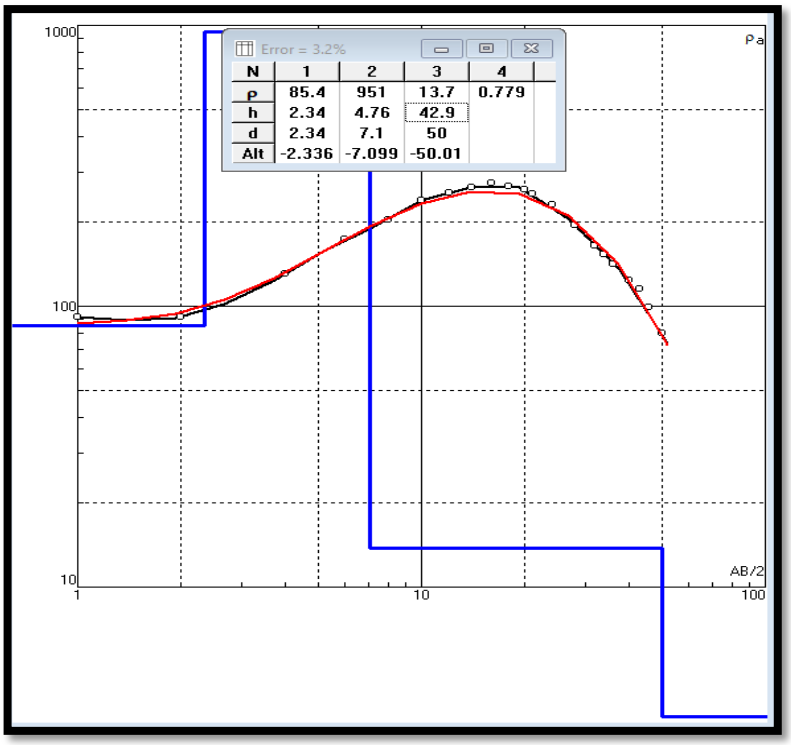

Figure 5.100. Vertical Electrical Sounding (VES)-3

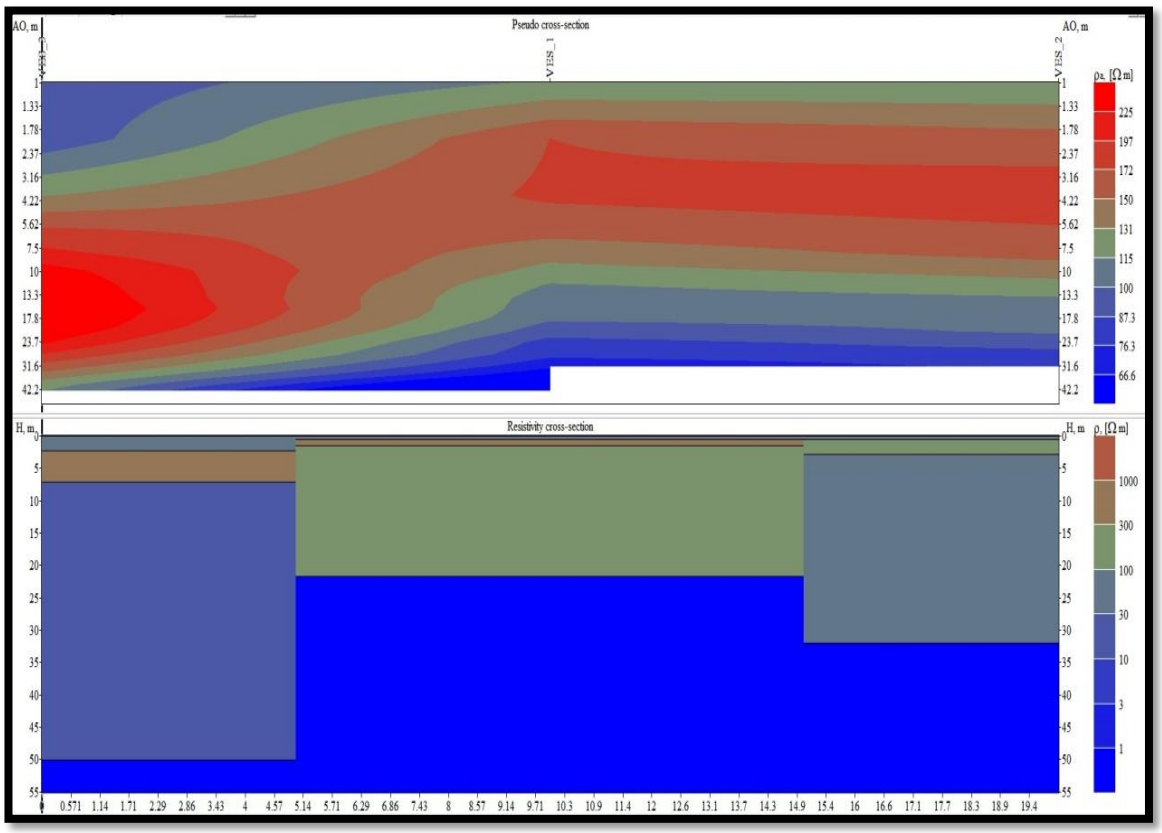

Figure 5.101. Pseudo cross-section and Resistivity cross-section

All three sounding curves of the resistivity survey performed in 3 locations showed a K-type curve which is a three-layer case of the resisitivity model, where $\rho_1 < \rho_2 > \rho_3$ represents each layer's resistivity. A K-type curve specifically refers to the characteristic shape observed on the graph when plotting apparent resistivity against the spacing between electrodes. In this study it can be observed that the first layer showed a low resistivity value and the second layer of the resistivity model has the highest resistivity and then decrease at the third layer.A K-type curves is used to interpret the layering and resistivity distribution of the subsurface.

5.1.6 CORE DRILLING

Drilling was carried out in location 2 and a depth of 28m was reached

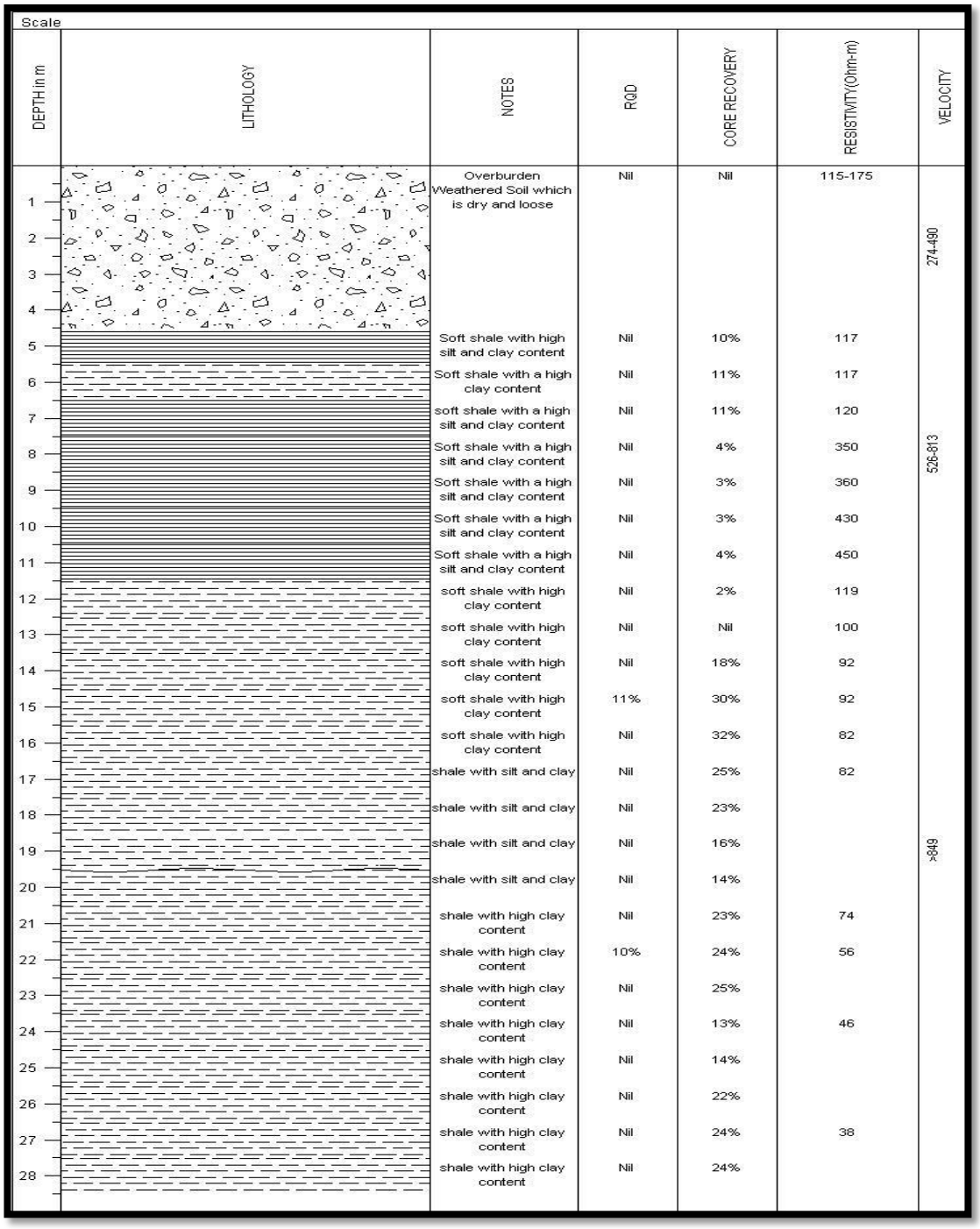

Figure 5.102. Correlation of Resistivity and Core Data

From the core data, the lithology of the subsurface can be encountered till the depth of 28m. An intercalation of soft shale with high silt and clay content and shale with high clay content was observed with low core recovery. 11% RQD is observed only at 15m depth which represents the highest RQD in the borehole.

5.1.7 ANALYSIS OF AIZAWL RAINFALL DATA

Aizawl rainfall data was collected from the State Meteorological Center, Directorate of Science and Technology, Government of Mizoram. Rainfall data from 2012 to 2022 was analyzed (Table 5.23 and 5.24) and is plotted in the graph (Figures 5.103 and 5.104)

Table 5.23: Aizawl Rainfall Data from 2012-2021

Year	Months											
	Jan	**Feb**	**Mar**	**Apr**	**May**	**June**	**July**	**Aug**	**Sep**	**Oct**	**Nov**	**Dec**
2012	15.3	7.3	46.9	277.5	202.1	505.5	292.1	448.6	328.9	297.1	121.8	0
2013	0	0	4.7	64.9	458.2	301.8	289.8	372.4	301.9	127.1	0	0
2014	0	13	16.2	45.1	276.1	332.9	376.7	248.6	414.1	67.9	0	0
2015	8.0	0.0	40.8	241.8	189.8	429.1	418.2	486.0	356.1	233.4	3.7	5.4
2016	1.0	11.8	80.6	124.3	351.7	396.3	290.5	328.4	380.6	106.0	89.9	0.0
2017	0.0	18.7	95.9	145.0	216.5	743.5	374.5	479.0	239.0	329.0	8.0	37.6
2018	8.0	8.0	47.0	115.0	232.0	463.0	233.0	420.0	131.0	89.0	3.0	0.0
2019	0.0	42.0	37.0	104.0	190.7	154.0	539.0	260.0	181.0	128.4	71.5	2.2
2020	48.1	20.2	0.0	108.3	290.0	218.3	243.1	156.9	238.1	385.0	33.5	0.0
2021	3.0	0.5	61.0	85.5	164.2	336.1	360.3	353.5	249.3	155.2	72.0	77.0

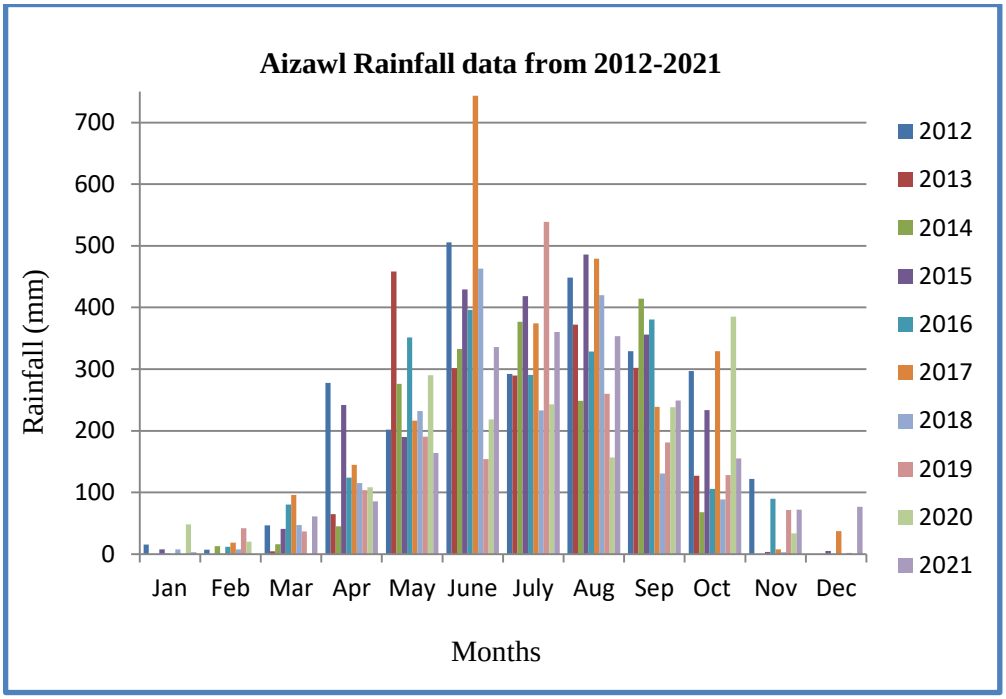

Figure 5.103. Average precipitation of Aziawl from 2012-2022

Table 5.24: Aizawl Average Rainfall in 2022

RAINFALL (in mm) OF AIZAWL, 2022												
Date	**Jan**	**Feb**	**Mar**	**Apr**	**May**	**Jun**	**Jul**	**Aug**	**Sep**	**Oct**	**Nov**	**Dec**
1	0.0	0.0	0.0	0.0	7.8	10.6	0.0	40.0	2.2	10.8	0.0	0.0
2	0.0	0.2	0.0	0.0	1.8	7.6	4.2	13.0	0.0	31.8	0.0	0.0
3	0.0	0.0	0.0	0.0	0.4	20.0	63.2	34.0	0.0	11.0	0.0	0.0
4	0.0	0.0	0.0	0.0	10.2	7.6	0.8	10.2	2.6	15.2	0.0	0.0
5	0.0	11.6	0.0	0.0	0.0	22.0	9.6	10.6	12.0	28.0	0.0	0.0
6	0.0	0.0	0.0	0.0	0.0	0.0	26.6	38.6	3.6	10.6	0.0	0.0
7	0.0	0.0	0.0	0.0	7.0	0.0	19.0	0.4	5.4	4.7	0.0	0.0
8	0.0	0.0	0.0	0.0	0.0	0.0	19.0	0.0	0.0	0.4	0.0	0.0
9	0.0	0.0	0.0	0.0	0.6	0.0	0.6	4.4	0.0	0.0	0.0	0.0
10	0.0	0.0	0.0	0.0	30.4	0.0	24.2	8.0	15.8	0.0	0.0	0.0
11	0.0	0.0	0.0	24.2	37.4	0.0	27.0	0.0	9.8	0.0	0.0	0.0
12	0.0	0.0	0.0	3.4	19.2	0.0	12.8	6.4	16.6	0.0	0.0	0.0
13	1.6	0.0	0.0	0.0	1.4	0.0	3.4	26.2	3.6	0.0	0.0	0.0
14	0.6	0.0	0.0	0.0	6.6	17.2	0.0	20.4	1.8	9.8	0.0	0.0
15	4.6	0.0	0.0	1.2	0.0	8.0	0.0	2.0	0.8	0.0	0.0	0.0
16	0.0	0.0	0.0	0.0	0.0	12.8	0.0	0.0	0.0	0.0	0.0	0.0
17	0.0	0.0	0.0	0.0	0.0	15.6	20.2	0.0	0.0	0.0	0.0	0.0
18	0.0	0.0	0.0	10.0	45.0	64.2	7.2	0.0	8.0	29.2	0.0	0.0
19	0.0	0.0	0.0	0.0	6.4	61.8	1.2	0.0	8.8	0.4	0.0	0.0
20	0.0	0.0	0.0	16.2	32.2	29.8	7.8	20.3	26.0	0.0	0.0	0.0
21	0.0	5.4	0.0	17.0	30.5	9.0	0.0	6.3	0.0	0.0	0.0	0.0
22	0.0	0.0	0.0	0.0	41.4	27.8	**65.0**	0.0	0.8	0.0	0.0	0.0
23	0.0	0.0	0.0	0.6	3.5	14.4	37.8	30.8	22.4	0.0	0.0	0.0
24	7.5	0.0	0.0	0.0	0.0	4.2	20.2	0.0	12.8	22.4	0.2	0.0
25	4.8	0.0	0.0	0.0	30.0	4.0	15.8	0.0	2.4	36.8	0.0	0.0
26	0.0	0.0	0.0	0.0	10.4	0.3	15.6	0.0	0.0	0.0	0.0	0.0
27	0.0	0.0	20.8	0.6	5.6	1.0	5.6	1.2	15.0	0.0	0.0	14.6
28	4.8	0.0	5.6	0.0	0.0	0.0	6.2	4.0	10.0	0.0	0.0	3.7
29	0.0		0.2	0.0	0.0	17.0	0.0	0.4	0.0	0.0	0.0	0.0
30	0.0		24.2	0.0	0.0	0.4	0.0	0.2	14.6	0.0	1.8	0.0

31	0.0		2.5		0.0		47.2	0.4		0.0		0.0
AVG	0.8	0.6	1.7	2.4	10.6	11.8	14.8	9.0	6.5	6.8	0.1	0.6
Total	23.9	17.2	53.3	73.2	327.8	355.3	460.2	277.8	195.0	211.1	2.0	18.3

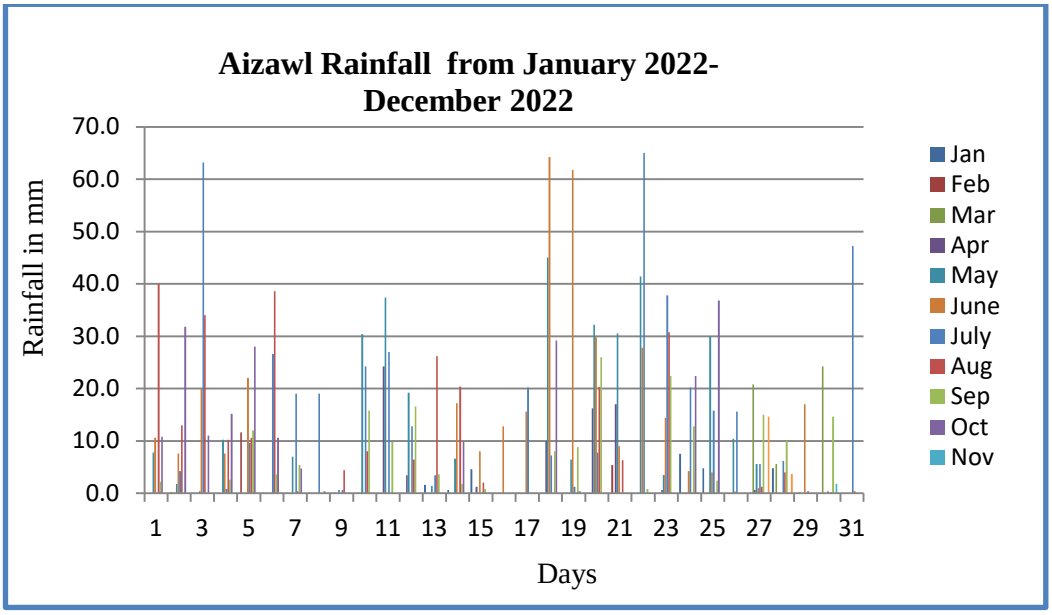

Figure 5.104. Average Precipitation of Aizawl in 2022

From the analysis, Precipitation was maximum in June 2017. An increase in rainfall from May to September is observed for every year. In 2022, precipitation increased from May and reached its peak in July. The amount of rainfall reduces from September.

5.1.8 TOTAL STATION MONITORING

Monitoring of ground motion was carried out monthly from September 2021 in two locations using the N6 Series Total Station instrument. From the data obtained, the change in elevation of the study area is plotted concerning the month (Figure 5.105 to 5.108).

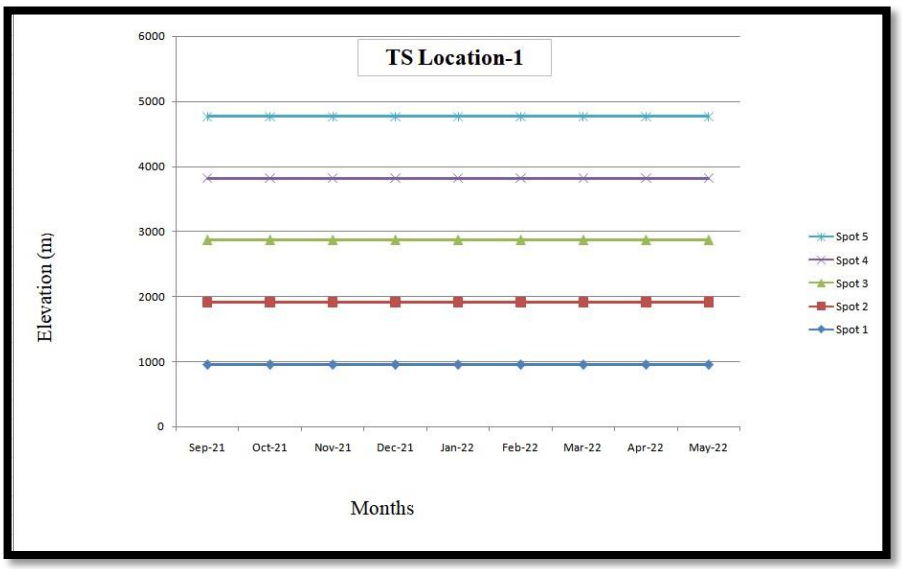

Figure 5.105. TS for location-1 (September 2021- May 2022)

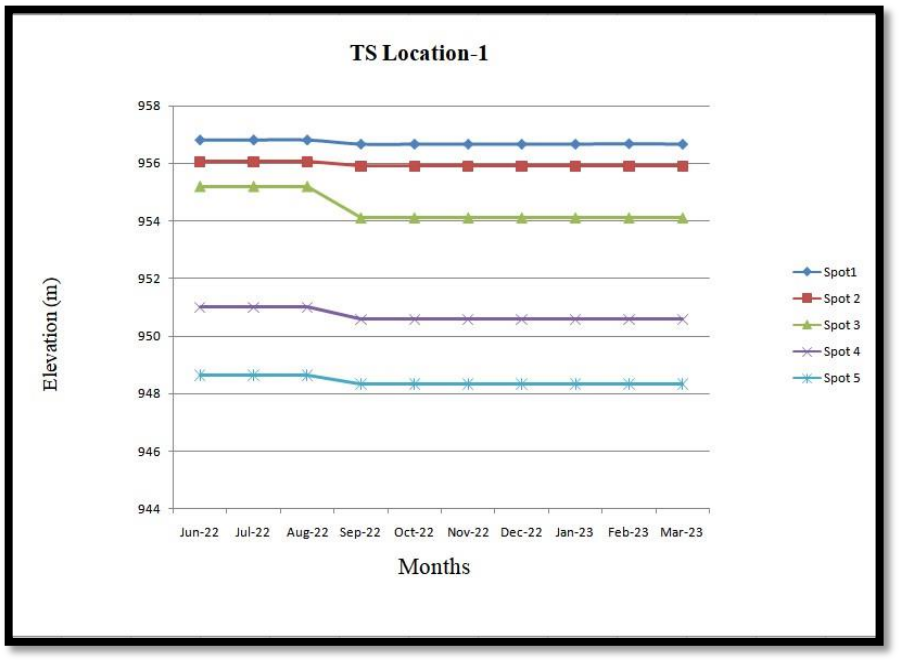

Figure 5.106. TS for location-1 (June 2021- March 2023)

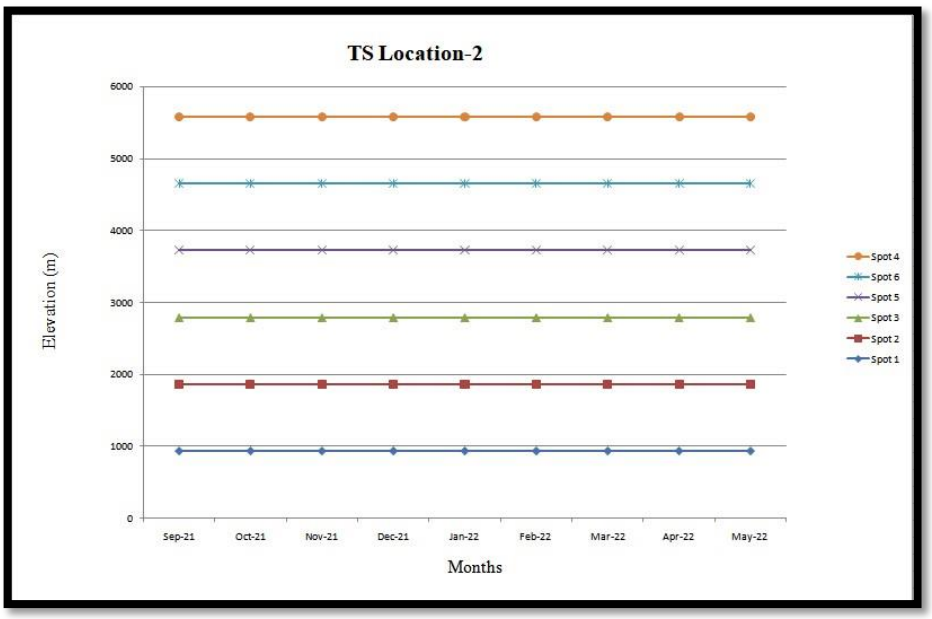

Figure 5.107. TS for location-2 (September 2021- May 2022)

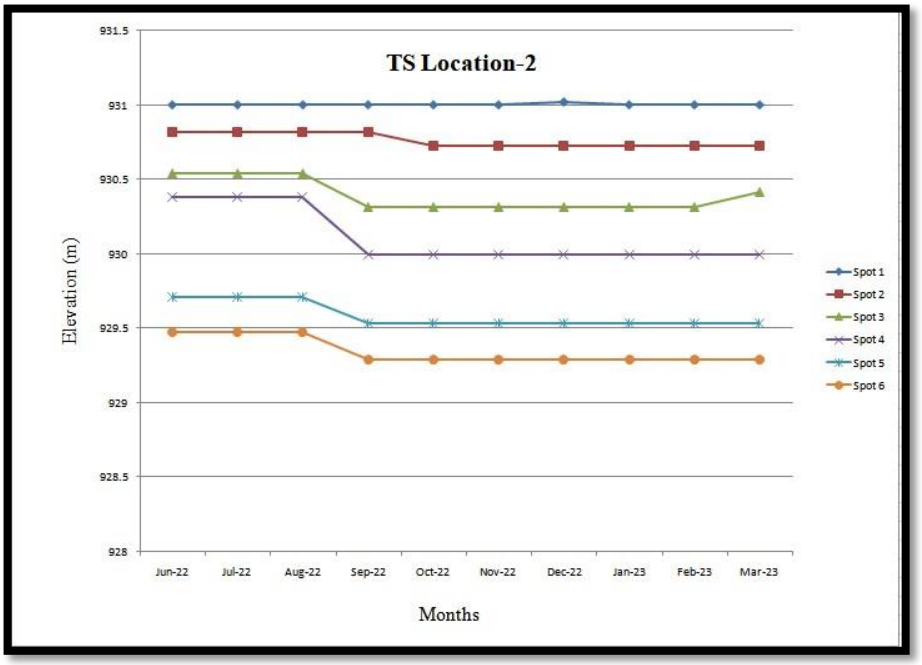

Figure 5.108. TS for location-2 (June 2021- March 2023)

5.1.8.1.COMPARATIVE ANALYSIS OF RAINFALL DATA WITH TOTAL STATION MONITORING DATA

The Total Station Monitoring data was compared with the rainfall data collected from the State Meteorological Center, Directorate of Science and Technology, Government of Mizoram, and the results are given in Tables 5.25 & 5.26 and Figures 5.109 & 5.110

Table 5.25: Aizawl Rainfall data and total station monitoring for the year 2021 to 2023 in Location-1

Months	**Rainfall (mm)**	**Spot-1**	**Spot-2**	**Spot-3**	**Spot-4**	**Spot-5**
September	249.3	956.81	956.059	955.184	950.996	948.641
October	155.2	956.81	956.059	955.184	950.996	948.641
November	72	956.81	956.059	955.184	950.996	948.641
December	77	956.81	956.059	955.184	950.996	948.641
January	23.9	956.81	956.059	955.184	950.996	948.641
Febuary	17.2	956.81	956.059	955.184	950.996	948.641
March	53.4	956.81	956.059	955.184	950.996	948.641
April	73.2	956.81	956.059	955.184	950.996	948.641
May	327.8	956.81	956.059	955.184	950.996	948.641
June	355.3	956.81	956.059	955.184	950.996	948.641
July	460.2	956.81	956.059	955.184	950.996	948.641
August	277.8	956.81	956.059	955.184	950.996	948.641
September	195	956.664	955.916	954.1	950.594	948.325
October	211.1	956.664	955.916	954.1	950.594	948.325
November	02	956.664	955.916	954.1	950.594	948.325
December	18.3	956.664	955.916	954.1	950.594	948.325
January	00	956.664	955.916	954.1	950.594	948.325

Febuary	00	956.664	955.916	954.1	950.594	948.325
March	78	956.664	955.916	954.1	950.594	948.325
April	32	956.664	955.916	954.1	950.594	948.325

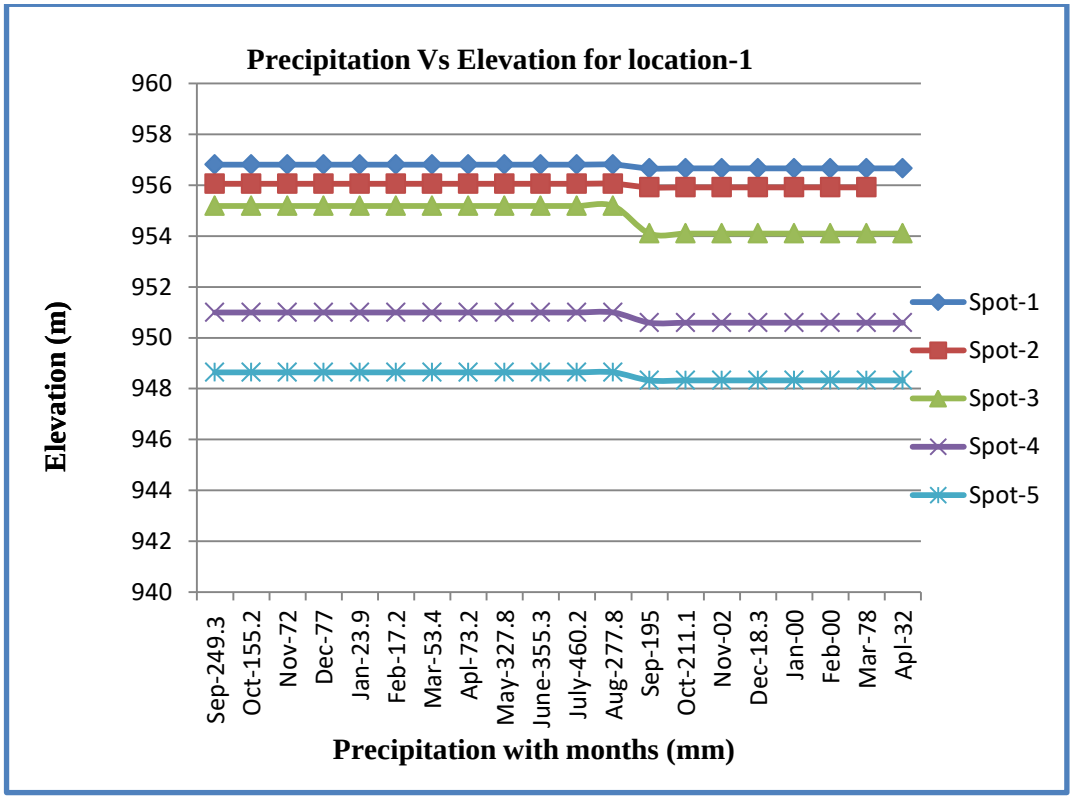

Figure 5.109. Ground subsidence with respect to precipitation from 2021 to 2022(Location-1)

Table 5.26: Aizawl Rainfall data and total station monitoring for the year 2021 to 2023 in Location-2

Months	**Rainfall (mm)**	**Spot-1**	**Spot-2**	**Spot-3**	**Spot-4**	**Spot-5**	**Spot-6**
September	249.3	931.001	930.813	930.536	930.378	929.707	929.473
October	155.2	931.001	930.01	930.536	930.378	929.707	929.473
November	72	931.001	930.813	930.536	930.101	929.707	929.473
December	77	931.001	930.813	930.536	930.378	929.707	929.473
January	23.9	931.001	930.813	930.536	930.378	929.707	929.473
Febuary	17.2	931.001	930.813	930.536	930.378	929.707	929.473
March	53.4	931.001	930.813	930.536	930.378	929.707	929.473
April	73.2	931.001	930.813	930.536	930.378	929.707	929.473
May	327.8	931.001	930.813	930.536	930.378	929.707	929.473
June	355.3	931.001	930.813	930.536	930.378	929.707	929.473
July	460.2	931.001	930.813	930.536	930.378	929.707	929.473
August	277.8	931.001	930.813	930.536	930.378	929.707	929.473
September	195	931.001	930.722	930.315	929.99	929.528	929.287
October	211.1	931.001	930.722	930.315	929.99	929.528	929.287
November	02	931.001	930.722	930.315	929.99	929.528	929.287
December	18.3	931.001	930.722	930.315	929.99	929.528	929.287
January	00	931.001	930.722	930.315	929.99	929.528	929.287
Febuary	00	931.001	930.722	930.315	929.99	929.528	929.287
March	78	931.001	930.722	930.315	929.99	929.528	929.287
April	32	931.001	930.722	930.315	929.99	929.528	929.287

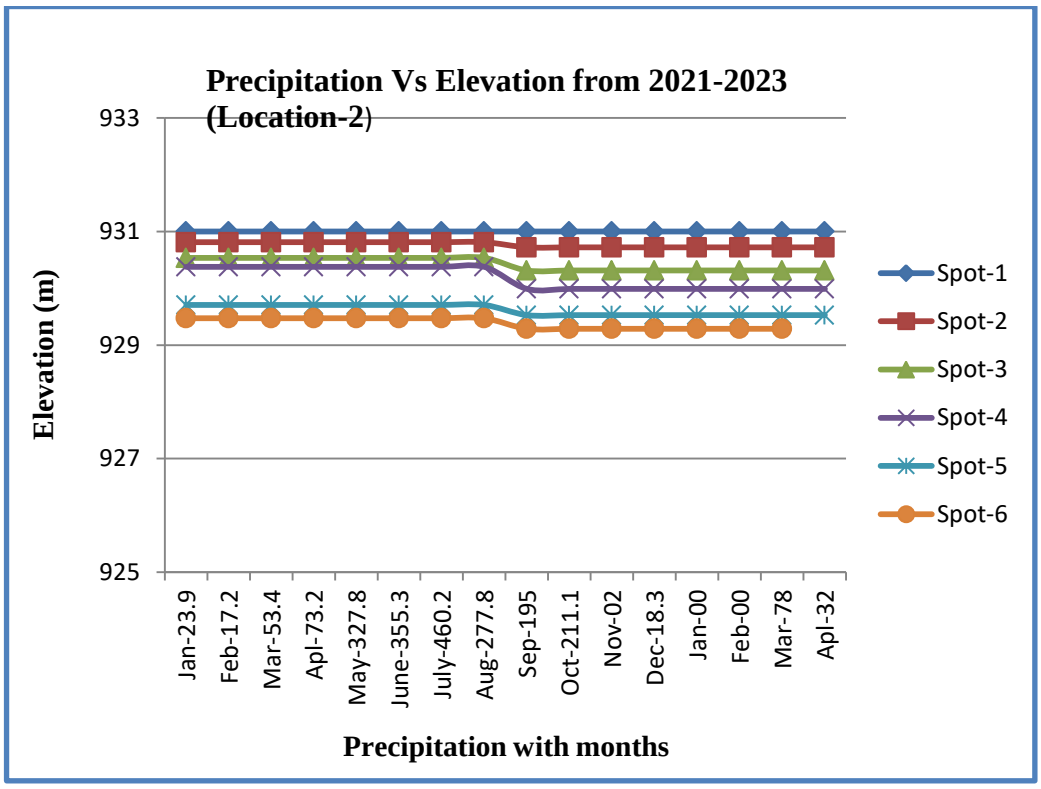

Figure 5.110.Ground subsidence with respect to precipitation from 2021 to 2023 (Location-2)

Based on the monitoring data from the study, a slight subsidence of approximately 1 foot was observed in both locations during September 2022. Additionally, a few human errors were documented in certain foresight points during this monitoring period. Also monitoring is not possible from April 2023 because of the development taking place in the area.

Further analysis involving the validation of rainfall data with total station monitoring data revealed a notable correlation. It was observed that following peak precipitation events, ground subsidence averaging 1 foot occurred in both locations. This finding suggests a potential link between heavy rainfall and subsequent ground movement, indicating a need for continued monitoring and investigation into the factors influencing subsidence in these areas.

5.2 DISCUSSION

The study area is divided into two locations. Location 1 lies on Zuangtui-Thuampui local council border and Location 2 covers P&E and PWD complex.

5.2.1 LOCATION-1

In Location-1, the natural moisture content is highest for ZS3 with an NMC value of 30.23 and lowest for ZS1 with 23.77 NMC. The liquid limit which is the minimum moisture content at which the soil behaves as liquid ranges from 40.22% to 40.95%. The plastic limit is low in ZS3 (24.36) compared to ZS2 (27.29). The maximum plasticity index obtained in location 1 is 16.31 and the soils are classified as slightly plastic (Table 5.4).

The consistency index ranges from 1.14 to 1.24 and the liquidity index from -0.24 to -0.14. From the value of the liquidity index and consistency index, all the samples in location-1 can be classified as semi-solid according to Coduto 1999. The average dry density of the soil is 1.67g/cc

From the direct shear test, ZS2 has a cohesion value of 0.12 kg/cm^2 which is the lowest and also has the greatest angle of internal friction(29.71°) among the sample study in location 1 and it indicates a higher chance of failure compared to the other areas. The other two samples ZS1 and ZS2 have a cohesion of 0.32 kg/cm^2 & 0.23 kg/cm^2 and an angle of internal friction of 27.95° & 29.02° respectively.

The cohesion value of 26KPa and 18° angle of internal friction is shown by ZS1 in the soil triaxial test.

From the slope stability analysis using the limit equilibrium method, it is analyzed that both the slope ZS1 AND ZS3 in location-1 have a factor of safety below unity in all the methods except for ZS1, the FoS is 1.33 in GLE/ Morgenstren-price method and 1.18 in Spencer method. So the area is considered to be unstable. Even though the FoS given by GLE/ Morgenstren-price method and the Spencer

method is unity, since it is below 1.5, the slope is still considered unstable when the soil is fully saturated with water during monsoon season.

Among the five-rock samples collected from location-1, three samples ZR1, ZR3 & ZR4 fall under high durability, with durability index of 84.97%, 82.74%, and 84.85% respectively (Table 5.17) under two cycles of alternate wetting and drying conditions. ZR2 has the highest durability with a durability index of 97.63% and can be classified as extremely highly durable according to Franklin and Chandra,1972. Among the five samples, ZR2 and ZR5 which were collected from an undisturbed area have higher durability compared to those collected from unstable areas.

The point load index strength of rock varies from 1MPa in ZR4 to 2.3MPa in ZR2. A sample representing an undisturbed area has a PLI of more than 2MPa (Table 5.19), while those samples collected from disturbed areas ZR1,ZR3 & ZR4 have PLI values of 1.8 MPa, 1.3MPa, and 1Mpa respectively which are below 2MPa. So the rock observed in undisturbed areas has higher strength compared to those in disturbed areas.

Based on the ground motion monitoring using total station data from September 2021 to March 2023, the slope remained stable initially from the start of monitoring until August 2022. However, a slight subsidence of approximately 1 foot was observed in September 2022. This subsidence coincided with significant changes in precipitation levels based on Aizawl rainfall data collected from the State Meteorological Center, Directorate of Science and Technology, Government of Mizoram (Table 5.26).

The rainfall data indicates that precipitation in July reached 460 mm, which is a substantial amount capable of fully saturating the soil. This high level of saturation likely persisted into August, although the precipitation decreased to 277.8 mm during that month. The saturation of the soil due to these heavy rainfall events can increase pore water pressure and reduce soil strength, leading to potential instability and failure of the slope observed in September 2022.

The observed subsidence in September 2022 following these rainfall events underscores the importance of understanding the influence of precipitation on slope stability

5.2.2 LOCATION-2

The study of geological and geomechanical properties of rock and soil is conducted along with a resistivity survey and core drilling. Ground monitoring using the total station was done monthly.

From the field investigation, it is observed that a shale bed is exposed in different sections of the study area. The area is covered by a thick layer of highly weathered soil in the upper slope sections, suggesting prolonged exposure to weathering processes. A notable difference was observed in the composition and grain size of the shale between undisturbed and disturbed areas. Shale in undisturbed zones exhibited a higher silt content, whereas shale in the sliding areas displayed a higher clay content. The presence of higher clay content in the sliding areas is particularly significant, potentially contributing to reduced slope stability and increased landslide susceptibility due to the clay's lower shear strength and greater water retention capabilities.

The natural moisture content of the soil is highest in ZS5 with a value of 23.671(Table 5.1) and lowest for ZS7 (Table 5.1).

Liquid limit ranges from 29.17% in ZS4 to 40.60% in ZS6 (table 5.2). ZS4 collected from a highly disturbed has the lowest liquid limit which shows that it will easily behave as a liquid when in contact with water compared to other samples. The highest value of liquid limit observed in location 2 is 40.60% shown by ZS6. The value of plastic limit ranges between 20.52 to 32.10. ZS4 has the lowest value of plastic limit which indicates that they require the least amount of moisture to behave as a plastic material. The soil ranges from 8.57 to 13.73 in the plasticity index, -0.21 to 0.07 in the liquidity index, and 0.92 to 1.21 in the consistency index. Hence all the samples fall under semi-solid types based on the value of consistency index and liquidity index, and can be classified as slightly plastic based on plasticity index. ZS4

has the highest dry density with a value of 1.88g/cc and the lowest value 1.53g/cc is shown by ZS6.

The direct shear test was performed in 5 different areas in location 2. The maximum cohesion value of 0.242kg/cm^2 is shown by ZS5 with an angle of internal friction 26.99°. The angle of internal friction falls between 26.99° to 28.9° (Table 5.13). A triaxial soil test is performed for ZS7 shows cohesion value and angle of internal friction of 39Kpa and 20° respectively which is lower compared to the cohesion and angle of internal friction obtained from the direct shear test.

Both the slopes ZS7& ZS8 and ZS4, ZS5&ZS6 in location-2 show a factor of safety below unity in all the methods employed in slope stability analysis using the limit equilibrium method. Except for Bishop Simplified Method in ZS4, ZS5 & ZS6, the FoS are below 0.6. From the value of FoS obtained from slope stability analysis (Table 5.15), we can interpret that the whole area in location 2 has a very high chance of slope failure. The FoS shown by the parameters obtained from the triaxial test is lower than the direct shear test.

Almost all the samples except ZR9 which was collected from a stable area show high durability after the second cycle of alternate wetting and drying(Table 5.18). ZR9 has the highest SDI value of 91% and is classified as a very highly durable rock. 76.43% is the lowest SDI value in location 2 and is shown by ZR7. With an increase in the cycle of wetting and drying conditions, most of the samples will fall under medium durability after the 4th cycle.

ZR9 which is collected from the stable area has a point load index strength of 1.59MPa which is the highest value of point load strength among the rocks studied in location 2. Except for ZR9 and ZR15 which are samples from undisturbed areas, all the other rock shows UCS values less than 20 MPa respectively (Table 5.20).

From the kinematic analysis performed in 5 different spots, planar failure, and wedge failure are the most common probable slope failures observed in location 2. For spot 1, wedge failure is 1.1%. Wedge failure is possible in spot 2 with a

percentage of 25.49. In spots 3 and 5, wedge failure is maximum with 2.8% and 1.9% respectively. Planar failure is 30% for spot 4.

Vertical Electrical Sounding (VES) with Schlumberger configuration was conducted in three locations VES-1 (Figure 5.98), VES-2 (Figure 5.99), and VES-3 (Figure 5.100). The pseudo-section and resistivity cross-sections were plotted from the combination of the three stations (Figure 5.101). All three sounding curves showed a K-type curve which is a three-layer case, where $\rho_1 < \rho_2 > \rho_3$ represents each layer's resistivity. The resistivity of each layer is compared with the drilling data up to a depth of 30m (Figure 5.102). The Vertical Electrical Sounding (VES) and the drilling data were interpreted to have a good correlation. The top layer up to a depth of 4.5m was composed of weathered shale and clay with a resistivity ρ_1 range of 115 to 175 Ohm-m, there is no core recovery and the RQD percentage was also zero. The second layer comprises of intercalation of shale with high silt content and shale with high clay content with the highest resistivity ρ_2 value (100-450 Ohm-m) compared to the other layer, this layer has a thickness of 7m (4.5m to 11.5m), this layer has a core recovery of 3% to 11% but the RQD% was zero. The lithology in the third layer was silty-clay with low resistivity value ρ_3 ranging from (38-100)Ohm-m, the thickness of this layer was 17m (11.5m to 28.5m), the low resistivity value of this layer could be due to the presence of clay, which act as impermeable layers which prevent further movement of water. The water present in this layer could act as a charge carrier and result in high conductivity and low resistivity. The RQD% at a depth of 14.5m and 22m was 11% and 10% respectively and a maximum core recovery of 32% at a depth of 16m.

From the drilling data and resistivity value we can interpret that bedrock was observed at a depth of 4.5m. A soft shale with high silt and shale content was observed with a low core recovery from 4.5m to 11.5m. The low core recovery and less RQD% showed that the bedrock was weak and highly weathered. From 11.5m to 28m, an alteration of soft shale with high clay content and shale with silt and clay content was encountered. The decrease in resistivity value at a higher depth with the presence of shale with high clay content represents high water content. The weak

rock mass and presence of water could be the triggering factor for the instability of the area.

From the analysis of rainfall data collected from the State Meteorological Center, Directorate of Science and Technology, Government of Mizoram from 2012 to 2022, it is observed that precipitation is mostly maximum in July for every year and reached a maximum of 743.5mm in June 2017. A subsidence of an average of 1ft is observed from the total station data during September 2022. Precipitation of 460mm in July 2022 was observed from the rainfall data which could greatly contribute to saturating the soil which can result in slope failure.

CHAPTER 6

CONCLUSION AND MITIGATION SUGGESTION

6.1 CONCLUSION

The geology of the research area is mainly composed of shale with high clay contents overlain by loose and weathered soil in most of the area. The research is based on field investigation, laboratory analysis, and analysis using software. From the field investigations, it is observed that the soil and the bedrock in the study area are displaced due to subsidence. So, we can interpret that not only the geomechanical properties of the soil but also the bedrock underlying the soil are responsible for triggering the ground subsidence. The field investigation revealed significant variations in shale bed characteristics across different areas of the terrain. A notable difference in composition and grain size was observed between undisturbed and disturbed areas. Shale in undisturbed zones showed higher silt content, while shale in the sliding areas exhibited higher clay content. The higher clay content in sliding areas is concerning, as it could contribute to reduced slope stability and increased landslide susceptibility due to the clay's lower shear strength and greater water retention capabilities.

From the Atterberg limit data, the soil in both locations can be classified as semi-solid with slightly plastic characters.

Based on the slope stability analysis using the limit equilibrium method with consideration of both direct shear and triaxial parameters, the findings indicate that the slope possesses a Factor of Safety (FoS) that is below unity. This conclusion implies that the study area is unstable and susceptible to slope failure, particularly when saturated with moisture. The FoS below 1 signifies that the forces acting to destabilize the slope (such as gravitational forces and pore water pressure) exceed the resisting forces provided by the soil and rock materials. Therefore, under saturated conditions, the slope is at risk of experiencing instability and potential slope failure.

Based on the analysis of samples ZR2, ZR5, and ZR9 collected from the undisturbed area, which exhibits durability above 90% and point load strength exceeding 2 MPa, it is evident that these samples demonstrate higher durability and strength compared to those obtained from the disturbed area. This discrepancy leads us to interpret that the subsidence area, characterized by lower durability and strength measurements in the collected samples, contrasts significantly with the stable surroundings. The observed differences highlight the impact of disturbance on the mechanical properties of the rock.

75% of the rock study in location 2 falls under the poor rock category under the RMR classification. Therefore, the rock observed in the study area can be classified as poor.

From Kinematic Analysis in location 2, the most probable failure is analyzed as wedge failure. Even though the slope and bed have an anti-dip relationship, due to the presence of joints and weak-strength rock, the area is still susceptible to wedge failure.

Based on the analysis of the 28-meter depth resistivity value and drilling data, it has been determined that the bedrock is situated at a depth of approximately 4.5 meters. The presence of intercalated shale layers with varying proportions of clay and silt content suggests complex sedimentary conditions in the subsurface. Zero percent RQD and a maximum core recovery of 11% indicate that the underlying bedrock is weak and highly weathered, compromising its structural integrity. Moreover, the decrease in resistivity values at greater depths, particularly in the presence of clay-rich shale layers, signifies elevated water content at lower depths. This high water content is likely a significant factor contributing to potential bedrock displacement and instability within the study area.

From the correlation between the total station data and the rainfall data, we can conclude that the ground movement of average 1ft displacement which occurred in September 2022 is rainfall-induced as the soil can be in its saturation stage due to a 460mm precipitation in July followed by continuous rainfall in the following months.

Based on the comprehensive field study, geotechnical analysis, and geophysical investigations conducted in the study area, several conclusions can be drawn regarding the factors contributing to slope instability and potential failures.

1. The research area is predominantly covered by loose and weathered soil, particularly susceptible to saturation during the monsoon season and the soil shows semi-solid with slightly plastic characters with low shear strength.

2. Beneath the soil layer lies a weak bedrock with high clay content, which behaves like a fluid upon contact with percolated water from the weathered soil, further compromising stability. Despite the anti-dip relationship between the bed and the slope, the weak point load strength and low durability coupled with the presence of joints and low RMR value serve as triggering factors for slope failure in both study locations. Additionally, comparing shale samples from disturbed and undisturbed areas in Zuangtui reveals that variations in silt and clay content play a significant role in weakening the rock during the rainy season, with high clay content observed in the study area exacerbating this susceptibility to instability.

3. From the 28m depth subsurface investigation, we can conclude that the underlying bedrock is weak, fractured, and highly weathered, compromising its structural integrity. The subsurface lithology is comprised of a shale bed with alternate variations of shale and clay proportion and also has an increase in water content with depth.

4. A 1ft ground movement was observed within a monitoring period of one and a half years. This indicates a moderate rate of movement. Further monitoring of the area is no longer feasible due to ongoing development activities occurring within the monitoring zone.

6.2 MITIGATION SUGGESTION

Some of the mitigation measures suggested for stabilization of the slope in the study areas area:

1. Given the area's composition of loose soil and rock with high clay content, it is imperative to implement a comprehensive drainage system to manage water flow effectively. This includes establishing proper channels to direct the flow of water (nallah) and installing shallow or surface drainage systems to control surface runoff(Figure 6.1 & 6.2). Since a shale bed is encountered at a depth of 4m and the bed observed in the study area dips towards South East, a deeper subsurface drainage system, extending to more than 4 meters in depth, is recommended for location-2 in the Western boundary so that a large amount of groundwater movement can be drained off from entering the sliding area (Figure 6.2).

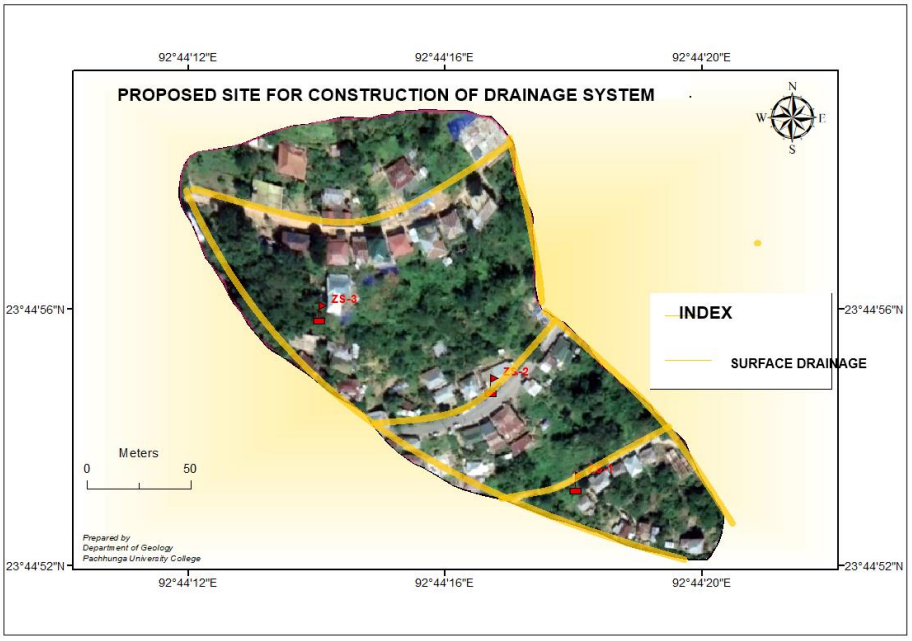

Figure: 6.1. Proposed drainage system for location-1

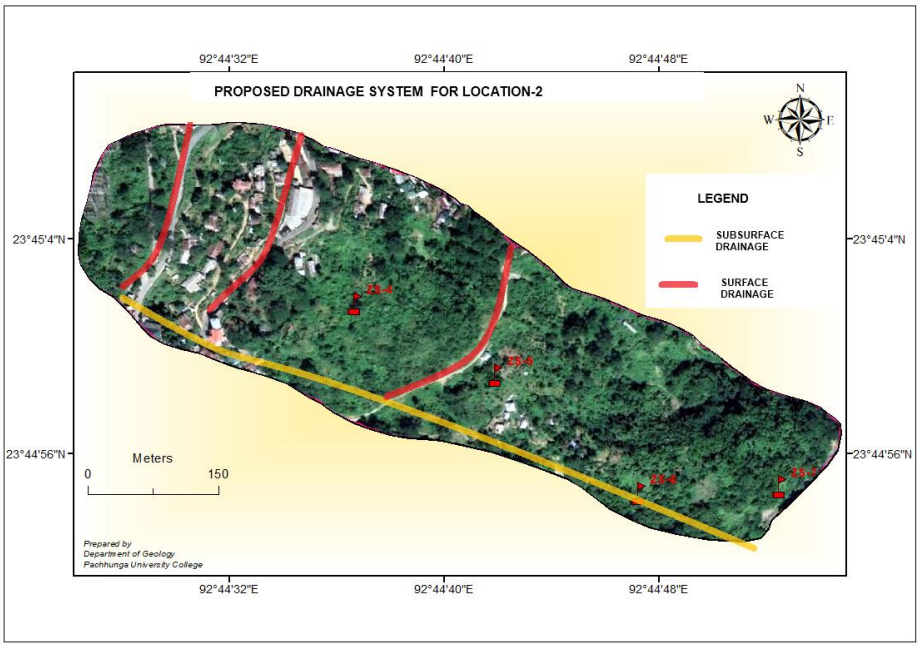

Figure: 6.2. Proposed drainage system location-2

2. To address the driving forces contributing to slope instability, measures should be taken to minimize construction loads, especially in the upper portions of the slope. This involves restricting building construction and reducing soil mass by removing loose debris and benching the slope.

3. Increasing the resisting force against landslides is crucial. Given the shallow water table in the study area, constructing gabion walls along the channel banks can effectively manage groundwater seepage. Moreover, constructing or reinforcing gabion walls along road sections is proposed (Figure 6.3 and 6.4). Strengthening the check dam at the toe of location 1 is also advised to provide additional stability and erosion control. These interventions collectively aim to enhance slope stability and mitigate landslide risks in the study area, considering the specific geological and hydrological conditions observed.

Figure: 6.3. Proposed mitigation site for location-1

Figure:6.4. Proposed mitigation site for location-2

6.3 LIMITATIONS

The shortage of advanced equipment poses a significant limitation in our ability to conduct comprehensive studies. Additionally, exploring deeper depths becomes a challenging task due to topographical obstacles. These constraints hinder our capacity to delvelop into more intricate aspects of research. Efforts to address these limitations and enhance technological resources are crucial for advancing our understanding. To address the driving forces contributing to slope instability, measures should be taken to minimize construction loads, especially in the upper portions of the slope. This involves restriction on building construction and reducing soil mass by removing loose debris and benching the slope.Conducting a comprehensive subsurface investigation using advanced geophysical methods holds the key to acquiring detailed and accurate information about slope problems. By employing sophisticated techniques, such as ground-penetrating radar or seismic surveys, we can delvelop deep into the subsurface layers. This in-depth analysis will yield a wealth of data on soil composition, geological structures, and potential hazards.

APPENDICES- PHOTO PLATE

Figure: Bulging of gabion wall in location-1

Figure: Collapsed of steps and pillar foundation

Figure: Crown of landslide

Figure: Collapsed of retaining wall

Figure: Cracks along the road

Figure: 1ft ground subsidence

Figure: Cracks on the groundfloor of the house steps

Figure: Fractures along private

Figure: Total station survey

Figure: Geological field work

Figure: Geological fieldwork

Figure: collapsed gabion wall

REFERENCES

Ahmed, B. (2021). The root causes of landslide vulnerability in Bangladesh. *Landslides*, *18*(5), 1707-1720. https://doi.org/10.1007/s10346-020-01606-0

Ahmed, K. S., Basharat, M., Riaz, M. T., Sarfraz, Y., & Shahzad, A. (2021). Geotechnical investigation and landslide susceptibility assessment along the Neelum road: a case study from Lesser Himalayas, Pakistan. *Arabian Journal of Geosciences*, *14*(11), 1019. https://doi.org/10.1007/s12517-021-07396-6

Alam, K., Abdullatif, O., El-Husseiny, A., & Babalola, L. (2022). Depositional and diagenetic controls on reservoir heterogeneity and quality of the Bhuban formation, Neogene Surma Group, Srikail Gas Field, Bengal Basin, Bangladesh. *Journal of Asian Earth Sciences*, *223*, 104985. https://doi.org/10.1016/j.jseaes.2021.104985

Alkhamaiseh, T., Mejus, L., Yusof, I., & Yaccup, R. (2018). Relationships between geophysical and geotechnical parameters focusing on a site specific results of a landslide risk area. *Amazonia Investiga*, *7*(15), 386-398.

Al-Taie, A. J. (2021, June). Assessment of durability and deterioration of rocks from western Iraq. In *IOP Conference Series: Materials Science and Engineering* (Vol. 1105, No. 1, p. 012112). IOP Publishing.

Al-Yasir, A. T., & Al-Taie, A. J. (2023). A new sand raining technique to reconstitute large sand specimens. *Journal of the Mechanical Behavior of Materials*, *32*(1), 20220228. https://doi.org/10.1515/jmbm-2022-0228

Amaral, P., Malheiro, A., Marques, F., Moniz, L., Furtado, S., & Loura, N. (2020, January). The use of total station for monitoring mass movements: application to Fajãzinha landslide at Flores Island (Azores Archipelago). In *Advances in Natural Hazards and Hydrological Risks: Meeting the Challenge: Proceedings of the 2nd International Workshop on Natural*

Hazards (NATHAZ'19), Pico Island—Azores 2019 (pp. 59-62). Cham: Springer International Publishing. https://doi.org/10.1007/978-3-030-34397-2_12

Araújo, J. R., Ramos, A. M., Soares, P. M., Melo, R., Oliveira, S. C., & Trigo, R. M. (2022). Impact of extreme rainfall events on landslide activity in Portugal under climate change scenarios. *Landslides*, *19*(10), 2279-2293. https://doi.org/10.1007/s10346-022-01895-7

Bahammou, Y. A., Benamara, A., Ammar, A., Hrittta, D., Dakir, I., & Bouikbane, H. (2021). Application of vertical electrical sounding resistivity technique to explore groundwater in the Errachidia basin, Morocco. *Groundwater for Sustainable Development*, *15*, 100648. https://doi.org/10.1016/j.gsd.2021.100648

Barman, J., Biswas, B., & Das, J. (2022). Mizoram, the capital of landslide: a review of articles published on landslides in Mizoram, India. *Monitoring and Managing Multi-hazards: A Multidisciplinary Approach*, 97-104. https://doi.org/10.1007/978-3-031-15377-8_6

Bejan, F. (2018). Comparative Study of Semi-Probabilistic and Probabilistic Approaches for Slope Stability Assessment. Study Case. *Bulletin of the Polytechnic Institute of Iasi-Construction & Architecture Section*, *69*(4), 43-56.

Bhusan, K., Pande, T., & Kayal, J. R. (2022). Landslide affected areas and challenges imposed in North Eastern Region of India: an appraisal. *Aust J Eng Innov Technol*, *4*, 32-44.

Borgohain, P., Hussain, M. F., Bezbaruah, D., Vanthangliana, V., Phukan, P. P., Gogoi, M. P., & Bharali, B. (2020). Petrography and whole-rock geochemistry of Oligocene Barail Sandstones of Surma basin: Implications for tectono-provenance and paleoclimatic condition. *Journal of Earth System Science*, *129*, 1-26. https://doi.org/10.1007/s12040-020-01431-y

Chen, Z., Song, D., Hu, C., & Ke, Y. (2020). The September 16, 2017, Linjiabang landslide in Wanyuan County, China: preliminary investigation and emergency mitigation. *Landslides*, *17*, 191-204.

Chitra, R., & Gupta, M. (2016). Geotechnical investigations and slope stability analysis of a landslide. *International Journal of Engineering Research & Technology (IJERT)*, *5*(02), 390-398.

Cho, I. K. (2020). Recent Trend in Electrical Resistivity Method. *Journal of the Korean Society of Mineral and Energy Resources Engineers*, *57*(5), 506-526. https://doi.org/10.32390/ksmer.2020.57.5.506

Choi, K. Y., & Cheung, R. W. (2013). Landslide disaster prevention and mitigation through works in Hong Kong. *Journal of Rock Mechanics and Geotechnical Engineering*, *5*(5), 354-365. https://doi.org/10.1016/j.jrmge.2013.07.007

Christopher, W. A. P. P., De Silva, N., Attanayake, A. M. A. N. B., & Jayasingha, P. (2023). Characterization of landslides: a vertical electrical sounding approach. *Geoscience Letters*, *10*(1), 1-10. https://doi.org/10.1186/s40562-023-00274-x

Coduto, D. P., Yeung, M. C. R., & Kitch, W. A. (1999). Geotechnical engineering: principles and practices.

Cotecchia, F., Santaloia, F., Lollino, P., Vitone, C., Cafaro, F., & Bottiglieri, O. (2016). A geomechanical approach to landslide hazard assessment: the Multiscalar Method for Landslide Mitigation. *Procedia Engineering*, *158*, 452-457.

Deshpande, S. M., Aher, R. K., Gaikawad, G. D., & Aher, K. R. (2018). Electrical resistivity method for groundwater exploration: A case study of ganori village area, Aurangabad District, Maharashtra, India. *Bulletin of Pure & Applied Sciences-Geology*, *37*(2), 125-137.

Duncan, J. M. (1996). State of the art: limit equilibrium and finite-element analysis of slopes. *Journal of Geotechnical engineering*, *122*(7), 577-596.

Evans, S., Bovis, M., & Hutchinson, J. (2001). Landslides of the flow type. *Environmental & Engineering Geoscience*, *7*(3), 221-238.

Franklin, J. A., & Chandra, R. (1972, May). The slake-durability test. In *International Journal of Rock Mechanics and Mining Sciences & Geomechanics Abstracts* (Vol. 9, No. 3, pp. 325-328). Pergamon.

Ganju, J. L. (1975). Geology of mizoram. *Bull. Geol. Min. Met. Soc. India*, *48*, 17-26.

Gazibara, S. B., Arbanas, S. M., Sinčić, M., Krkač, M., Lukačić, H., Jagodnik, P., ... & Arbanas, Ž. (2022). LandSlidePlan-scientific research project on landslide susceptibility assessment in large scale. In *Proceedings of the 5th regional symposium on landslides in Adriatic-Balkan Region* (pp. 99-106). University of Zagreb.

Herianto, P., Kunsuwan, B., Mairaing, W., Chalermpornchai, T., & Srisook, W. (2020). GIS-Based Landslide Susceptibility Map Verification by its Geotechnical and Geological Characteristics. *International Journal of Geoinformatics*, *16*(4).

Islam, M. S., Shijan, M. H. H., Saif, M. S., Biswas, P. K., & Faruk, M. O. (2021). Petrophysical and petrographic characteristics of Barail Sandstone of the Surma Basin, Bangladesh. *Journal of Petroleum Exploration and Production Technology*, *11*(8), 3149-3161.

Jianjun, G., Zhang, Y. X., & Xiao, L. (2020). An application of the high-density electrical resistivity method for detecting slide zones in deep-seated landslides in limestone areas. *Journal of applied geophysics*, *177*, 104013.

Jongmans, D., & Garambois, S. (2007). Geophysical investigation of landslides: a review. *Bulletin de la Société géologique de France*, *178*(2), 101-112.

Kabeta, W. F., Tamiru, M., Tsige, D., & Ware, H. (2023). An integrated geotechnical and geophysical investigation of landslide in Chira town, Ethiopia. *Heliyon*, *9*(7).

Kamal, M., Shen, J., Othman, A. A. A., Sultan Araffa, S. A., Tekin, H. O., Ene, A., ... & Zakaly, H. M. (2023). Integrated geophysical techniques applied for petroleum basins structural characterization in the central part of the Western Desert, Egypt. *Open Chemistry*, *21*(1), 20220293.

Khan, M. A., Hossain, M. S., Khan, M. S., Samir, S., & Aramoon, A. (2017). Impact of wet-dry cycles on the shear strength of high plastic clay based on direct shear testing. In *Geotechnical Frontiers 2017* (pp. 615-622).

Kumar, A., & Sanoujam, M. (2007). Landslide studies along the national highway (NH39) in Manipur. *Natural hazards*, *40*(3), 603.

Laldinpuia(2019). Geological investigation and monitoring of Ramhlun Sport Complex landslide,Aizawl,India. *Sci vision,* 19(3), 80-99

Laldinpuia, K. S., & Singh, T. N. (2013). The 2013 rockslide disaster of Aizawl, Mizoram, India. *Sci Vis*, *13*(2), 58-63.

Laldintluanga, H., Ramhmachhuani, R., Mozumder, R. A., & Lalbiakmawia, F. (2023). Hydrogeological Effects on Premature Failure of Flexible Pavement in Hilly Area Along State Highway-I in Mizoram, India. *Indian Geotechnical Journal*, *53*(1), 29-41.

Lalhlimpuia, H. (2022). *Geotechnical studies of selected rockfall sites In and around aizawl, mizoram* (Doctoral dissertation, Mizoram University).

Lalitha, M., Kumar, K. A., Nair, K. M., Dharumarajan, S., Koyal, A., Khandal, S., ... & Hegde, R. (2021). Evaluating pedogenesis and soil Atterberg limits for inducing landslides in the Western Ghats, Idukki District of Kerala, South India. *Natural Hazards*, *106*, 487-507.

Mahmud, S., Hamza, S., Irfan, M., Huda, S. N. U., Burke, F., & Qadir, A. (2022). Investigation of groundwater resources using electrical resistivity sounding and Dar Zarrouk parameters for Uthal Balochistan, Pakistan. *Groundwater for sustainable development*, *17*, 100738.

McColl, S. T. (2022). Landslide causes and triggers. In *Landslide hazards, risks, and disasters* (pp. 13-41). Elsevier.

Mehmood, Z., Khan, N. M., Sadiq, S., Mandokhail, S. U. J., & Ashiq, S. Z. (2020). Assessment of subsurface lithology, groundwater depth, and quality of UET Lahore, Pakistan, using electrical resistivity method. *Arabian Journal of Geosciences*, *13*(6), 281.

Misbahudin, M. (2020). Landslide susceptibility analysis in Kabandungan District and Salak Geothermal Field, West Java. *Jurnal Geografi Lingkungan Tropik (Journal of Geography of Tropical Environments)*, *4*(2), 1.

Mohamaden, M. I. I., Hamouda, A. Z., & Mansour, S. (2016). Application of electrical resistivity method for groundwater exploration at the Moghra area, Western Desert, Egypt. *The Egyptian Journal of Aquatic Research*, *42*(3), 261-268. 10.1088/1742-6596/995/1/012094

Munshi, K. N., & Dey, A. K. (1964). Spectrophotometric Determination of Rare Earth Metals with 4-(2-Pyridylazo) resorcinol. *Analytical Chemistry*, *36*(10), 2003-2004.

Pal, R., Biswas, S. S., Mondal, B., & Pramanik, M. K. (2016). Landslides and floods in the Tista Basin (Darjeeling and Jalpaiguri Districts): Historical evidence, causes and consequences. *J. Ind. Geophys. Union*, *20*(2), 66-72.

Parkash, S., Awasthi, A. K., & Virdi, N. S. (2003). Stability assessment of rock slopes using modified SMR technique and kinematic analysis along SH-53 between Dunda and Uttarkashi, Uttaranchal. *Geological Society of India*, *61*(5), 595-606.

Pasierb, B., Grodecki, M., & Gwóźdź, R. (2019). Geophysical and geotechnical approach to a landslide stability assessment: a case study. *Acta Geophysica*, *67*(6), 1823-1834.

Popescu, M. E., & Sasahara, K. (2009). Engineering measures for landslide disaster mitigation. *Landslides–Disaster Risk Reduction*, 609-631. https://doi.org/10.1007/978-3-540-69970-5_32

Rusydy, I., Al-Huda, N., Fahmi, M., & Effendi, N. (2019). Kinematic analysis and rock mass classifications for rock slope failure at USAID highways. *Structural Durability & Health Monitoring*, *13*(4), 379.

Salamov, A. M., Mammadov, V. A., Khalilova, H. K., Zamanova, A. G., & Gasimov, E. E. (2021). Research into landslide processes in the coastal zone of the Takhtakorpureservoir using vertical electrical sounding method (the southeastern slope of the Great Caucasus). *Geofizicheskiy Zhurnal*, *43*(6), 209-220. https://doi.org/10.24028/gzh.v43i6.251563

Sardana, S., Verma, A. K., Singh, A., & Laldinpuia. (2019). Comparative analysis of rockmass characterization techniques for the stability prediction of road cut slopes along NH-44A, Mizoram, India. *Bulletin of Engineering Geology and the Environment*, *78*, 5977-5989. https://doi.org/10.1007/s10064-019-01493-3

Schepers, R., Rafat, G., Gelbke, C., & Lehmann, B. (2001). Application of borehole logging, core imaging and tomography to geotechnical exploration. *International Journal of Rock Mechanics and Mining Sciences*, *38*(6), 867-876. https://doi.org/10.1016/S1365-1609(01)00052-1

Senthilkumar, V., Chandrasekaran, S. S., & Maji, V. B. (2017). Geotechnical characterization and analysis of rainfall—induced 2009 landslide at Marappalam area of Nilgiris district, Tamil Nadu state, India. *Landslides*, *14*, 1803-1814.

Shible, H., Hollender, F., Traversa, P., & Bard, P. Y. (2023). Ground-motion model for hard-rock sites by correction of surface recordings (Part 1): Comparison of site-response estimates at KiK-Net sites. *Bulletin of the Seismological Society of America*, *113*(5), 2164-2185.

Shrestha, H. K., Yatabe, R., & Bhandary, N. P. (2008). Groundwater flow modeling for effective implementation of landslide stability enhancement measures: a case of landslide in Shikoku, Japan. *Landslides*, *5*, 281-290. https://doi.org/10.1007/s10346-008-0121-8

Shrivastava, S., & KK, R. (1979). Stratigraphy of eastern Mizo hills. *Bulletin of the Oil and Natural Gas Commission* 16: 87-94

Siddique, T., Alam, M. M., Mondal, M. E. A., & Vishal, V. (2015). Slope mass rating and kinematic analysis of slopes along the national highway-58 near Jonk, Rishikesh, India. *Journal of Rock Mechanics and Geotechnical Engineering*, *7*(5), 600-606. https://doi.org/10.1016/j.jrmge.2015.06.007

Siddiqui, F. I., & Osman, S. B. A. S. (2012). Integrating geo-electrical and geotechnical data for soil characterization. *International Journal of Applied Physics and Mathematics*, *2*(2), 104-106.

Singh, P. K., Ratan, D., Singh, K. K., & Singh, T. N. (2016, November). Landslide in fractured and stratified rocks-a case from Aizawl, Mizoram, India. In *Recent Advances in Rock Engineering (RARE 2016)* (pp. 375-380). Atlantis Press. https://doi.org/10.2991/rare-16.2016.59

Singh, T. N., & Singh, V. (2005). An intelligent approach to prediction and control ground vibration in mines. *Geotechnical & Geological Engineering*, *23*, 249-262.

Sloan, S. W. (2013). Geotechnical stability analysis. *Géotechnique*, *63*(7), 531-571. https://doi.org/10.1680/geot.12.RL.001

Stark, T. D., Choi, H., & McCone, S. (2005). Drained shear strength parameters for analysis of landslides. *Journal of Geotechnical and Geoenvironmental Engineering*, *131*(5), 575-588.

Tamrakar, N. K., Kushwaha, S. P., & Maharjan, S. (2021). Slake durability indices and slaking characteristics of mudrocks of the Siwalik Group, Central

Nepal. *International Journal of Engineering Research and Applications*, *11*(1), 59-73.

Tsiambaos, G.,& Sabatakakis, N. (2004).Considerations on strength of intact sedimentary rocks. *Engineering Geology*, *72*(3-4), 261-273. https://doi.org/10.1016/j.enggeo.2003.10.001

Vyzhva, S., Onyshchuk, V., Onyshchuk, I., Reva, M., & Shabatura, O. (2019, May). Application of geophysical methods in the study of landslides. In *18th International Conference on Geoinformatics-Theoretical and Applied Aspects* (Vol. 2019, No. 1, pp. 1-5). European Association of Geoscientists & Engineers.https://doi.org/10.3997/2214-4609.201902066.

WANG, J. Q., CHANG, Z. C., Tang, Y., & Tang, Y. (2021). Dynamic triaxial test analysis of reinforced gravel soil under cyclic loading. *Rock and Soil Mechanics*, *41*(9), 1.

Wieczorek, G. F. (1996). Landslides: investigation and mitigation. Chapter 4-Landslide triggering mechanisms. *Transportation Research Board Special Report*, (247).

Yalcin, A. (2011). A geotechnical study on the landslides in the Trabzon Province, NE, Turkey. *AppliedClay Science*, *52*(1-2), 11-19. https://doi.org/10.1016/j.clay.2011.01.015

Zieher, T., Pfeiffer, J., van Natijne, A., & Lindenbergh, R. (2021, July). Integrated monitoring of a slowly moving landslide based on total station measurements, multi-temporal terrestrial laser scanning and space-borne interferometric synthetic aperture radar. In *2021 IEEE International Geoscience and Remote Sensing Symposium IGARSS* (pp. 942-945). IEEE. https://doi.org/10.1109/IGARSS47720.2021.9553324

BRIEF BIO-DATA

Personal Details:-

Name : **LALHMINGSANGI**

Address : **RAMTHAR VENG, AIZAWL**

Phone No. : **7628000776**

Email address : **sangby90@gmail.com**

Father's Name : **LALRAMHLUNA**

Mother's Name : **LALHMUNHLUI**

Marital Status : **SINGLE**

EDUCATION:

Year	Institution	Board	Class	Subject	Division	Percentage
2008	SPHSS	MBSE	X	-	D	75.2%
2010	SPHSS	MBSE	XII	Science	II	58.4%
2014	PUC	MZU	B.Sc.	Geology	I	81.16%
2016	DIBRUGARH UNIVERSITY	UGC	MSc.	Geology	I	73.2%
2021	MZU	MZU	Ph.D.	Geology	A+	8 SGPA

PERFORMANCE:

PUBLICATIONS:

1. Published a paper entitled ‘Slake durability and point load indices of shale in Zuangtui sliding area, Aizawl, Mizoram’,*Sci Vision,* Vol.23(1):2-5, ISSN: 0975-6175
2. Published a paper entitled ‘Characteristics of soil with seasonal change and their effects on slope stability’, *Sci vision,* Vol.23(1):19-24,ISSN: 0975-6175

PRESENTATIONS:

1. Presented a paper on ‘Application of Total Station for Landslide Monitoring: A Case Study of Aizawl, Mizoram, ’ at Mizoram Science Congress 2020.
2. Presented a paper on ‘Kinematic Analysis and Hazard Assessment of Zemabawk Landslide, Aizawl ’ at Mizoram Science Congress 2018.
3. Presented a paper on ‘Geotechnical Investigation and Slope Stability Analysis using Limit Equilibrium Method(LEM) of Zuangtui Area in Aizawl, Mizoram, ’ at Mizoram Science Congress 2022.
4. Presented a paper on ‘Geomechanical Study of Zuangtui Slumping Area in Aizawl, Mizoram, ’ at NETC 2022, IIT Guwahati.
5. Presented a paper on ‘Geophysical and Geotechnical Investigation of Zuangtui Subsidence, Aizawl, Mizoram ’ at International Conference on Exploring the complexities of physical and earth system dynamics through modeling and data analysis, PUC, Aizawl 2024

TRAINING AND SEMINAR ATTEND:

1. 3 Days National Workshop on 'Landslide Hazard in Southern Mizoram' during 24th - 26th October 2019 at Lunglei organized by MISTIC, DGMR, LGC and GSM
2. E-training on 'Application of Geographic Information System' conducted by GSI during 30th June to 7th July 2020
3. E-Training on "Refresher Course on NGCM Data Handling and Interpretation" conducted by RTD, NER, GSITI, Shillong from 20.07.2020 to 24.07.2020.
4. Participated in the National Training Programme on Earthquake Risk Mitigation jointly organized by the National Institute of Disaster Management, Ministry of Home Affairs, Government of India, New Delhi, and North-Eastern Hill University, Shillong from July 08 -10, 2020 using online mode.

PARTICULARS OF THE CANDIDATE

NAME OF CANDIDATE : **LALHMINGSANGI**

DEGREE : **Doctor of Philosophy**

DEPARTMENT : **Department of Geology**

TITLE OF THESIS : **'Geotechnical Investigations and Monitoring of Zuangtui Area, Aizawl, Mizoram'**

DATE OF ADMISSION : **16th April 2021**

APPROVAL OF RESEARCH PROPOSAL:-

1. BOS : **23rd April 2021**
2. School Board : **5th May 2021**

:

MZU REGISTRATION NO. : **2100410**

PH.D. REGISTRATION NO.: **MZU/Ph.D./1738 of 16.04.2021**

AND DATE

EXTENSION (IF ANY) : **NIL**

Head Department of Geology

ABSTRACT

GEOTECHNICAL INVESTIGATIONS AND MONITORING OF ZUANGTUI AREA, AIZAWL, MIZORAM

AN ABSTRACT SUBMITTED IN PARTIAL FULFILLMENT OF THE REQUIREMENTS FOR THE DEGREE OF DOCTOR OF PHILOSOPHY

LALHMINGSANGI

MZU REGISTRATION NO.:2100410

Ph.D. REGISTRATION NO.:MZU/Ph.D./1738 of 16.04.2021

DEPARTMENT OF GEOLOGY

SCHOOL OF EARTH SCIENCES AND NATURAL RESOURCE MANAGEMENT

APRIL, 2024

GEOTECHNICAL INVESTIGATIONS AND MONITORING OF ZUANGTUI AREA, AIZAWL, MIZORAM

BY

LALHMINGSANGI
DEPARTMENT OF GEOLOGY

SUPERVISOR Dr.V.VANTHANGLIANA

JOINT SUPERVISOR Dr.LALDINPUIA

Submitted

In partial fulfillment of the requirement of the degree of Doctor of Philosophy in Geology of Mizoram University, Aizawl

ABSTRACT

Introduction:

A landslide is defined as the "movement of a mass of earth debris or rock down a slope," landslides can be triggered by various factors such as rainfall, earthquakes, toe erosion from flooding or river erosion, and other natural phenomena. Anthropogenic causes like slope modification, overgrazing, and excessive development also contribute to landslide occurrences.

These hazards are widespread, particularly in hilly terrains worldwide, and pose a significant threat in the North Eastern part of India, where landslides are the most serious hazard. In Mizoram, over 50% of natural hazards are attributed to landslides, primarily caused by topography, stream or river undercutting of slopes, slope modification for development, differential erosion, earthquakes, and the reduction in the engineering properties of rock and soil due to moisture.

The structural features of Mizoram reflect its position within the broader tectonic framework of the Assam Arakan geosynclines. The region exhibits a series of synclines and anticlines, with structural complexity gradually increasing from west to east. Along the Tripura-Mizoram border, various fold types, including overturned, box, and recumbent folds, signify the dynamic tectonic history of the area. Mizoram is flanked by narrow molasses basins like the Tipam basin on its western side, while the southern part of the Shillong plateau features the bell-shaped Surma basin sloping towards the southwest. These basin formations and structural characteristics underscore the complex interplay of tectonic forces shaping the geological landscape of Mizoram. Given the high-slope terrain and dense population in Aizawl, understanding mitigation measures is crucial for reducing the impact of landslide-related disasters.

Location and geology of the study area:

Mizoram is in the northeastern part of India. Its capital, Aizawl, sits centrally within the state, marked by the coordinates 23°39'N to 23°50'N latitude and 92°03'39"E to 92°04'47"E longitude, encapsulated within toposheets 84A/09,

84A/10, and 84A/13.

Zuangtui, a locality within Aizawl, falls under ward no. 1 of the Aizawl Municipal Corporation (AMC). Its coordinates range approximately from 23°44'54.54"N to 23°44'53.16"N latitude and 92°04'14.82"E to 92°04'18.6"E longitude, and elevation of around 965 meters above sea level. This area is delineated within top sheet 84A/9 for geographical reference.

Transportation-wise, the study area resides about 30 kilometers from Lengpui Airport, crucially linking Aizawl with major cities such as Kolkata, Guwahati, and Imphal. Moreover, National Highway 54 (NH-54) serves as a vital road artery, facilitating connectivity to Assam and other Indian states.

Geologically, the study area belongs to the Upper Bhuban Formation, a constituent of the Surma Group, having an age of Miocene-Oligocene age. Characterized by alternating sandstone and shale layers, a pronounced 40°E dip is evident in the southern part of the region, as documented by the Geological Survey of India in 1974 and 2011.

Surface-wise, the Upper Bhuban Formation is capped by thick layers of loose soil. Rock exposures, notably along the Zuangtui-Thuampui border stream and road sections, predominantly exhibit shale formations rich in clay content. These shale formations hint at sedimentary deposits likely formed in tranquil aquatic environments.

In this study, we focused on Zuangtui area, a pivotal locality in Aizawl, the capital of Mizoram, which has been experiencing ground movement since 1987. The slumping movement has resulted in the demolition of numerous buildings, the evacuation of government quarters, and the dislocation of the 132Kv Sub-Station. Given that Zuangtui serves as a crucial link to various essential centers, industries, and government offices for the residents in and around Aizawl, a thorough investigation of both surface and subsurface conditions is imperative.

Scope of the study:

Mizoram characterized by soft rocks and high hill slopes, compounded by random faulting and folding, creates inherently unstable slope conditions. In particular, the susceptibility to landslides is exacerbated by the presence of

groundwater in loose, weathered soil, and unconsolidated rock formations, particularly pronounced in areas like Aizawl. These factors contribute to frequent landslides during the rainy season, posing significant risks to habitat areas and infrastructure. Given these challenges, understanding the geological and geomechanical properties of the soil and rock is crucial, especially in the context of moisture influence. Conducting geophysical surveys can provide valuable insights into subsurface lithology and groundwater presence, aiding in the assessment of landslide risks. By integrating geotechnical investigations to evaluate material properties and groundwater conditions, it becomes possible to develop effective mitigation strategies to address landslide hazards.

Aims and Objectives

The objectives of this study are as follows

a) To assess geo-mechanical properties of soil and rock.

b) To monitor the rate of ground movement and to determine sub-surface structure

c) To suggest appropriate mitigation measures

Methodology

The area is divided in two locations, location 1 and location 2. A comprehensive investigation was conducted, involving detailed field and laboratory assessments. Geo-mechanical properties of the soil were evaluated through the Atterberg limit test, direct shear test, and triaxial test. The strength and durability of the rock were assessed using the point load test and slake durability test respectively. Slope stability was determined through kinematic analysis and the Limit Equilibrium Method. Rock mass classification was performed using Rock Mass Rating. To understand subsurface conditions, resistivity data were cross-validated with core drilling data. Ground motion was systematically monitored over three years using a total station instrument monthly.

The Attreberg limit test is performed according to IS: 2720 (Part 5). It is used

in the determination of the moisture content of the soil at which clay and silt soil transit in different phases. It is used for finding the plastic limit(PL), liquid limit(LL), and shrinkage limit(SL) of the soil sample. The natural water content of the soil is determined by the amount of water present in the soil expressed as a percentage of the oven dry weight. The liquid limit is determined using the Casagrande apparatus. For finding the plastic limit for the soil paste, alternate rolling and kneading until the thread crumbles under pressure, typically occurring at a diameter exceeding 3 mm is performed. The Plasticity Index is calculated as the difference between its liquid limit and plastic limit.

The compaction test is performed as per IS: 2720 Part VII-1980. The direct shear test is performed as per IS: 2720 (Part 13)-1986. Soil triaxial test was performed as per IS 2720(Part 11): 1993.

Slope stability analysis was performed using SLIDE 6.0, using Bishop simplified method, GLE/Morgenstern method, Ordinary/Fellenius method, Janbu simplified method, Janbu corrected method, and Spencer method. These methods are based on limit equilibrium, stress, and strain analysis. The mode of failure is pre-assumed where the failure occurs when the driving force exceeds the resisting force. Only the equilibrium of forces is satisfied in the simplest form of limit equilibrium analysis. The sum of the forces triggering the sliding of the slope is compared with the sum of the force resisting the failure along an assumed plan.

Slake durability test is to be carried out as per IS: 10050 -1981 guidelines to assess the rock resistance to disintegration under drying and wetting in a slaking fluid.

The determination of rock strength using the Point Load test was conducted in the study area using the Point Load Strength Index apparatus according to IS 8764:1998. The RMR, developed by Bieniawski in South Africa during 1972-1973, is a quantitative rock mass classification system or Geomechanics Classification system. Its primary purpose is to assess the stability and support requirements of tunnels. Moreover, the RMR method extends its applicability beyond tunnels, serving to evaluate the stability conditions of rock slopes and critical sections of rock masses susceptible to slope failure. The UCS of an intact rock material can be determined by the point load strength index test of rock cores and lumps. Rock

quality designation (RQD) is a quantitative assessment of rock quality. Joint spacing or discontinuity spacing can be defined as the perpendicular distance between the adjacent discontinuities or between the joints of the same joint set. It is widely accepted that the spacing of joints is of great importance in appraising a rock mass structure. The very presence of joints reduces the strength of a rock mass and their spacing governs the degree of such a reduction. Joint conditions parameters encompass the roughness of the discontinuity surfaces, their separation length of the discontinuity and continuity of the joints, weathering of the joints surface, slickenside, and infillings or gouge

Kinematic analysis is the determination of the possible modes of slope failure such as planar, wedge, and toppling based on the dip amount and dip direction of the discontinuities in a stereographic projection.

Conditions that must be satisfied during stereographic projection in kinematic analysis in different types of slope failure such as planar failure, wedge failure, and toppling failure.

a) Planar failure

The plane on which sliding occurs must strike parallel or nearly parallel (Approximately ±20º) to the slope face, the sliding plane must be 'daylight ' in the slope face, which means that the dip of the plane must be less than the dip of the slope face.

b) Wedge failure

Wedge failure occurs when two or more discontinuities intersect. Certain geometrical conditions must be satisfied for a wedge failure to occur.

c) Toppling failure

Toppling failure occurs when the discontinuity or joints are at a high angle (~ 70º) and the dip of the discontinuity must be within 10º in the direction of the face such that several slabs formed in the same trend with the face.

The electrical resistivity method using the Vertical Electrical Sounding (VES) technique was used in the study area for determining the relation between the resistivity of the subsurface rock and soil and their engineering properties. Signal

Stacking Resistivity Metre (SSRMT-ATS) instrument was used for the survey. Schlumberger configuration is the most suitable configuration for Vertical Electrical Sounding (VES) and gives the best resolution compared to the other configurations.

The total station is an electronic theodolite integrated with an electronic distance meter (EDM) for reading distances from the instrument to a particular point. It is used for measuring angles, heights, and distances. N6 series total station is used for monitoring the ground movement in the study area

A core drilling was performed at location 2 using the Diamond Core Drill TRD 80s Model. A 28m depth was reached. NX(types of core barrel) casing pipe of 3.4m and BX casing pipe of 8.20m were introduced in the borehole. The core samples were identified and litholog was prepared in comparison with the resistivity data.

Results and Discussion

A ground displacement of 1ft was observed in September 2022 at a location in the study area

In Location-1, the natural moisture content is highest for ZS2 with an NMC value of 30.23 and lowest for ZS1 with 23.77 NMC. The liquid limit which is the minimum moisture content at which the soil behaves as liquid ranges from 40.22% to 40.95%. The plastic limit is low in ZS3 compared to ZS2 . The maximum plasticity index obtained in location 1 is 16.31 and the soils are classified as slightly plastic.

The consistency index ranges from 1.14 to 1.24 and the liquidity index from -0.24 to -0.14. From the value of the liquidity index and consistency index, all the samples in location-1 can be classified as semi-solid according to Coduto 1999. The average dry density of the soil is 1.67g/cc

From the direct shear test, ZS2 has a cohesion value of 0.12 kg/cm^2 which is the lowest and also has the greatest angle of internal friction among the sample study in location 1 and it indicates a higher chance of failure compared to the other areas. The other two samples ZS1 and ZS2 have a cohesion of 0.32 kg/cm^2 & 0.23 kg/cm^2 and ^{an} angle of internal friction of 27.95° & 29.02° respectively.

From the slope stability analysis using the limit equilibrium method, it is analyzed that both the slope ZS1 AND ZS3 in location-1 have a factor of safety below unity in all the methods except for ZS1, the FoS is 1.33 in GLE/ Morgenstren-

price method and 1.18 in Spencer method.

Among the five-rock samples collected from location-1, three samples ZR3, ZR4 & ZR5 fall under high durability, with durability index of 82.74%, 84.85%, and 84.9% (respectively under two cycles of alternate wetting and drying conditions. Among the five samples, ZR2 and ZR5 which were collected from an undisturbed area have higher durability compared to those collected from unstable areas.

The point load index strength of rock varies from 1MPa in ZR4 to 2.3MPa in ZR2. The rock observed in undisturbed areas has higher strength compared to those in disturbed areas.

Based on the ground motion monitoring using total station data from September 2021 to March 2023, the slope remained stable initially from the start of monitoring until August 2022. However, a slight subsidence of approximately 1 foot was observed in September 2022. This subsidence coincided with significant changes in precipitation levels based on Aizawl rainfall data collected from the State Meteorological Center, Directorate of Science and Technology, Government of Mizoram.

The rainfall data indicates that precipitation in July reached 460 mm, which is a substantial amount capable of fully saturating the soil. This high level of saturation likely persisted into August, although the precipitation decreased to 277.8 mm during that month. The saturation of the soil due to these heavy rainfall events can increase pore water pressure and reduce soil strength, leading to potential instability and failure of the slope observed in September 2022. The observed subsidence in September 2022 following these rainfall events underscores the importance of understanding the influence of precipitation on slope stability.

The study of geological and geomechanical properties of rock and soil is conducted along with a resistivity survey and core drilling. Ground monitoring using the total station was done monthly.

In location-2, the natural moisture content of the soil is highest in ZS5 with a value of 23.671 and lowest for ZS7 . ZS4 collected from a highly disturbed has the lowest liquid limit which shows that it will easily behave as a liquid when in contact with water compared to other samples. The highest value of liquid limit observed in

location 2 is 40.60% shown by ZS6. The value of plastic limit ranges between 20.52 to 32.10. ZS4 has the lowest value of plastic limit which indicates that they require the least amount of moisture to behave as a plastic material. The soil ranges from 8.57 to 13.73 in the plasticity index, -0.21 to 0.07 in the liquidity index, and 0.92 to 1.21 in the consistency index

The direct shear test was performed in 5 different areas in location 2. The maximum cohesion value of 0.242kg/cm^2 is shown by ZS5 with an angle of internal friction 26.99°.

Both the slopes ZS7& ZS8 AND ZS4, ZS5&ZS6 in location-2 show a factor of safety below unity in all the methods employed in slope stability analysis using the limit equilibrium method.

Almost all the samples except ZR9 which was collected from a stable area show high durability after the second cycle of alternate wetting and drying. With an increase in the cycle of wetting and drying conditions, most of the samples will fall under medium durability after the 4th cycle.

ZR9 which is collected from the stable area has a point load index strength of 1.59MPa which is the highest value of point load strength among the rocks studied in location 2.

From the kinematic analysis performed in 5 different spots, planar failure, and wedge failure are the most common probable slope failures observed in location 2. For spot 1, wedge failure is 1.1%. Wedge failure is possible in spot 2 with a percentage of 25.49. In spots 3 and 5, wedge failure is maximum with 2.8% and 1.9% respectively. Planar failure is 30% for spot 4.

Vertical Electrical Sounding (VES) with Schlumberger configuration was conducted in three locations. The pseudo-section and resistivity cross-sections were plotted from the combination of the three stations. All three sounding curves showed a K-type curve which is a three-layer case, where $\rho_1 < \rho_2 > \rho_3$ represents each layer's resistivity. The Vertical Electrical Sounding (VES) and the drilling data were interpreted to have a good correlation. The top layer up to a depth of 4.5m was composed of weathered shale and clay with a resistivity ρ_1 range of 115 to 175 Ohm-m, there is no core recovery and the RQD percentage was also zero. The second layer comprises of intercalation of Silty-clay and Silty-Shale with the highest resistivity ρ_2

value (100-450 Ohm-m) compared to the other layer, this layer has a thickness of 7m (4.5m to 11.5m), this layer has a core recovery of 3% to 11% but the RQD% was zero. The lithology in the third layer was silty-clay with low resistivity value ρ_3 ranging from (38-100)Ohm-m, the thickness of this layer was 17m (11.5m to 28.5m), the low resistivity value of this layer could be due to the presence of clay, which act as impermeable layers which prevent further movement of water.

From the analysis of rainfall data collected from the State Meteorological Center, Directorate of Science and Technology, Government of Mizoram from 2012 to 2022, it is observed that precipitation is mostly maximum in July for every year and reached a maximum of 743.5mm in June 2017. A subsidence of an average of 1ft is observed from the total station data during September 2022. Precipitation of 460mm in July 2022 was observed from the rainfall data which could greatly contribute to saturating the soil which can result in slope failure.

The studies indicate that the area is characterized by weak and highly fractured shale beds covered by a thin, loose, and weathered soil. The underlying bed exhibits weak loading strength and is weathered with a high water content. The proportion of sand and clay content in a shale bed exhibits variability between stable and unstable areas. Specifically, the clay content is higher in unstable areas when compared to stable areas. This variation suggests that the stability of the shale bed is influenced by the relative proportions of sand and clay. Despite an anti-dip relationship between the bed and the slope, the slope is prone to failure due to the weak geomechanical properties of the soil and rock, lithological variation, presence of joints, toe erosion resulting from nala water cutting in the southeast, and heightened precipitation during the monsoon season. These factors collectively contribute to slope failure in both locations within the study area. A ground movement of 5 feet was recorded during the monitoring period.

Mitigation Measures

Some of the suggested mitigation measures for the stabilization of the slope area include implementing a proper surface and subsurface drainage system, reducing the slope through benching, prohibiting the construction of RCC buildings, and constructing or reconstructing gabion walls and check dams. Given the area's composition of loose soil and rock with high clay content, it is imperative to

implement a comprehensive drainage system to manage water flow effectively.To address the driving forces contributing to slope instability, measures should be taken to minimize construction loads, especially in the upper portions of the slope. This involves restricting building construction and reducing soil mass by removing loose debris and benching the slope. Given the shallow water table in the study area, constructing gabion walls along the channel banks can effectively manage groundwater seepage.

Limitations

The shortage of advanced equipment poses a significant limitation in our ability to conduct comprehensive studies. Additionally, exploring deeper depths becomes a challenging task due to topographical obstacles. These constraints hinder our capacity to delve into more intricate aspects of research. Efforts to address these limitations and enhance technological resources are crucial for advancing our understanding. To address the driving forces contributing to slope instability, measures should be taken to minimize construction loads, especially in the upper portions of the slope. This involves restriction.

building construction and reducing soil mass by removing loose debris and benching the slope.

Conducting a comprehensive subsurface investigation using advanced geophysical methods holds the key to acquiring detailed and accurate information about slope problems. By employing sophisticated techniques, such as ground-penetrating radar or seismic surveys, we can delve deep into the subsurface layers. This in-depth analysis will yield a wealth of data on soil composition, geological structures, and potential hazards.